DEVELOPMENT AND MODELLING OF A NEW CATALYTIC DISTILLATION PROCESS

by

Gary G. Podrebarac

A thesis
presented to the University of Waterloo
in fulfilment of the
thesis requirement for the degree of
Doctor of Philosophy
in
Chemical Engineering

Waterloo, Ontario, Canada, 1996

The University of Waterloo requires the signatures of all persons using or photocopying this thesis. Please sign below, and give address and date.

ABSTRACT

Catalytic Distillation (CD) is a relatively new process used by the petrochemical industry. The process involves placing a heterogeneous catalyst inside of a distillation column so that a chemical reaction and product separation can take place simultaneously in the same piece of equipment. The first commercial application of CD was introduced in 1980 for the production of methyl *tertiary*-butyl ether (MTBE), and the success of this process has created a great deal of interest in using CD as a more generally applied reaction technique.

This thesis describes a new application of CD for the production of diacetone alcohol (DAA) via the base-catalyzed aldol condensation of acetone. This reaction is equilibrium limited to only 4.3 wt% conversion of acetone to DAA at 54°C. As well, DAA can dehydrate to mesityl oxide (MO). MO can continue to react with acetone to form heavier byproducts. DAA is a very useful chemical intermediate and an environmentally friendly cleaning solvent. Therefore, this reaction is commercially relevant, while providing an opportunity to study product selectivity and verify that CD can increase the conversion of acetone beyond the equilibrium limit.

An important goal of this thesis is to develop a new model of CD that takes into account mass transfer between the catalyst and the liquid phase. It is well known that mass transfer can influence the reaction rate and product selectivity of a heterogeneously catalyzed reaction. Yet, as the literature currently exists, no models of CD take mass transfer into account.

In order to develop a model of CD, an experimental program was completed to obtain basic data for reaction kinetics and mass transfer. The rate of DAA formation over the anion exchange resin catalyst was found to be strongly limited by pore diffusion, having an estimated Thiele modulus of 11. However, reaction rates in the batch reactor were not influenced by external mass transfer to the catalyst surface. The reaction rate was also found to be extremely sensitive to the background concentration of water in the reaction mixture. Although high water concentrations slow down the rate of DAA formation, they improve the selectivity of the reaction toward DAA and improve the lifetime of the catalyst.

Mass transfer experiments were also conducted. Mass transfer rates between the catalyst structure and the liquid flowing through the column and mass transfer coefficients for rate-based distillation were measured. The rate of mass transfer between the liquid and the catalyst, however, was found to be extremely sensitive to the flow pattern which is established in the column. This created certain difficulties since flow patterns in packed distillation columns establish themselves in a random way. Thus, it is impossible to make the model of CD completely predictive. Certain steps may be taken, however, such as using liquid

distributors, to improve the reproducibility and the predictability of the CD process.

Several CD experiments were conducted in the bench scale and pilot scale CD facilities at the University of Waterloo. These experiments provided operating data for a variety of liquid flow rates and catalyst bed heights. It was also verified that the CD process can exceed the equilibrium conversion of acetone, as a product containing 50 wt% DAA was easily obtained.

A differential rate-based model was developed which describes the reaction zone of the CD column. The model takes into consideration the kinetic data obtained in the absence of external mass transfer and modifies the kinetic equations to incorporate the various types of external mass transfer which exist in the CD column. The model was fitted to the CD operating data so that the rate of DAA production predicted by the model matched the experimental data. Agreement between the model and other experimental variables which were not fitted was very good. The predicted flow patterns were in agreement with the earlier work of Porter and Templeman (1968), and the model was also able to provide a good estimate of the expected product selectivity and MO production rate. Several samples from within the catalyst bag were also taken, and they confirmed that the predicted concentration profiles in the catalyst bag were close to measured values.

Several experiments were conducted with a proper liquid distributor located just above the catalyst zone of the column. Improving the liquid distribution over the catalyst bag resulted in 45 - 240% gains in DAA production and 112 - 343% gains in product selectivity (measured as mol DAA/mol MO). The distributor also reduced the variability of the system. Clearly, liquid distribution and mass transfer are two of the most important issues in catalytic distillation.

A major problem encountered with this process is catalyst deactivation. If a catalyst can be found that has improved lifetime characteristics, the production of DAA with Catalytic Distillation could easily be commercialized.

ACKNOWLEDGEMENTS

Although nobody was willing to write my thesis for me, there are many people who were instrumental in helping to complete this research....

First of all, I would like to thank my supervisors, Dr. F.T.T. Ng and Dr. G.L. Rempel. They both placed a tremendous amount of faith in me from my first days as a graduate student, and I have appreciated that tremendously.

I would also like to thank the Natural Sciences and Engineering Research Council (NSERC) for providing a strategic grant for this project, and a scholarship for myself. Given the current scarcity of government dollars, I sincerely hope that this investment in Canadian research was a good one. Technical support and advice was received from Chemical Research and Licensing Co. (CR&L) of Houston, Texas. To truly complete this list of project backers I must also thank Dr. G.R. Podrebarac and K.L. Podrebarac for their support, financial and otherwise.

Chunchen Huang, who became my full-fledged side-kick, was very helpful in conducting the mass transfer experiments in Section 3.3 and 3.4. Thanks for your patience and hard work, CC! Dr. Bongani Nkosi conducted the surface area analyses, and sat through many discussions of the current "state of the nation". Conducting CD experiments is a demanding task, and I would like to thank CC Huang, Dr. Bongani Nkosi, and Dr. Lida Yang for helping out.

Dave Stradiotto, Dennis Herman, and Dr. Mark Pritzker deserve thanks for helping me to unlock the mysteries of gPROMS. In addition, Frank Wassmer, Ron Neal, Ralph Dickhout, and G. Waddle deserve thanks. Building, blowing, maintaining, and acquiring decent equipment is difficult, and these staff members were always ready to jump into the fray.

I thank Mark Beasy, Derek Creaser, Marc Dubé, Jungfu Huang, Laila Kott, Cindy Lang, Celia Lee, Dr. Ray Legge, Rob Lutzer, Mr. Liu, Neil McMannus, Scott Parent, Harriot Phillips, Rob Rintjema, Francesca Rodrigues, Chris Rourke, Cecile Siewe, Gail Walker, and all the guys at "Friday Afternoon Hockey" for letting me hang out with them.

I would also like to express my appreciation to my brother Scott
and my new sister Andrea for letting me crash at
their nice, clean townhome, and to my brother
Craig for letting me drive him
out to Calgary. Is there a
meal plan at the
Huether,
yet?

TABLE OF CONTENTS

LIST OF TABLES

LIST OF FIGURES

NOMENCLATURE

Symbols used for Rate Constants - k :

Superscripts

I, II, III- referring to a specific step in the reaction mechanism (Figure 2.2.2-1)
* - denotes an intrinsic rate constant
′ - denotes a rate constant per unit bulk volume of catalyst

Subscripts

1 - forward rate constant for DAA production (M^{-1} min^{-1})
-1 - reverse rate constant for DAA decomposition (min^{-1})
2 - pseudo-zero order rate constant for MO production (M min^{-1})
d - deactivation rate constant
for - constant for the forward reaction
i - rate constant for the disappearance of component i
MO - first order rate constant for MO production (min^{-1})
rev - constant for the reverse reaction
S - rate constant per unit surface area (m/s)
V - rate constant per gross volume of the catalyst pellet (1/s)

Other Variables

a - fraction of catalytic sites which are active
A - interfacial area per unit height of column (m^2/m)
A′ - interfacial area (m^2)
A″ - interfacial area per unit bulk volume (m^2/m^3)
b - intercept of the linear approximation to the vapour-liquid equilibrium curve
c - number of components in a closed system
c_i - vapour phase concentration of component i
C_i - liquid phase concentration of component i
d - diameter (m)
D - diffusion coefficient (m^2/s)
D_{eff} - effective diffusion coefficient (m^2/s)
Đ - dispersion coefficient (m^2/s)
f - fraction of liquid flowing through the catalyst bags in the CD column
F - volumetric liquid flow rate (m^3/s)
F - degrees of freedom

G	- gas phase flow rate (mol/s)
h_L	- Thiele modulus for plate shaped catalyst defined in equation (3.10)
h_S	- Thiele modulus for spherical catalyst pellets defined in equation (3.13)
HETP	- height equivalent to a theoretical plate
HTU	- height of a transfer unit defined in equation (3.26)
j_D	- j-factor for liquid-solid mass transfer defined in equation (3.22)
j_G	- j-factor for vapour liquid mass transfer based on gas-side compositions (3.28)
j_L	- j-factor for vapour liquid mass transfer based on liquid-side compositions (3.28)
k_C	- solid-liquid mass transfer coefficient based on concentrations (m/s)
k_f	- film mass transfer coefficient based on concentrations (m/s)
K_{EQ}	- reaction equilibrium constant
K_O	- overall vapour-liquid mass transfer coefficient based on mole fractions ($mol/m^2 \cdot s$)
L	- length of a catalyst pore (m)
L	- liquid phase flow rate (mol/s)
m	- slope of the approximation to the vapour-liquid equilibrium curve
n	- reaction order in Chapter 3
n	- index referring to a specific bag in the CD column in Chapter 5
N	- total number of catalyst bags in the CD column
N_i	- mass transfer rate (mol/s)
$\mathbb{N}_i$	- mass transfer flux ($mol/m^2 \cdot s$)
NTU	- number of transfer units defined in equation (3.26)
p	- parameter defined in equation (3.16)
p	- number of phases in a closed system
P_i^{vap}	- vapour pressure of pure component i
P_T	- total pressure
Pe	- Peclet number
Q	- a constant
r	- number of independent reactions in a closed system
r	- radial position (m)
R	- radius of pore, particle, or catalyst bag (m)
R_i	- rate of generation of component i ($mol/m^3 \cdot s$)
Re	- Reynolds number
S	- selectivity ratio defined in equation (3.14)
Sc	- Schmidt number
Sh	- Sherwood number
t	- time (s or min)
T	- temperature (°C or K)
v_0	- superficial (empty tube) velocity (m/s)
V	- volume of reactor (mL, L, or m^3)
V	- vapour phase volumetric flow rate in chapter 5 (m^3/s)
w	- parameter defined in equation (3.16)
x	- position in a catalyst pore (m, or dimensionless)
x_i	- liquid phase mole fraction of component i

X^0 - parameter defined in equation (3.16)
y_i - vapour phase mole fraction of component i
z - vertical position in the column or catalyst bag (m)
Z - total height of the column or of a catalyst bag (m)

Greek

α - stoichiometric coefficient in equation (3.16)
β - parameter defined in equation (3.16)
γ - parameter defined in equation (3.16)
γ_i - liquid phase activity coefficient of component i
Γ - parameter defined in equation (3.16)
δ - parameter defined in equation (3.16)
ϵ - parameter defined in equation (3.16)
η - catalyst effectiveness factor defined in equations (3.12) and (3.13)
κ - rate parameter defined in equation (3.5)
λ - parameter defined in equation (3.16)
μ - viscosity
ν_i - stoichiometric coefficients, $\nu_i < 0$ for reagents, $\nu_i > 0$ for products
ρ - density
ε - void fraction of catalyst particles

Superscripts

n - index referring to a specific catalyst bag in the CD column
O - property of a pure component

Subscripts

b - bottom of distillation column
bag - inside of the catalyst bag
B - bulk conditions
EQ - equilibrium condition
G - referring to the gas phase

i - referring to component i
L - referring to the liquid phase
p - catalyst particle or random packing element
r - in the radial direction, or in the reboiler of the distillation column
S - conditions at the catalyst surface

t - tube, or top of distillation column
0 - an initial condition

-1-

INTRODUCTION

1.1 Introduction to Catalytic Distillation

Catalytic Distillation (CD) is a method of simultaneously conducting a chemical reaction and separating the reagents/products in a distillation column. It was patented by Smith (1980, 1982) along with the first application of this technology for the production of methyl *tertiary*-butyl ether (MTBE). Rapid growth in demand for MTBE has attracted a great deal of interest in using CD as a more general reaction technique.

Catalytic Distillation, for the purposes of this work, is defined as the process by which a heterogeneously catalyzed chemical reaction and distillation of the products/reagents occur simultaneously within a distillation column. A key characteristic of this process is the fact that the heterogeneous catalyst acts as the catalyst for the reaction as well as a distillation packing. This aspect separates CD from Reactive Distillation, where a homogeneous catalyst is used.

CD belongs to the more general class of 'two-phase flow fixed-bed catalytic reactors'. An upward flow of vapour and downward flow of liquid comprise the two flowing phases in the CD reactor. CD is also a 'counter-current' process since the liquid and vapour flow in opposite directions. Other flow configurations within this reactor class have the vapour and liquid phases in concurrent downward flow (ie. a trickle bed reactor), or concurrent upward flow.

Catalyst particles are typically small spherical or cylindrical particles, and the resulting catalyst bed has a low void fraction of 0.3 - 0.4. On the other hand, typical packings used in counter-current distillation have a void fraction near 0.7, and some structured packings boast a void fraction of 0.97 (Kister, 1992). The low void fraction of catalyst beds makes the operation of a counter-current reactor difficult. Flow rates must be carefully controlled since these beds are highly susceptible to flooding. However, trickle bed reactors do not flood and

as a result, are far more common in industry.

Following the introduction of the MTBE process, however, new methods of supporting small catalyst particles inside of distillation columns were disclosed (Smith, 1984; Jones, 1984, 1985). These catalyst structures maintain a void fraction of at least 0.5 in the column, and make the counter-current operation of fixed bed reactors practical.

The increasing importance of CD as a reaction technique raises the fundamental question of whether or not there are any advantages associated with operating a reactor in counter-current flow, as opposed to co-current upward or downward flow. Mills et. al. (1984) studied the hydrogenation of α-methylstyrene to cumene (a first order, irreversible reaction) in all three flow configurations using the same catalyst bed, and concluded that there were no major differences in the observed α-methylstyrene conversion.

Trambouze (1990) compared counter-current and trickle bed reactor models for several types of reactions. In his models, the void fraction of the catalyst bed was taken to be 0.35 for the trickle bed reactor, and 0.7 for the counter-current reactor. The use of such a high void fraction in the counter-current reactor model implies that the catalyst can be manufactured in the shape of a distillation packing. In practice, the preparation of specially shaped catalysts may be difficult. The results from all of the reaction scenarios showed a higher conversion per unit mass of catalyst for the counter-current reactor. Only a small increase in conversion was predicted for a first order irreversible reaction, which agrees reasonably well with the findings of Mills et. al. (1984). However, more substantial increases in conversion were predicted for reversible reactions and highly exothermic reactions.

Therefore, it appears that the conversion of some types of reactions may be increased with counter-current flow. There are many other advantages specifically offered by CD, and some of these are outlined below (Stadig, 1987):

1) CD efficiently uses the heat released by a reaction. In conventional reactors, the heat of reaction is removed by cooling coils or heat exchangers. Since the catalyst is surrounded by boiling liquid in the CD process, however, the heat of reaction improves distillation by increasing the vapour flow. This results in energy savings since reboiler duties can be lowered in CD columns.

2) Since the catalyst is surrounded by liquid at its boiling point, the danger of 'hot spots' forming in the CD column is eliminated. The temperature of the liquid in the CD column cannot exceed its boiling point, and the high flow rates in a distillation column ensure that the catalyst pellets remain 'wetted'. Thus, the catalyst is restricted to a temperature very near the boiling point of the liquid phase.

3) Keeping the temperature of the catalyst particles near the boiling point of the liquid gives CD columns precise isothermal control of the reaction temperature. In conventional tubular reactors, radial and axial temperature gradients are the norm.

4) Conducting two unit operations in one piece of equipment offers significant capital savings over a conventional reactor-distillation column scheme and typically results in simpler process flowsheets.

5) Catalysts are often corrosive and hazardous materials. In CD columns, the catalyst does not contact the walls or internals of the column. Therefore, expensive corrosion resistant materials of construction can be avoided.

6) CD processes can be operated so that the reaction product is selectively removed from the reaction zone by distillation. Le Chatelier's principle implies that the removal of product from a system at equilibrium will cause more product to form. Therefore, CD is able to increase the conversion of equilibrium limited reactions beyond the thermodynamic limits.

7) Distillation columns operate at high liquid and vapour flow rates. Thus, a fast removal of products from the reaction zone is possible. The fast removal of products from the reaction zone reduces the probability of consecutive reactions taking place and improves product selectivity.

8) Catalyst lifetime can be improved since the material that contacts the catalyst has been distilled. By careful placement of the catalyst zone relative to the feed point, poisons may be excluded from the catalyst zone and deactivation may be avoided.

Although there are a number of advantages to CD, this technology cannot be applied in every situation. There are a number of criteria that a reaction must satisfy before CD may be considered. Some of these criteria are outlined as follows:

1) Distillation must be a practical method of separating the reagents/products of the reaction. If the boiling points of the components are too close, distillation is not an effective way to separate them and other technology is likely more suitable.

2) The reaction must take place in the liquid phase since the catalyst pellets are completely 'wetted'.

3) The reaction must take place at a temperature equivalent to the boiling point of the liquid in the column. There is some flexibility in this condition since the boiling point can be altered by changing the pressure in the column. However, there is an upper limit to the temperature that can be used since two phases are required for distillation. Thus, the reaction temperature must be below the critical temperature of at least one of the components present.

4) The reaction cannot be overly endothermic. A highly endothermic reaction condenses vapour in order to obtain the energy necessary for the reaction. This results in poor distillation and increased reboiler duties. Other types of reactors, with more effective ways of getting heat to the reaction zone, are preferred for highly endothermic reactions.

5) A heterogeneous catalyst with a long lifetime must be available. It is expensive and labour intensive to change the catalyst in a CD column. The catalyst must typically last 1-2 years in service to be commercially viable.

These criteria preclude the application of CD for a large number of very useful chemical reactions. However, there are still many types of reactions that do, in general, satisfy the above conditions. Some general types of reactions that may benefit from CD are hydrolysis, hydrogenations, etherifications, esterifications, dimerizations, alkylations, and others (Guang-run and Nai-ju, 1991; Stadig, 1987).

1.2 Applications of Catalytic Distillation

Although CD is a relatively new process, there are already a number of applications that have been investigated. In this section, some of these reaction systems will be discussed, and the benefits that CD offers will be presented.

1.2.1 Etherification

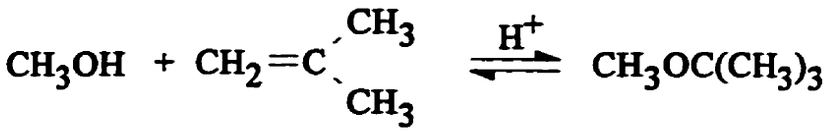

Figure 1.2.1-1: The acid catalyzed production of MTBE.

The manufacture of methyl *tertiary*-butyl ether (MTBE) was the first commercial CD process, and has become so important that one cannot discuss CD without at least mentioning it. MTBE is produced from an acid catalyzed reaction between methanol and isobutylene, as shown in Figure 1.2.1-1.

MTBE is an environmentally friendly octane enhancer that is blended into gasoline. The main competition for MTBE as a fuel oxygenate comes from ethanol. MTBE offers several advantages over ethanol, however, such as improved solubility with gasoline, a higher octane number (108 vs. 101 for ethanol), and a higher energy content per unit volume (Ecklund and Mills, 1989). MTBE is also a more economical source of octane than ethanol, even with the US tax subsidies that ethanol enjoys (Weiszmann et. al., 1992).

A study was initiated in the winter of 1987 to verify that the use of MTBE would reduce environmental CO levels, and gasoline containing 8 vol% MTBE was successfully tested in the Denver, Colorado area. In 1988-89, MTBE levels were increased to 11 vol% (Ecklund and Mills, 1989). The 1990 US Clean Air Act amendments now require that areas in the US that do not meet federal CO standards use oxygenated fuels containing 2.7% oxygen, which is equivalent to 15 vol% MTBE (Anderson, 1993). In the winter of 1992-93, 39 metropolitan areas exceeded the allowable CO levels. Despite MTBE's favourable environmental impact, however, a major incentive for its use is octane improvement. As lead usage in gasoline is phased out/down in the USA and Europe, MTBE is added to meet the required octane levels (Weirauch, 1995).

Growth in MTBE production over the past 15 years is unprecedented. MTBE production in the US was 190 million gallons in 1982, 1.03 billion gallons in 1987 (Mills and

Ecklund, 1989), and 2.17 billion gallons in 1994 (Kirschner, 1995). World production has increased from 3.07 billion US gallons in 1990 to an estimated 6.9 billion US gallons in 1995 (Thomas, 1994). Despite a spate of health complaints in 1992, studies indicate that MTBE is a safe gasoline additive (Anderson, 1993), which bodes well for continued growth. With cities in Asia such as Bangkok, Taipei and Jakarta facing rapidly deteriorating air quality, world demand for MTBE will likely remain strong for years to come (Weirauch, 1995). However, growth has recently shifted the economics of the MTBE process. Methanol prices increased from $130 US/tonne in 1993 to $440 US/tonne in 1994, peaking at $600 US/tonne, mainly on demand from MTBE producers (Bell, 1995). This past performance, however, has established a great deal of credibility for CD as a practical reaction technique.

Conventional MTBE processes have a very similar design. Processes from Gulf Canada (Chase and Galvez, 1981) and Hüls-UOP (Hutchings et. al., 1992) are nearly identical. Schematics of the Hüls-UOP and CD Tech (Hutchings et. al., 1992) processes are shown in Figure 1.2.1-2 and 1.2.1-3, respectively.

Perhaps the most striking difference between these schematics is the simplicity of the CD process. While the water-wash section and excess methanol recovery and recycle are identical in both diagrams, the reaction section of the CD process is much simpler. In the CD Tech process, there is no external cooling or recycle through reactor (1) and one less reactor. This gives the CD Tech process a lower capital cost. The adiabatic reactor (1) prolongs the life of the catalyst in the CD column by removing catalyst poisons. In addition, the heat of reaction released in (1) preheats the feed to the CD column (2). The reaction releases such quantities of heat that a mixture of boiling liquid and vapour is actually fed to the CD column. Isobutylene conversions up to 99.99% are possible for the CD Tech process vs. 97-99% for the Hüls-UOP process. CD provides a slight advantage in isobutylene conversion due to its ability to increase conversions beyond the equilibrium limit. The amount of improvement is small, however, since the equilibrium of the MTBE system favours product formation. High isobutylene conversions can be obtained (>95%) by using two times the stoichiometric amount of methanol (Rehfinger and Hoffmann, 1990), and for this reason conventional reactors will remain fairly competitive.

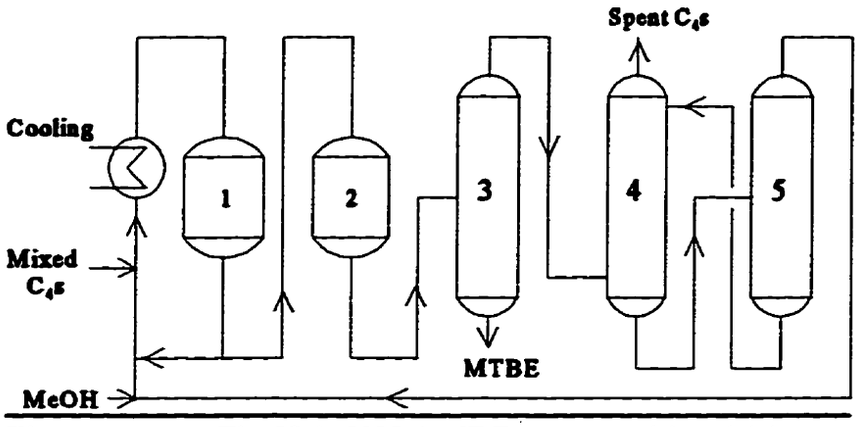

Figure 1.2.1-2: The Hüls-UOP MTBE process. (1) and (2) - adiabatic reactors, (3) - MTBE purification, (4) - C_4 water wash, (5) - methanol/water separation (Hutchings et. al., 1992).

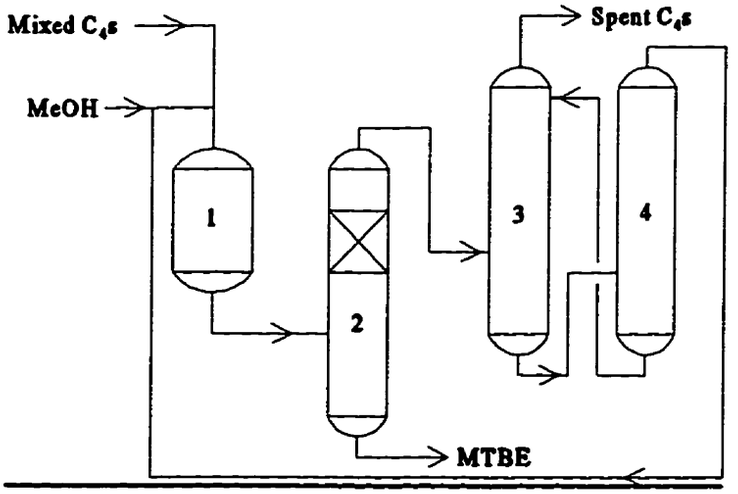

Figure 1.2.1-3: The CD Tech MTBE process. (1) - adiabatic reactor, (2) - CD column, (3) - C_4 water wash, (4) - water/methanol separation (Hutchings et. al., 1992).

In addition to MTBE, there is interest in producing tertiary amyl methyl ether (TAME) (Bravo et. al., 1993) and ethyl tertiary butyl ether (ETBE) as gasoline additives. MTBE processes, however, can usually manufacture different ethers with very little modification.

Not surprisingly, CD can also be used to obtain *extremely* pure isobutylene for use in the manufacture of butyl rubber and polyisobutylene (Convers et. al., 1981). By feeding MTBE to a CD column, deetherification takes place and isobutylene is obtained as an overhead product (Smith, 1985). This process simplifies the difficult separation of isobutyiene from other C_4 isomers.

1.2.2 Alkylation of Benzene

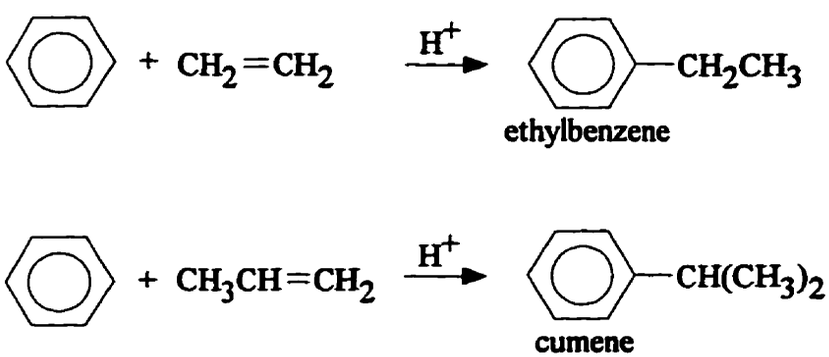

Figure 1.2.2-1: The alkylation of benzene to produce ethylbenzene and cumene.

The alkylation of benzene with ethylene or propylene leads to ethyl benzene and cumene, as shown in Figure 1.2.2-1. Of the top 50 most produced chemicals in 1994, ethyl-benzene is ranked 19th and cumene is ranked 31st (Kirschner, 1995). CD can successfully manufacture both of these important chemicals (Doherty and Buzad, 1992; Stadig, 1987; Shoemaker and Jones, 1987). Since the processes are fairly similar, we will focus on the cumene process (Shoemaker and Jones, 1987).

The process schematic is shown in Figure 1.2.2-2. CD offers many advantages over conventional cumene production methods.

Firstly, the concentration of propylene in the reaction section of the CD column is low, which slows down the propylene oligomerization side reaction and reduces the amount of diisopropylbenzene (DIPB) and triisopropylbenzene (TIPB) produced. The DIPB and TIPB that are formed are separated from cumene in (2) and recycled back to the CD column where transalkylation with benzene yields more cumene. This process boasts a 50% energy savings over conventional technology, a 25% lower capital cost, and eliminates the need to recycle a large quantity of benzene.

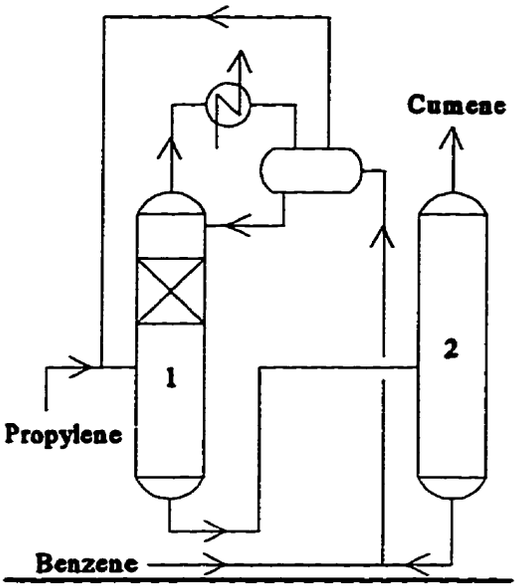

Figure 1.2.2-2: CD Tech cumene process. (1) - CD column, (2) - cumene/(DIPB&TIPB) separation (Shoemaker and Jones, 1987).

1.2.3 Esterification and Hydrolysis

Another reaction that has received attention is the reversible esterification of methanol or ethanol with acetic acid to form methyl acetate (MeOAc) (Fuchigami, 1990; Agreda et. al., 1990) or ethyl acetate (EtOAc) (Savković-Stevanović et. al., 1992), respectively. These reactions are a major focus of reactive distillation work and are now being tested with heterogeneous catalysts. The reactions are shown in Figure 1.2.3-1. The reverse reaction, or the hydrolysis of MeOAc, is important since MeOAc is a by-product of polyvinyl alcohol production. MeOH and acetic acid produced from the hydrolysis can then be recycled within the polyvinyl alcohol manufacturing process (Fuchigami, 1990).

For MeOAc, the equilibrium constant ($K_{EQ} = 5.2$, Agreda et. al., 1990) favours

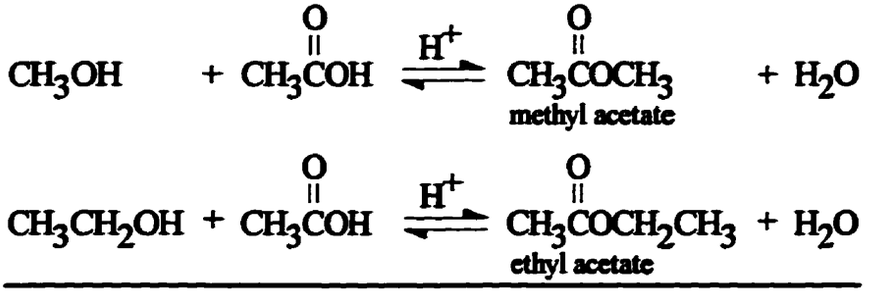

Figure 1.2.3-1: The production of esters from alcohols and acetic acid.

production of the ester. Therefore, CD would likely benefit the hydrolysis reaction more than the esterification reaction. The equilibrium restriction in either case is not severe. Fuchigami (1990) notes that the hydrolysis process is greatly simplified when CD is used. The CD process requires one CD column and two distillation columns, whereas the conventional process requires one reactor and *four* distillation columns.

Another hydrolysis reaction that has been studied is the formation of ethylene glycol from ethylene oxide (EO) and water (Ciric and Miao, 1994). This reaction is shown in Figure 1.2.3-2. The CD column operates by refluxing water over the catalyst zone. EO, which is very volatile (boiling point is 10°C), is fed below the catalyst zone in the same way that propylene is fed to the cumene process (Figure 1.2.2-2). This operating procedure leads to low reactant and product concentrations in the reaction zone which should inhibit consecutive

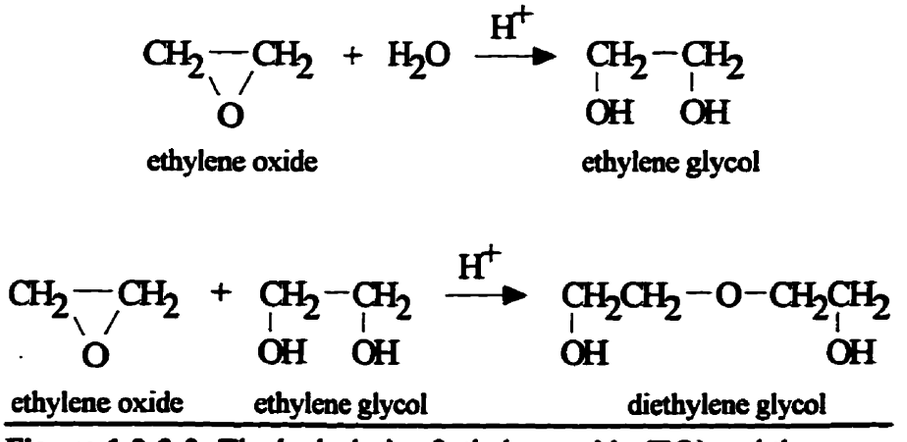

Figure 1.2.3-2: The hydrolysis of ethylene oxide (EO) and the formation of diethylene glycol.

reactions. Indeed, it was reported that diethylene glycol production (the main byproduct) was quite low.

1.2.4 Hydrogenation

A process has been developed for the selective hydrogenation of diolefins (Hydrocarbon Processing, 1994). The removal of traces of diolefins from hydrocarbon feeds is very important, as these compounds frequently deactivate catalysts in downstream operations or participate in undesirable side reactions. For example, the severe deactivation of Ni-based oligomerization catalysts by butadiene is discussed by Podrebarac et. al. (1996).

A process schematic for the selective hydrogenation of the C_4 fraction from a catalytic cracker is shown in Figure 1.2.4-1. This process is very convenient since it separates C_5+ from the C_4 stream, and simultaneously hydrogenates butadiene. The placement of the hydrogenation catalyst (eg. Pd on alumina) above the feed point also prevents foulants and heavy catalyst poisons from reaching the catalyst. This type of catalyst protection is not possible in fixed bed reactors. Although hydrogenation reactions are very exothermic, the catalyst section in the CD column operates in an isothermal manner. This is in sharp contrast with fixed bed reactors where temperature gradients are inevitable. The elimination of a separate hydrogenation reactor and hydrogen stripper also reduces the capital cost of this system.

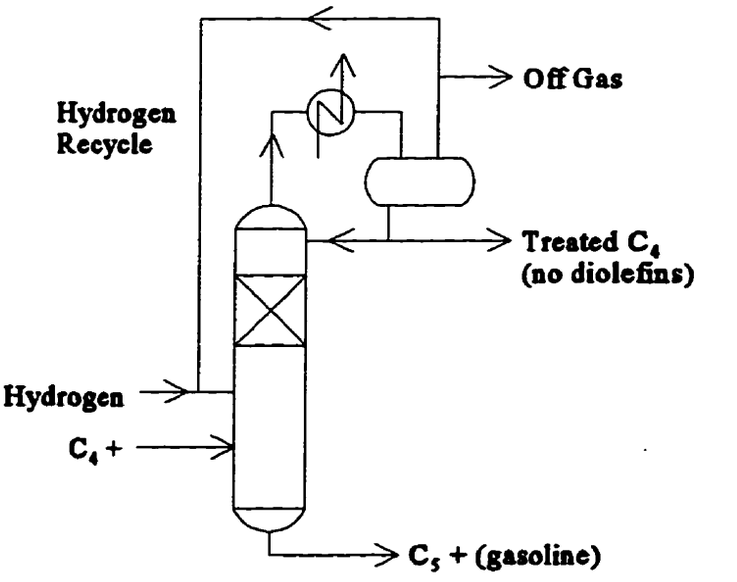

Figure 1.2.4-1: CD based process for the selective hydrogenation of diolefins (Hydrocarbon Processing, 1994).

The CD hydrogenation system may also be used to remove traces of sulfur compounds from the hydrocarbon feed. Heavy sulfur-containing compounds will remain in the C_5+ fraction, while volatile sulfur-containing compounds are hydrogenated to produce H_2S gas. H_2S is recovered as part of the 'Off Gas' stream shown in Figure 1.2.4-1.

1.2.5 Alkylation

Huss and Kennedy (1990) have disclosed a CD process that can be used for the alkylation of isobutane with butenes. Conventional alkylation processes currently provide a great deal of octane for blending into premium gasoline. CD appears to have great potential as a reaction technique for alkylation. It may be able to improve the selectivity of this process by quickly removing the octane product from the reaction zone, thus reducing the rate of consecutive reactions. Alkylation processes typically operate at a high ratio of paraffin:olefin to minimize olefin oligomerization side reactions. CD should also reduce the amount of paraffin recycling that is required and simplify the flowsheet considerably when compared to conventional alkylation systems.

The usual catalysts for conventional alkylation processes are homogeneous sulfuric acid and hydrofluoric acid, and are extremely corrosive and hazardous. Clearly, there is strong incentive to develop a heterogeneous catalyst for this reaction and eliminate the use of hazardous liquid catalysts. The process described by Huss and Kennedy (1990) requires the co-feeding of BF_3 to the CD column. Obviously, it would be preferable to eliminate the BF_3 feed from this process. Despite CD's potential advantages, it appears that CD alkylation is a process in need of a good heterogeneous catalyst. Industrial competition in this area is intense, and as a result, publications describing CD alkylation are scarce.

1.2.6 Oligomerization

There is interest in using CD to oligomerize light olefins into heavier 'liquid' products. Smith et. al. (1991) have disclosed a CD based process for the acid catalyzed oligomerization of C_4 and C_5 isoolefins. This reaction is highly exothermic, yet the CD process is able to maintain an isothermal reaction zone.

With the objective of oligomerizing linear olefins, a detailed study of 1-butene and mixed C_4 raffinate dimerization was conducted at this laboratory (Podrebarac, 1992). However, the oligomerization of linear olefins requires more severe reaction conditions than isoolefin oligomerization if an acid catalyst is to be used. In order to permit the use of milder reaction conditions, a Ni-Y zeolite catalyst was selected.

Podrebarac (1992) postulated that the reaction product (octenes) would be removed quickly from the catalyst zone of the column by the high liquid flow rates used in CD. The fast removal of products from the reaction zone should improve the product selectivity by slowing consecutive reactions that form less desirable C_{12}s, and improve catalyst lifetime since large oligomers ($\geq C_{16}$) are responsible for catalyst deactivation. Unfortunately, these benefits were not observed. Catalyst deactivation was faster in the CD column than in a tubular reactor, and the initial product selectivity to octenes was worse in the CD product. It was reasoned that mass transfer between the bulk liquid and the catalyst was rather poor in the CD process. Processes described previously may actually take advantage of poor mass transfer to improve selectivity. For example, cumene production requires a high benzene:propylene ratio to improve the cumene yield, and poor mass transfer of propylene to the catalyst helps maintain this high ratio. Rapid product removal is required to achieve good selectivity from a system with consecutive reactions, however, and this may not be possible with the current method of supporting catalysts in CD columns. The fact that significant quantities of DIPB and TIPB form in an environment starved for propylene may, in fact, be evidence of slow product removal in the cumene process. It should be mentioned that cumene is alkylated more easily than benzene, however, and this feature makes the selective formation of cumene a relatively difficult task.

1.3 Research Overview and Problem Statement

Despite repeated musings that CD should improve product selectivity by restricting consecutive reactions, this has never been adequately demonstrated. In fact, results from our laboratory (Podrebarac, 1992) are to the contrary. Our preliminary results suggest that CD does not improve the product selectivity for a system of consecutive reactions. One goal of this research is to examine carefully how the CD process influences the selectivity of consecutive reactions.

Claims that CD improves the conversion of equilibrium limited reactions also abound. Yet the majority of the reactions that use CD are not severely limited by equilibrium. In the MTBE process, for example, the conversion of isobutylene is increased by only 1-2% by switching to CD. A second goal of this work is to test the effectiveness of CD at conducting a reaction that is severely restricted by equilibrium.

Recently, a number of publications have appeared that describe mathematical models of the CD process. The literature in this area will be reviewed in Chapter 5 of this thesis. Most models treat the CD process as an equilibrium stage operation. Solving CD problems in this way, however, holds the emphasis on traditional distillation issues such as concentration profiles, temperature profiles, and product purities. The assumptions made in developing these models tend to sacrifice accuracy in the reaction rate equations in order that conventional distillation algorithms can be used to solve the models. As a result, the reaction rate expressions are often simplified to the point that they are meaningless.

Reaction rates over heterogeneous catalysts are strongly influenced by mass transfer, and this *must* be taken into account. Indeed, the observations in Section 1.2.6 suggest that this issue is of paramount importance. Rather than a conventional equilibrium model, a more appropriate approach would be a 'rate-based' model. This type of model consists of differential equations which take into account the various mass transfer steps. While solving such a model is more difficult, the results would be more meaningful. Thus, the final goal of this work is to develop a 'rate-based' model of the reactive zone in a catalytic distillation column that effectively considers mass transfer.

The research required to achieve these goals was divided into chronological phases. Each phase of the research is described briefly in the paragraphs below, and constitutes a chapter of this work.

Phase I: The goal of Phase I is to identify a reaction that could benefit from the application of Catalytic Distillation. A system that is strongly limited by equilibrium and that has a consecutive reaction is required to accomplished the outlined goals.

Phase II: The purposes of Phase II are to conduct a kinetic study of the reaction selected in Phase I and to experimentally determine mass transfer coefficients for the CD column. This is a highly experimental section, and will provide mass transfer coefficients which are essential for the CD process.

Phase III: In this phase, bench and pilot scale CD experiments will be conducted using facilities at the University of Waterloo. The main points of interest are the reaction rate and product selectivity, and how these compare with batch results from Phase II.

Phase IV: This phase is concerned with modelling the CD process. In phase IV, the kinetic and mass transfer data from phase II will be used to model the behaviour of the CD process observed in phase III. CD will be modelled as a 'rate-based' process with differential equations that take into account many of the mass transfer steps that occur in the CD process. Such a model would be invaluable in *a priori* evaluations of how a CD column will behave based on easily obtained batch kinetic data.

-2-

PHASE I - SELECTING A REACTION

2.1 Reactions Considered

The purpose of Phase I is to identify a new application for Catalytic Distillation (CD). Basically, this involves selecting a chemical reaction that will benefit from the application of CD, but that hasn't been previously tested.

In Section 1.1, many restrictions on the reactions that may be conducted in a CD column were outlined. In addition to satisfying these restrictions, the selected reaction must also help accomplish the stated goals. The following conditions apply:

- The reaction should be severely equilibrium limited.
- The reaction products should take part in consecutive reactions.

Many reactions were considered for further study, but only the serious candidates will be mentioned in the paragraphs that follow.

Oligomerization: Additional work which builds on previous work conducted in this laboratory was proposed (Podrebarac, 1992). The oligomerization of linear butenes to octenes is a good way of upgrading the value of C_4's from cracking operations. However, this reaction is not limited by equilibrium, and was not selected for further study.

Hydration: The hydration of olefins to alcohols was also considered. Perhaps the most important reaction in this group is the hydration of isobutylene to tertiary butyl alcohol (TBA) (Doherty and Buzad, 1992). The oligomerization of isobutylene to octenes is a side reaction, and the dehydration of TBA to an ether is a consecutive reaction. This reaction is also equilibrium limited (Delion et. al., 1986). The major drawback of this reaction is the poor miscibility between the olefin and water phases. Thus, this reaction was not considered further.

Etherification: The production of MTBE and TAME was covered in Section 1.2.1, and is the major application of CD technology. This process has become a very popular research topic, and the subject of many publications. Although the literature is becoming crowded in this area, there is still original work that could be done with alternative olefin and alcohol feeds. This process, however, is not severely limited by equilibrium and does not have consecutive reactions. For these reasons this system was not considered further.

Hydrogenation: This is a class of reactions that could likely benefit from CD. Hydrogenations are highly exothermic, and the CD process could efficiently use the heat released to improve distillation and reduce the reboiler duty. The hydrogenation of aniline to cyclohexylamine was seriously considered for this work, and a literature review on this subject was presented in the research proposal which was prepared for this thesis (Podrebarac, 1994). The overall chemical reaction is shown in Figure 2.1-1.

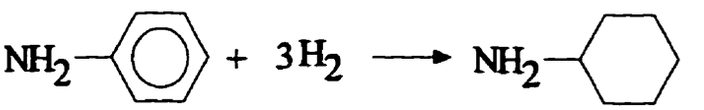

Figure 2.1-1: The hydrogenation of aniline to cyclohexylamine.

Due to the toxicity of aniline, and the fact that this reaction is irreversible (Freifeider, 1971), it was not considered further.

Aldol Condensation: The aldol condensation is a class of reactions which is widely used in organic synthesis. It may be conducted in the liquid or vapour phase, with a variety of catalysts (Scheidt, 1964). Condensations may be conducted with aldehydes or ketones. The equilibrium typically does not favour the ketone condensation product, and for this reason the reaction is not considered to be as useful for ketones as it is for aldehydes (Fessenden and Fessenden, 1986).

The self-condensation of acetone was considered for further study. This reaction is illustrated in Figure 2.1-2. Under mild reaction conditions, diacetone alcohol is formed (Fessenden and Fessenden, 1986). At higher temperatures diacetone alcohol readily undergoes dehydration to mesityl oxide (Scheidt, 1964).

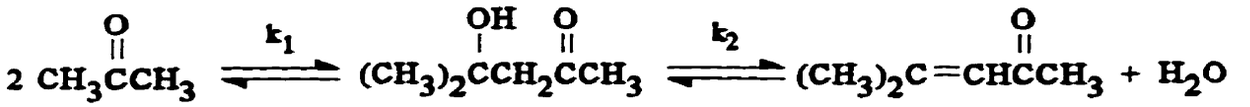

Figure 2.1-2: The aldol condensation of acetone to diacetone alcohol, followed by dehydration to mesityl oxide.

Being equilibrium limited, and having a consecutive reaction, the aldol condensation of acetone is a good candidate for this research. However, the question of whether this reaction has been previously tested in a CD column still remains.

Belck (1955) appears to have previously considered this system. He did some theoretical work with a reaction 2A⇌ B, where B has the higher boiling point and can be removed from the bottom of the column. Belck's hypothetical column is shown in Figure 2.1-3. Although he did not specify the chemicals 'A' and 'B', he did provide some of their properties. Table 2.1-I compares the properties given by Belck (1955) with properties of acetone and diacetone alcohol.

The similarity between 'A' and acetone, and 'B' and DAA in Table 2.1-I is striking. It seems likely that Belck considered conducting this reaction in a distillation column. The schematic in Figure 2.1-3 shows that operating this column would be very difficult. Belck planned to use a homogeneous catalyst, and shows that the catalyst would have to be removed from the column at a stage where the reaction reaches equilibrium. This difficult operation made the cost of the process prohibitive.

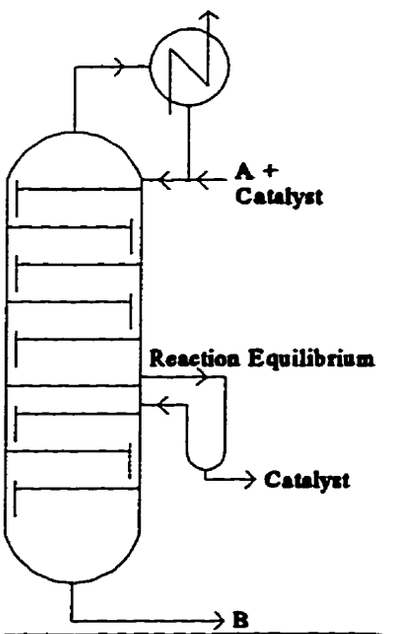

Figure 2.1-3: The column considered by Belck (1955).

No other references to conducting this reaction in a reactive distillation column were found. However, Kunin (1972, 1973) outlines a laboratory technique for producing DAA in a Soxhlet extractor. Acetone vapours that emerge from a boiling flask are condensed and passed through a thimble containing the catalyst. The DAA/acetone mixture then flows back into the flask. Since acetone is much

Table 2.1-I: Comparison of Belck's (1955) compounds A and B with Acetone and Diacetone Alcohol.

Property	'A'	Acetone	'B'	DAA
Molecular Wt. (g/mol)	58	58.08	116	116.16
Density (kg/L) at 56°C	0.7	0.748	0.9	0.907
Normal Boiling Point (°C)	60	56.3	165	165.6
Heat of Vaporization (kJ/mol) at 165°C	22.61	21.4	40.19	44.68

more volatile than DAA, the reaction product concentrates in the flask. While this type of technique uses distillation to purify DAA, it can hardly be called Catalytic Distillation.

The commercial importance of DAA is also an attractive consideration. There are currently many commercial applications for DAA, and the future for this product looks somewhat promising. DAA is being marketed as a cleaning solvent that could replace acetone (Kirschner, 1994). Stronger environmental regulations concerning solvent use are providing the incentive to seek alternative solvents with low volatility. DAA has a lower flash point, and 1/10 the volatility of acetone, so it can provide a safer working environment and last longer than acetone.

The aldol condensation of acetone seems to meet the criteria outlined for selecting a reaction for this research. A detailed literature review, which summarizes our knowledge of this reaction, follows in Section 2.2.

2.2 The Aldol Condensation of Acetone - Literature Review

2.2.1 Uses of DAA and Production Techniques

The aldol condensation of acetone leads to a variety of useful products. The product of the initial condensation reaction is 4-methyl-4-hydroxy-2-pentanone or diacetone alcohol (DAA). Since DAA contains an alcohol group and a ketone group, it has rather unusual and useful solvent properties. It is a solvent for cellulose acetate, nitrocellulose, vinyl chloride-vinyl acetate, epoxy resins, and a good additive for brushing lacquers. Its solvating ability makes it a useful additive in hydraulic brake fluids and gasoline where it is used to prevent freezing and dissolve carbon deposits (Braithwaite, 1995).

DAA is usually produced by a low temperature liquid-phase self-condensation of acetone in the presence of a solid base catalyst, such as NaOH (Godet, 1959). Suitable catalysts also include the hydroxides of potassium, calcium, or barium (Braithwaite, 1995). A wide variety of alternative catalysts have been discovered, such as hydrotalcites (Reichle, 1984 and 1985), rutile (Griffiths and Rochester, 1978), alumina (Bell and Gold, 1983), organometallic cobalt complexes (Tencer et. al., 1991), alkali metal phosphates (Tada, 1975), γ-Fe_2O_3 and α-Fe_2O_3 (Watanabe and Seto, 1991), anion exchange resins (Schmidle and Mansfield, 1952), and others. The aldol condensation is also catalyzed by acids, but a rapid dehydration of the intermediate product is usually observed with acid catalysts (March, 1985). Low reaction temperatures are preferred due to the unfavourable equilibrium that exists. The equilibrium concentration of DAA is 9.1 wt% at 30°C and increases to 16.9 wt% at 10°C (Craven, 1963).

DAA is an intermediate product of the aldol condensation of acetone. Many consecutive reactions take place once DAA is formed and lead to other very useful products.

Perhaps the most common chemical manufactured from DAA is methyl isobutyl ketone (MIBK). In 1973, 120,000 tons of MIBK were manufactured in the United States (Papa and Sherman, 1978). By 1992, MIBK production had declined to 97,000 tons

(Braithwaite, 1995). MIBK was identified as a hazardous air pollutant (HAP) in the 1990 US Clean Air Act amendments, which has contributed to this decline.

The reactions involved in producing MIBK from acetone are shown in Figure 2.2.1-1. In the Hibernia Scholven process, shown in Figure 2.2.1-2, a separate reactor is used for each step (Braithwaite, 1995). 'Three-step' processes were the preferred technology until the late 1960's. Since then, MIBK producers have opted for a 'one-step' synthesis of MIBK from acetone and hydrogen due to the lower capital cost. Veba-Chemie introduced a 'one-step' process in 1976 (Papa and Sherman, 1978). The conversion of acetone was reported to be 35% per pass, with 96% selectivity to MIBK, at 135°C and a hydrogen pressure of 6.2 MPa. The catalyst for the 'one-step' process must effect aldolization, dehydration, and hydrogenation. A cation-exchange resin loaded with 0.05 wt% Pd is an example of such a multi-functional catalyst. This process, however, is less selective than 'three-step' processes.

$$\text{Acetone} \underset{293\ \text{K}}{\overset{\text{alkali}}{\rightleftharpoons}} \text{Diacetone Alcohol} \underset{373\ \text{K}}{\overset{\text{acid}}{\rightleftharpoons}} \text{Mesityl Oxide} + H_2 \xrightarrow[423\ \text{K}]{\text{Ni or Cu}} \text{MIBK}$$

Figure 2.2.1-1: The steps involved in the manufacture of MIBK.

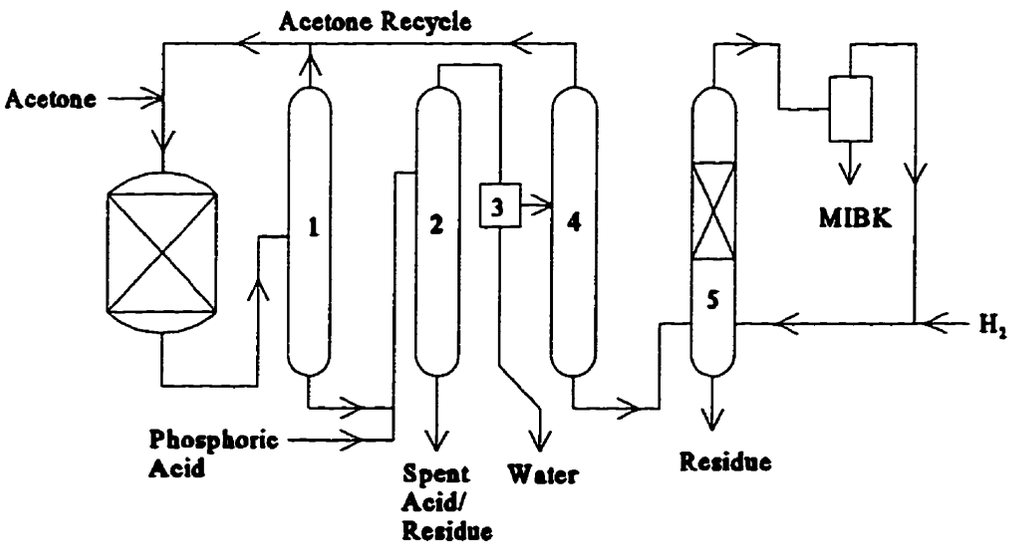

Figure 2.2.1-2: A 'three-step' process for MIBK. (1) - acetone/DAA column, (2) - dehydration, (3) - phase separation, (4) - acetone/MO column, (5) - hydrogenation (Braithwaite, 1995)

Despite the refinements that have been made to the 'one-step' MIBK process, many 'three-step' processes are still in operation since they offer the flexibility of removing diacetone alcohol (DAA) and mesityl oxide (MO) as intermediate products (Braithwaite, 1995).

MO is produced from the dehydration of DAA and, as just described, is an intermediate in MIBK production. MO is also used in the production of methyl isobutyl carbinol and isophorone. The addition of alcohols to MO leads to diacetone alcohol ethers (Lorette, 1958). MO may be produced and consumed on site, but bulk sales in the US ceased in 1986 due to health concerns (Braithwaite, 1995).

DAA has also found a niche as a specialty reaction intermediate. Hydrogenation of the ketone group of DAA leads to hexylene glycol, which is widely used in hydraulic brake fluids. As shown in Figure 2.2.1-3, DAA reacts with *p*-phenetidine to produce 'Santoquin', an antioxidant produced by Monsanto and added to animal feeds (Braithwaite, 1995).

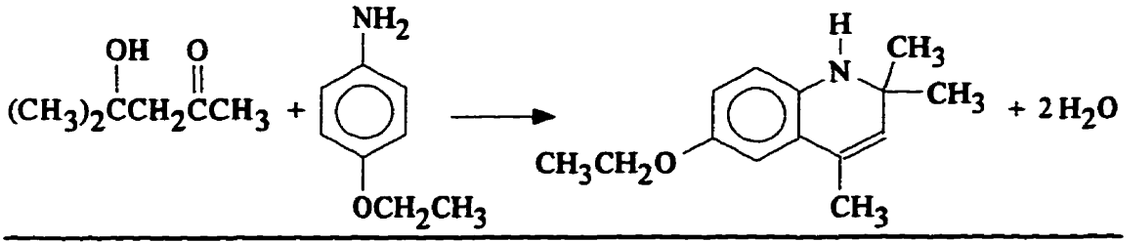

Figure 2.2.1-3: The production of 'Santoquin' from DAA and *p*-phenetidine.

2.2.2 The Reaction Mechanism

Early kinetic studies with this system focus on the decomposition of DAA to acetone, which is the reverse of the reaction that is being considered in this work. Åkerlöf (1926) and French (1929) studied the decomposition of DAA in aqueous solutions using NaOH and KOH catalysts. The effect of adding various salts (ie. NaCl, NaBr, NaI) on the reaction rate was studied. The reaction was reported to be first order with respect to [OH^-] and [DAA] and, in general, the presence of other salts slowed the rate of reaction. The presence of a few salts (involving F^-, CO_3^{2-}, and SO_4^{2-} anions) however, caused the reaction rate to increase.

Åkerlöf (1928) also studied the effect of adding various alcohols to the aqueous solutions, being careful that the catalyst would remain dissolved. He studied the influence of isopropyl, n-propyl, ethyl, and methyl alcohols. All of the alcohols, except isopropyl, caused the reaction rate constant to decrease. Isopropyl alcohol caused the reaction rate constant to increase, but the effect was insignificant below 10 wt% alcohol content.

Murphy (1931) and La Mer and Miller (1935) confirmed that the decomposition of DAA was first order with respect to catalyst concentration and DAA concentration. They also investigated the effect of added salts, and determined that the activation energy was independent of the amount of salt added. An activation energy of 16,000-18,000 cal/mol (67 - 75 kJ/mol) for the decomposition of DAA was reported.

More recent investigations of the aldol condensation of acetone in the forward direction were conducted by Tanabe et al. (Tanabe et. al., 1989; Zhang et. al., 1988) The mechanism of the reaction was investigated using H-D exchange experiments with acetone and acetone-d_6 (Zhang et. al., 1988b). The accepted reaction mechanism for DAA production is provided in Figure 2.2.2-1. It was concluded that steps I and III in the proposed mechanism are both faster than step II. Thus, step II is the rate determining step. It is interesting to note that this same conclusion was reached much earlier by Westheimer and Cohen (1938), but their reasoning was not as clear.

Zhang et. al. (1988) tested the catalytic activity of a variety of metal oxides for the condensation of acetone. It was shown that Mg and Ca oxides were more active than Ba and Sr oxides. When the catalysts were arranged according to their activity per unit surface area, the order became Ba>Sr>Ca>Mg, which is the same order that these metals are found in the periodic table. Temperature Programmed Desorption (TPD) experiments showed that the base strength of the metal oxides follows the same order. Thus, stronger base sites are better able to catalyze the reaction. This seems consistent with the mechanism in Figure 2.2.2-1. A stronger base site should shift step I to the right, giving a higher enolate ion concentration and a proportionally increased rate.

Zhang et. al. (1988) also demonstrated that the active site for the aldol condensation is surface OH^-, and not O^{2-}. Carbon dioxide was used to selectively poison the O^{2-} sites on the

surface. When catalysts were poisoned prior to the reaction, the condensation of acetone was not severely inhibited. Other base catalyzed reactions which require O^{2-} sites, such as butene isomerization, were completely inhibited. The addition of small amounts of water to the surface of the catalyst improved the aldol condensation activity of the catalyst. Water dissociates on the surface generating more hydroxyl sites. Added water also reduced the amount of mesityl oxide formed as a byproduct. The addition of too much water, however, deactivated the catalyst. The amount of water added was measured very carefully.

Tanabe et. al. (1989) studied the addition of many other cations to the MgO catalyst and it was reported that the addition of Na^{+}, Zr^{4+}, and Zn^{2+} (as nitrates) increased the activity of the catalyst. This was attributed to the creation of stronger basic sites on the catalyst surface. Doses of these cations were most effective at concentrations between 0.5-1 wt%. The activity of the catalyst declined after a loading of 1 wt% was exceeded.

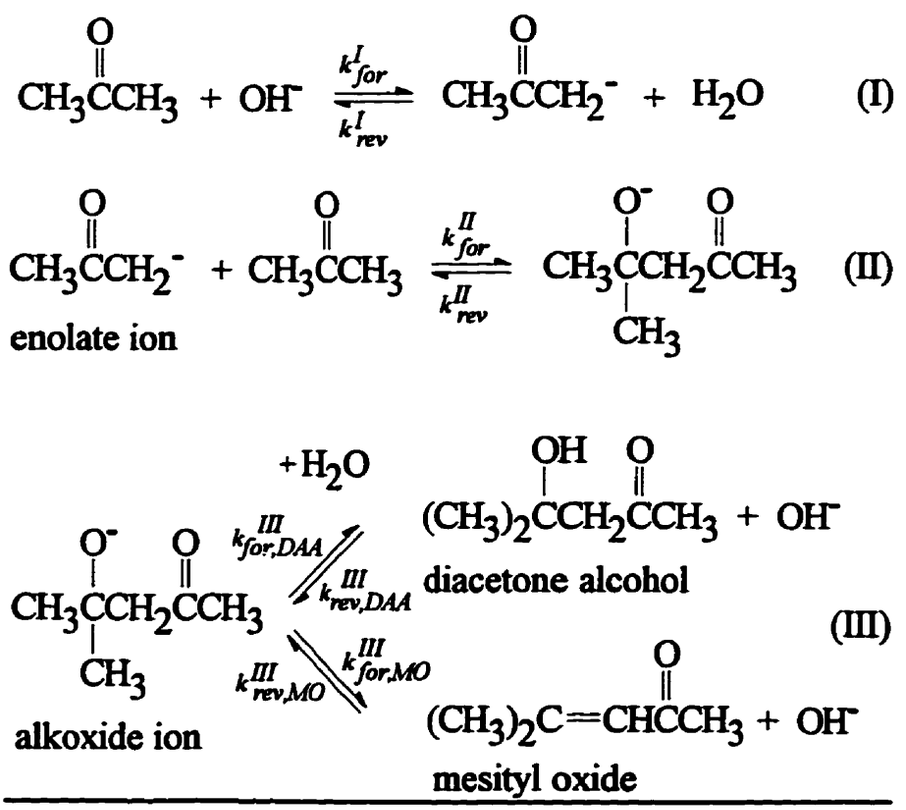

Figure 2.2.2-1: The proposed reaction mechanism for the production of DAA and MO from acetone (forward and reverse rate constants are indicated for each step of the reaction).

While the mechanism of DAA formation has been thoroughly studied and is well understood, the mechanism for the dehydration of MO to DAA is not as clear. The production of MO is shown to proceed through the alkoxide ion in Figure 2.2.2-1. This treatment should be adequate for the kinetic work in Chapter 3 of this thesis, however, another possible pathway exists. A diagram showing two possible routes from DAA to MO is shown in Figure 2.2.2-2. The left side of the diagram shows the production of MO via an alkoxide ion intermediate and the right side of the diagram shows the involvement of an enolate ion intermediate.

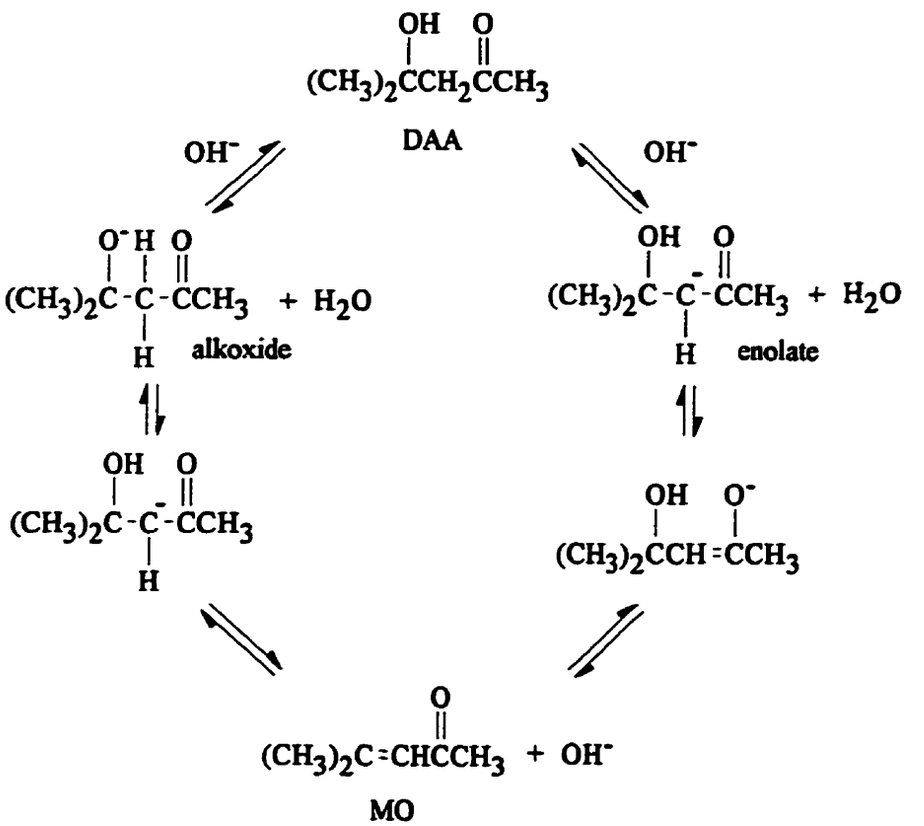

Figure 2.2.2-2: Possible mechanisms for MO production from DAA involving alkoxide and enolate ion intermediates.

2.2.3 Consecutive Reactions

Many reactions can follow the initial formation of DAA. The first is the dehydration of DAA, which leads to MO. The dehydration of DAA is not difficult since the new double bond which forms is in conjugation with the C=O bond and is very stable (March, 1985). This reaction is catalyzed by acids and bases, but acids are more effective and far more selective toward MO formation (Kim and Hatfield, 1985; Paushkin et. al., 1970). For example, the phosphoric acid catalyzed dehydration of DAA to MO causes no regeneration of acetone below 70°C (Kim and Hatfield, 1985). The acid catalyzed dehydration of DAA involves a stable 3° carbonium ion, which accounts for the effectiveness of this route to MO.

Base catalyzed dehydration of DAA is quite slow at the low temperatures commonly encountered in the liquid phase condensation of acetone (ie. 0-20°C). At temperatures greater than 30°C, however, the rate of MO formation increases significantly (Sišul et. al., 1992). The proposed mechanism of the base-catalyzed dehydration of DAA is shown in step III of Figure 2.2.2-1. This was placed on the same diagram to show that DAA and MO are likely produced from a common alkoxide ion intermediate.

At higher temperatures the number of consecutive reactions that can occur increases tremendously. The number of products obtained is further complicated if a heterogeneous catalyst with a combination of basic and acidic sites is used.

Reichle (1980) observed the formation of several products in vapour phase reactions at 300°C over $MgO-Al_2O_3$, $NaOH-Al_2O_3$, and $Li_3PO_4-Al_2O_3$ catalysts. When MO forms, it may condense with another acetone molecule to form phorone (P) and isophorone (IP). The structures of P and IP are shown in Figure 2.2.3-1. IP is a very stable product, and its formation is thought to be irreversible. It is formed in significant quantities at high temperatures. The combination of MO and acetone can also lead to two other compounds (DHD & DHO) which are shown in Figure 2.2.3-2. These compounds are not formed in large quantities and can rearrange to form the stable IP. DHO can undergo a 1,6 self-aldol reaction to form another very stable product called mesitylene. The formation of mesitylene, the structure of which is shown in Figure 2.2.3-2, is also considered to be irreversible.

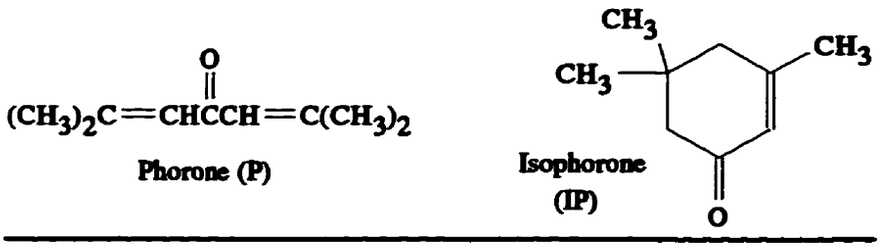

Figure 2.2.3-1: The structures of phorone and isophorone.

Bell and Gold (1983) conducted another investigation with C^{13} NMR to detect reaction products from an alumina catalyst. The reactor was operated at room temperature initially, then the temperature was slowly increased and new compounds were documented as they appeared. At 345 K isophorone was detected, and at 575 K (302°C) mesitylene was detected. This work nicely compliments the earlier work of Reichle (1980).

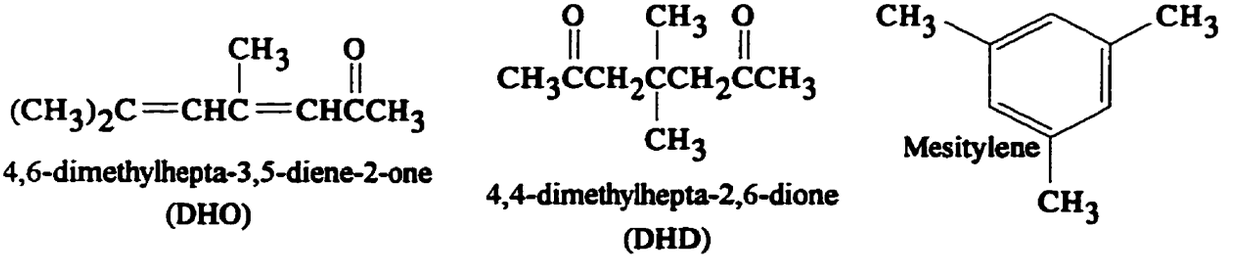

Figure 2.2.3-2: Structures of 4,6-dimethylhepta-3,5-diene-2-one, 4,4-dimethylhepta-2,6-dione, and mesitylene.

Lippert et. al. (1991) made use of the micropulse reactor technique used by Reichle, but directly connected their reactor to a GC-MS system. The reaction was conducted between 200 and 400°C. Metal oxide catalysts were used and the selectivity toward the formation of various products was noted.

The same compounds that were identified in earlier publications were verified, but at temperatures above 300°C some new compounds were found. Above 300°C, IP takes part in reactions that form larger molecules, such as isoxylitones. Another consequence of the higher temperatures is the cracking of DAA on acid sites to yield acetic acid and isobutene. The inclusion of this and other cracking reactions greatly increases its complexity and the variety of products which are possible. A diagram of the many possible reaction pathways is

provided in Figure 2.2.3-3.

The reaction scheme presented in Figure 2.2.3-3 is quite complicated. Fortunately, at the mild temperatures used for this work (liquid phase at 56°C), we anticipate that the only major byproduct should be MO.

2.2.4 Reaction Kinetics and Equilibrium

The reverse reaction, or the decomposition of DAA to acetone, is accompanied by a small increase in volume. Early kinetic studies relied on the measurement of this volume change to track the progress of the reaction (Åkerlöf, 1926). Due to the unfavourable reaction equilibrium, this technique could not be used to measure reaction rates in the forward direction. However, the reverse rate constant and the equilibrium constant can be used to calculate the value of the forward rate constant. Although this approach is valid, we will endeavour to directly determine forward rate constants. Based on the reaction mechanism shown in Figure 2.2.2-1, one would postulate that the forward reaction should be second order with respect to acetone.

Maple and Allerhand (1987) directly measured the reaction rate in the forward direction. One volume of 0.1 M NaOH was added to 20 volumes of a 4:1 (by volume) mixture of acetone and cyclohexane-d_{12}. Using NMR, the concentration of DAA was measured as a function of time. The data were fitted to a kinetic model and the values for the rate constant and the equilibrium constant were determined. The concentration of acetone and diacetone alcohol were 9.3 M and 0.49 M, respectively, at equilibrium. The value of the forward rate constant was reported to be $.12 \times 10^{-4}$ M^{-1} min^{-1} at room temperature. This work verifies that the reaction is second order with respect to acetone. Another interesting observation was the detection of 0.01% DAA in "pure" acetone. The formation of such small amounts of DAA could be catalyzed by trace impurities dissolved in the acetone or by hydroxyl groups on the glass container.

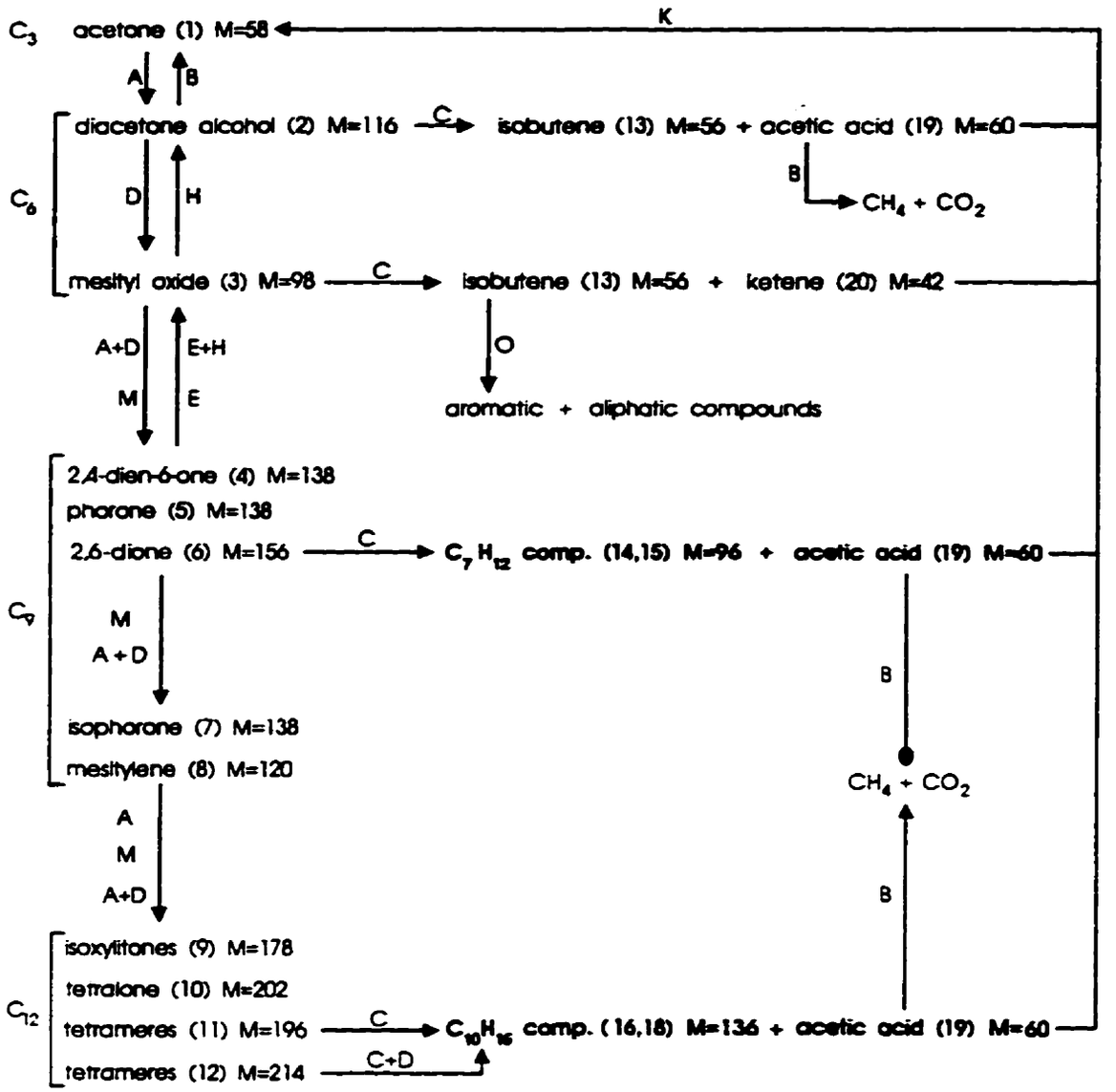

Figure 2.2.3-3: Diagram of the possible reactions of acetone over catalysts with acid-base properties. Taken from Lippert et. al., 1991. Reprinted, with permission, from the *Journal of Molecular Catalysis.* © Elsevier Sequoia, 1991.

A - aldol addition	B - breaking (cleavage)	C - cracking
D - dehydration	E - elimination	H - hydration
K - ketonization	M - Michael addition	O - oligomerization

Craven (1963) reported the equilibrium conversion of acetone at various temperatures. Table 2.2.4-I shows the equilibrium conversion (in wt%) of acetone to DAA, along with equilibrium constants calculated from the conversion data. The equilibrium conversion of acetone increases, but the rate of reaction decreases, as the reaction temperature decreases. The reaction rate becomes very slow below 0°C, and Craven advises caution in using his data below this temperature since the slow reaction rates may have caused errors in his experimental results.

Table 2.2.4-I: Equilibrium conversions of acetone at various temperatures.

Temp. (°C)	54	45	32.5	30[a]	20[a]	10[a]	0[a]	-10[a]	-20[a]
Conv. (wt%)	4.3	5.5	7.7	9.1	12.1	16.9	23.1	25.6	27.3
K_{EQ} (M^{-1})	.0019	.0024	.0035	.0040	.0056	.0086	.0135	.0157	.0173

[a]data taken from Craven (1963)

Figure 2.2.4-1 shows a plot of $\ln(K_{EQ})$ vs. 1/T based on the data in Table 2.2.4-I. A straight line fits the data obtained above 0°C, and agrees with the data determined in this research. The slope of this line yields the heat of reaction. Craven (1963) estimated ΔH_R = -3.5 kcal per mol of acetone condensed (-29.3 kJ/mol DAA). This is quite close to Davis and Burrows' (1936) result of ΔH_R= -8190 cal per mol of DAA (-34.2 kJ/mol DAA). Combining our data and Craven's (1963) data, the result is ΔH_R= -27.35 kJ/mol.

An attempt was made to calculate the heat of reaction at 56°C based on thermochemical data provided by Daubert and Danner (1989) (see Appendix A for details). The attempt gave a very poor result of ΔH_R= -97 kJ/mol of DAA. This prediction is roughly 3.5 times higher than the measured value. This problem is not unique, however, and was previously encountered by Davis and Burrows (1936). Their attempt to calculate the heat of reaction at 25°C gave ΔH_R= +6100 cal/mol (+25.5 kJ/mol). This result predicts that the reaction is endothermic! Davis and Burrows speculated on the source of the problem:

> 'Here as frequently the thermochemical calculation involves the inaccuracy inherent in a small difference between large quantities.'

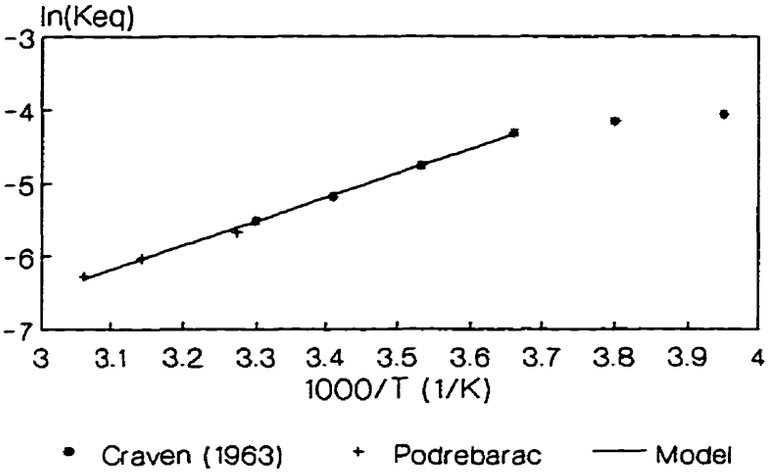

Figure 2.2.4-1: Plot of $\ln(K_{EQ})$ vs. 1/T to determine the heat of reaction.

The heats of formation of acetone and DAA are, indeed, large quantities. The heat of formation of acetone is known within ±1%, but the ideal gas heat of formation of DAA was *predicted* to be -546 kJ/mol, and has an expected accuracy of ±10% (Daubert and Danner, 1989). Clearly, we cannot expect a good prediction of the heat of reaction.

The activation energy of the forward reaction was reported in the literature. Watanabe and Seto (1991) calculated an activation energy of 70 kJ/mol with iron oxide catalysts, and their experimental procedures seem quite reliable. Slow reaction rates were observed over the iron catalysts, which makes it likely that diffusion did not influence the results. Samples were analysed by gas chromatography, which is considered more reliable than optical or density techniques.

The enthalpy of reaction for the dehydration of DAA to MO was also calculated in Appendix A, with a prediction of ΔH_R =+70.2 kJ/mol. Kim and Hatfield (1985) agree that this reaction is endothermic, but the value of ΔH_R obtained from their equilibrium data is +25 kJ/mol. Kim and Hatfield (1985) also report an activation energy of 78.3 kJ/mol for this reaction with homogeneous phosphoric acid.

2.2.5 Reactor Studies

Godet (1959) was issued a patent for the production of DAA in a tubular flow reactor. A heterogeneous catalyst that consisted of solid NaOH supported on asbestos was used. Acetone flowed through the 3 cm diameter x 4 m reactor at 18°C and a flow rate of 7 L/h. It was reported that there was a maximum in conversion with respect to distance along the reactor. Godet rationalized that this was due to the exothermic nature of the reaction. As conversion increases, the temperature of the product increases and the equilibrium conversion decreases. Thus, a point is reached where the amount of DAA formed slightly exceeds the equilibrium amount and the decomposition reaction begins to dominate. The optimal length of the reactor was found to be 60 cm, at which point the temperature is 23°C and the conversion is 11 wt%. This equilibrium composition is consistent with the data reported by Craven (1963).

Rao et al. studied the formation of DAA in a batch reactor (1966) and a trickle bed reactor (1967) using a heterogeneous $Ba(OH)_2$-Na_2SiO_3 (4:1 ratio by mass) catalyst. The effects of varying the catalyst concentration, the temperature, the stir speed, and the reaction time were studied in a batch reactor. The reaction was fast at 27°C, however, their reported equilibrium conversion of acetone (12.7 wt%) is higher than that reported by Craven. This discrepancy is likely due to inaccuracies in the optical analysis technique (refractive index) that was used. Trace amounts of catalyst particles or small amounts of MO can corrupt optically determined concentrations.

In the trickle bed study by Rao et. al. (1967), it was stated that elevated pressure is required to form DAA at temperatures above 40°C. The basis for making this statement was not clear. Also, after indicating that the reaction is <u>not</u> diffusion controlled, an activation energy of only 2700 cal/mol (11.3 kJ/mol) was reported. This is much lower than the value of 70 kJ/mol reported by Watanabe and Seto (1991), which indicates that the reaction studied by Rao et. al. (1967) actually was diffusion controlled.

Ray and Ghosh (1972) conducted experiments to determine reaction rate constants under conditions of very little solvent. In a batch reactor, 80 g of acetone and 1 or 2 mL of

strong aqueous NaOH were mixed together. These results are difficult to interpret since NaOH is not soluble in pure acetone. Of value, however, are the results of tests conducted to determine the densities of pure acetone, pure DAA, and mixtures of acetone and DAA. It was found that these two compounds follow ideal mixing laws.

Sišul et. al. (1992, 1991, 1989) published a series of papers describing the production of DAA and MO with strongly basic anion exchange resin catalysts. In the earliest study, a mixture of DAA and acetone was boiled and the overhead vapour (consisting mainly of acetone) was condensed and passed through a temperature-controlled bed of anion exchange resin. The composition of the liquid in the boiling flask was measured as a function of time. After approximately 8 hours of operation, the composition of DAA reached a maximum value of 70-80 wt% and remained constant. They also compared the optical (refractive index) and GC analysis techniques, and found the optical technique to be rather inaccurate. It was demonstrated that anion exchange resins are very active, and they were tested at temperatures up to 50°C.

A similar reactor setup was used to examine the catalyst lifetime (Sišul et. al., 1991). Rather than boiling the liquid, however, a pump was used to recirculate a controlled flow of liquid through the resin. Each batch of catalyst was used for 5 days. At temperatures up to 30°C, it was reported that the yield of DAA declined by approximately 6% per day.

The formation of MO was also observed (Sišul et. al., 1992). MO production was most significant when the reaction temperature exceeded 30°C. After 12 h of operation of the same apparatus described in 1991, the ratio of DAA:MO (mass ratio) in the collection flask was 4:1 when the reactor was at 50°C and was 16.5:1 when the reactor was at 30°C. Although the studies by Sišul et. al. (1992, 1991, 1989) provide some useful guidelines and demonstrate that anion exchange resins are effective catalysts, many important details were missing from the experimental sections of these publications. Thus, catalyst activities could not be calculated.

The production of DAA is relatively simple. As reported in Section 2.2.1, the usual production technique is to pass acetone through a tubular reactor at 10-20°C. With such a simple procedure, it is surprising to find many reactor studies of dubious quality.

-3-

PHASE II - REACTION KINETICS AND MASS TRANSFER

3.1 Batch Kinetics

Kinetic studies of the aldol condensation of acetone were conducted in a batch reactor. The temperature used for most of these reactions was 54°C. This temperature was selected since it is very close to the boiling point of acetone (56°C) but will not cause excessive evaporative losses of acetone during the experiments.

A batch reactor was selected because of its simple operating procedure. Kinetics can be studied by removing small samples from the reactor at various times and fitting the concentration data to a kinetic model. Another benefit of using a batch reactor is that the liquid and the catalyst can be very well mixed. This eliminates the possibility of mass transfer between the liquid and outer catalyst surface, or 'external mass transfer', controlling the rate of the reaction. Although one must experimentally verify that external mass transfer is not a problem, it is easier to avoid in batch reactors than in fixed bed flow reactors.

3.1.1 Kinetic Equations

In order to determine rate constants, a kinetic model must be fitted to the experimental data. In this section, a kinetic model for the aldol condensation of acetone is developed.

The reaction mechanism in Figure 2.2.2-1 shows the elementary steps involved in the production of DAA. Steps I and III were reported to be faster than step II. This leaves step II as the 'rate determining step' for the production of DAA. At our reaction conditions, MO production is much slower than DAA production. If we assume MO production is negligible, equation (3.1) can be used to describe the rate of DAA production.

$$\frac{d[DAA]}{dt} = -\frac{1}{2}\frac{d[Ac]}{dt} = k_{for}^{II}[Ac][enolate\ ion] - k_{rev}^{II}[alkoxide\ ion] \qquad (3.1)$$

Since steps I and III are both faster than step II, we may assume that steps I and III are at equilibrium. This allows the substitution of equilibrium expressions for the concentrations of the ionic intermediates in (3.1). With these substitutions, we arrive at equation (3.2).

$$\frac{d[DAA]}{dt} = k_{for}^{II}[Ac]\left(\frac{K_{EQ}^{I}[Ac][OH^-]}{[H_2O]}\right) - k_{rev}^{II}\left(\frac{[DAA][OH^-]}{K_{EQ}^{III}[H_2O]}\right) \qquad (3.2)$$

In equation (3.2), the second order dependence of the rate on acetone concentration, [Ac], and the first order dependence of the rate on DAA concentration and catalyst concentration are evident. This is in agreement with the data presented in Section 2.2. There is also an inverse dependence of the reaction rate on water concentration. Clearly, water will play an important role in this reaction system.

The equation can be simplified by grouping terms which remain essentially constant during the reaction (ie. $[H_2O]$, $[OH^-]$). New constants, k_1 and k_{-1}, are used in the simplified equation. Thus, the rate constants and equilibrium constants for each elementary step of the mechanism do not need to be individually determined. The simplified equation is shown in (3.3).

$$\frac{d[DAA]}{dt} = k_1[Ac]^2 - k_{-1}[DAA]$$

$$where:\ k_1 = \frac{k_{for}^{II}K_{EQ}^{I}[OH^-]}{[H_2O]};\quad k_{-1} = \frac{k_{rev}^{II}[OH^-]}{K_{EQ}^{III}[H_2O]};\quad K_{EQ} = \frac{k_1}{k_{-1}} = \frac{[DAA]_{EQ}}{[Ac]_{EQ}^2} \qquad (3.3)$$

$$K_{EQ}^{I} = \frac{[enolate\ ion]_{EQ}[H_2O]_{EQ}}{[Ac]_{EQ}[OH^-]_{EQ}};\quad K_{EQ}^{III} = \frac{[DAA]_{EQ}[OH^-]_{EQ}}{[alkoxide\ ion]_{EQ}[H_2O]_{EQ}}$$

Equation (3.3) shows the basic differential equation from which the final rate model will emerge. In equation (3.3), k_{-1} can be expressed in terms of k_1 and K_{EQ}. This reaction is strongly limited by equilibrium and the conversion of acetone will always be small. We can assume, therefore, that the system has a constant volume. This allows us to replace the term [Ac] with ($[Ac]_O$ - 2[DAA]), where $[Ac]_O$ is the initial concentration of acetone in the reactor, and [DAA] is the concentration of DAA at any time. These substitutions are shown in equation (3.4).

$$\frac{d[DAA]}{dt} = k_1 \left([Ac]_O - 2[DAA]\right)^2 - k_1 \frac{[Ac]_{EQ}^2}{[DAA]_{EQ}} [DAA] \qquad (3.4)$$

The above expression can be rearranged to separate the time and DAA concentration variables, and integrated. Although the expression looks somewhat intimidating, an analytical solution is available (Spiegel, 1968). After stipulating that [DAA] = 0 at t=0, the solution can be simplified to a more manageable form. The final form is shown as equation (3.5).

$$[DAA] = \frac{[Ac]_O^2 \, [DAA]_{EQ} \, (1 - e^{\kappa})}{4[DAA]_{EQ}^2 - [Ac]_O^2 \, e^{\kappa}}$$

$$\textit{where:} \quad \kappa = \frac{[Ac]_O^2 - 4[DAA]_{EQ}^2}{[DAA]_{EQ}} k_1 t \qquad (3.5)$$

This equation was previously used by Maple and Allerhand (1987), and is utilized in Section 3.1.3 to determine values of k_1 from experimental data. Although this model can be linearized, it is preferable to obtain k_1 values from non-linear regression. The SYSTAT† statistical software package was used to fit this model to the experimental data.

It is important to recall that the production of mesityl oxide (MO) was ignored in the development of equation (3.5). Since the rate of MO production is much slower than DAA

---

†SYSTAT for DOS personal computers. ©1990, SYSTAT, Inc.

production at our reaction conditions, this should not introduce significant errors.

We should now like to develop an expression for the rate of MO production. MO is produced via the dehydration of DAA. For the purposes of this work, we will assume that MO is produced according to the mechanism in Figure 2.2.2-1. The literature indicates that step III for the formation of DAA is a fast reaction (Zhang et. al., 1988b). Therefore, the rate determining step for MO production is likely step III, or the decomposition of the alkoxide ion. The basic differential equation describing the rate of MO production is shown in (3.6).

$$\frac{d[MO]}{dt} = k^{III}_{for,\,MO}\,[alkoxide\ ion] - k^{III}_{rev,\,MO}\,[MO][OH^-] \qquad (3.6)$$

Since equilibrium between DAA and the alkoxide ion in step III is rapidly established, one can substitute this equilibrium relationship in place of the alkoxide ion concentration in equation (3.6).

$$\frac{d[MO]}{dt} = k^{III}_{for,\,MO}\left(\frac{[DAA][OH^-]}{K^{III}_{EQ}\,[H_2O]}\right) - k^{III}_{rev,\,MO}[MO][OH^-] \qquad (3.7)$$

The form of equation (3.7) is quite interesting. The forward rate of MO formation is first order with respect to [DAA] and catalyst concentration and inversely related to the water concentration. It appears that the presence of water will play an important role in this reaction as well.

The formation of MO is reversible, but slow at our conditions. The equilibrium concentration of MO is also quite high. At 56°C, the equilibrium ratio of [MO]:[DAA] should be approximately 2.5 (Kim and Hatfield, 1985). As will be shown, MO:DAA ratios at the end of batch experiments remain very much lower than this value. For this reason, the reverse reaction can be neglected in the kinetic expression. This equation can also be simplified by grouping terms which remain constant. The water concentration will be considered as a constant since the amount produced is small. With these modifications, the overall expression takes the form of equation (3.8).

$$\frac{d[MO]}{dt} = k_{MO}[DAA] \;, \quad where \quad k_{MO} = \frac{k^{III}_{for,MO}[OH^-]}{K^{III}_{EQ}[H_2O]}$$

$$k_2 = \frac{d[MO]}{dt} = k_{MO}[DAA]_{EQ} \tag{3.8}$$

Equation (3.8) shows that the rate of production of MO should depend on [DAA] so long as catalyst and water concentrations are held constant. Substituting equation (3.5) into (3.8) to replace [DAA] would give a rather complicated expression. It is more convenient to realize that after some time the equilibrium between acetone and DAA is established, and that [DAA] will remain constant after this time. After the equilibrium concentration ($[DAA]_{EQ}$) is reached, therefore, a plot of [MO] vs. time should yield a straight line with a slope of k_2. The value of k_2 can be easily obtained from a linear regression of the kinetic data. In fact, k_2 proved to be very useful in this kinetic work and k_{MO} was seldom used.

The previous equations treat the catalyst as if it were homogeneous, or dissolved in the solution. It is well known, however, that when a chemical reaction process occurs within a porous particle its behaviour may deviate appreciably from true chemical kinetics. For example, the *intrinsic* reaction rate may follow a first order rate law, $-dC/dt = kC$, where C is the reactant concentration. However, the *observed* rate may not equal kC_O, where C_O is the reactant concentration external to the catalyst pellet. This situation can arise if mass transfer resistance creates an appreciable concentration drop within the pellet.

Ernest Thiele was the first to develop a convenient expression describing the effect of pore diffusion in heterogeneous catalysis. Wheeler (1951) expanded on his work in a classic and comprehensive treatise entitled "Reaction Rates and Selectivity in Catalyst Pores". These reaction/diffusion equations provide important background and will be presented here. For a more detailed discussion, however, one of the references by Wheeler (1951), Levenspiel (1972) or Satterfield (1981) should be consulted. It should also be mentioned that the following analysis is for <u>isothermal</u> reactions. The non-isothermal case has been examined (Weisz and Hicks, 1962) and is also covered in the texts by Levenspiel (1972) and Satterfield (1981).

Figure 3.1.1-1 shows an idealized cylindrical catalyst pore. The irreversible decomposition of compound A occurs at the pore wall. The rate of disappearance of A (mol/s) within the differential slice is given by $k^*_S C_A^n (2\pi r)dx$, where k^*_S is the intrinsic reaction rate constant *per* unit catalyst surface area, and n is the order of the reaction.

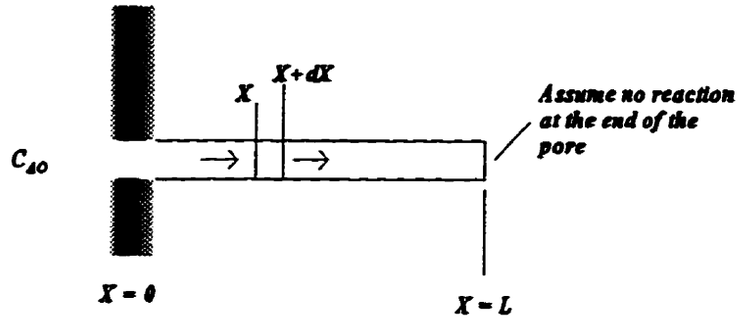

Figure 3.1.1-1: Idealized model of a cylindrical catalyst pore.

The diffusive flux of A is proportional to the concentration gradient of A at any point along the pore. It is assumed that the diffusion coefficient D is constant. The basic differential equation and boundary conditions that describe this situation are shown in (3.9).

$$\frac{d^2C_A}{dx^2} - \frac{2k_S^*}{Dr} C_A^n = 0$$

$$at\ x = 0,\ C_A = C_{AO} \qquad (3.9)$$

$$at\ x = L,\ \frac{dC_A}{dx} = 0$$

The solution to this equation defines the concentration of A as a function of position in the pore. For a first order reaction (ie. n=1), an analytical solution to (3.9) is possible. The solution is shown in equation (3.10). In developing the solution, it is convenient to gather the constants together into a dimensionless group. This group, given the symbol h_L by Wheeler (or 'mL' by Levenspiel, or 'ϕ' by Satterfield), is called the Thiele modulus and is widely used in heterogeneous reaction kinetics.

$$\frac{C_A}{C_{AO}} = \frac{\cosh\left[h_L\left(1 - \frac{x}{L}\right)\right]}{\cosh(h_L)}, \quad \textit{where: } h_L = L\sqrt{\frac{2k_S^*}{Dr}} \tag{3.10}$$

It should be clear that equation (3.10) is a concentration profile and does not directly provide a reaction rate. However, the overall rate of reaction equals the rate at which the reactant A diffuses into the mouth of the pore. Determining the rate of diffusion at x=0 involves taking the derivative of (3.10) and this is shown in (3.11).

$$Rate = -\pi r^2 D\left[\frac{dC_A}{dx}\right]_{x=0} = \pi r^2 D\,\frac{h_L\,C_{AO}}{L}\tanh(h_L) \tag{3.11}$$

The *effectiveness factor* (η) is defined as the ratio of the reaction rate with pore diffusion to a hypothetical rate without pore diffusion. In the absence of diffusion, the reaction rate in the pore would be $2\pi rLk^*_sC_{AO}$. Dividing (3.11) by this hypothetical rate gives the analytical expression for η.

$$\eta = \frac{1}{L^2}\left(\frac{rD}{2k_S^*}\right) h_L \tanh(h_L) = \frac{1}{h_L}\tanh(h_L) \tag{3.12}$$

The form of equation (3.12) is sensitive to the catalyst geometry. For this research, it is also convenient to consider the case of a spherical catalyst particle. Following the same basic approach, Satterfield (1981) developed an expression for η for a first order irreversible reaction which is shown in (3.13).

$$\eta = \frac{3}{h_S}\left[\frac{1}{\tanh(h_S)} - \frac{1}{h_S}\right] \qquad \textit{where} \quad h_S = R\sqrt{\frac{k_V^*}{D_{eff}}} \tag{3.13}$$

Satterfield's definition of the Thiele modulus is similar to, but slightly more practical than, the definition for a single catalyst pore. In this definition of the Thiele modulus (h_S), k^*_V is the rate constant per gross volume of the catalyst pellet, D_{eff} is the effective overall diffusion coefficient, and R is the radius of the catalytic sphere. A plot of the effectiveness factor for spherical particles (equation 3.13) and for a flat plate-shaped catalyst (equation 3.12) is shown in Figure 3.1.1-2.

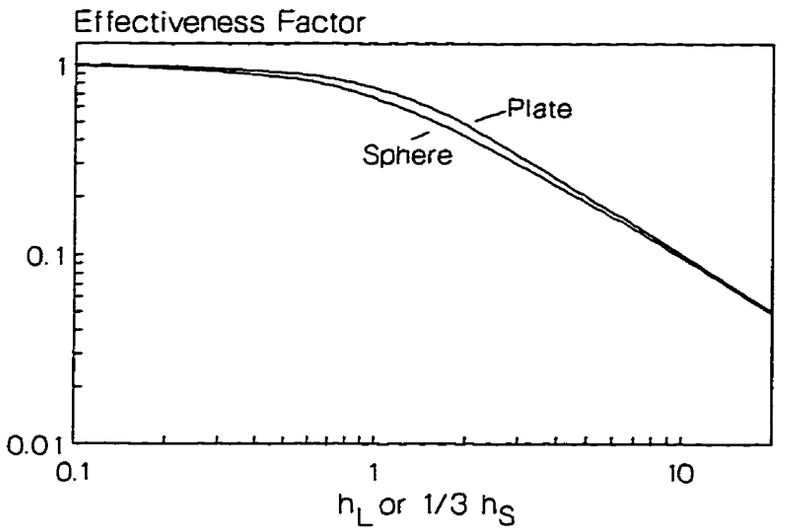

Figure 3.1.1-2: Effectiveness factors as a function of Thiele moduli for spherical catalyst particles and flat particles.

Some important trends are obvious from this graph. Firstly, the effectiveness factor approaches unity as the radius of the particle decreases. Therefore, smaller catalyst particles are used more efficiently. Secondly, very active catalysts (large rate constants) tend to have low effectiveness factors. These are important considerations when catalysts are being 'designed' for a specific application and/or efficient use of a very expensive catalyst is required. Another interesting feature is the similar shapes of the curves, despite the differences in geometry. Thus, one can often use data from a simple geometry to describe a more complicated geometry without introducing excessive errors.

Determining effectiveness factors is not a simple task. Although it is possible to

measure the pore sizes and surface area of catalysts, determining D_{eff} is often difficult. Problems with determining D_{eff} are further compounded if the reaction takes place at extreme conditions of temperature and pressure. Fortunately, methods are available to determine effectiveness factors from experimental rate data (Satterfield, 1981; Smith and Amundson, 1951).

To this point, the discussion has focused on the fact that pore diffusion slows down the rate of a reaction. Another important aspect of pore diffusion, especially for this research, is its impact on product selectivity. Wheeler (1951) derived equations for the consecutive reactions A→B→C occurring in a single pore (Figure 3.1.1-1), where both reactions are first order and irreversible and both compounds have the same diffusion coefficient. Østergaard (1961) later extended this analysis to an infinite series of consecutive reactions (A→B→C→...).

The results of Wheeler's analysis show that the concentration profile of A is unaffected by the consecutive reaction, and is described by equation (3.10). A new differential equation was developed for the concentration profile of B, however, and its solution is shown below.

$$\frac{C_B}{C_{BO}} = \left(1 + \frac{C_{AO}}{C_{BO}}\,\frac{S}{S-1}\right)\frac{\cosh\left[\frac{h_L}{\sqrt{S}}\left(1-\frac{x}{L}\right)\right]}{\cosh\left[\frac{h_L}{\sqrt{S}}\right]} - \frac{C_{AO}}{C_{BO}}\,\frac{S}{S-1}\,\frac{\cosh\left[h_L\left(1-\frac{x}{L}\right)\right]}{\cosh[h_L]} \qquad (3.14)$$

$$S = \frac{k^{*}_{S,A}}{k^{*}_{S,B}} \qquad h_L = L\sqrt{\frac{2k^{*}_{S,A}}{rD}}$$

In equation (3.14), the selectivity ratio (S) is defined as the ratio of the intrinsic first order rate constants for the disappearance of A and B. In his theoretical analysis, Wheeler (1951) compared the selectivity of a catalyst with large pores ($h_L < 0.1$) and small pores ($h_L > 5$) for

the case S=4. The findings of this comparison are shown in Figure 3.1.1-3. In this figure, it is clear that diffusion in the small-pore catalyst significantly reduces the selectivity toward the intermediate product B.

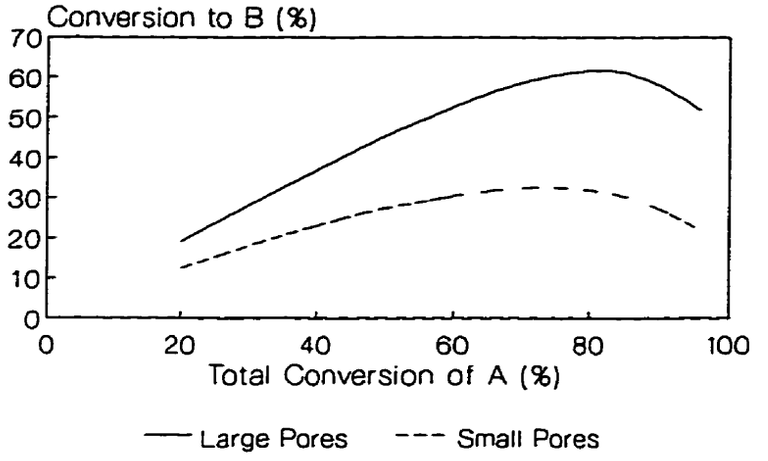

Figure 3.1.1-3: The influence of pore diffusion on the observed product selectivity (Wheeler, 1951).

The selectivity of consecutive reactions is significantly altered by pore diffusion. In addition to this, other phenomena occur when pore diffusion controls a reaction rate. When $h_L \geq 5$, the expression for η in (3.12) can be approximated by $\eta = 1/h_L$ (Levenspiel, 1972). This changes the rate expression, as shown in (3.15).

$$\textit{Observed rate}\left[\frac{mol}{m^2\,s}\right] = k_S^{\cdot}\,C_{AO}\,\eta = \frac{k_S^{\cdot}\,C_{AO}}{h_L} = \frac{1}{L}\sqrt{\frac{k_S^{\cdot}\,r D}{2}}\,C_{AO} \qquad (3.15)$$

In equation (3.15), the observed reaction rate is proportional to the root of the rate constant. It follows that the observed activation energy may only be ½ of the intrinsic value. Pore diffusion can also change the observed order of a reaction from n (intrinsic kinetics) to (n+1)/2. First order reactions remain first order, but others are affected.

Recently, Gottifredi et. al. (1994) published general equations which can describe the reaction $\alpha A \leftrightarrow B \rightarrow$ products, where 'α' is a stoichiometric coefficient and all reactions are first order. If we consider that 'A' is acetone, 'B' is DAA, 'products' are MO and water, and α=2, this hypothetical system bears a striking familiarity. Gottifredi et. al. (1994) set up dimensionless mass conservation equations for three particle shapes having a characteristic length L. For spherical particles, the characteristic length is L = Radius/3 (Levenspiel, 1972). Equations for the concentration profiles of A and B are given in equation (3.16), and variable definitions are available in the Nomenclature section of this thesis.

$$C_A = (1-\lambda X^0)\,\frac{\cosh(\epsilon h_L x)}{\cosh(\epsilon h_L)} - \lambda X^0\,\frac{\cosh(\beta^{1/2} h_L x)}{\cosh(\beta^{1/2} h_L)}$$

$$C_B = X^0\,\frac{\cosh(\beta^{1/2} h_L x)}{\cosh(\beta^{1/2} h_L)} - \Gamma C_A$$

$$X^0 = \Gamma + C_{B0}\ ;\quad \epsilon^2 = (1+w+p-\beta)\ ;\quad \lambda = p/(\beta-\epsilon^2) \qquad (3.16)$$

$$\beta = 1/2[(1+w+p)-(1-p-w)\delta]\ ;\quad \delta = \sqrt{1+\frac{4p}{(1-p-w)^2}}\ ;\quad \Gamma = \frac{\gamma}{p}(w+p-\beta)$$

$$h_L^2 = L^2\frac{k^*_{V,A}}{D_{A,eff}}\ ;\quad w = \frac{k^*_{V,B} D_{A,eff}}{k^*_{V,A} D_{B,eff}}\ ;\quad \gamma = \frac{1}{\alpha}\,\frac{D_{A,eff}}{D_{B,eff}}\ ;\quad p = \frac{\gamma}{K_{EQ}}$$

Equation (3.16) is an unwieldy collection of equations and constants, but the entire problem hinges on just a few parameters. These parameters are the diffusion coefficients for A and B, the equilibrium constant for the first reaction (K_{EQ}), the size of the catalyst particle (L), and the intrinsic forward rate constants for the disappearance of A and B ($k^*_{V,A}$ and $k^*_{V,B}$ respectively). Recall that these rate constants are based on the gross catalyst volume. With reasonable estimates of these parameters, this solution should adequately represent the behaviour of the Acetone-DAA-MO system.

As mentioned, equation (3.16) is dimensionless. The space coordinate 'x' is the radial

position over the total radius ($x = r/R$). The concentrations of A and B are normalized with respect to the concentration of A at the surface of the catalyst (at $x = 1$) to make them dimensionless. Therefore, at the outer surface of the catalyst, C_A always equals 1. The surface concentration of B (C_{B0}) must be specified, and must be normalized with respect to the surface A concentration.

It has been demonstrated that an effectiveness factor (η) can correct intrinsic reaction rates that are influenced by diffusion. Although Gottifredi et. al. (1994) proceeded to develop an expression for the effectiveness factor based on equation (3.16), the size and complexity of this expression makes its application unrealistic. In addition, the value of η in a batch reactor is time dependent. It is clearly not practical to alter the rate equations derived in (3.5) and (3.8) to take into account the effects of pore diffusion. It should be clearly understood, therefore, that the experimental rate constants determined from (3.5) and (3.8) are *observed* rate constants, which will undoubtedly be quite different from *intrinsic* rate constants.

3.1.2 Experimental Procedure for Batch Reactions

ACS Reagent grade acetone was purchased from BDH (Toronto). The acetone was batch distilled at atmospheric pressure before use, and typically contained 0.4 wt% water. DAA, MO, isophorone, and phorone were obtained from Aldrich Chemical Co. (Milwaukee). Amberlite IRA-900 anion exchange resin was also purchased from Aldrich Chemical Co. (Milwaukee). This macroreticular resin was used as the catalyst for the reaction. Some of the properties of Amberlite IRA-900 are presented in Table 3.1.2-I.

One general concern about the use of anion exchange resins as catalysts is their limited thermal stability. As shown in Table 3.1.2-I, the thermal limit for IRA-900 is only 60°C. The maximum temperature that will be considered in this work is 56°C (the normal boiling point of acetone). At temperatures exceeding the 60°C limit, however, it is suspected that an elimination reaction takes place, with $N(CH_3)_3$ leaving the resin (March, 1985).

Table 3.1.2-I: Properties of IRA-900 Ion Exchange Resin

Functional Group[a]	$-N^+(CH_3)_3\ X^-$
Effective Size[b]	0.53 mm
Uniformity Coefficient[b]	1.8
Surface Area[a]	27 m^2/g
Porosity[a]	0.27 mL/mL
Exchange Capacity[a]	4.4 meq/g
Max. Temperature[b] (hydroxide form)	60°C

[a] taken from Tanabe (1989)
[b] taken from Rohm and Haas Company (1991)

The resin catalyst is supplied in the chloride form. In order to activate the resin, it was usually soaked in 0.8 M - 1.5 M NaOH (BDH, Toronto) to exchange some of the Cl^- for OH^-. A fairly strong NaOH solution is required since OH^- is the least favoured replacing ion for strongly basic resins (Kunin, 1972b). Consequently, the water used to wash the resin must be very pure in order to avoid deactivating the catalytic sites. Accordingly, water was treated by a Millipore Milli-Q purification system before use.

The time allowed for the exchange is also important. Most catalyst samples were exchanged for 3 h, but a few were left in the basic solution overnight and were exchanged for 24 h. The effect of 'exchange time' will be discussed in Section 3.1.3. Following the exchange, the resin was washed with water until phenolphthalein indicated that all excess NaOH had been removed.

In order to determine the OH^- loading of the freshly prepared catalysts, samples of the resin were neutralized with acid. The procedure for this determination follows:

- 2 mL of resin (in water) was transferred into a fritted glass filter funnel.
- 30 mL of 0.1 N HCl was slowly passed over the resin, and the acid was collected.
- the resin was washed slowly with 60 mL of deionized water and the wash water was also collected.

- using phenolphthalein as an indicator, the wash water/acid mixture was titrated with 0.1 N NaOH

In this procedure the amount of acid passed through the resin is known, and the amount of acid collected is known. The difference between these values represents the amount of basicity contained within 2 mL of the resin.

It is important to realize that the volume of a given mass of IRA-900 resin can change depending upon its anionic form and the solvent in which it is immersed. Volumes of resin in the OH^- form were compared in water, isopropanol, and acetone. The volume of resin in water is 1.29 times larger than the volume in isopropanol, and the volume in propanol is 1.12 times larger than the volume in acetone. The volume changes were also shown to be reversible. Throughout this thesis, reported volumes of resin catalyst are measured in water, unless otherwise indicated.

The surface area, pore size distribution, and pore volume of the resin catalyst were determined using an Autosorb-1 instrument from Quantachrome. Samples were washed in ACS grade isopropanol (BDH, Toronto), then pretreated under vacuum before the analysis. The pretreatment procedure for the samples will be specified as these data are reported.

Batch reactions were conducted in a 250 mL, double neck round bottom flask that was fitted with a condenser and a thermometer. The amount of catalyst to be used (usually 2 mL) was measured in water, then washed for 15 minutes with 50-60 mL of isopropanol to displace most of the water. The catalyst, slightly wet with isopropanol, was then placed in the reaction flask, and the flask was immersed in a water bath. The temperature of the water bath was controlled by a Haake FF circulator. After preheating 100 mL of acetone to the desired reaction temperature, it was quickly poured into the reaction flask. Magnetic stir bars kept the reactor solution and water bath well mixed.

Several batch reactions were conducted under very dry conditions. For these experiments the acetone was dried using 3A molecular sieves (Aldrich, Milwaukee), and the experiment was conducted under nitrogen (Praxair, Kitchener) to exclude atmospheric moisture. Molecular sieves could not be left in the acetone during the reaction, because they

were catalytically active for the aldol condensation.

Concentrations of Ac, DAA, MO and water were monitored by taking approximately 0.55 mL of liquid sample from the flask with a syringe, being careful not to remove any of the catalyst. Each sample was mixed with 0.5 mL of 1-propanol (or n-propanol from BDH, Toronto) in a 10 mL volumetric flask and then diluted to the mark with isopropanol.

Organics were analyzed on a Perkin Elmer Autosystem gas chromatograph (GC) with a 30 m x 0.32 mm DB-Wax column from J&W Scientific, and an FID detector. The samples were also analyzed for water on another Perkin Elmer Autosystem GC equipped with an 8 ft. x 1/8 in. column packed with Hayesep P, and a TCD detector. In both cases, helium was used as the carrier gas and the 'Internal Standard' calibration method was used. The concentration of a component (g/mL) was measured relative to the known concentration of 1-propanol. Response factors for the compounds of interest are shown in Table 3.1.2-II. A few samples were also tested on a VG Lab Base Trio-1 GC/MS. The column used for the GC/MS analysis was a 60 m x 0.32 mm DB-1 from J&W Scientific.

Table 3.1.2-II: Response factors with 1-propanol as the internal standard.

Compound Name	Response Factor
Acetone	1.1655
Diacetone Alcohol	1.1986
Isophorone	0.6137
Mesityl Oxide	0.8585
Water[a]	0.8566

[a]Analyzed by TCD

For the analysis of organics, the inlet GC pressure was set to 10 psig. The oven temperature was initially set to 40°C, and then held at this level for 3 minutes. The temperature was then increased at 9 C°/min to 120°C, held for 2.12 minutes, and then increased at 15 C°/min to 160°C. This program resulted in a very clear separation of all of the components. A typical chromatogram is shown in Figure 3.1.2-1.

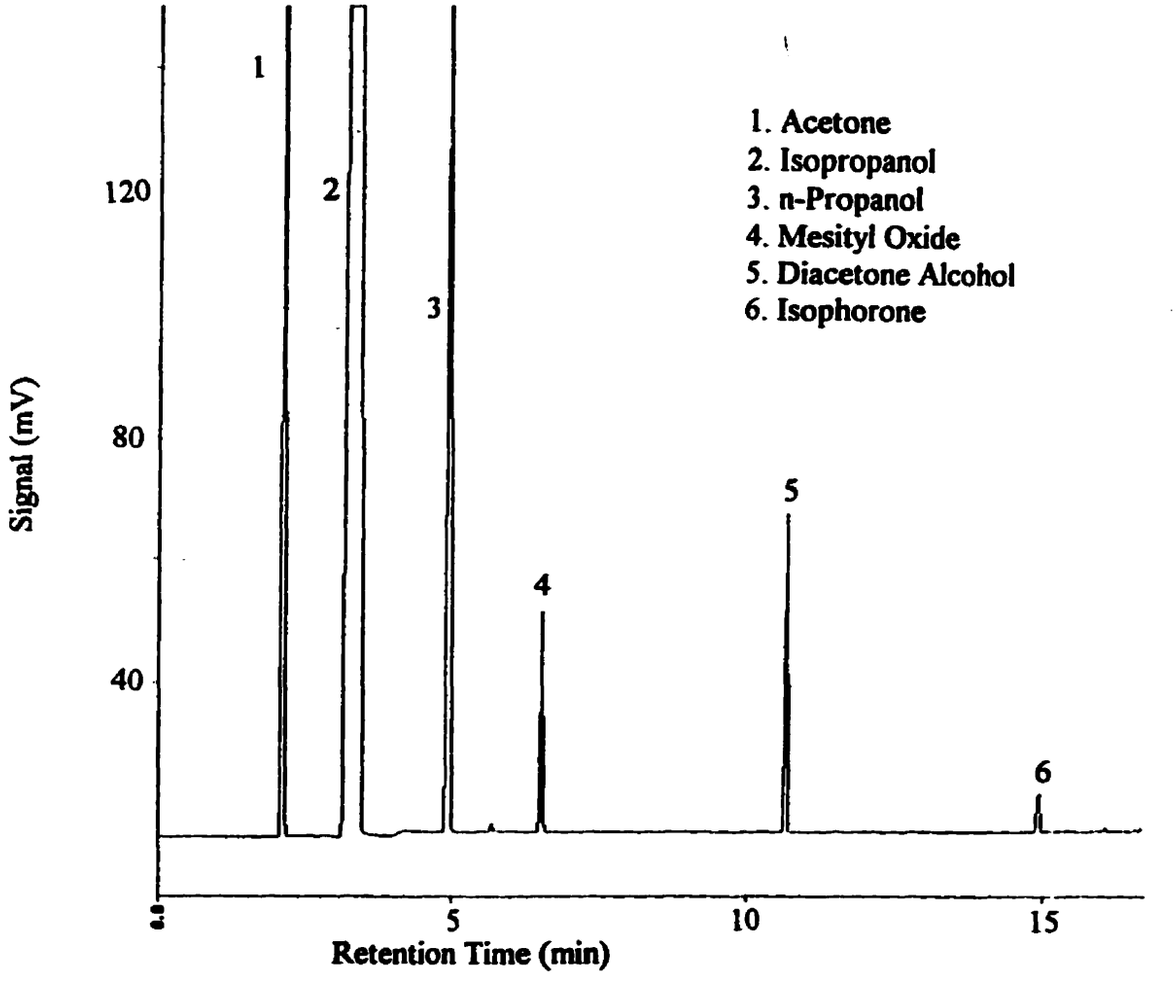

Figure 3.1.2-1: Analysis of a CD sample for organics with the DB-Wax column.

For the analysis of water, the inlet column flow rate was set to approximately 20 mL/min. The oven temperature was initially 140°C. This was held for 8 minutes, and then increased at 20 C°/min to 220°C. A sample chromatogram of a typical water analysis is shown in Figure 3.1.2-2.

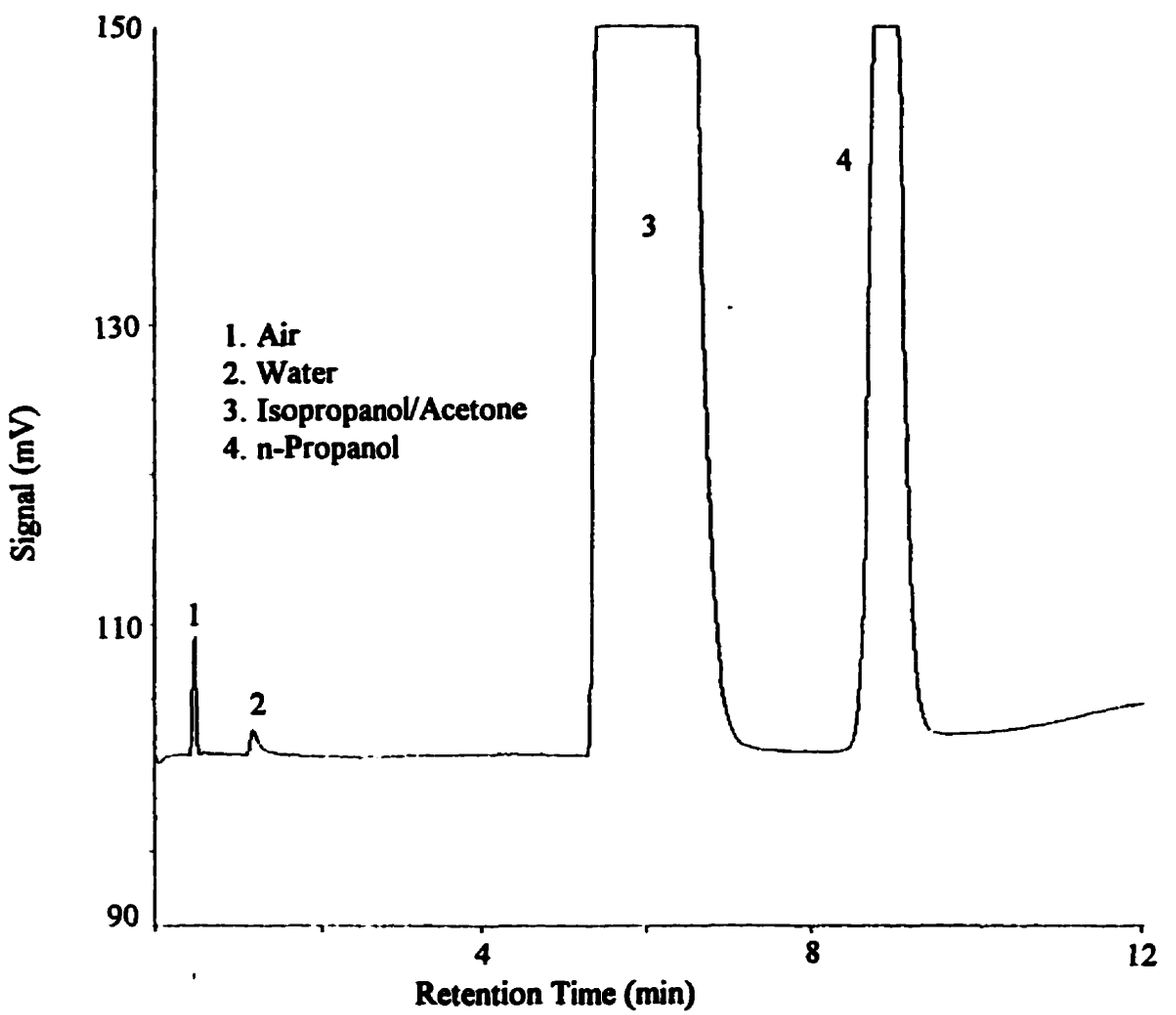

Figure 3.1.2-2: Analysis of a sample from a batch reaction for water content with the 1/8" Hayesep P column.

The solvents used to dilute the samples were dried in order to increase the accuracy of the water determinations. Isopropanol and 1-propanol were kept in sealed bottles and dried with 3A molecular sieves. The background water content in the solvents was determined by GC analysis. The water content of a sample was then calculated by subtracting the background water concentration from the water concentration of the sample. It is estimated that the accuracy is approximately ±8% when the water concentration is near 0.17 M. The accuracy of the water determinations improves as the water content increases. However, samples were typically injected two or three times to ensure that a reliable average measurement was obtained. The analysis of the organic phase was very accurate and reliable. For example, the typical DAA concentration is known within ±0.1 wt%.

Although data from the GCs provide the wt% of each component in the sample, the kinetic expressions require concentration data. This conversion is possible if the density of each component is known at the reaction temperature, and ideal mixing laws are used. In Section 2.2.5 it was stated that ideal mixing laws are followed by mixtures of DAA and acetone. Since this system involves very small quantities of water, which is likely non-ideal, the assumption of ideal mixing seems reasonable. Table 3.1.2-III shows some of the liquid densities required to make these calculations.

Table 3.1.2-III: Liquid densities at various temperatures.

Temperature (°C)	Acetone[a] (g/L)	DAA[a] (g/L)	MO[a] (g/L)	Water[b] (g/L)
10	802.80	947.08	865.60	999.89
20	791.40	938.55	856.66	998.19
32.5	776.80	927.72	845.33	994.84
45	761.85	916.67	833.80	990.14
54	751.95	909.03	825.85	985.87

[a]from Daubert and Danner (1989)
[b]from McCabe et. al. (1985)

3.1.3 Kinetic Data

As mentioned in Section 3.1.1, kinetic data were obtained by sampling from a batch reactor and monitoring the changes in composition over time. A sample calculation and data from some of the experiments are available in Appendix B. Concentration vs. time data from a typical experiment is plotted in Figure 3.1.3-1. This graph was constructed from an experiment at 54°C with 100 mL of acetone and 2 mL of catalyst exchanged within 3 h to 0.45 mmol OH^-/mL (expt. #75). The points on the graph represent the measured data, and the lines represents the models shown in equation (3.5) and (3.8). For the production of DAA, the model fits the data very well. The rate constant provided by Figure 3.1.3-1 is k_1 = 0.34 x 10^{-3} M^{-1} min^{-1}.

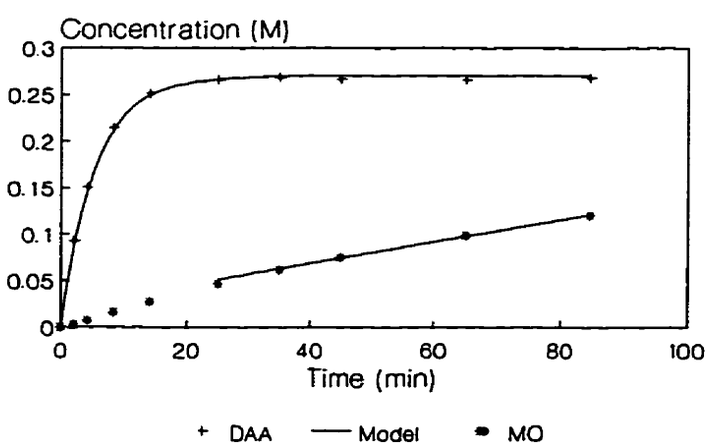

Figure 3.1.3-1: [DAA] and [MO] vs. time in a batch reaction at 54°C with 100 mL of acetone and 2 mL of catalyst exchanged for 3 h to 0.45 mmol OH^-/mL (expt. 75).

It is convenient to assume that no concentration gradients exist between the catalyst surface and the bulk liquid. While this assumption can usually be made in well mixed batch reactors, it must be verified. If external mass transfer is important, the reaction rate depends on the rate of mass transfer to and from the catalyst surface. The molar transfer rate of component i, N_i,

is given in equation (3.17). The surface area for mass transfer is represented by A', while B and S denote bulk liquid and catalyst surface concentrations. The mass transfer coefficient, k_C, is a function of the stirring speed.

$$N_i = k_C A'([i]_S - [i]_B) \tag{3.17}$$

A good way to check for external mass transfer, therefore, is to conduct experiments at different stirring speeds and compare the observed reaction rate constants. Two different stir speed settings were selected, and several experiments with 2 mL of catalyst at 54°C were conducted at each setting. The results are shown in Table 3.1.3-I.

Table 3.1.3-I: Experiments to check for external mass transfer in the batch reactor.
(54°C, 2 mL catalyst at 0.49 mmol OH^-/mL, 100 mL acetone)

Stir Speed Setting	1000 x k_1 (M^{-1} min^{-1})	$[DAA]_{EQ}$ (M)	Expt. #
1	0.377	0.270	4
1	0.370	0.280	5
1	0.365	0.280	6
1	0.360	0.277	7
1	0.350*	0.268	13
1	0.350*	0.279	14
2	0.365	0.278	8
2	0.375	0.275	10
2	0.365	0.271	11
2	0.350	0.280	33
2	0.340*	0.274	16

* rate constant from 1 mL of catalyst was doubled
(ie. a 1st order catalyst dependence was assumed)

Although the stir speeds were not measured in rpm, the increment from 1 to 2 represents an approximate doubling in the rotational speed. The jump from a setting of 1 to 2 is, therefore, a very significant increase. These results demonstrate that the stir speed does not influence the observed rate constant for DAA formation, and it follows that external mass transfer is negligible in the batch reactor. Along with the observed rate constant, the 'best-fit' equilibrium concentration of DAA was determined by the non-linear regression.

Table 3.1.3-I also demonstrates that these experiments show good reproducibility. Taking the average of all 11 rate constants (since stir speed was not important over the range used) provides $k_1 = 0.3606 \times 10^{-3}$ M^{-1} min^{-1}. Using the Student's T distribution with 10 degrees of freedom (Box et. al., 1978), the 95% confidence interval of this rate constant is $\pm 0.026 \times 10^{-3}$ M^{-1} min^{-1}, which gives it an accuracy of ±7%.

MO concentrations were also monitored during these experiments, although the MO data from the first few experiments were erratic. The MO peak is small, and the integrator frequently assigned inappropriate integration limits. Thus, each MO peak had to be checked to ensure that reasonable integration limits were selected.

The plot of [MO] vs. time in Figure 3.1.3-1 is typical of other [MO] vs. time plots. The MO data display some curvature early in the experiment, but become fairly linear after 20 minutes of reaction. Experiments were usually terminated after 80 minutes, but a longer experiment (expt. #7) showed that the slope of the MO data remains essentially constant for long periods of time. This is illustrated in Figure 3.1.3-2.

The MO data in Figures 3.1.3-1 and 3.1.3-2 reveal an unexpected trend. As a 'consecutive' reaction, one would expect the slope of the [MO] vs. time data to increase as [DAA] increases. The slope of the MO data should be greatest and remain constant once $[DAA]_{EQ}$ is reached. However, this is not observed. The initial slope of the MO data in Figure 3.1.3-1 is 0.002063 M min^{-1}, whereas the slope of the data after 20 minutes is 0.00117 M min^{-1}. There are several possible explanations for this behaviour, including pore diffusion control of the reaction rate, catalyst deactivation, the reverse hydration of MO to DAA, and water concentrations increasing as a function of time in the batch reactor. Each of these issues will receive attention in this thesis.

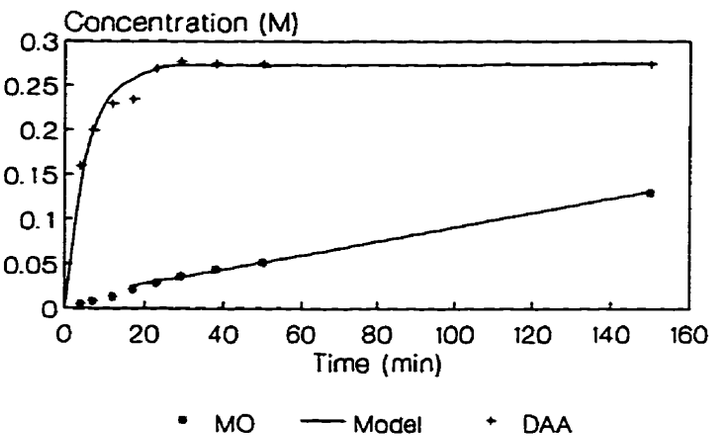

Figure 3.1.3-2: [DAA] and [MO] vs. time in a batch reaction at 54°C with 100 mL of acetone and 2 mL of catalyst exchanged for 24 h to 0.49 mmol OH^-/mL (expt. 7).

As discussed during the derivation of equation (3.8), it was decided to use the slope of the best fit line at times between 20 and 80 minutes as the value of k_2. This is convenient since [DAA] remains constant at its equilibrium value during this time period, which permits the use of a simplified rate expression. This also ensures that these rate data will be useful in predicting the performance of other types of continuous reactors which operate for longer periods of time. An initial rate is not helpful for this purpose. The best fit line for the data after 20 minutes is shown in Figure 3.1.3-2, and its slope gives $k_2 = 0.00079$ M min^{-1}. The best fit line for the MO data in Figure 3.1.3-1 is $k_2 = 0.00117$ M min^{-1}.

Figures 3.1.3-1 and 3.1.3-2 confirm that MO formation is slow relative to DAA formation. Therefore, it is reasonable to assume that the production of MO is negligible in developing the kinetic equation for DAA production in (3.5). In Section 2, it was estimated that the equilibrium molar ratio of [MO]/[DAA] at 54°C was 2.5, while the ratio in Figure 3.1.3-1 after 80 minutes is close to 0.4. Since MO concentrations only reach 16% of this

equilibrium value, it may be reasonable to ignore the reverse hydration of MO in developing equation (3.8). To provide further support for this assumption, however, a batch reaction was conducted in which pure MO and water were initially mixed and the rates of acetone and DAA production were measured. The reaction mixture, consisting of 20 mL each of MO and water diluted to 100 mL with isopropanol (this is necessary since MO and water are mutually insoluble), was added to 5 mL of catalyst at 54°C. The production rates of acetone and DAA were 0.00023 and 4.15×10^{-6} M min^{-1}, respectively. Thus, MO was hydrated at a rate of 0.00012 M min^{-1}. This is very slow when compared to the rate of MO production observed in many of the batch reactions. Considering that this rate was measured with 5 mL of catalyst and at $[H_2O] = 11$ M, whereas the batch experiments usually involved 2 mL of catalyst and $[H_2O] = 0.17$ M, one is certainly justified in ignoring the reverse reaction when developing equation (3.8).

The MO production rates (k_2) observed during several experiments are displayed in Table 3.1.3-II. These data show that k_2 is fairly reproducible, but that there is a large difference when the catalyst is soaked in the NaOH solution for different times. Oddly, the exchange time does not seem to significantly alter the value of k_1. This effect was not anticipated at the outset of this work, and consequently, the catalyst exchange time was not carefully controlled during early catalyst preparations. IRA-900 anion exchange is reported to be stable in acids and bases. However, the large differences in k_2 caused by varying the exchange time brings the stability of this resin into question. Two samples of fresh catalyst were subjected to a pore radius, pore volume, and surface area analysis to compare their pore structures. Before the analysis, each sample was washed with isopropanol, then heated to 60°C under vacuum for 1 h to remove any isopropanol and water from the surface. The results of these measurements are shown in Table 3.1.3-III.

The data in Table 3.1.3-III show that the exchange time does not significantly alter the total number of catalytic sites, or the average pore radius of the catalyst samples. However, soaking the resin for 24 hours increases the pore volume and the surface area by 17%. The surface area of the resin exchanged for 3 h is quite close to Tanabe's (1989) value of 27 m^2/g. Differences in the pore volume and surface area are a likely source of the differences in k_2. In

addition to the pore structure, however, other properties of the basic sites within the resin may have been altered. More research is required, however, to fully explain this phenomenon.

Table 3.1.3-II: MO production rates during experiments at 54°C.
(54°C, 2 mL catalyst, 0.49 mmol OH^-/mL, 100 mL acetone)

Stir Speed	Exchange Time (h)	k_2 ($M\ min^{-1}$)	Expt. #
1	3	0.00135	5
1	3	0.00131	6
2	3	0.00136	8
2	3	0.00116	10
2	3	0.00132	11
1	24	0.00079	7
1	24	0.00084*	13
1	24	0.0009*	14
2	24	0.00094*	16
2	24	0.0008	33

* slope from 1 mL of catalyst was doubled
(ie. a 1st order catalyst dependence was assumed)

Table 3.1.3-III: Properties of IRA-900 resin exchanged for 3 h and 24 h in 1.5 M NaOH.

Property	Exchange Time (h) 3	24
OH^- Loading (mmol/mL)	0.49	0.49
Pore Volume (mL/g)	0.23	0.27
Average Pore Radius (Å)	177.8	178.3
Surface Area (m^2/g)	25.84	30.26

As noted earlier, the locus of the MO data points in Figure 3.1.3-1 and 3.1.3-2 is unusual. Based on equation (3.8), the rate of MO production should increase as [DAA] increases and remain constant once $[DAA]_{EQ}$ is reached. This behaviour is worthy of further attention.

Several experiments were conducted over a wide range of initial DAA concentrations ($[DAA]_0$), and the results are summarized in Table 3.1.3-IV. The catalyst used for this set of experiments was exchanged to 0.45 mmol OH^-/mL within 3 h, and was all prepared in the same batch. These data show that k_2 and the initial slope of the MO vs. time data are both essentially independent of $[DAA]_0$ over the range $0 \leq [DAA]_0 \leq 1$ M, and are much more

Table 3.1.3-IV: The effect of increasing $[DAA]_0$ on k_1, k_2 and the initial MO slope at 54°C[a].

$[DAA]_0$ (M)	$[Ac]_0$ (M)	k_1 (M^{-1} min^{-1})	k_2 (M min^{-1})	Initial Slope (M min^{-1})	Expt. #
0	12.95	0.34×10^{-3}	0.00117	0.00206	75
0.32	12.36	-	0.00121	0.00200	76
0.58	11.90	0.27×10^{-3}	0.00124	0.00205	77
1.08	11.08	0.20×10^{-3}	0.00110	0.00188	78
2.77	8.24	0.11×10^{-3}	0.00094	0.00153	79
6.75	1.6	0.03×10^{-3}	0.00062	0.00099	80

[a]catalyst was exchanged to 0.45 mmol OH^-/mL and washed within 3 h.

reproducible when variations in the catalyst preparation time are avoided. Values of k_2 and the initial MO slope actually decline at the highest values of $[DAA]_0$. This is most likely the result of catalyst deactivation, and will be discussed in more detail later in this section.

Despite literature data showing that the formation of MO is first order with respect to [DAA] in homogeneous systems (Kim and Hatfield, 1985), the values of k_2 in Table 3.1.3-IV

suggest that the formation of MO is zero order over the range $0 \leq [DAA]_0 \leq 1$ M. This could be a consequence of diffusion inside of the catalyst pellet. The pore volume and surface area data in Table 3.1.3-III suggest that k_2 is influenced by the pore structure of the catalyst. If pore diffusion influences the rate of DAA formation, it is possible that [DAA] inside of the catalyst bead is always near its equilibrium value regardless of the external DAA concentration. This would result in the driving force for MO production remaining essentially constant, and make the reaction appear to be zero order with respect to [DAA].

According to Levenspiel (1972), a good way to verify that a reaction rate is diffusion controlled is to measure the activation energy. As reported in section 3.1.1, diffusion controlled reactions have activation energies that are much lower than kinetically controlled reactions. A series of reactions was conducted at 32.5, 45, and 54°C with 100 mL of acetone and 2 mL of a catalyst exchanged for 3 h to 0.6 mmol OH^-/mL. Equilibrium data from these experiments were shown in Figure 2.2.4-1 as part of the literature review. Figures 3.1.3-3 and 3.1.3-4 show the results of these experiments in the form of Arrhenius plots.

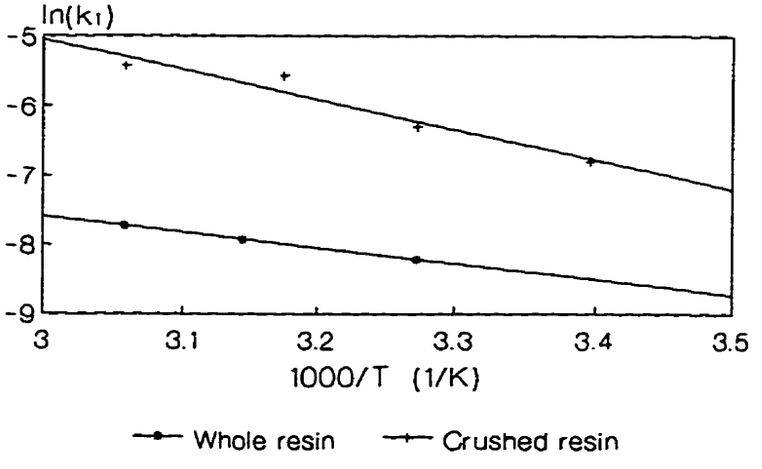

Figure 3.1.3-3: Arrhenius plot of k_1 using a catalyst exchanged to 0.6 mmol OH^-/mL.

The slope of the 'Whole resin' line in Figure 3.1.3-3 gives an activation energy of 18.8 kJ/mol for the formation of DAA, which is much lower than Watanabe and Seto's (1991) value of 70 kJ/mol for a kinetically controlled reaction. Such a low value suggests that the reaction rate is almost completely controlled by pore diffusion.

Values of k_{MO}, the first order rate constant for MO formation, were used to construct Figure 3.1.3-4. The values of k_{MO} were calculated from k_2 values using equation (3.8). To facilitate the calculations, it was assumed that [DAA] is constant at its equilibrium value throughout the catalyst pellet. This is a reasonable assumption, and will be supported by the results of upcoming calculations (for a preview, see Figure 3.1.3-5). The slope of the 'Whole resin' line in Figure 3.1.3-4 provides an activation energy of 75 kJ/mol for MO production. This value is reasonable for kinetically controlled reactions, and agrees well with the value of 79 kJ/mol obtained with homogeneous phosphoric acid as the catalyst (Kim and Hatfield, 1985).

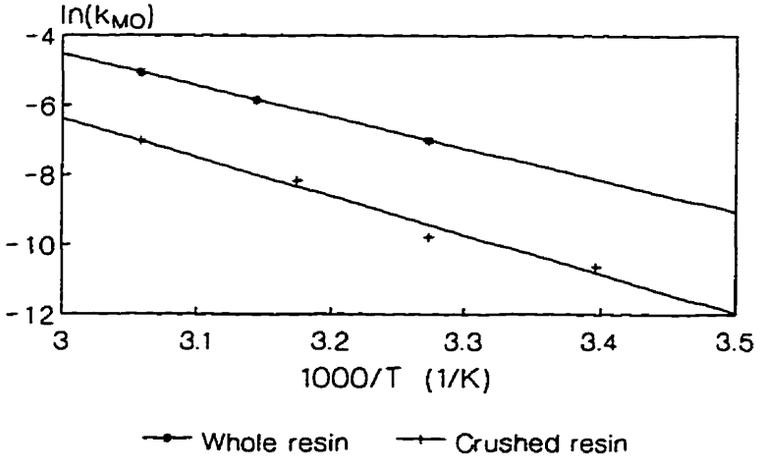

Figure 3.1.3-4: Arrhenius plot of k_{MO} using a catalyst exchanged to 0.6 mmol OH^-/mL.

Another series of experiments was conducted in which the catalyst was crushed with a mortar and pestle before the reaction. The discussion in Section 3.1.1 reveals that the rate of a diffusion controlled reaction can be increased by using smaller catalyst particles. For a kinetically controlled reaction, however, the particle size of the catalyst is not important. The results of the second set of experiments are also available in Figures 3.1.3-3 and 3.1.3-4.

The 'crushed resin' data in Figure 3.1.3-3 show that reducing the particle size of the catalyst (although the new size was not measured) results in dramatically increased DAA production rates. Each aliquot of catalyst used for these experiments was crushed separately, and the increased scatter of the data for the crushed catalyst may be a result of poor control over the particle size during the crushing procedure. There are also increased errors involved in measuring the much faster reaction rates. The slope of the 'Crushed resin' data provides a higher activation energy of 35.9 kJ/mol for DAA production. While this value remains lower than 70 kJ/mol reported by Watanabe and Seto (1991), it indicates that the reaction rate may be influenced by a combination of diffusional and kinetic effects. It is now very clear, however, that the rate of DAA formation in the whole catalyst pellets is controlled by pore diffusion.

The data in Figure 3.1.3-4 reveals that crushing the catalyst produced a slight decline in the MO production rate. The activation energy for MO production with the crushed catalyst was found to be 92.8 kJ/mol, which is reasonably close to 75 kJ/mol observed for the 'Whole resin' and 79 kJ/mol reported for phosphoric acid (Kim and Hatfield, 1985). In either case, the rate of MO production does not appear to be limited by pore diffusion.

In order to fully appreciate the effect of pore diffusion on MO production, the DAA concentration profile inside of a catalyst pellet can be approximated with equation (3.16). This calculation will also add credibility to the assumption of a constant concentration of DAA throughout the catalyst pellet. Before using this equation, however, effective diffusion coefficients, intrinsic first-order rate constants, and an equilibrium constant are required to calculate the parameters h_L, w, γ, and p. The equilibrium concentration of DAA is 0.28 M at 54°C, and the value of the equilibrium constant to be used in (3.16) is approximated with the equation K_{EQ} = 0.28 M / (12.95-2(0.28) M) = 0.0226.

Effective diffusivities of A (acetone) and B (DAA) in the catalyst must also be estimated. The binary liquid phase diffusion coefficient for an infinitely dilute solution of DAA in acetone ($D_{DAA,Ac}$) can be obtained using methods described by Reid et. al. (1986), and was estimated to be 4.6×10^{-9} m^2/s. As described in Appendix C, the values of $D_{A,eff}$ and $D_{B,eff}$ are taken to be 15% of this estimated value, or 6.9×10^{-10} m^2/s. In a binary system, $D_{AB} = D_{BA}$. Although we are considering a multi-component system, pseudo-binary diffusion coefficients may be used if the solutions are dilute (Taylor and Krishna, 1993). Since we are considering a dilute solution of several components in acetone, it is acceptable to let the effective diffusivity of acetone equal the effective diffusivity of DAA.

The value of $k^*_{V,B}$, the intrinsic rate constant for MO formation, was estimated from experimental data by assuming that the average DAA concentration within the pellet is 0.28 M. This calculation is also shown in Appendix C, and the value of $k^*_{V,B}$ is 0.0084 s^{-1}.

Instead of an *a priori* estimate of $k^*_{V,A}$, the values of h_L and w were varied by trial and error until the diffusion rate of DAA out of the pellet (with $[DAA]_{r=R} = 0$ M) matched the experimentally observed DAA production rate. Data from a representative experiment (expt. #6) were used, and a detailed description of these calculations is available in Appendix C. The final values assigned to the constants are $h_L = 11$, $w = 0.00226$, $\gamma = 0.5$ and $p = 22.124$. The value of h_L (the Thiele modulus) is high, which is typical of diffusion controlled reactions.

DAA concentration profiles were calculated at wall concentrations of 0, 0.5, and 1 M while the values of h_L, w, γ and p were held constant. Thus, the effect of changing $[DAA]_{r=R}$ on the DAA concentration profile inside of the pellet can be shown. The results are presented in Figure 3.1.3-5, and show that the internal DAA concentration is essentially constant, and is insensitive to the external DAA concentration. Only in a very narrow region near the outer wall of the catalyst pellet does [DAA] stray appreciably from the equilibrium value. Since [DAA] remains constant inside of the pellet, it is now clear why MO production is a pseudo-zero order reaction. We will continue to use the pseudo-zero order rate constant (k_2) to describe the MO production rate.

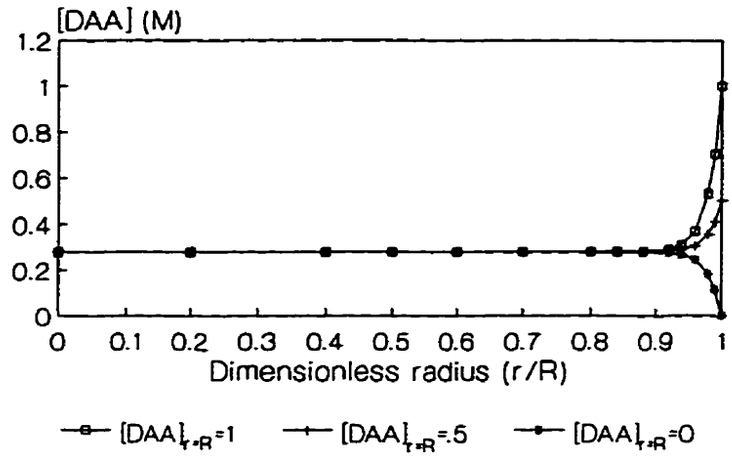

Figure 3.1.3-5: DAA concentration profiles inside the catalyst pellet predicted from equation (3.16) with h_L=11, w=0.00226, γ=0.5, and p=22.124.

The fact that diffusion controlled reactions can change their apparent reaction order was discussed in Section 3.1.1. In theory, an intrinsically second order reaction should change to 1.5 order under the influence of pore diffusion. Thus, one might expect a 1.5 order rate model to be more appropriate for describing the kinetic data. Unfortunately, it is very difficult to distinguish between models that are 1st, 1.5, and 2nd order in the forward direction and first order in the reverse direction. Rate constants can be found that make each of these models appear virtually identical (see Appendix D). The second order rate model in equation (3.5) was selected for this work since it provides a logical link to the reaction mechanism and has a convenient analytical solution.

Several experiments were conducted to investigate the dependence of the reaction rate on the number of OH^- groups within the resin. Batch experiments were run with 2 mL of catalyst in 100 mL of acetone at 54°C to determine k_1 and k_2. In this comparison, all of the catalysts were usually prepared within 3 h. The results of these experiments are summarized in Table 3.1.3-V.

Table 3.1.3-V: Changes in k_2 and k_1 as the OH^- loading of the catalyst is varied.

OH^- loading (mmol/mL)	k_2 ($M\ min^{-1}$)	k_1 ($M^{-1}\ min^{-1}$)	Expt. #
0.00	0.00000	0.00×10^{-3}	-
0.29	0.00075	0.24×10^{-3}	81
0.35	0.00086	0.30×10^{-3}	74
0.45	0.00117	0.34×10^{-3}	75
0.49[a]	0.00079	0.36×10^{-3}	7
0.49	0.00135	0.37×10^{-3}	5
0.61	0.00173	0.44×10^{-3}	62

[a]catalyst exchanged for 24 h

A graphical form of the data in Table 3.1.3-V is provided in Figure 3.1.3-6. This graph confirms that the values k_1 and k_2 are proportional to the number of catalytic sites in the resin. The catalyst used to obtain most of the data in Figure 3.1.3-6 was prepared within 3 h. However, this figure also includes one value of k_2 which was obtained with catalyst exchanged for 24 h in 1.5 M NaOH. As was previously observed in Table 3.1.3-II, the MO production rate is very sensitive to the amount of time used to exchange the catalyst. Figure 3.1.3-6 illustrates the magnitude of the change that occurs to k_2 as the catalyst is soaked for a longer period of time. Oddly, no significant changes in the value of k_1 were noticed with these different catalyst exchange times.

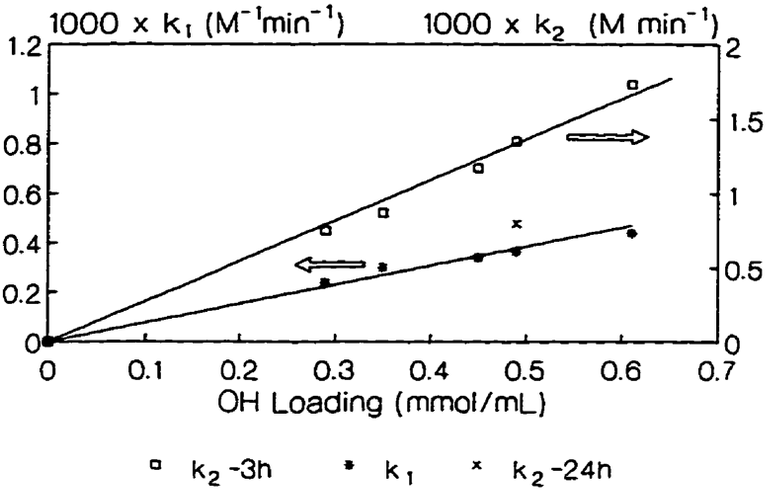

Figure 3.1.3-6: Plot of k_1 and k_2 vs. the OH^- loading of the catalyst.

Catalyst deactivation is a vital issue, but is difficult to study in batch reactors. Some convincing evidence of deactivation is found in Table 3.1.3-IV, however, where higher concentrations of DAA lead to lower values of k_1 and k_2. The data in Table 3.1.3-IV suggest that the reaction products or higher molecular weight condensation products cause deactivation. Kunin (1972b) mentions that aldol condensations commonly foul anion exchange resin catalysts with 'resinous materials'. Although Figure 2.2.3-3 shows that there are many high molecular weight products which form during the aldol condensation of acetone, nothing heavier than DAA was ever detected with the usual GC analysis of the batch reaction products.

In an attempt to dislodge these elusive, high molecular weight byproducts from the catalyst surface, a sample of spent catalyst was rinsed with isopropanol, and then treated with 0.05 N HCl. The acidic solution turned yellow within several minutes. Organic compounds were extracted from the aqueous phase with n-hexane, and were analyzed by GC. An identical treatment with a fresh catalyst sample was also performed to establish a

'background' chromatogram, and to ensure that any compounds which were detected in the hexane did not leach from the catalyst itself. Figure 3.1.3-7 allows a comparison of the 'background' chromatogram with the chromatogram from the spent catalyst. Given that the residence times of DAA and isophorone are 10.7 and 14.9 minutes, respectively, it is clear that many heavier reaction products were dislodged from the resin.

The hexane sample taken from the spent catalyst was analyzed with GC/MS in an attempt to identify some of the peaks shown in Figure 3.1.3-7. Unfortunately, the DB-1 column in the GC/MS was unable to completely separate the peaks and the identifications were ambiguous. A sample of the liquid product from a batch reaction was also analyzed with GC/MS. The method used on the VG Lab-Base GC/MS is able to detect very low concentrations, and a trace of isophorone was identified in the liquid product. Isophorone is shown in Figure 2.2.3-1, and is a product of condensation reactions between MO and acetone. These heavier condensation products are formed despite the fact that the reaction temperature used for this work is quite mild. Since these heavy compounds tend to remain in the catalyst structure as Kunin (1972b) suggests, they are a very likely cause of catalyst deactivation. Clearly, catalyst deactivation is a concern, and a closer examination of the rate of catalyst deactivation will be presented in Section 3.2.

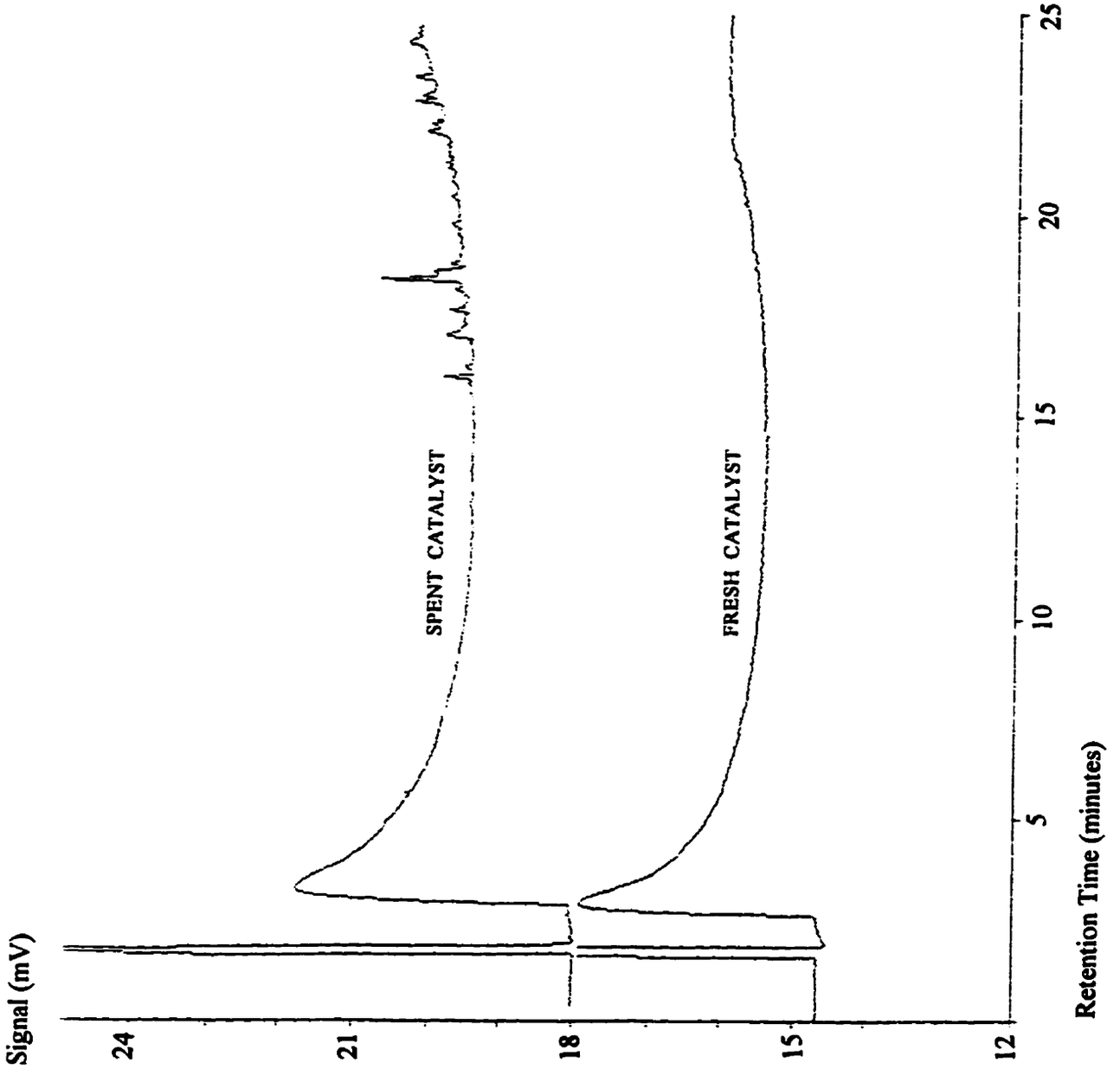

Figure 3.1.3-7: Chromatograms of the hexane extract obtained from fresh and spent catalyst samples reveals high molecular weight material removed from the spent catalyst.

3.1.4 The Role of Water

In this section, the influence of water on the reaction rate is investigated. The reaction mechanism presented in Figure 2.2.2-1 shows that water plays an important role in this reaction. Water is involved in steps I and III of the reaction mechanism for the formation of DAA and is released as a product when MO forms.

For the production of DAA, the literature indicates that step II of the mechanism is rate determining (Westheimer and Cohen, 1938; Zhang et. al., 1988b). The amount of water in the reaction mixture directly influences the concentration of the enolate ion by shifting the equilibrium in step I. This is reflected in kinetic equations (3.2) and (3.3), which reveal an inverse dependence of the rate of DAA production on water concentration. A series of experiments was conducted with 2 mL of catalyst (exchanged to 0.49 mmol OH^-/mL for 24 h) and 100 mL of an acetone/water mixture at 54°C to investigate this effect.

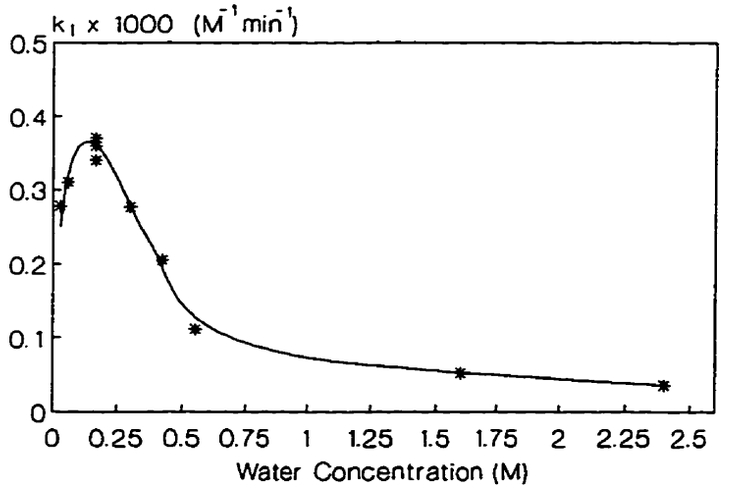

Figure 3.1.4-1: The effect of the initial water concentration on the observed rate constant for DAA production (k_1) in batch reactions at 54°C with 100 mL of acetone and 2 mL of catalyst.

ACS Reagent grade acetone contains 0.17 M of water (0.4 wt%). It should be noted, perhaps, that all of the experiments presented in Section 3.1.3 were conducted with this background concentration of water.

At water concentrations greater than 0.17 M, the rate constant decreases as expected. Figure 3.1.4-1 clearly shows, however, that there is a maximum in k_1 near $[H_2O] = 0.17$ M. We suspect that the rate constant decreases at very low water concentrations because of a change in the rate controlling step of the reaction. Recall that DAA formation requires the presence of water in step III of the mechanism. As the water concentration decreases the rate of step III decreases, and could eventually become rate controlling. Thus, at very low water concentrations, the rate of DAA production should be directly proportional to the concentration of water. A second possible explanation for the existence of this maximum, however, is increased catalyst deactivation at lower water concentrations. Very low water concentrations shift the equilibrium in steps I and III to increase the concentration of the enolate and the alkoxide ions. Thus, there is an increased probability that these ionic intermediates will react with DAA or MO to form heavier byproducts which contribute to catalyst deactivation.

The production rate of MO is also sensitive to the water concentration. As the water content of the reaction mixture increases, the equilibrium between the alkoxide ion and DAA in step III shifts to lower the concentration of the alkoxide ion. Since step III of the mechanism is likely the rate controlling step for MO production, one would expect to observe an inverse dependence of k_2 on water concentration, as shown in equation (3.7). However, one would not expect a maximum to exist in a plot of k_2 vs. water concentration since step III is the only step of the reaction which is expected to control the rate of MO production.

The MO production rate (k_2) is shown as a function of water concentration in Figure 3.1.4-2, and a maximum is observed. The decline in the value k_2 as anhydrous conditions are approached is not as significant as the decline in the value of k_1, and is likely a result of catalyst deactivation rather than mechanistic phenomena. As mentioned previously, the concentration of the enolate and alkoxide ions should increase as the water concentration decreases. This will increase the likelihood of consecutive reactions which lead to higher

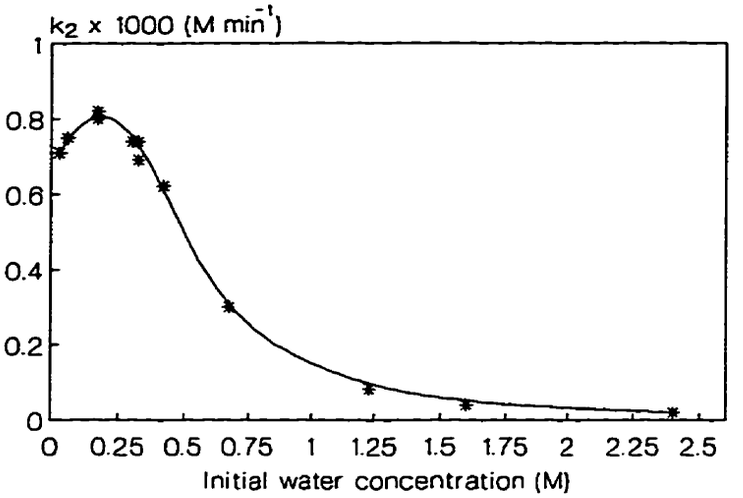

Figure 3.1.4-2: MO production rate (k_2) as a function of the initial water concentration in batch reactions at 54°C with 100 mL of acetone and 2 mL of catalyst..

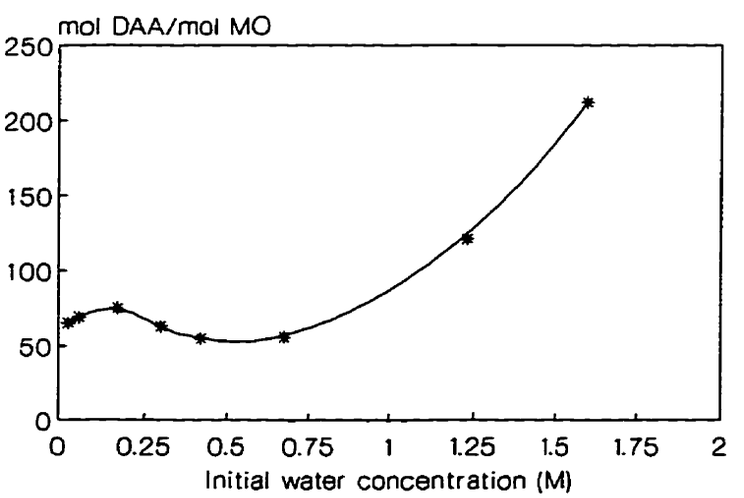

Figure 3.1.4-3: Selectivity (mol DAA/mol MO) as a function of the initial water concentration in batch reactions at 54°C with 100 mL of acetone and 2 mL of catalyst..

molecular weight compounds that deactivate the catalyst.

Figure 3.1.4-3 shows the *initially observed* reaction selectivity toward DAA formation. These selectivity values were calculated by dividing $k_1[Ac]_o^2$ (ie. the rate of DAA production when [DAA] = 0 M) by the MO production rate (k_2) at a given water concentration. There is an interesting local maximum in this data at lower water concentrations. However, this trend would not likely be discernable in a continuous reactor. As long as the reaction rate is sufficient to produce the equilibrium concentration of DAA, the DAA production rate would appear to be constant over a wide range of water concentrations. Therefore, in a continuous reactor, such as a CSTR, the ratio of DAA/MO should simply increase with increasing water concentrations. This was found to be true in the experiments of Section 3.2.

Based on the arguments that low water concentrations encourage catalyst deactivation, one might expect the catalyst to have a longer lifetime if water is added to the reaction mixture. The effect of added water on catalyst lifetime is investigated in CSTR experiments in Section 3.2.

3.1.5 Batch Reactions with a Catalyst Bag

In Catalytic Distillation, the catalyst beads must be placed inside of a fibreglass bag to prevent them from falling to the bottom of the distillation column. However, bundling the catalyst beads in this fashion causes external mass transfer to become more important. In order to investigate the changes that take place when the catalyst is bagged, two batch reactions were conducted with catalyst exchanged for 24 h to 0.49 mmol OH^-/mL.

Two experiments were conducted with stir speed settings of 1 and 2, where speed 2 is approximately twice as fast as 1. The catalyst (2 mL) was placed inside of a fibreglass bag, which was then sewn shut. The bag was just large enough to hold the catalyst. The catalyst bag was then held in the reaction liquid from the end of a thread like a 'tea bag'. This was done since the bag interfered with the normal motion of the magnetic stir bar if left at the

bottom of the reaction flask.

It was anticipated that the rate of this reaction would be 'external mass transfer controlled'. The kinetic expression that applies in this case is equation (3.17) in Section 3.1.3. The instantaneous production rate of DAA is given by the expression $N_{DAA} = k_C A'([DAA]_S - [DAA]_B)$, where the production rate of DAA depends on the area (A') available for mass transfer, the mass transfer coefficient (k_C), and the concentration difference between the surface of the bag (S) and the bulk liquid (B). The instantaneous production rate of MO is governed by an analogous expression.

The formation of DAA is a fast, reversible reaction. It is safe to assume, therefore, that $C_{DAA,S}$ is always 0.28 M. With this assumption, (3.17) can be integrated to give the bulk concentration of DAA as a function of time. This equation is shown in equation (3.18).

$$[DAA]_B = [DAA]_S \left(1 - e^{-(k_C A'/V)\, t} \right) \qquad (3.18)$$

In (3.18), V is the volume of liquid in the batch reactor and t is time measured in minutes. The group $k_C A'/V$ has units of min^{-1}, and its value can be determined by fitting the experimental data to the equation. This was done for two different stir speeds, and the results are shown in Figure 3.1.5-1.

With the stirrer set at 1, $k_C A'/V$ has a value of 0.0043 min^{-1}. When the speed is increased to 2, however, the value of $k_C A'/V$ increases to 0.0082 min^{-1}. Clearly, the stir speed has a tremendous impact on the mass transfer rate at these conditions.

The fit between the model and the data in Figure 3.1.5-1 is excellent. This supports the assumption that the surface DAA concentration is near 0.28 M. However, a liquid sample was removed from within the catalyst bag in order to try to verify this assumption. This sample was taken at the end of the experiment stirred at 2, and the DAA concentration is plotted on Figure 3.1.5-1. The measured concentration is quite close to the equilibrium DAA concentration of 0.28 M, and shows that the assumption of a constant surface concentration of DAA is reasonable.

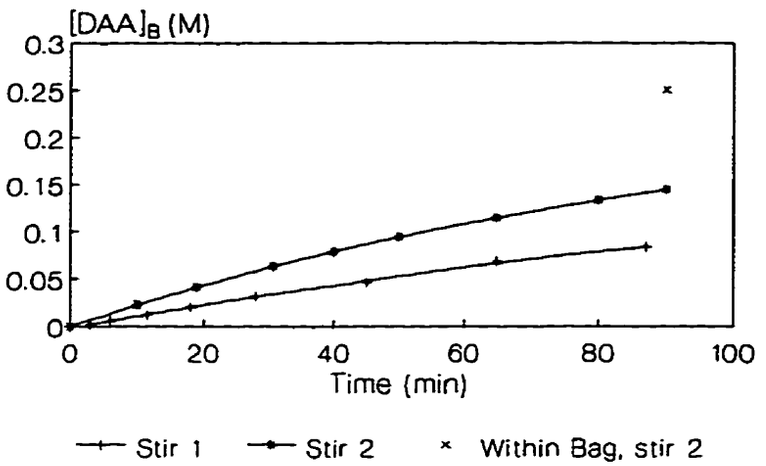

Figure 3.1.5-1: DAA production in a batch reaction at 54°C with 100 mL of acetone and 2 mL of catalyst (exchanged to 0.49 mmol OH^-/mL for 24 h) inside of a fibreglass bag.

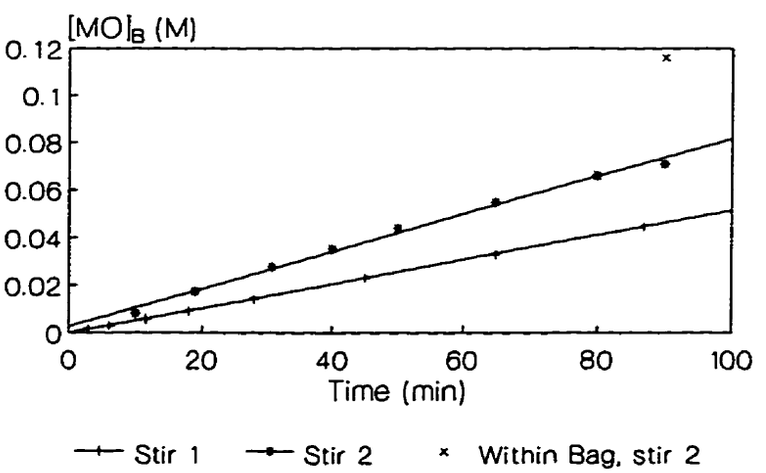

Figure 3.1.5-2: MO production in a batch reaction at 54°C with 100 mL of acetone and 2 mL of catalyst (exchanged to 0.49 mmol OH^- /mL in 24 h) inside of a fibreglass bag.

Figure 3.1.5-2 shows [MO] vs. time data from the same experiments presented in Figure 3.1.5-1. It was anticipated that the MO production rate would be similar to the rate observed in previous batch reactions, and would not be as sensitive to the stir speed as DAA production. The MO data in Figure 3.1.5-2 was fitted to a linear model since the production of MO is a pseudo-zero order reaction.

Figure 3.1.5-2 demonstrates that the rate of MO production is also influenced by stir speed. The production rate is nearly linear at 0.00083 M/min with a stir speed of 2, but drops to 0.00051 M/min at the slower stir setting of 1. The production rate observed at the faster stir setting of 2 agrees very well with the rate of 0.0008 M/min observed with loose catalyst. At the slower speed of 1, however, the MO production rate is much lower.

The initial MO production rate should be independent of the stir speed. To transfer MO out of the bag, however, [MO] inside of the bag must become higher than [MO] outside of the bag. A liquid sample was taken from within the bag, at the end of the experiment stirred at 2, which confirms that the MO concentration inside the bag was much higher than the bulk MO concentration. Since water is also produced in a 1:1 molar ratio with MO, water concentrations inside of the bag should be greater than in the bulk solution. The concentrations of MO and water inside of the bag, however, should depend on the value of the mass transfer coefficient. One would expect [H_2O] and [MO] inside of the bag to be higher during the experiment stirred at 1 than the experiment stirred at 2 because of the value of k_cA' is higher for the experiment stirred at 2. It is likely that the higher concentration of water inside of the bag at slower stir speeds caused the decline in the MO production rate which was observed. Although this explanation is offered, it is unfortunate that samples which could confirm that MO and water concentrations increase as the stir speed decreases were not taken.

The most important result of these experiments is the considerable change in selectivity that occurs when the catalyst is placed in a bag. In Figure 3.1.4-3, the molar ratio of DAA:MO that is initially possible with loose catalyst at 0.17 M H_2O is 75. At a stir setting of 2 with bagged catalyst, however, the molar ratio of DAA/MO in the bulk liquid is nearly constant at 2.4! The external mass transfer limitation introduced to the system by bagging the

catalyst slows the rate of escape of DAA into the bulk solution. Since the formation of DAA is reversible, no additional DAA can form until some is transferred out of the bag. MO formation, on the other hand, is a pseudo-zero order reaction and proceeds more or less unchanged. Thus, selectivity changes are achieved largely at the expense of DAA production, and the bagged catalyst appears to have a much lower activity than the loose catalyst.

One of the goals of this work is to develop a model for catalytic distillation (CD) which incorporates the batch kinetic data described in this chapter. However, the catalyst in the CD process is also placed inside of fibreglass bags. As demonstrated, the reaction rates from the bagged catalyst are very different from those observed with loose catalyst particles. In order to use kinetic data obtained with loose catalyst in the CD model, the effects of external mass transfer will have to be taken into account.

3.2 Catalyst Lifetime Studies

Catalyst deactivation is always a serious concern in CD processes because of the expense and labour associated with changing the catalyst structures. Some evidence was presented in the batch kinetic study (in Figure 3.1.3-7) which indicates that deactivation is taking place. In order to better observe and quantify deactivation, however, experiments must be conducted in a continuous reactor. A Continuous-flow Stirred Tank Reactor (CSTR) was selected for this work. In this section an outline of the equations and equipment used to study catalyst lifetime and experimental results will be presented.

3.2.1 Deactivation Equations

Equations are required to describe the concentration of DAA and MO as a function of time in the CSTR. In constructing this model, the following assumptions will be made:

- the reactor is perfectly mixed and contains no dead-volume
- the feed is instantaneously mixed in the reactor as it enters
- the feed contains no DAA or MO
- the volume of liquid in the reactor is constant

The model must also take into account that the production of DAA is second order with respect to [Ac] and that the decomposition of DAA to acetone is first order with respect to [DAA]. The production of MO is treated as a zero order reaction, since this was observed in Section 3.1.3. In light of these assumptions and requirements, the differential model of the CSTR is shown in equation (3.19).

In (3.19), F represents the volumetric flow rate, and V represents the volume of liquid in the CSTR. The rate constants k_1 and k_2 are for the production of DAA and MO, respectively, with a fresh catalyst. Their values were taken from the batch data discussed previously. Catalyst deactivation is introduced by multiplying the rate constants by 'a', where 'a' represents the fraction of catalytic sites which are active, and its value declines from 1 to 0

$$\frac{d[DAA]}{dt} = k_1 a\,([Ac]_O - 2[DAA])^2 - \frac{k_1 a}{K_{EQ}}[DAA] - \frac{F}{V}[DAA]$$

$$\frac{d[MO]}{dt} = k_2 a - \frac{F}{V}[MO] \qquad (3.19)$$

$$\frac{da}{dt} = -k_d\, a\,([DAA]+[MO])$$

as time passes (Froment and Bischoff, 1990). The evidence in Figure 3.1.3-7 suggests that higher condensation products are responsible for deactivation. It is assumed that the rate of formation of compounds which are deleterious to catalyst lifetime depends on the concentrations of DAA and MO. Thus, the rate of deactivation of the catalyst (da/dt) is proportional to [DAA], [MO], and the number of active sites remaining. The deactivation constant, k_d, is used to quantify the amount of deactivation which takes place. Catalysts which deactivate quickly will have large values of k_d.

Equation (3.19) was solved numerically on a spreadsheet. Euler's method was used to simultaneously integrate these equations and calculate [DAA] and [MO] as a function of time. The model was fitted to experimental data by varying the value of k_d until the sum of squares of the error for the DAA data was minimized. The initial conditions of the simulation are [DAA] = 0, [MO] = 0, and a = 1. The concentration of water is ignored in the kinetic expressions, and is assumed to be constant for the duration of the experiment.

3.2.2 Experimental Procedure for the CSTR

A 250 mL three-neck round bottom flask was used as the CSTR. The flask was immersed in a water bath (described in Section 3.1.2) to maintain a constant reaction temperature. The water bath was stirred with a magnetic stir bar to ensure that the temperature of the bath was constant. A magnetic stir bar could not be used to stir the reaction mixture, however. After several hours of stirring, the catalyst particles were crushed

by the stir bar and the fines swept out in the product stream. Thus, an impeller-style stirrer that did not contact the bottom of the flask was used. The stirrer shaft passed through a rubber septum to prevent the escape of acetone vapour.

A condenser, through which the feed was also introduced, was placed on another neck of the flask. The acetone feed was pumped at a constant volumetric rate by a Milton Roy LCD Mini positive displacement pump. The product was collected by siphoning liquid through a copper tube which was covered with a fine-mesh screen to prevent the catalyst from escaping. This tube was inserted through the third neck of the flask and its height had to be adjusted very carefully.

The volume of liquid in the reactor was held constant at 150 mL and the reaction temperature was 54°C. The same temperature was used for most of the batch kinetic work. The catalyst used for these experiments was exchanged to 0.49 mmol OH^-/mL for 3 h, and 3 mL of catalyst was used in an experiment. The performance of this catalyst was determined in a batch experiment at 54°C with 100 mL of acetone, and values of k_1 and k_2 are available in Table 3.1.3-V (see expt. #5). Since the ratio of catalyst to liquid is the same in the batch and CSTR experiments, these rate constants can be used without modification. The value of the equilibrium constant is $K_{EQ} = [DAA]_{EQ}/[Ac]^2_{EQ} = 0.28\ M/(12.2\ M)^2 \approx 1.9 \times 10^{-3}\ M^{-1}$.

The product analysis technique was described in Section 3.1.2.

3.2.3 CSTR Results

Figure 3.2.3-1 shows data for a CSTR experiment with a flow rate of 152 mL/h. The data points and model predictions from (3.19) are both provided on the same figure, and show good agreement. Therefore, this simple deactivation model should be useful for quantifying deactivation. The value of k_d for the data in Figure 3.2.3-1 is 0.046 $M^{-1}\ min^{-1}$. Although the catalyst deactivates, it is encouraging that these experiments were run for a lengthy period of time. Some of the variables that influence catalyst lifetime will now be investigated.

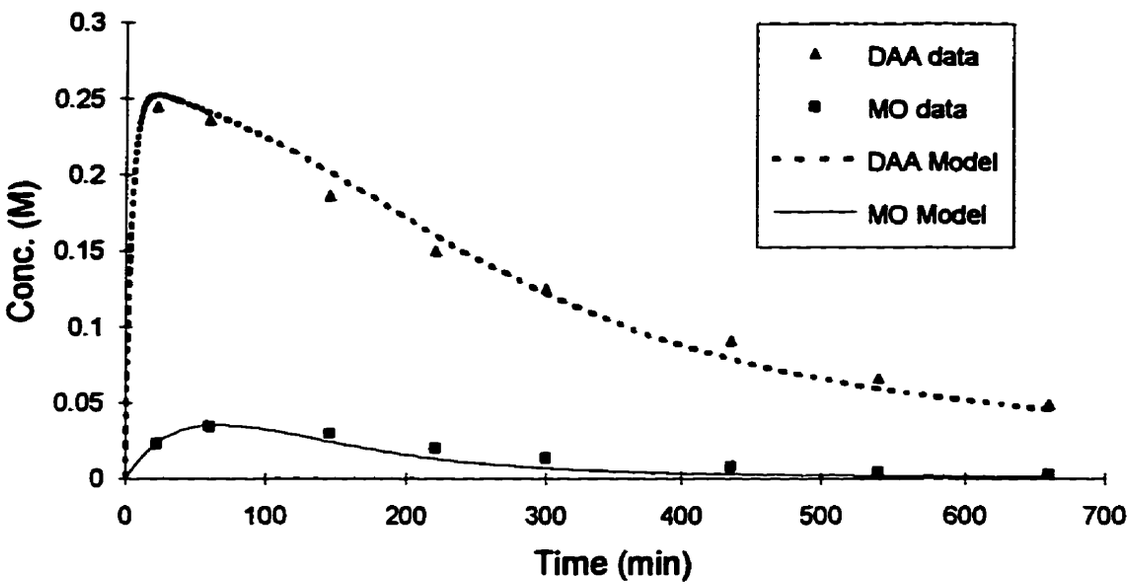

Figure 3.2.3-1: A concentration vs. time plot from a CSTR experiment at 54°C with 3 mL of catalyst, 150 mL of liquid, and an acetone feed rate of 152 mL/h.

A variable that has a very strong impact on the catalyst lifetime is the flow rate of acetone through the reactor. As shown in Figure 3.2.3-1, a flow rate of 152 mL/h results in k_d = 0.046 M^{-1} min^{-1}. An experiment conducted at 76 mL/h of acetone with the same conditions gave k_d = 0.026 M^{-1} min^{-1}, which is a significant increase in lifetime. A reduced acetone feed rate gives a much better catalyst lifetime, despite the fact that [DAA] and [MO] are similar in both experiments (since DAA is limited by equilibrium). This is strong evidence that there may be an impurity in the acetone which causes deactivation.

Over the course of 11 h at 152 mL/h, the catalyst is exposed to a total of 1.8 L of acetone. According to information label provided on the ACS Reagent grade acetone, there are many impurities in acetone which are present at low levels. The compounds which are most likely to cause deactivation are reported to be present at a level of '0.0003 meq/g as acetic acid'. In 1.8 L of acetone, this amounts to 0.43 meq of 'acetic acid'. The 3 mL sample of catalyst used in the CSTR only contains 1.47 meq of OH^-. Therefore, enough acid passes through the reactor in 11 h to neutralize nearly 30% of the catalytic sites. Even though acetic

acid is a weak acid, the removal of the OH^- groups from the resin is very likely since OH^- is the least favoured replacing anion (Kunin, 1972b), and is neutralized by H^+ to produce water. Attempts were made to try to remove acetic acid from the acetone feed via distillation, and to neutralize the acid by adding dilute NH_4OH to the feed. However, none of these measures appreciably improved the catalyst lifetime.

Based on the reaction mechanism and the discussions in Section 3.1.4, it was postulated that adding water to the acetone feed should increase the catalyst lifetime and improve the product selectivity toward DAA. Conventional wisdom has maintained that a low concentration of water is required in the acetone since this leads to higher production rates of DAA. However, this philosophy is now changing. Some corporations have investigated the advantages of using a higher concentration of water in acetone, and have reported their findings in the patent literature (Kyowa Yuka Co., 1983 and 1983b; Sumitomo Chemical Co., 1986). These patents verify that a longer catalyst lifetime and improved selectivity toward DAA are possible if water is added to the acetone feed. Unfortunately, these experiments were conducted at a fairly low temperature (10-20°C) and water concentrations ranging from 3-10 wt%. We are obviously interested in temperatures that approach the boiling point of acetone and lower water concentrations of water which may be present in the CD column.

In order to assess the impact of added water at our conditions, a CSTR experiment was conducted at 54°C with acetone containing 2 wt% water (0.85 M). The feed rate was 153 mL/h, and the results of this experiment were compared to the results from the run with 0.4 wt% water which are provided in Figure 3.2.3-1. Values of the kinetic parameters k_1 and k_2 can be taken from batch reaction data, but must take into account the presence of the added water. Based on Figures 3.1.4-1 and 3.1.4-2, values for k_1 and k_2 can be estimated. Table 3.2.3-I summarizes the results of these two experiments.

The values of k_d in Table 3.2.3-I clearly show that the lifetime of the catalyst is improved by adding 2 wt% water. However, adding water will not completely prevent catalyst deactivation. While we suspect that added water discourages consecutive reactions, it does nothing to solve the problem of acetic acid in the acetone.

Table 3.2.3-I: CSTR experiments at 54°C with 3 mL of catalyst, a 150 mL reactor volume, and acetone feed containing 0.4 and 2 wt% water.

Water in Feed (wt%)	$[H_2O]$ (M)	k_1[a] (M^{-1} min^{-1})	k_2[a] (M min^{-1})	k_d (M^{-1} min^{-1})	Selectivity[b] (mol DAA /mol MO)
0.4	0.17	0.37×10^{-3}	0.00135	0.046	7.5
2.0	0.85	0.10×10^{-3}	0.000338	0.024	28.3

[a]values taken from the results of batch experiments (see batch expt. #5)
[b]selectivity after 1 h of operation

In fact, water which is added to the acetone feed must be very pure or it may also be a source of catalyst deactivation. Most of the anions commonly found in water can exchange with the OH^- sites to deactivate the catalyst. It would be a relatively expensive undertaking to purify water to this extent for an industrial application.

As shown in Table 3.2.3-I, the addition of water to the acetone feed seems to improve the selectivity of the reaction to favour DAA production. Based on the data in Figure 3.1.4-2, the value of k_2 at 2 wt% water (0.85 M) is 4 times lower than k_2 at 0.4 wt% water (0.17 M). This is reflected in the values of k_2 which appear in Table 3.2.3-I. The rate constant for DAA formation is large enough that equilibrium is reached during both of the experiments shown in Table 3.2.3-I. Therefore, the rate constants from batch data predict that the selectivity of the reaction, measured as mol DAA/mol MO, should increase by a factor of 4. The experimentally observed selectivity increased from 7.5 to 28.3 mol DAA/mol MO after 1 hour of operation (Table 3.2.3-I). This shows good agreement between the batch and CSTR data. Therefore, even at fairly low levels, adding water will improve the catalyst lifetime and change the product selectivity to favour the production of DAA. However, it is clearly not possible to use CSTR data to reproduce the selectivity vs. $[H_2O]$ trend which was constructed in Figure 3.1.4-3.

3.3 Mass Transfer between the Catalyst Bag and Bulk Liquid

Section 3.1.5 clearly demonstrates that mass transfer plays an important role in determining reaction rates and product selectivity. The type of mass transfer that will be considered in this section takes place between the catalyst particles immediately inside the catalyst bag and the bulk liquid flowing outside the catalyst bag.

Liquid-solid mass transfer is of vital importance in the area of reactor design. The importance of mass transfer is substantiated by the large amount of space apportioned to it in the classic paper by Satterfield (1975), the monograph by Gianetto and Silveston (1986), and the extensive review by Zhukova et. al. (1990). Many researchers have studied liquid-solid mass transfer, and correlations relating the mass transfer coefficient to liquid properties, liquid and/or gas flow rates, and the particle size of the catalyst abound in the literature (Carberry, 1960; Gianetto and Silveston, 1986; Goto and Smith, 1975; Satterfield, 1981 and 1975; Satterfield et. al., 1978; Steinberger and Treybal, 1960; Treybal, 1980; Zhukova et. al., 1990).

Mass transfer coefficients are a function of the system geometry and the literature covers many common geometries encountered in fixed bed and trickle bed reactors. However, the geometry of a CD column is unique. In a CD column, the catalyst is held within fibreglass bags, and mass transfer must take place through these bags. Therefore, correlations developed for typical reactor geometries will not apply.

A single reference was found in which mass transfer coefficients were determined for a CD geometry. Zheng and Xu (1992) studied mass transfer in the catalyst zone of a CD column with a 45.8 mm (1.8 inch) diameter. During CD experiments, the catalyst was supported inside of 20 mm wide pockets sewn into a 200 mm wide cloth belt. The belt was then twisted and rolled inside of corrugated wire mesh to produce a round catalyst bundle with the same diameter as the column. A schematic diagram of the top view of a catalyst bundle is shown in Figure 3.3-1. In order to determine mass transfer coefficients, however, the bags were filled with naphthalene particles with a similar size as the catalyst. The liquid phase used in these experiments was water, and the gas phase was air. The mass transfer data were presented in the form of a dimensionless j-factor correlation so that results obtained with

air and water can be generalized to other chemical systems.

Our method of supporting the catalyst in the column and our column diameter are both different from that of Zheng and Xu (1992). However, since these are the only CD mass transfer data available, we will use them to compare with our results.

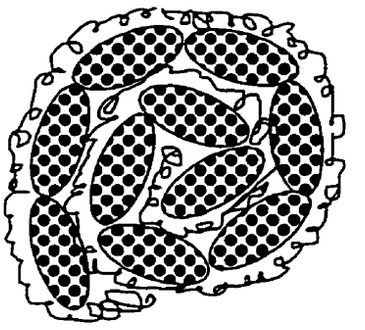

Figure 3.3-1: Top view of a catalyst bundle.

3.3.1 Equations Describing Liquid-Solid Mass Transfer

The rate at which benzoic acid dissolves into water was used to calculate the mass transfer coefficients that are required. A schematic diagram of the column used to study mass transfer is shown in Figure 3.3.1-1. It should be clear that Z refers to the total height of the catalyst zone, and not the total height of the column. A mass balance for the solute within a volume element of thickness dz at a height z from the top of the packing is shown below:

$$FC|_{z+\Delta z} - FC|_z = k_C A(C_{EQ} - C|_z)dz \tag{3.20}$$

where:
- F = volumetric flow of water (m^3/s)
- C = concentration of solute outside of bag (mol/m^3)
- z = position in column (m)
- C_{EQ} = solubility of solute in water (mol/m^3)
- k_C = mass transfer coefficient (m/s)
- A = interfacial area per unit height (m^2/m)

Equation (3.20) is based on the assumption that the equilibrium concentration of solute (C_{EQ}) always exists at the solid surface immediately inside of the catalyst bag. If the volumetric flow rate of water is constant, this equation can be integrated to describe the concentration as a function of height. The integrated equation is shown as (3.21) in a form that is useful for determining the value of the mass transfer coefficient.

$$k_C A = \frac{F}{Z} \ln\left(\frac{C_{EQ}-C_0}{C_{EQ}-C_Z}\right) \tag{3.21}$$

Equation (3.21) shows that the value of $k_C A$ can be determined if the height of the packing and the concentrations of the solute at the top and bottom of the column are known. An independent knowledge of k_C and A is not required since these variables are always used together.

Values of $k_C A$ must be correlated with the flow rates of liquid and gas in the column. This is usually accomplished with a j-factor correlation (Satterfield, 1981). The basic definition of the j-factor, and the empirical equation relating it to the liquid and gas flow rates, is shown in (3.22). This correlation involves the use of two common dimensionless groups. The Reynolds number (Re) is a dimensionless ratio of inertial to viscous forces and is influenced by the liquid and gas flow rates. The Schmidt number (Sc) is a dimensionless ratio of the rate of momentum transfer to the rate of diffusion and incorporates important properties of the solvent. These dimensionless groups facilitate the use of these data with different chemical systems.

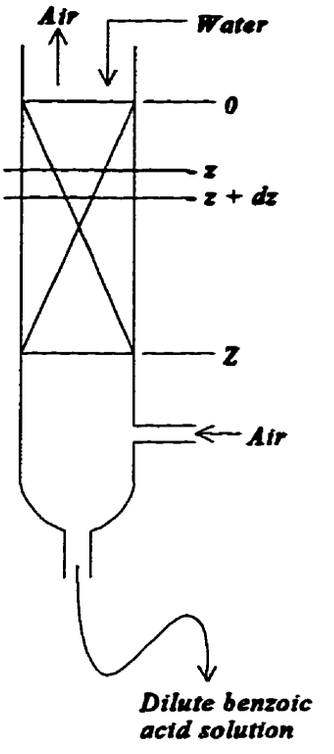

Figure 3.3.1-1: Sketch of the glass column.

$$j_D = \frac{k_C A}{d_t v_L} Sc^{2/3} = Q_1 Re_L^{Q_2} Re_G^{Q_3} \qquad (3.22)$$

$$Sc = \frac{\mu_L}{\rho_L D_L} \qquad Re_L = \frac{d_t v_L \rho_L}{\mu_L} \qquad Re_G = \frac{d_t v_G \rho_G}{\mu_G}$$

In (3.22), D_L represents the Fick diffusion coefficient of the solute in the liquid phase. The subscripts L and G refer to the properties of the liquid and gas phases, respectively.

Once values of $k_C A$ have been measured at a variety of liquid and gas flow rates, the values of the constants Q_n can be determined by fitting (3.22) to the experimental data. If logarithms of (3.22) are taken, linear regression techniques can be used with the linearized form of the equation. This is useful for obtaining initial guesses of the constants, but it is best to use non-linear regression to determine the final values of Q_n.

3.3.2 Liquid-Solid Mass Transfer - Experimental

This mass transfer study was conducted in a glass column built especially for this purpose. A schematic diagram of the column is provided in Figure 3.3.1-1. The column was approximately 60 cm tall with an internal diameter of 1 inch ($d_t = 2.54$ cm). Air and water were used as the gas and liquid phases, and benzoic acid was the solute. Benzoic acid is sparingly soluble in water, and has a long history of use in mass transfer experiments. Some relevant properties of benzoic acid are summarized in Table 3.3.2-I.

Table 3.3.2-I: Some properties of benzoic acid.

Property	Value	Reference
Molecular weight (g/mol)	122.12	Himmelblau (1982)
Specific gravity (28°/4°)	1.316	Himmelblau (1982)
Melting Point (K)	395.4	Himmelblau (1982)
Solubility (C_{EQ}) at 25°C (mol/L)	0.0272 0.028	Steinberger and Treybal (1960) Umland (1993)
Diffusion coefficient in water at 25°C (cm^2/s)	0.908×10^{-5} 1.210×10^{-5}	Steinberger and Treybal (1960) Satterfield (1981)

ACS Reagent grade benzoic acid (BDH, Toronto) was pressed into cylindrical pellets approximately 1.4 cm in diameter by 0.5 cm high. These pellets were stacked on top of each other inside a fibreglass catalyst bag of nearly the same diameter. The height of one bag was typically 12.5 cm, and the top of the bag was sewn closed. This procedure resulted in a bag completely filled with benzoic acid, and having almost no void space. A single catalyst bag was then wrapped in demister wire, and placed in the column.

Contrary to the procedure followed by Zheng and Xu (1992), small (~1 mm) benzoic acid particles were not packed into the catalyst bag. This was done for an important reason.

The goal of this work is to measure the mass transfer coefficient between the solid immediately inside the bag and the liquid flowing outside the bag. If a bed of benzoic acid particles is packed inside the bag, then some liquid will flow through the fixed bed of particles, dissolve a great deal of benzoic acid, and rejoin the remaining liquid at the bottom of the bag. Clearly, not all of the benzoic acid exiting the bottom of the column would be transferred through the sides of the bag in this situation. Yet, equation (3.21) assumes that *all* of the benzoic acid was transferred through the sides of the bag. Therefore, the value of the mass transfer coefficients calculated by (3.21) would be too high. Cylindrical pellets of benzoic acid, which leave no void space inside of the bag, preclude liquid from flowing 'through the bed'. Thus, all of the flow must travel along the outside of the bag, and benzoic acid has no alternative but to transfer through the side walls of the bag. This procedure is expected to result in more accurate values of $k_C A$.

All of the experiments were conducted with fresh deionized water so that C_0 is always zero. The water flow was provided by a small centrifugal pump, and the flow rate was measured with a rotameter. Oil-free plant air from the University of Waterloo was used as the gas phase, and its flow rate was also measured with a rotameter. The benzoic acid concentrations of the liquid samples collected at the bottom of the column were determined with a Perkin Elmer Lambda 3B UV spectrophotometer at a wavelength of 228 nm.

Preliminary experiments were conducted to monitor the value of $k_C A$ as a function of time. The results of these tests indicated that it takes approximately 1 h for the concentration of benzoic acid to reach steady state. A plot of the observed benzoic acid concentration vs. time is provided in Figure 3.3.2-1. Typically, the benzoic acid concentration would remain constant between 1 and 2 h, and then begin to decline. The decline was attributed to the dissolution of a significant amount of benzoic acid and the subsequent decrease in surface area for mass transfer. Therefore, experiments were usually run for 1-1½ h, and a fresh batch of benzoic acid pellets was used for each experiment.

Preliminary experiments were also conducted in which 4-5 inches of ¼" Intalox saddles (a random distillation packing) was placed above the catalyst bag. This packing was intended to distribute the water and provide flow conditions similar to the CD column.

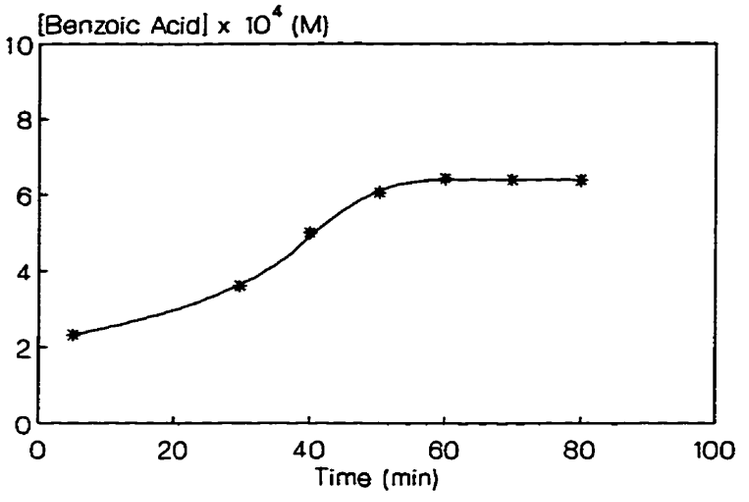

Figure 3.3.2-1: Benzoic acid concentration vs. time for F = 100 mL/min and V = 40 L/min.

However, each time the flow of water was initiated with a fresh bag, the flow pattern established itself in a unique way with a different amount of liquid contacting the bag. Thus, the experiments were *never* reproducible with the random packing in place. The irregular flow pattern is partially due to a phenomena called the 'wall effect'. The diameter of our column is 2.54 cm, while the nominal size of the Intalox saddles is ¼ inch (0.635 cm), and the diameter of the catalyst bag is 1.4 cm. Such a large ratio of packing size to column diameter does not create an even flow distribution in the column, and most of the flow tends to travel down the walls of the column. This phenomena will be discussed in more detail in Chapter 4. To eliminate the uncertainty caused by the Intalox saddles, the flow of water was introduced so that it would directly contact the top of the catalyst bag.

An experiment was repeated several times to ensure that the results were reproducible. Three experiments were operated at an air flow rate of 30 L/min, and a water flow rate of 90 mL/min. The results of these experiments are summarized in Table 3.3.2-II, and show that the value of k_CA remains nearly constant over a variety of different packing heights. Thus, the 'wall effect' is no longer a source of unacceptable error in these experiments, and this

approach yields reasonably reproducible values of $k_C A$.

Table 3.3.2-II: Results from three mass transfer experiments at an air flow rate of 30 L/min and a water flow rate of 90 mL/min.

Packing Height (m)	[Benzoic Acid] (mol/m^3)	$k_C A$ (m^2/s)	j_D
0.125	2.96×10^{-3}	1.34×10^{-6}	1.47
0.13	3.45×10^{-3}	1.52×10^{-6}	1.66
0.26	5.62×10^{-3}	1.29×10^{-6}	1.41
Average values ----->		1.38×10^{-3}	1.51

3.3.3 Liquid-Solid Mass Transfer Coefficients

Mass transfer experiments were conducted at water flow rates (F) of 11, 32.5, 70, 90, 117, 144, and 170 mL/min. Gas flow rates were set to 15, 30, 45, and 62.7 L/min. Nearly all possible combinations of the gas and liquid flow rates were tested in the glass column. The results are provided in Appendix E, and are summarized in Figure 3.3.3-1.

The data in Figure 3.3.3-1 were correlated to the liquid and gas phase Reynolds numbers using equation (3.22). The best fit correlation is represented by the solid lines in Figure 3.3.3-1, and is shown in equation (3.23).

$$j_D = 40.554\ Re_L^{-0.608}\ Re_G^{-0.103} \qquad (3.23)$$

The 95% confidence intervals for the parameters Q_1, Q_2, and Q_3 in equation (3.23) are 40.554 ± 19.1, -0.608 ● 0.034, and -0.103 ± 0.064, respectively.

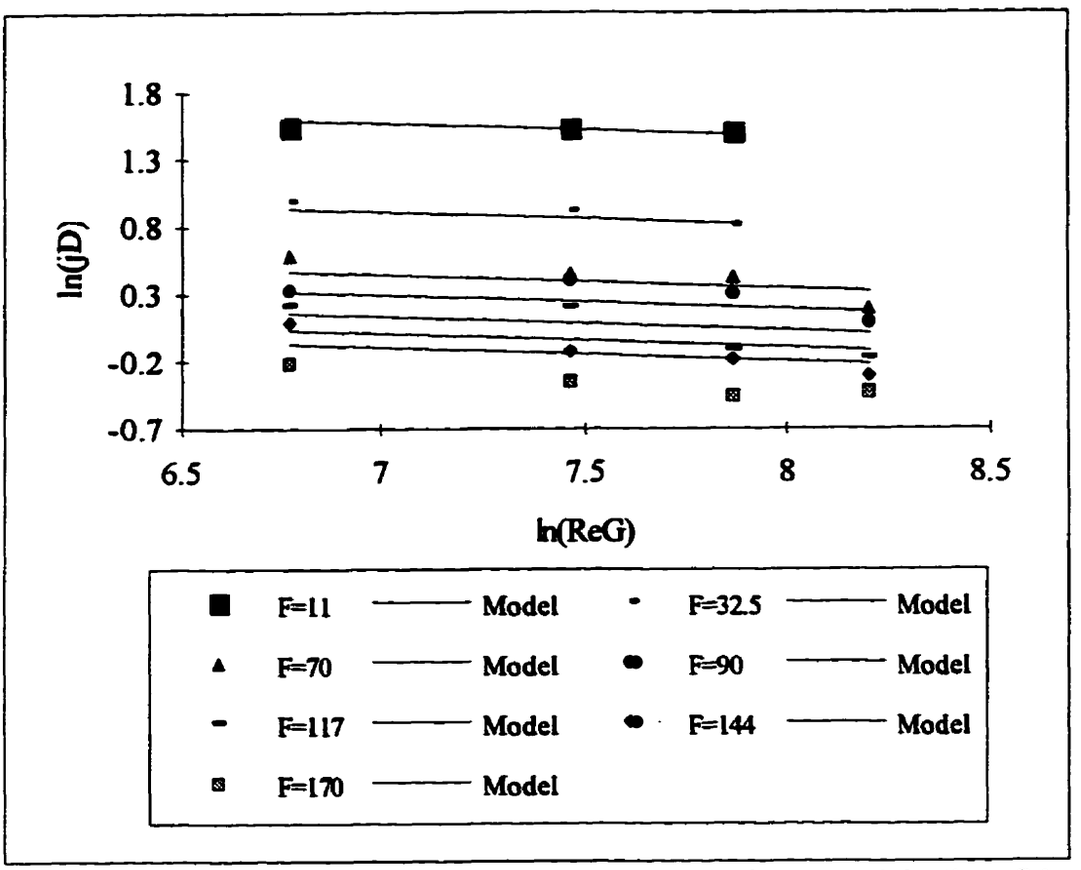

Figure 3.3.3-1: A plot of the experimentally determined j-factors and the 'best fit' correlation vs. the gas phase Reynolds number.

Equation (3.23) seems to estimate values of j_D quite well, although it consistently overestimates the data at the highest liquid flow rate. However, it is likely that errors have been distorted in this region of the graph due to the logarithmic scale. Figure 3.3.3-2 is provided to verify that this correlation is reasonable. This figure shows a plot of the predicted value of the mass transfer coefficient (equation (3.23)) vs. the measured value. If the model fit the data perfectly, all of the points on the graph would fall on a line with a slope of 1. Figure 3.3.3-2 demonstrates that the data and the model are not a perfect fit. However, the data points are distributed on both sides of the line, showing that the model is reasonable.

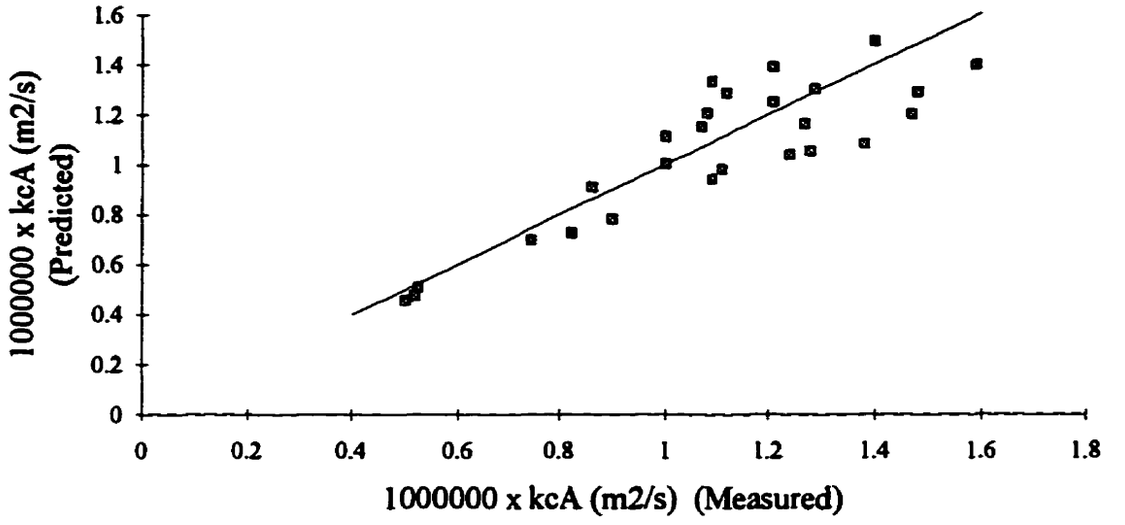

Figure 3.3.3-2: A plot of the predicted vs. the measured value of k_CA.

In (3.23), the exponent of the gas phase Reynolds number is -0.103. This value is fairly close to zero, which implies that the gas flow rate does not have a large influence on the value of k_CA. This compares fairly well with Zheng and Xu's value of -0.28. However, the more negative value from Zheng and Xu's work indicates that the gas flow rate was a more significant variable in their system. This suggests that their packing has a higher pressure drop and/or a lower void fraction, which would cause the upward gas flow to exert a greater shearing force on the liquid phase. The exponent of Re_L is -0.608, which is much more negative than Zheng and Xu's value of -0.27. This indicates that these mass transfer coefficients are much more sensitive to the liquid flow rate than in Zheng and Xu's system, which suggests that they achieved better contact between the liquid and the bags.

It is interesting to try to compare one of our values of k_CA with the data from Zheng and Xu (1992). Their data, however, were reported in different units. They defined the variable A in their mass transfer coefficient as the area available for mass transfer per unit *volume* of the column (m^2/m^3). In order to convert mass transfer coefficients of Zheng and Xu (s^{-1}) to match the units of this work (m^2/s), we must multiply them by a constant representing the volume of the column per unit height (1.647×10^{-3} m^3/m). They also used a

belt of 10 bags of naphthalene pellets wrapped in demister wire, whereas we only used one bag. At flow conditions giving $k_cA = 1.4 \times 10^{-6}$ m^2/s in our work, Zheng and Xu (1992) report a value near 0.004 s^{-1}, or 6.6×10^{-6} m^2/s. These values are of the same order of magnitude, and are reasonably close to each other. However, Zheng and Xu's value is approximately 5 times higher than the value from this work.

There are a number of possible causes for this discrepancy. Perhaps the most significant is that Zheng and Xu used small particles of naphthalene, and likely had a significant amount of flow passing through their bags of particles. For reasons outlined in Section 3.3.2, we did not use 'particles' of benzoic acid and therefore had no flow passing through our catalyst bag. This is likely the major reason for the difference between the observed mass transfer coefficients. Another important difference is the fact that Zheng and Xu used 10 catalyst bags (sewn together), whereas only one was used in this work. This would clearly increase the surface area available for mass transfer.

It seems clear that changes in catalyst packing techniques have a large influence on the mass transfer coefficients in Catalytic Distillation. Therefore, a great deal of care must be taken if attempting to use correlations from the literature.

3.4 Vapour-Liquid Mass Transfer

The exchange of material between the vapour and liquid phases accounts for the distillation which occurs in the CD column. Vapour-liquid mass transfer coefficients are not required for 'equilibrium stage' distillation models. However, such models are not appropriate for describing CD processes. Since the goal of this work is a rate-based model, these mass transfer coefficients must be obtained.

Owing to the fundamental importance of this type of data, it is not surprising that an enormous number of publications address this subject. Vapour-liquid mass transfer data are available from reaction engineering references (Gianetto and Silveston, 1986; Morsi, 1989; Satterfield, 1975 and 1981; Zhukova, 1990), as well as from distillation and absorption references (Billet and Schultes, 1993; Hines and Maddox, 1985; Hung and Taylor, 1990). Some reasons for distinguishing between these sources of mass transfer data are as follows:

- Absorption towers are generally operated at liquid and gas flow rates which are substantially greater than those used in reactors.
- Absorption towers generally use larger packing sizes, a high void fraction, and different shapes, such as Berl saddles and Raschig rings, whereas catalysts are generally smaller spherical or extruded pellets.
- In laboratory-scale absorption towers, a considerable portion of the absorption may occur in the liquid trickling down the wall. In a reactor, however, the wall contributes nothing to the reaction and wall flow is simply a mechanism for bypassing.

Judging from these differences, it appears that data from the distillation/absorption class of publications is most appropriate. Unfortunately, the issue of system geometry arises. The geometry of a CD column is unique, and the only study which addresses liquid-vapour mass transfer for a CD geometry is by Zheng and Xu (1992). As outlined in Section 3.3, however, there are also significant differences in geometry between our column and the column used by Zheng and Xu. We must also obtain these mass transfer coefficients through experimentation.

Sharma and Danckwerts (1970) discuss the general use of chemical methods to determine mass transfer coefficients in two-fluid systems. Some common methods involve absorbing CO_2 in dilute solutions of NaOH or carbonate buffer solutions, O_2 in dilute acid

solutions of CuCl, NH_3 in dilute acid solutions, and COS, H_2S, or CS_2 in amine solutions. Clearly, some of these systems are easier to work with and safer than others. By far, the most popular system is CO_2 and dilute NaOH or carbonate buffers.

For this work, it was decided to determine mass transfer coefficients by conducting simple distillation experiments in the absence of a chemical reaction. By selecting a suitable binary system, equations can be developed relating the overhead and reboiler compositions to the vapour-liquid mass transfer coefficients.

3.4.1 Equations Describing Vapour-Liquid Mass Transfer

In packed columns, vapour-liquid equilibrium (VLE) never exists, nor is it assumed to exist. The difference between an actual phase composition and its equilibrium composition is the driving force for mass transfer. The equation describing the flux of component 'i' between the gas and liquid phase is shown in equation (3.24).

$$N_i = K_{OG}(y_{i,EQ} - y_i) = K_{OL}(x_i - x_{i,EQ}) \qquad (3.24)$$

where:
N_i = molar flux (mol/m^2·s)
K_{OG}, K_{OL} = overall mass transfer coefficients (mol/m^2·s)
$y_{i,EQ}$, $x_{i,EQ}$ = equilibrium mole fractions of vapour and liquid phases
y_i, x_i = mole fractions in vapour and liquid phases

Equation (3.24) is based on overall mass transfer coefficients, and the relationship between these overall coefficients and single-phase mass transfer coefficients is provided in Appendix F. In (3.24), the compositions $y_{i,EQ}$ and $x_{i,EQ}$ are the hypothetical mole fraction that would be in equilibrium with x_i and y_i, respectively. A positive value of N_i indicates mass transfer from liquid to vapour.

The flux of material between the phases causes the mole fractions to change as a function of height in the column. Within a differential height of the column, dz, the changes in the vapour and liquid composition are given the symbols dy_i and dx_i, respectively. These changes in composition are related to the height of the column by (3.25).

$$N_i A\,dz = G\,dy_i = L\,dx_i \tag{3.25}$$

where: A = interfacial area per unit column height (m^2/m)
G, L = molar flow rates of vapour and liquid phases (mol/s)
dz = differential height of the column (m)

Substituting equation (3.24) into (3.25) to replace the flux term, and integrating through the entire height of the column leads to

$$Z = \frac{G}{K_{OG}A}\int_{y_{i,b}}^{y_{i,t}} \frac{dy_i}{y_{i,EQ}-y_i} = \frac{L}{K_{OL}A}\int_{x_{i,b}}^{x_{i,t}} \frac{dx_i}{x_i - x_{i,EQ}} \tag{3.26}$$

$$Z = HTU_{OG}\,NTU_{OG} = HTU_{OL}\,NTU_{OL}$$

where t and b represent the top and bottom of the column. Equation (3.26) assumes that G and L are constant, which is reasonable if the components being distilled have similar heats of vaporization. The portion of equation (3.26) in front of the integral is called the 'Height of a Transfer Unit' (HTU) and may be defined in terms of the overall vapour or liquid phase mass transfer coefficients. The portion of (3.26) inside of the integral is called the 'Number of Transfer Units' (NTU), and may also be defined in terms of vapour or liquid phase compositions.

In our experiments, the height of the column (Z) can be measured, the liquid and vapour flow rates (L and G) can be determined (see the description in Section 3.4.2), and the composition of the liquid phase (x) can be found by sampling from the condenser and reboiler of the column. If one can evaluate the NTU integral based on these measured compositions, the value of the mass transfer coefficient can easily be evaluated.

The integral shown in equation (3.26) is difficult to evaluate, but an analytical solution is possible if the equilibrium relationship for a binary system is approximated with a straight line. For an equilibrium line with a slope m and an intercept b, and a system at total reflux, the integrated form of (3.26) is shown as equation (3.27) (Hines and Maddox, 1985). A derivation of this equation is also available in Appendix F.

$$NTU_{OG} = \frac{1}{1-m} \ln\left(\frac{(1-m)(mx_r + b) - b}{(1-m)y_t - b} \right)$$
$$NTU_{OL} = \frac{m}{1-m} \ln\left(\frac{(1-m)(mx_r + b) - b}{(1-m)y_t - b} \right). \quad (3.27)$$

In (3.27), x_r is the liquid phase composition measured in the reboiler. Since the column has a total condenser, the liquid and vapour compositions in the condenser are the same (ie. $y_t = x_t$).

Equations are now available to determine the mass transfer coefficients $K_{OL}A$ and $K_{OG}A$. These mass transfer coefficients must be correlated with the liquid and vapour flow rates. Since the mass transfer coefficients are determined with chemicals that are different from the acetone/DAA system, j-factor correlations (previously used in Section 3.3) must be applied. The definition of the j-factor for vapour-liquid mass transfer is shown below.

$$j_L = \frac{Sh_L}{Re_L\, Sc_L^{1/3}} = Q_1\, Re_L^{Q_2} \qquad j_G = \frac{Sh_G}{Re_G\, Sc_G^{1/3}} = Q_3\, Re_G^{Q_4} \quad (3.28)$$

$$\textit{where:}\quad Sh_L = \frac{K_{OL}A}{C_L D_L},\quad Sc_L = \frac{\mu_L}{\rho_L D_L},\quad Re_L = \frac{d_t v_L \rho_L}{\mu_L}$$

$$Sh_G = \frac{K_{OG}A}{C_G D_G},\quad Sc_G = \frac{\mu_G}{\rho_G D_G},\quad Re_G = \frac{d_t v_G \rho_G}{\mu_G}$$

d_t = diameter of column (m)
v = superficial velocity (m/s)
μ = viscosity (Pa·s)
ρ = density (kg/m^3)
C = total concentration (mol/m^3)
D = diffusivity (m^2/s)
Q_n = constants to be determined

In (3.28), the mass transfer coefficients are correlated with a single Reynolds number because there is only one independent flow rate in the column. Since the column is operated at total

reflux, the liquid and vapour molar flow rates are not independent variables. Therefore, we cannot independently assess the impact of the flow rate of each phase. Equation (3.28) also involves the Sherwood number (Sh). This is a dimensionless group which is commonly encountered in mass transfer correlations, and is a ratio of convective mass transfer to diffusive mass transfer.

Finally, it should be stressed that this is a simplified treatment of a complex issue. Since distillation does not strongly influence the reaction rate of the aldol condensation of acetone, a more detailed treatment is not required. However, when systems with reagents that exist primarily in the gas phase are being considered, such as the production of cumene or MTBE, vapour-liquid mass transfer must be treated more rigorously. In such situations, the use of overall mass transfer coefficients would likely be unacceptable.

3.4.2 Vapour-Liquid Mass Transfer - Experimental

The ethanol/1-propanol binary system was selected for these experiments. Ethanol denatured with 5 wt% methanol (BDH, Toronto) and Omnisolv grade 1-propanol (BDH, Toronto) were used. Some properties of these pure solvents are shown in Table 3.4.2-I. A very important consideration in selecting these compounds was that they have similar molar heats of vaporization. Thus, equimolar counter diffusion and constant molar flow rates in the distillation column can be assumed without introducing excessive error.

These experiments were conducted in a 1 inch (2.54 cm) diameter x 1.2 m glass distillation column. A schematic diagram of the column is shown in Figure 3.4.2-1. The liquid (and vapour) flow rates in the column were estimated from a calibration of the reboiler. A correlation was developed relating the power used to produce vapour with the power supplied to the reboiler, Vapour (J/s) = 0.7194 W - 14.074, where W is in units of Watts.

Five catalyst bags, filled with IRA-900 ion exchange resin in the chloride form (maximum operating temperature is 77°C in the chloride form), were packed into the column giving a total height of 0.7 m. The column was then carefully insulated to reduce heat loss.

Table 3.4.2-I: Some properties of ethanol and 1-propanol.

Property[a]	Ethanol	1-Propanol
Molecular Wt. (g/mol)	46.07	60.10
Boiling Point (°C)	78.3	97.2
ΔH_{VAP} at 88°C (kJ/mol)	38.6	41.2
Density at 20°C (g/mL)	0.789	0.804
Vapour viscosity (90°C, μP)	105	90
Liquid viscosity (90°C, cP)	0.363	0.555
Vapour Diffusivity (cm^2/s) (90°C)	9.56×10^{-2}	-
Liquid Diffusivity (cm^2/s) (60% EtOH at 90°C)	4.45×10^{-5}	-

[a]Taken or estimated from Reid et. al. (1987)

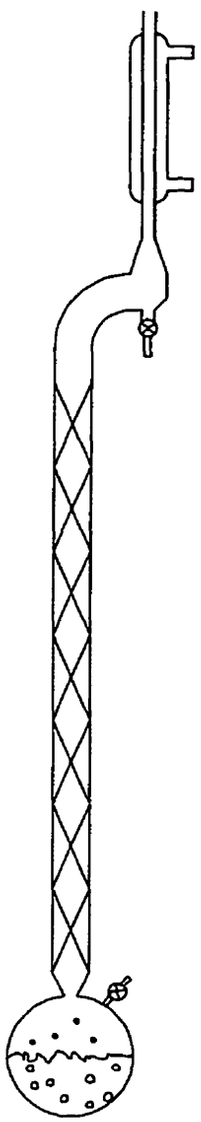

Figure 3.4.2-1: Schematic of the bench scale column.

The reboiler (a round bottom flask) had a capacity of 1 L, and approximately 0.7 L of the alcohol mixture was charged at the beginning of the distillation. The condenser water was turned on, and power was started to the reboiler. Once liquid flow in the column was established, some overhead product was removed until the methanol (used to denature the ethanol) concentration in the condenser was negligible. The column was operated at total reflux, and small liquid samples were removed from the reboiler and condenser until steady state was reached. The samples were analysed on the Perkin Elmer Autosystem GC with the 0.32 mm x 30 m DB-Wax column. Once a steady state was confirmed, the reboiler duty was changed and a new steady state was evaluated.

Literature VLE data for the ethanol/1-propanol system is available (Gmehling and Onken, 1977). These data are plotted in Figure 3.4.2-2, and show that the behaviour is nearly

ideal. The slope of the linear approximation (m) was taken to be 0.6887, and the intercept (b) was 0.3292. These values are substituted for m and b, respectively, in equation (3.27), and reasonably approximate the equilibrium data between $0.30 < x_{EtOH} < 0.94$.

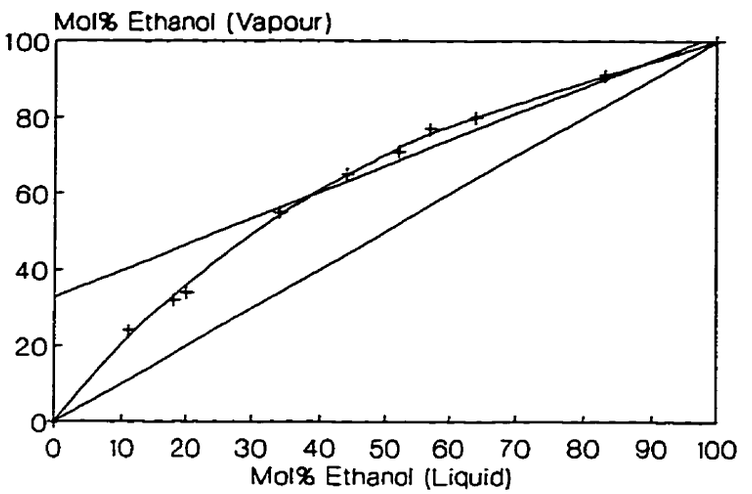

Figure 3.4.2-2: VLE diagram for ethanol/1-propanol at 101.3 kPa, and the linear approximation to the VLE data.

3.4.3 Vapour-Liquid Mass Transfer Coefficients

Distillations were conducted at seven different reboiler duties, resulting in seven different flow rates inside of the distillation column. The results of these experiments are shown in Table 3.4.3-I. The data in this table were used to find the values of the constants Q_n in equation (3.28), and the final correlations are shown in equation (3.29).

$$j_L = \frac{Sh_L}{Re_L\, Sc_L^{1/3}} = 3.186\, Re_L^{-0.202} \qquad j_G = \frac{Sh_G}{Re_G\, Sc_G^{1/3}} = 0.303\, Re_G^{-0.212} \qquad (3.29)$$

Plots of the predicted and measured values of $K_{OL}A$ and $K_{OG}A$ are provided in Figures 3.4.3-1 and 3.4.3-2, respectively. These plots show that there is good agreement between the experimental data and equation (3.29).

Table 3.4.3-I: Results from the vapour-liquid mass transfer experiments.

Power (W)	G or L (mol/min)	x EtOH reboiler	x EtOH distillate	NTU_{OG}	HTU_{OG} (m)	$K_{OG}A$ (mol/m.s)	j_G	NTU_{OL}	HTU_{OL} (m)	$K_{OL}A$ (mol/m.s)	j_L
71	0.0554	0.3570	0.9404	4.6316	0.1511	0.0061	0.1019	3.1898	0.2195	0.0042	2.2859
102	0.0887	0.3495	0.9026	3.8545	0.1816	0.0081	0.0848	2.6546	0.2637	0.0056	1.9024
141	0.1308	0.3699	0.8922	3.5499	0.1972	0.0111	0.0781	2.4448	0.2863	0.0076	1.7520
190	0.1834	0.3532	0.8658	3.1897	0.2195	0.0139	0.0702	2.1968	0.3187	0.0096	1.5742
238	0.2349	0.3463	0.8638	3.1932	0.2192	0.0179	0.0703	2.1991	0.3183	0.0123	1.5759
297	0.2981	0.3335	0.8633	3.2536	0.2151	0.0231	0.0716	2.2408	0.3124	0.0159	1.6058
365	0.3717	0.3553	0.8694	3.2353	0.2164	0.0286	0.0712	2.2282	0.3142	0.0197	1.5968

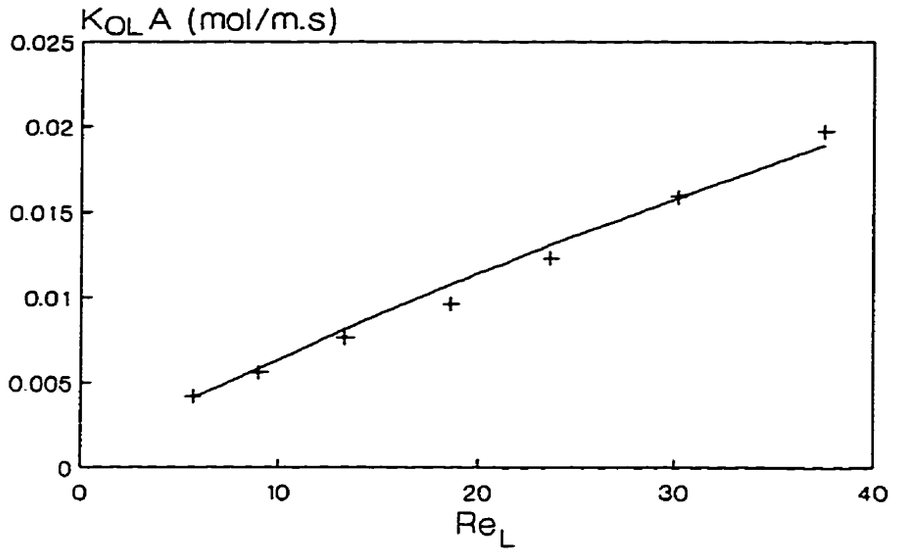

Figure 3.4.3-1: Overall liquid phase mass transfer coefficients as a function of the liquid phase Reynolds number.

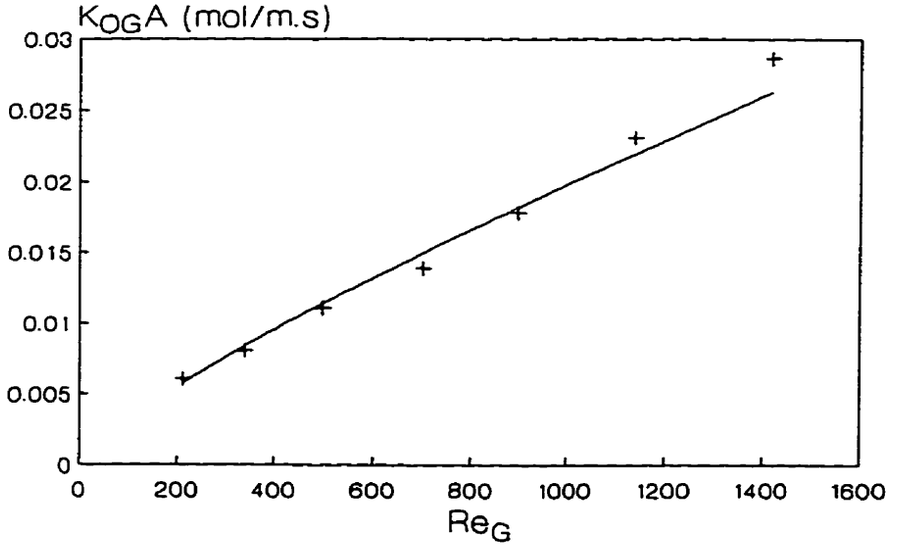

Figure 3.4.3-2: Overall gas phase mass transfer coefficients as a function of the gas phase Reynolds number.

The values of the parameters Q_1 - Q_4 in equation (3.29) were found by non-linear regression. In the equation for j_L, the 95% confidence intervals for Q_1 and Q_2 are 3.186 ● 0.814 and -0.202 ● 0.094, respectively. In the equation for j_G, the 95% confidence intervals for Q_3 and Q_4 are 0.303 ± 0.180 and -0.212 ● 0.094, respectively.

Previous work in a larger distillation apparatus shows that the height equivalent to a theoretical plate (HETP) for these types of CD structures is a strong function of the flow rates in the column (Cox, 1989). The definitions of HETP and HTU_{OG} are different and are related by equation (3.30).

$$HETP = \frac{HTU_{OG} \ln(mG/L)}{(mG/L - 1)} \qquad (3.30)$$

For an ideal system at total reflux and of low relative volatility, values of HETP and HTU_{OG} are virtually identical (Perry, 1984). These conditions were satisfied in the work conducted by Cox (1989). The HETP for a CD bundle was reported to be 6 ft (1.8 m) at a vapour velocity of 7.45 ft/s, and 12 ft (3.6 m) at a vapour velocity of 3.6 ft/s (Cox, 1989). This compares with an experimental HETP value of 2.4 ft (0.73 m) for 1" pall rings, which was independent of vapour velocity (Cox, 1989). These data suggest that catalyst bundles are poor distillation packings. Cox's data also demonstrate that when vapour (and liquid) velocities are increased, the value of HETP decreases.

Table 3.4.3-I, however, shows a very different trend. Contrary to Cox's data, the values of HTU increase when the vapour and liquid flow rates are increased. Our data were taken at superficial vapour velocities between 0.054 and 0.362 m/s (.17 and 1.2 ft/s), which were much lower than Cox's velocities. The vapour velocitites in this work were all much lower than Cox's velocities since smaller distillation packings were used, and smaller packings flood at lower velocities. However, this work covers a wide range of vapour velocities, and some of the lower velocities were far below the capacity of the packing. The heat loss from the insulated column may have also comprised a significant portion of the total heat input to the column at such low velocities. Due to this heat loss, the liquid and vapour flow rates may have been different from their expected values, and the mass transfer coefficients may have

also been affected. For these reasons, the data at low flow rates are likely somewhat unreliable.

At 190 W, the value of $K_{OG}A$ was 0.0139 mol/m·s. At similar flow velocities, the value of k_GA (gas-side only) from the work of Zheng and Xu (1992) is 0.2 mol/m^3·s·kPa. To convert the units of this value to match our units, we must multiply by the pressure of the system and by the volume of the column per unit height. This gives a value of 0.033 mol/m·s, which is more than twice the value of our result. One would expect the catalyst structure used by Zheng and Xu to provide better contact between the vapour and liquid phases because of the larger number of bags used and the larger surface area available for mass transfer. Zheng and Xu's result may also be higher since it does not take into account mass transfer resistance from the liquid phase. It is reassuring, however, to see that these data agree within an order of magnitude. Unfortunately, a lack of information in Zheng and Xu's (1992) paper prevents us from extracting the liquid side coefficients, and therefore, from comparing our result with an overall coefficient from Zheng and Xu's work.

The value of the exponents in (3.29) is near -0.2 for both of the overall liquid and vapour phase correlations developed in this thesis. The exponents of the liquid-side and gas-side correlations from Zheng and Xu (1992) were -0.7 and -0.08, respectively. The exponent for the gas phase correlation is fairly close to our value, but their liquid phase exponent is not close. This suggests that the rate of mass transfer in Zheng and Xu's column is much more sensitive to the liquid flow rate.

-4-

PHASE III - CATALYTIC DISTILLATION EXPERIMENTS

Batch and continuous CD experiments were conducted to measure catalyst activity and product selectivity. The results in Section 3.1.5 showed a much lower DAA activity and much lower ratios of DAA:MO when a catalyst bag is used in a batch reactor. Since the catalyst is bagged in the CD process, one would expect the catalyst activity and DAA:MO ratios from the CD column to be much lower than in batch reactions with loose catalyst.

4.1 Batch Catalytic Distillation Experiments

The purpose of the batch CD experiments is to study the effect of changing the liquid flow rate on the product selectivity, and catalyst activity.

In order to model the CD process, however, some knowledge of the liquid flow patterns inside of the column is required. These experiments were conducted in the bench-scale glass column, which permitted a visual inspection of the flow pattern. It was confirmed that some of the liquid flow in the column flows through the catalyst bag, while most of the flow in the column bypasses the bag. The flow pattern in the column is an extremely important variable, as it directly influences mass transfer rates in the column. Since the liquid is distributed over the catalyst bags by a layer of random packing, a brief discussion of flow patterns in random packing is worthwhile.

It is known that a uniform liquid distribution is vital in achieving optimum performance from any random packing. Perry et. al. (1990) and Harriot (1989) provide good examples of the liquid distribution influencing the performance of packed columns. In one example, the number of theoretical stages in an existing ethylene oxide absorber was doubled by simply improving the liquid distribution (Perry et. al., 1990).

Liquid flow in a packed column is inherently non-uniform because of the random arrangement of the packing and the limited number of liquid distribution points. Early workers in this area suggested that the spread of liquid in a column is analogous to a 'random walk', and Porter (1968) agrees that this is suitable for the first liquid droplets which pass through the column. Once this vanguard of liquid wets certain paths through the packing, however, the liquid which follows flows along these paths in the form of rivulets. Since the liquid flow is confined to these preferred paths, local flow rates may actually be several times higher than the average (Hoek et. al., 1986). Thus, the flow pattern in a packed column is established in a random way, then tends to remain stable with respect to time.

Engineers have historically been reluctant to rely on large-scale packed columns since their unpredictable performance necessitates the use of large safety factors, which increases the size and cost of the equipment. The uncertainty associated with predicting mass transfer rates in packed columns is generally ascribed to the impossibility of controlling the flow in packed beds (Hoek et. al., 1986). Only in the past 10 years, with significant advances in liquid distributors and structured packings, have large diameter packed columns made inroads in the chemical industry (Porter, 1995).

It is accepted that packings have a natural or equilibrium flow distribution (Hoek et. al., 1986). If the initial liquid distribution is more uniform than the natural distribution, the flow pattern rapidly deteriorates to the natural distribution within 10 layers of packing. If the initial distribution is more non-uniform, then the flow pattern also tends toward the natural distribution, but this occurs much more gradually.

Perhaps the most important type of liquid maldistribution in small columns is wall flow. When a random packing is dumped into a column, the column wall interferes with the random arrangement of the packing elements. This results in wide variations in void fraction in the radial direction up to a distance of two particle diameters from the column wall. Figure 4.1-1 provides an example of the changes in void fraction as a function of the column radius for a spherical packing (Papageorgiou and Froment, 1995). Owing to the high void fraction of the packing near the column wall, there is less resistance to flow and the liquid tends to accumulate in this region of the column.

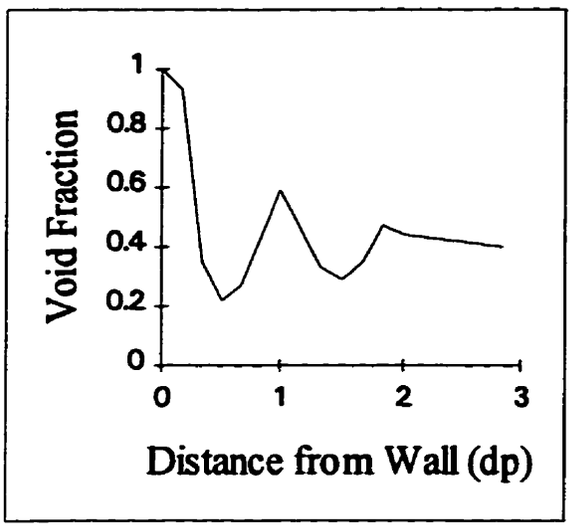

Figure 4.1-1: A plot of void fraction vs. the number of particle diameters away from the column wall (d_p) for spheres with $d_t/d_p = 5.8$ (from Papageorgiou and Froment, 1995).

Different workers have suggested the empirical rule that the ratio of the column diameter to the packing diameter (d_t:d_p) be greater than 8:1, 10:1, or 25:1 to avoid severe wall effects. Such large column diameters ensure that most of the liquid flow remains in the packing (Porter and Templeman, 1968). A 1" diameter column and ¼" Intalox saddles were used for our CD experiments, making our value of d_t:d_p = 4. This is a low value, and suggests that wall effects will significantly influence these results.

Although wall effects reduce the efficiency of absorption or distillation columns, they are far more serious in packed bed reactors. Gas-liquid mass transfer still occurs with liquid flowing down the wall of a column, albeit at a reduced rate. Wall flow in a fixed bed reactor, however, bypasses the catalyst altogether. This leads to lower conversions, and different selectivity when compared to the case of uniform flow.

Porter and Templeman (1968) provide valuable insight into the wall effect. Various sizes of packings and columns were used to determine the percentage of liquid flowing along the wall. These data are shown as a function of the d_t:d_p ratio and the total liquid flow rate in Figure 4.1-2. The fraction of liquid flowing along the wall decreases as the liquid flow rate increases. The results also show a very large drop in the percentage wall flow as d_t:d_p increases. Clearly, wall effects will be much more pronounced in bench-scale and laboratory equipment when compared to production-scale equipment. This is one of the major difficulties encountered when attempting to scale-up any type of packed column.

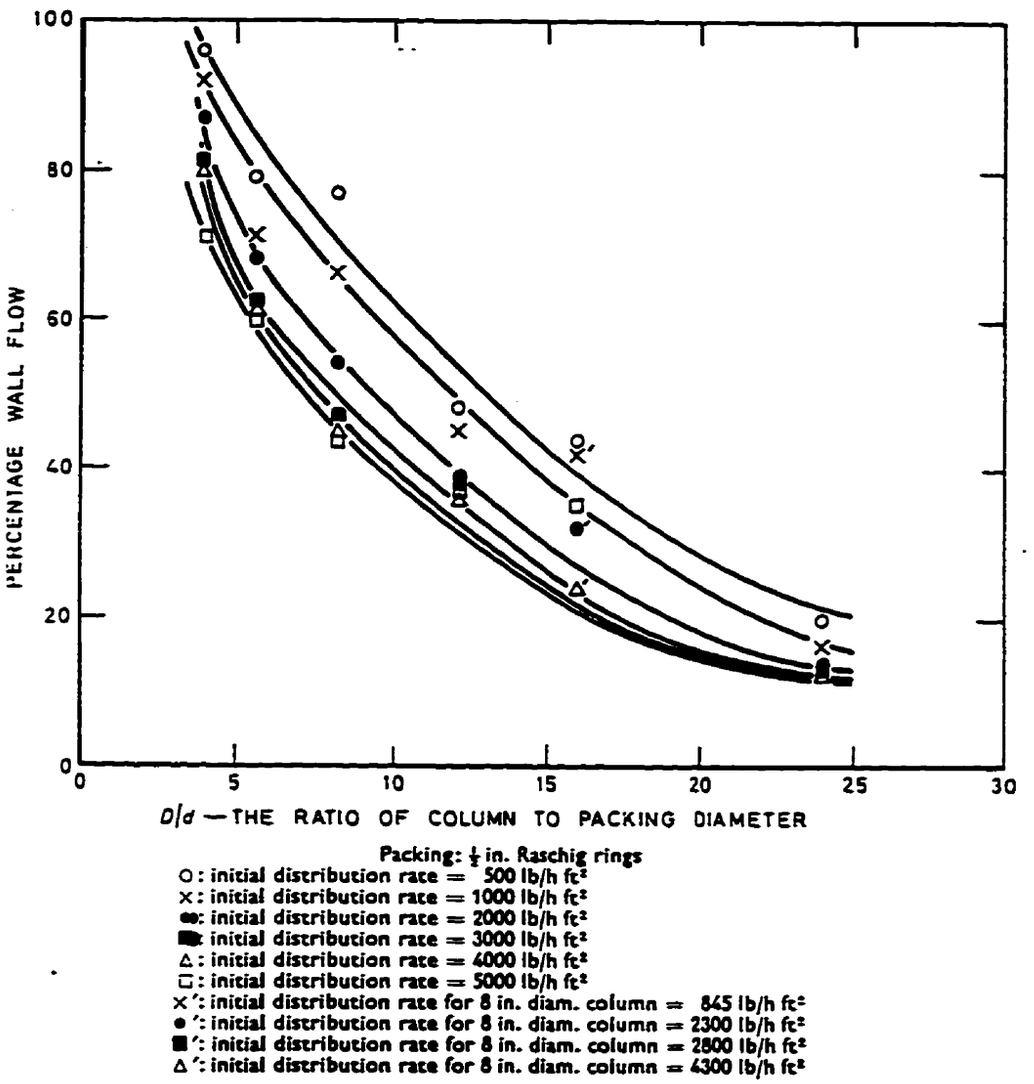

Figure 4.1-2: The 'percentage wall flow' determined with water at various flow rates as a function of d_t/d_p (Porter and Templeman, 1968). Reprinted, with permission, from *Trans. Instn. Chem. Engrs.*, ©The Institution of Chemical Engineers, 1968.

4.1.1 Batch CD Experiments - Experimental

Batch CD experiments were conducted in the glass column described in Section 3.4.2. A schematic diagram of the column is shown in Figure 3.4.2-1. The catalyst for this work was tested in a batch reaction at 54°C with 100 mL of acetone and 2 mL of catalyst, and gave k_1=0.37 x 10^{-3} M^{-1} min^{-1} and k_2=0.001 M min^{-1}. This catalyst was packed into fibreglass bags which were approximately 1.5 cm in diameter and 11 cm tall, then wrapped in demister wire to form a bundle. Each bag was filled with catalyst, then the top of the bag was sewn closed with about 4 or 5 stitches. This method of packing the catalyst was patented by Smith (1984), and an full scale diagram of a typical catalyst bundle is shown in Figure 4.1.1-1. Since several different bags were used in these experiments, a slightly different amount of catalyst was used in each experiment. Typically, each bag was packed with 17 mL of catalyst soaked in isopropanol (22 mL if soaked in water). The catalyst would then shrink to approximately 15.2 mL in the presence of acetone. At least 10" (25 cm) of Intalox saddles were dumped above the catalyst bundle. This packing was intended to help distribute the liquid above the catalyst bag, and mimic the operation of the pilot scale CD column. The remainder of the column below the catalyst (50 cm) was also filled with ¼" Intalox saddles to improve distillation.

At the start of an experiment, the 1 L reboiler was charged with 750 mL (592.5 g) of acetone. Heating commenced, and a stop-watch was started when the acetone vapour was seen to make contact with the catalyst bag. The time at which each sample was removed from the reboiler was noted. The sample analysis was identical to the procedure outlined in Section 3.1.2. All of the reaction products are much less volatile than acetone, and they accumulate in the reboiler. Since the liquid holdup in the column is small compared to the capacity of the reboiler, essentially all of the DAA, MO, isophorone, and water produced to that point are considered to be in the reboiler.

Experiments were also conducted to measure the liquid flow rate that passes through the catalyst bag. A special catalyst bag was prepared with a small glass funnel at the bottom to direct the liquid flow into a small tube. The tube then carried the liquid outside the column where samples were timed and weighed to calculate the flow rate. A cross-sectional view of this arrangement is shown in Figure 4.1.1-2.

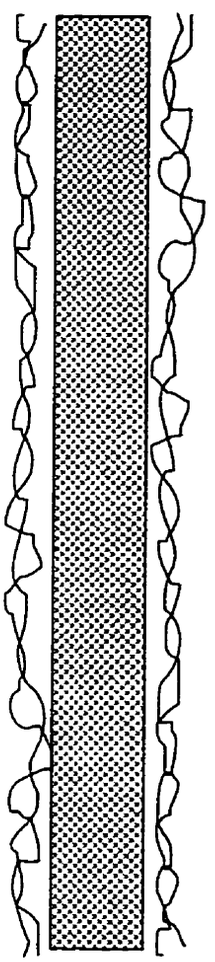

Figure 4.1.1-1: A diagram of the catalyst bundle (also called a 'Texas Tea Bag') used in the CD experiments (Smith, 1984).

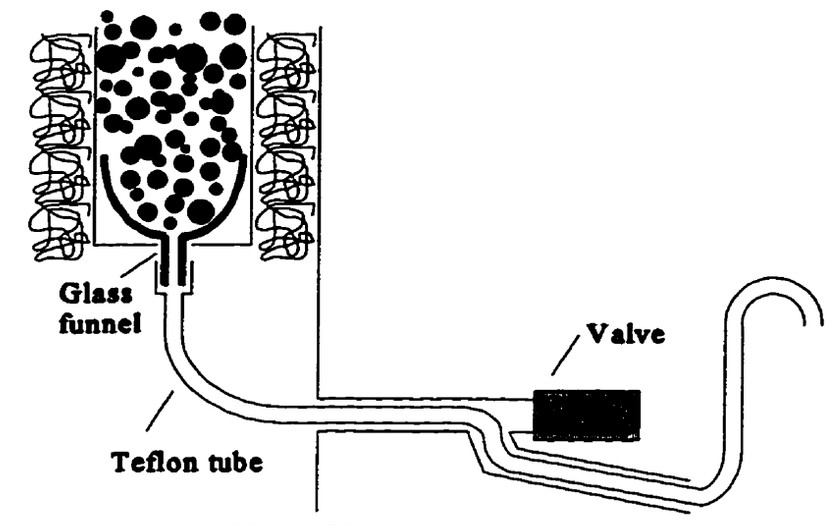

Figure 4.1.1-2: Cross-sectional view of the apparatus used to measure the liquid flow rate through the catalyst bag.

As shown in Figure 4.1.1-2, any liquid captured at the bottom of the catalyst bag passes through an existing valve in the wall of the column. The internal valve parts were removed to allow the passage of the Teflon tube through the fitting.

Most of the collected samples were 10 mL in volume, although several larger samples of 50 g were also obtained. The amount of energy which produces vapour is correlated to the total power input to the reboiler (W) by the relation *Vapour Production (J/s) = 0.7194 W - 14.074* (see Section 3.4.2). The total flow rate inside of the column was determined by dividing the rate of energy input by the enthalpy of vaporization of acetone (ΔH_{vap} = 520 J/g). Thus, the fraction of liquid which passes through the bag is calculated by dividing the mass flow rate of material through the tube by the total flow rate inside of the column.

4.1.2 Fraction of Liquid Flowing Through the Bag

The flow rate of liquid inside of the bag was measured at four different reboiler power settings. Thus, four different flow rates of liquid and vapour were tested. Table 4.1.2-I provides a summary of the experimental results.

Table 4.1.2-I: Values of f determined at various liquid flow rates.

Power Setting (V)	Total Liquid Flow (g/min)	Total Liquid Flux ($lb/h \cdot ft^2$)	Fraction of liquid flowing inside of the bag (f) Test 1	Test 2	Test 3
55	5.49	133	$.12^3$ $.21^3$	$.85^2$ $.82^2$	0.73^2
65	8.76	212	$.16^2$ $.29^4$	$.42^1$ $.53^1$	0.64^1
75	12.27	296	$.36^5$ $.36^5$	$.62^3$	
85	16.36	396	$.39^1$ $.28^1$ $.33^1$ $.51^6$ $.43^6$	$.66^4$	

$^{1,2,3...}$ indicates the order in which the measurements were made

The results in Table 4.1.2-I demonstrate that random packings are, in fact, random. At a $d_t:d_p$ ratio of 4, Porter and Templeman (1968) report that 70-95% of the total flow occurs along the wall. Thus, only 5-30% of the total flow should have a chance of contacting the catalyst bag. While many of the observations in Table 4.1.2-I are within this range, there are many which are not even close. This may be a result of the relatively short section of packing above the catalyst bag. The liquid was introduced at a point in the center of the column, and it may take up to 24" (61 cm) of packing before the wall flow builds up to its equilibrium level (Hoek et. al., 1986). The columns used by Porter and Templeman (1968) were always tall enough to ensure that the equilibrium flow pattern was attained. The column used for this work, however, had only 10" (25.4 cm) of packing above the catalyst bag. Thus, the equilibrium flow distribution may not have been established when the measurements were taken. This could explain some of the unusually high values of f observed in Table 4.1.2-I.

Porter and Templeman's data (1968) show that a lower fraction of the liquid tends to flow down the wall of a column at higher flow rates. The data in Table 4.1.2-I does not show

any clear pattern as flow rates are increased. However, the 'Total Liquid Fluxes' in Table 4.1.2-I are all quite low when compared to Porter and Templeman's work. Hoek et. al. (1986) indicate that once a flow pattern is established in a packed column, the flow pattern then tends to remain stable with respect to time. Our data seem to support this observation. Note that values of f seem consistently high during Test 2, and consistently low in Test 1.

More consistent values of f may be possible with taller sections of random packing above the catalyst, larger diameter columns, and improved liquid distributors. It is possible to use a taller section of packing above the catalyst zone in the pilot scale CD column in Section 4.2, and the use of a liquid distributor is also discussed in Section 4.3. Despite these steps to reduce the variability of f, however, it seems clear that an accurate prediction of the value of f is impossible.

4.1.3 Results from the Batch CD Experiments

The first batch CD experiment was conducted at a reboiler setting of 85 V, which provided an acetone flow rate of 16.36 g/min, and the catalyst bag was filled with 17 mL of catalyst. Figure 4.1.3-1 shows a plot of the amount of DAA, MO, and isophorone in the reboiler and the boiling temperature as a function of time.

Initially, the amount of DAA increases linearly as a funciton of time, which indicates constant catalyst activity. However, DAA production cannot continue indefinitely. The composition of DAA in the vapour will slowly increase over time until it reaches the reaction equilibrium concentration of 4.3 wt% DAA, at which point DAA production will stop. This time is reached after approximately 20 h of operation, and the liquid in the reboiler is 54.2 wt% DAA. Although the net production of DAA is halted by equilibrium, the production of MO and water continues. This is clearly shown in Figure 4.1.3-1. After approximately 51 h of operation, there is actually more MO in the reboiler than DAA. This experiment also produced significant amounts of isophorone. Unfortunately, the production of isophorone was unexpected and the GC method was not programmed with enough time to allow the

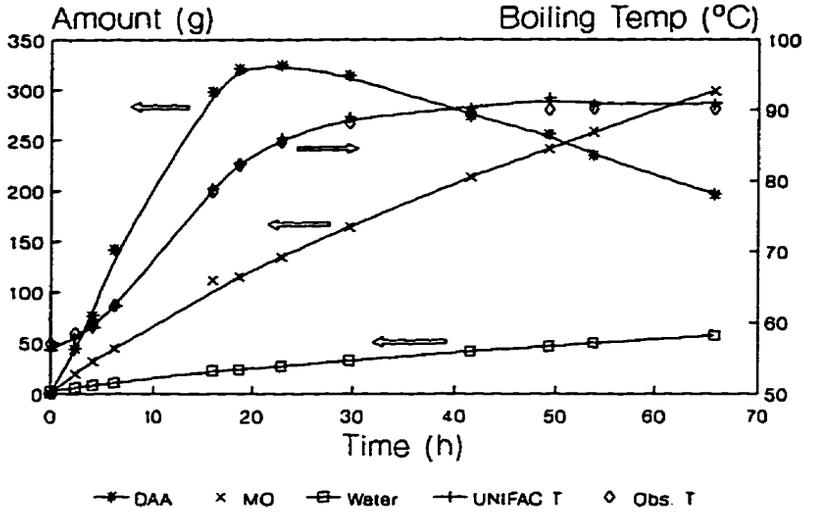

Figure 4.1.3-1: Amounts of DAA, MO and Water produced and the reboiler temperature vs. time in a batch CD experiment at 16.36 g/min.

isophorone to be quantified. This oversight was corrected in subsequent experiments.

Figure 4.1.3-1 also provides an opportunity to compare the observed boiling temperature (Obs. T) with predicted temperatures (UNIFAC T) based on the reboiler composition. Predictions based on ideal vapour-liquid equilibrium (VLE) behaviour were unacceptable, and activity coefficients of acetone, DAA, MO, and water were calculated with the UNIFAC method (Smith and Van Ness, 1987). Activity coefficients are plotted as a function of time in Figure 4.1.3-2. This graph shows that MO and water are primarily responsible for the non-idealities. This is not surprising since MO and water are mutually insoluble. The calculated and observed temperatures, shown in Figure 4.1.3-1, are in good agreement even though isophorone was not accounted for in the VLE equations.

There is some non-linearity to the MO vs. time data in Figure 4.1.3-1, which could indicate a very slow rate of catalyst deactivation. Unlike the CSTR experiments (see Section 3.2.3), however, the catalyst remains active for a very long period of time in the CD column.

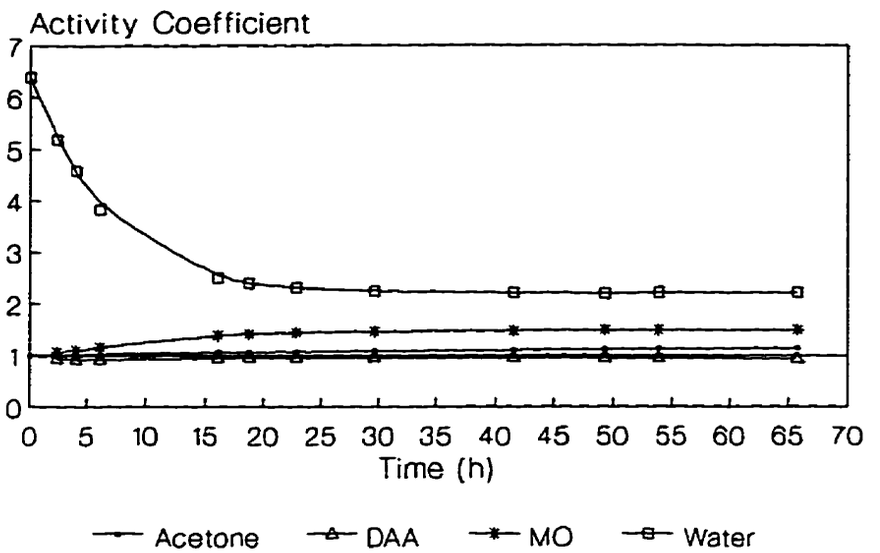

Figure 4.1.3-2: The activity coefficients of acetone, DAA, MO, and water during the batch CD experiment depicted in Figure 4.1.3-1.

The catalyst lifetime in the batch CD column is excellent, and the following three factors are likely responsible:

1) The catalyst is not subjected to a continuous flow of fresh acetone, which means that there is a fixed amount of the acid impurity which can deactivate the catalyst. Once this acid is neutralized by some of the catalytic sites, this deactivation mechanism is no longer a concern.
2) The reaction products are continuously removed from the reaction zone. This slows the rate of formation of heavy byproducts which lead to catalyst deactivation. The rate of product removal from the CSTR is much slower than the batch CD column because of the long residence time (approximately 1 h).
3) Water concentrations in the reaction zone of the batch CD column are higher than in the batch reactor and CSTR. It will be shown in Section 5.1.6 that an azeotrope exists between acetone and water. This azeotrope ensures that the concentration of water in the reaction zone of the column is at *least* 0.7 wt%, whereas only 0.4 wt% water was present in most

batch reactions and CSTR experiments. In Section 3.2, it was clearly demonstrated that the addition of water to the ACS Reagent grade acetone improves the lifetime of the catalyst.

To gather more information about the CD process, four additional batch CD experiments were performed in the glass column. These experiments were conducted at reboiler settings of 55 V, 65 V, 75 V, and 85 V. Composition vs. time data for all of the batch CD experiments is available in Appendix G. Figure 4.1.3-3 shows data from an experiment conducted with 22.3 mL of catalyst and the reboiler at 75 V (12.27 g/min). These results confirm that isophorone (IP) production is slow. The MO data in Figure 4.1.3-3 is also non-linear. This is similar to the trend observed in batch experiments (see Figure 3.1.3-1), but the non-linearity exists over a much longer time frame. The curvature of the MO vs. time data warrants further attention. A comparison of MO data from experiments at 55, 65, 75, and 85 V can be made by examining Figure 4.1.3-4.

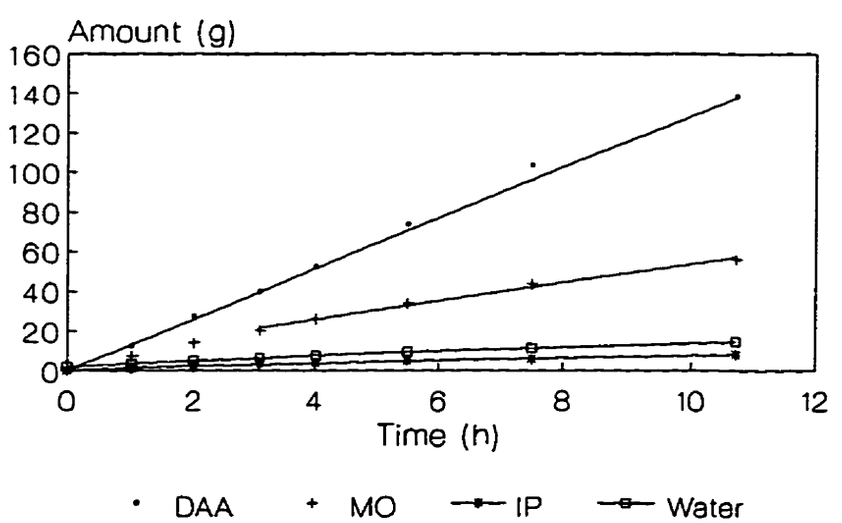

Figure 4.1.3-3: Results from a batch CD experiment with 21.4 mL of catalyst at a reboiler rate of 12.27 g/min (heater set to 75V).

Figure 4.1.3-4 shows clearly that higher flow rates (higher reboiler duties) result in higher production rates of MO. The MO vs. time data at the lowest reboiler setting (55 V) is very nearly linear, whereas the data obtained at 85 V exhibits very noticeable curvature. The initial activity (slope of the MO vs. time curve) of the catalyst at 85 V is quite high, but lessens over the course of the experiment. However, the deactivation is not as serious as observed in the CSTR. As shown in Figure 4.1.3-1, the production of MO continues for a very long period of time.

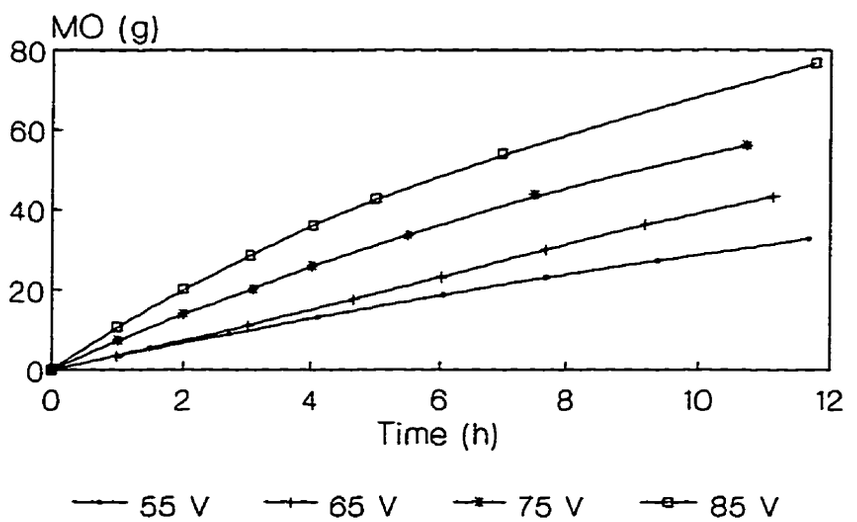

Figure 4.1.3-4: MO vs. time plots for the batch CD experiments conducted at reboiler settings of 55, 65, 75, and 85 V.

As the catalyst deactivates, the rate of catalyst deactivation becomes slower. The catalyst undergoes a fairly rapid initial deactivation, but eventually appears to reach a "steady state" activity. The term "steady state" is placed inside of quotations because it is not a true steady state; catalyst deactivation still occurs, but at a very much reduced rate. The same behaviour was observed in a batch reactor, with the catalyst reaching "steady state" after 20 - 30 minutes of reaction (see Figure 3.1.3-1). Initial deactivation is hard to detect in the batch

CD column at 55 V, which indicates that initial deactivation may occur fairly quickly at low flow rates. High flow rates (ie. a higher voltage setting), however, are able to stave off this initial catalyst deactivation for several hours. This is likely due to faster rates of product removal at higher reboiler duties, which discourage the formation of high molecular weight byproducts that deactivate the catalyst.

When reporting the MO production rates, therefore, it was decided to take the slope of the line near 10 h. This allows time for the catalyst to deactivate toward its "steady state" activity. Thus, a more meaningful comparison of the batch CD results with the batch reaction data, which were reported after 20 minutes, can be made.

A summary of the batch CD experimental data is available in Appendix G, and the results from all of the experiments presented in Figures 4.1.3-4 and 4.1.3-1 are summarized in Table 4.1.3-I. Two important trends are evident from this data. Firstly, the DAA production rate increases very significantly as the reboiler duty (the liquid flow rate) is increased. The DAA activity increases because the production rate of DAA is limited by mass transfer rather than kinetics. Higher reboiler duties provide higher flow rates through the bag, which increase mass transfer rates and the DAA productivity. Secondly, there is a trend of increasing MO productivity as the reboiler duty increases. MO and water are both produced inside of the catalyst bag, and must be transferred out of the bag. At higher reflux flow rates, MO and water should both be removed from the bag more promptly, and their average concentrations inside of the bag should be lower. As clearly demonstrated in Section 3.1.4, lower concentrations of water generally lead to higher MO activities. This suggestion is investigated further in Section 4.3.

It is interesting to compare the results obtained from loose catalyst in the batch reactor with the results reported in Table 4.1.3-I. In a batch experiment at 54°C with 100 mL of acetone and 2 mL of this catalyst, $k_1 = 0.37 \times 10^{-3}\ M^{-1}\ min^{-1}$. If the decomposition of DAA to acetone is ignored, an activity of 21.04 g DAA/mL_{cat}·h is theoretically possible. This is initially achieved in batch reactions when [DAA] = 0 M, and is very much higher than any of the DAA activities reported in Table 4.1.3-I. Clearly, the production of DAA is extremely sensitive to mass transfer effects.

Table 4.1.3-I: Results from batch CD experiments.

Reboiler Duty Setting (V)	Flow Rate (g/min)	Amount of Catalyst[a] (mL)	DAA Activity ($g/mL_{cat} \cdot h$)	MO Activity ($g/mL_{cat} \cdot h$)	Selectivity (mol DAA/ mol MO)
55	5.49	20.5	0.11	0.12	0.760
65	8.76	21.8	0.33	0.17	1.685
75[b]	12.27	21.4	0.60	0.18	2.848
85[c]	16.36	17.0	1.07	0.23	3.946
85	16.36	23.3	1.54	0.20	6.405

[a]batch reaction at 54°C: $k_1 = 0.37 \times 10^{-3}\ M^{-1}\ min^{-1}$, $k_2 = 0.001\ M\ min^{-1}$
[b]shown in Figure 4.1.3-3
[c]shown in Figure 4.1.3-1

For the production of MO in a batch reactor, $k_2 = 0.001\ M\ min^{-1}$, which translates to an activity of 0.294 g $MO/mL_{cat} \cdot h$. This is higher than any of the activities in Table 4.1.3-I. One would expect water concentrations inside of the catalyst bag to be much higher than in the batch reactor because of the acetone/water azeotrope. The results in Figure 3.1.4-2 show that higher water concentrations reduce MO production rates. Therefore, the rate of MO production in the CD column should be lower than the batch reactor. However, the production rate of MO is not as sensitive to mass transfer conditions as the production of DAA. This is consistent with the zero-order nature of MO production which was observed in Section 3.1.

Table 4.1.3-I shows that the product selectivity depends heavily on the flow conditions in the CD column. With this catalyst in a batch reactor, the initial selectivity is 60.47 mol DAA/mol MO. This value is a theoretical maximum, however, since it assumes that there is no DAA decomposition to acetone. A more realistic measure of selectivity might be to stop a batch reaction after 15 minutes once $[DAA]_{EQ}$ is reached (see Figure 3.1.3-1). After 15 minutes, the product selectivity would be 18.67 mol DAA/mol MO. Although this is lower than the initial selectivity, it is still much greater than the results from any of the batch CD

experiments. The highest selectivity reported in Table 4.1.3-I is 6.405 mol DAA/mol MO. At the lowest flow rate studied, the amount of MO produced actually exceeds the amount of DAA.

It is also interesting to compare these batch CD results with the results of the batch experiments in which the catalyst was placed inside of a fibreglass "tea bag". These experiments were presented in Section 3.1.5. For the experiment with a stir speed of 2, the initial production rate of DAA was 0.8 g DAA/mL_{cat}·h. This is comfortably within the range of the results shown in Table 4.1.3-I. The product selectivity is also similar, being 2.4 mol DAA/mol MO in the batch reactor with bagged catalyst.

The importance of mass transfer when the catalyst is placed into a fibreglass bag is obvious. Significant gains in DAA production and product selectivity toward DAA formation are realized when the stir speed in the batch reactor is increased. Analogously, similar gains are realized in the batch CD column by increasing the reboiler duty, and thus, the liquid flow rate inside of the column.

4.2 Continuous Catalytic Distillation Experiments

In Section 4.1, the bench-scale glass CD column was used to study the effect of the liquid flow rate on the catalyst activity and product selectivity. This column is quite short, however, and is not able to hold more than one catalyst bag. In practice, the catalyst zone of a CD column could be much taller. The glass column is also not equipped to handle a continuous flow of acetone. To obtain continuous operating data from taller catalyst sections, some experiments were conducted in a much larger apparatus.

4.2.1 Continuous CD Experimental

Continuous experiments were conducted in the CD pilot plant at the University of Waterloo. This column is based on designs provided by Chemical Research & Licensing Co. (CR&L) of Houston, Texas. Descriptions of the column, its ancillary equipment, and detailed operating procedures were presented in earlier work (Podrebarac, 1992). A schematic diagram of the column is provided in Figure 4.2.1-1. This diagram shows the flow paths for the overhead and bottom products, and the preferred location of the catalyst zone for this work.

The column has a total height of 23 ft. (7 m) and a diameter of 1" (2.54 cm). This is the same diameter as the columns used to study mass transfer. The non-reactive sections of the column were packed with ¼" Intalox saddles. In the reactive section of the column, the catalyst was placed inside of fibreglass bags as described in Section 4.1.1. The bundles were spaced approximately 5 cm apart so that they would not be punctured by the thermocouples. The 3" (7 cm) gaps between the catalyst bundles were also filled with ¼" Intalox saddles to encourage mixing of the liquid phase and disrupt the flow path of the wall flow. The steps involved in conducting an experiment are briefly outlined below:

- Load the catalyst bags into the column, and purge the column with nitrogen.
- Charge approximately 500 mL of acetone into the reboiler.

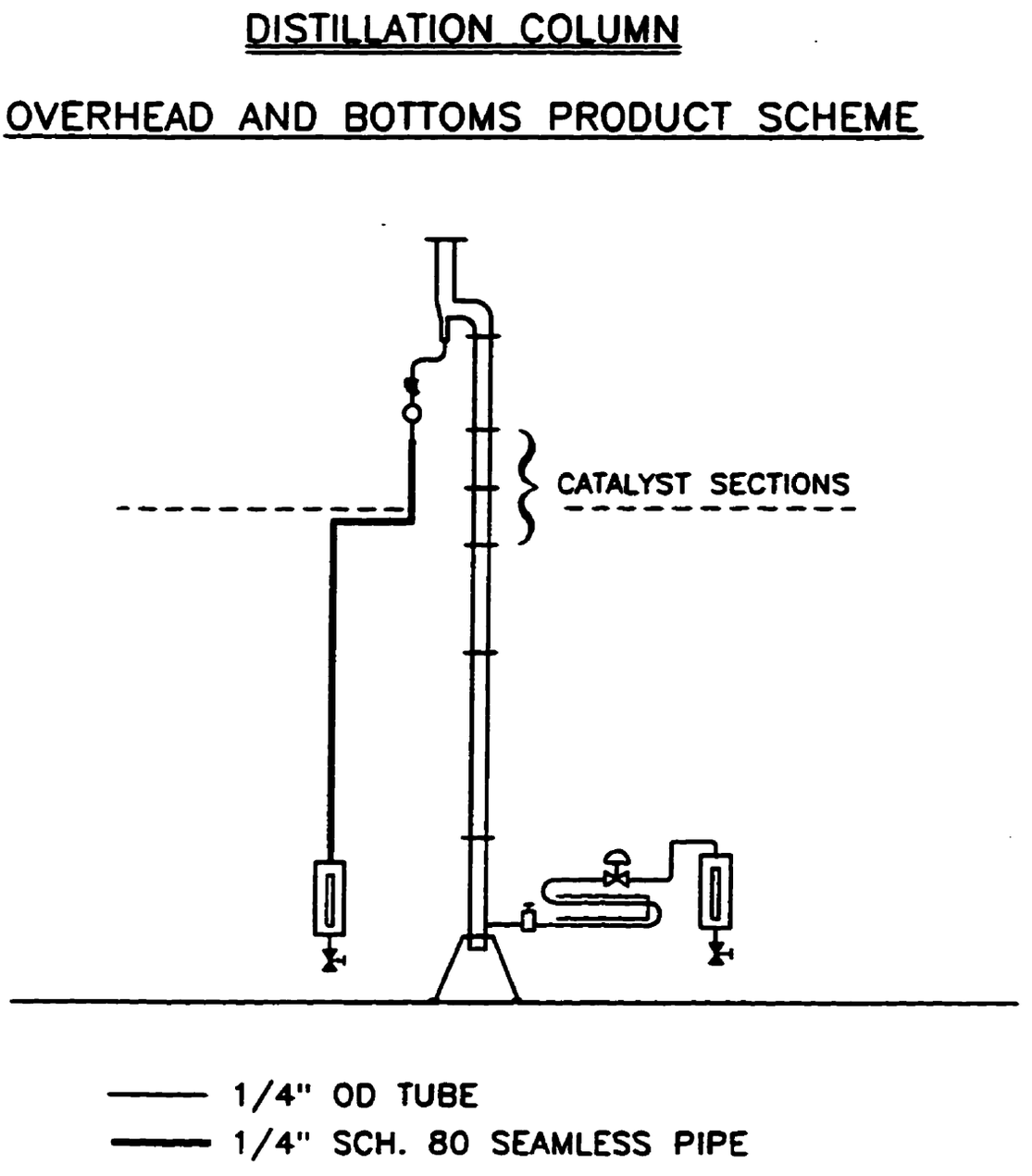

Figure 4.2.1-1: Schematic diagram of the pilot scale CD column.

- Start heating the reboiler at about 25% of its capacity (ie. 250 W), and wait for the column to reflux acetone. This takes 1 - 1½ h.
- Once operating at total reflux, the temperature in the reboiler should slowly increase from 56°C as DAA, MO, and water begin to concentrate. Leave the column refluxing for ½ h.
- Turn on the feed pump to start feeding acetone just below the catalyst zone. The feed point is located below the catalyst in an attempt to prevent catalyst poisons, such as acetic acid, from reaching the catalyst.
- Start the removal of bottom product at the same mass flow rate as the feed entering the column (no overhead product removal is required). This balance is achieved by manually maintaining a constant liquid level in the reboiler. Unfortunately, this is a source of error during these experiments. Due to turbulence in the reboiler, the liquid level can be difficult to read, and the operator can occasionally allow too much or too little liquid to flow out of the reboiler. The official start of an experiment (time "0") is taken to be the time at which the product removal from the reboiler is commenced.
- Keep the feed rate and product removal rate constant so that the product composition reflects the catalyst activity.

The flow rate of acetone to the column was purposely set much higher than the rate at which acetone can possibly be converted to DAA or MO by the catalyst. Thus, the overall acetone conversion was usually kept lower than 60%. With this operating procedure, one can be certain that the reaction rate in the column is not controlled by the availability of the reagent.

The product from the reboiler was immediately passed through a heat exchanger to reduce its temperature, and stored in 250 mL sample bottles. The sample bottles were kept on ice, and kept closed as much as possible to minimize evaporative losses of acetone. One bottle is capable of storing the product from 1½ h of operation. The samples were analyzed for water and organics with the same GC methods outlined in Section 3.1.2. Knowing the total mass of the sample, the composition of the sample, and the time taken to collect the

sample, one may calculate the production rate of each component. Other important data from the column, such as temperature profiles, differential pressure across the column, and heat duties, were recorded by a computer which monitors the column operation. Some variables, however, such as the condenser duty and the liquid feed rate supplied by the pump, must be recorded manually.

The packed section of the pilot scale CD column is approximately 17 feet (5.2 m) tall, and there is a considerable amount of heat lost between the reboiler and the condenser (Podrebarac, 1992). Thus, the liquid flow rates in the CD column should not be based on the reboiler duty, as was done with the short batch CD column. For the pilot scale CD column, the liquid flow rates were determined by measuring the condenser duty. Since the catalyst is placed quite close to the top of the column, this should yield satisfactory results. The condenser duty calculation is based on the flow rate of water in the condensing coil, and the temperature difference of the water between the inlet and outlet of the condensing coil.

4.2.2 Continuous CD Results

Figure 4.2.2-1 shows a plot of the composition of the bottom product vs. time for an experiment conducted with 4 catalyst bags. The catalyst for this experiment was exchanged to 0.49 mmol OH^-/mL in 24 h, and 91.26 mL of this catalyst was loaded into the column. The rate constants from this catalyst in a batch reaction at 54°C can be found in Table 3.1.3-V. The feed rate of acetone to the column was maintained at 152 mL/h. Although some isophorone (IP) is produced, its concentration never exceeds 1.2 wt%. As the catalyst deactivates, the composition of IP declines to .56 wt%. A similar decline is observed with MO production. The MO concentration reaches a maximum of 12 wt% from 7-8 h into the experiment, but eventually drops to 5.6 wt% after 45 h of operation. The declining MO and IP concentrations indicate that the catalyst is deactivating. However, there are no significant changes in the rate of DAA production. The rate of DAA production remains essentially

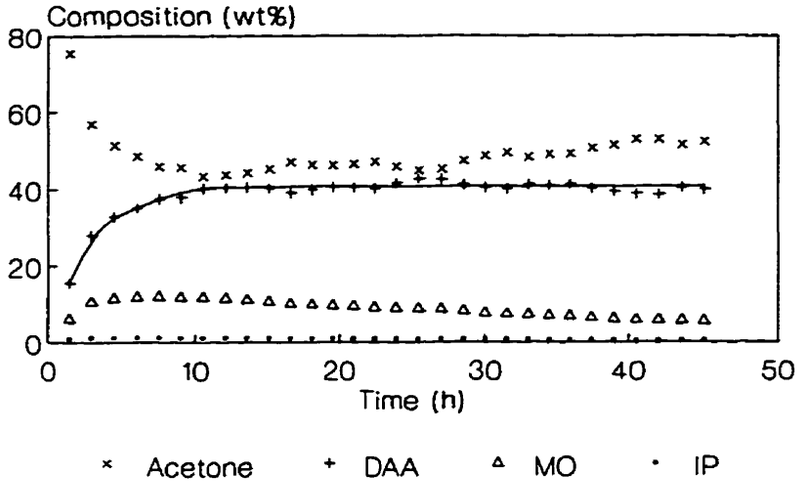

Figure 4.2.2-1: Liquid composition in the reboiler during the continuous CD experiment with 91.26 mL of catalyst in 4 catalyst bags and an acetone feed rate of 152 mL/h (see Expt. #3 in Table 4.2.2-II).

constant because it is limited by mass transfer rather than kinetics. If the experiment in Figure 4.2.2-1 was permitted to continue for a longer period of time, catalyst deactivation would eventually become significant enough that a reduction in the rate of DAA production would be observed.

A strange feature of Figure 4.2.2-1 is the fact that MO reaches its maximum concentration after 4-5 hours, but DAA reaches its steady state after approximately 12 h. In the batch CD experiments of Section 4.1, and the batch experiments of Section 3.1, it was noticed that this catalyst has a high initial activity toward MO production, but deactivates fairly quickly. As the catalyst deactivates, the rate of catalyst deactivation declines. In the batch CD and batch experiments, the rate of deactivation became slow enough that the catalyst activity appeared to be essentially constant. The continuous CD experiments last for a much longer period of time, however, and a slow rate of deactivation was noticed. As a result of the initially high activity for MO production and the initially fast rate of catalyst deactivation, the concentration of MO reaches a maximum long before DAA reaches its

steady state concentration.

Since catalyst deactivation occurs in the CD column, one must be cautious when using batch kinetic data to model results from the CD column. The rate of MO production in batch reactions (k_2) was measured after the catalyst appeared to reach its "steady state" activity. Therefore, results from the CD model in Chapter 5, which rely on batch kinetic data, should be compared to "steady state" CD data. For this reason, the MO production rates in Table 4.2.2-II are reported after 12-15 hours of operation when steady state DAA production is achieved. This allows sufficient time for the initially rapid catalyst deactivation to occur, and for "steady state" MO production to be reached before catalyst deactivation becomes excessive. However, this also means that suitable MO production rates can only be obtained 12-15 h into an experiment.

One cause of catalyst deactivation is the formation of heavy byproducts in the catalyst pores. Evidence of high molecular weight byproducts was presented in Figure 3.1.3-7. In the CD column, consecutive reactions which cause deactivation should be more significant in catalyst bags which are located further down the column since concentrations of DAA and MO progressively increase at points further down the column. As a result of pore-blocking and fouling, one would expect that the surface areas of spent catalyst samples taken further down the column to become progressively lower.

To verify this hypothesis, the surface areas of catalyst samples from bag 1 (top) to bag 4 (bottom) were measured. The equipment used to conduct the surface area analysis was described in Section 3.1.2. Before being analyzed, the samples were evacuated and heated to 60°C for 24 h to remove any volatile reagents or products from the surface. The resulting BET surface areas are provided in Table 4.2.2-I. These data clearly show that catalyst samples taken from lower points in the reaction zone have lower surface areas.

Figure 4.2.2-2 shows the observed temperature profile from the run depicted in Figure 4.2.2-1 after 12 hours of operation. Since there is a large difference in the volatility of DAA and acetone, these components are easily separated by distillation. Most of the separation is completed in the reboiler and the first few feet of packing at the bottom of the column. The remainder of the column is essentially isothermal and near the boiling point of pure acetone.

Table 4.2.2-I: Catalyst surface areas from the CD experiment shown in Figure 4.2.2-1 with 4 catalyst bags.

Catalyst Sample	Single-Point BET (m^2/g)	Multi-Point BET (m^2/g)
Fresh catalyst	36.0	37.4
Bag 1 (Top)	33.6	35.3
Bag 2	32.4	34.7
Bag 3	29.2	31.9
Bag 4 (Bottom)	27.8	30.1

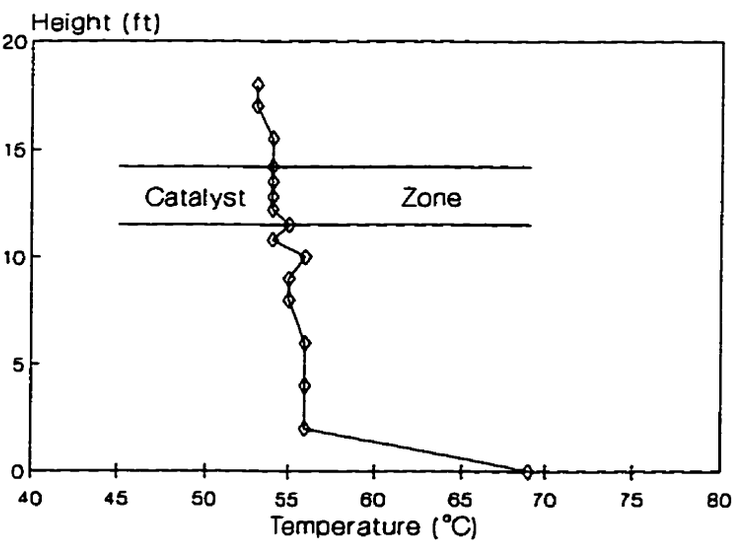

Figure 4.2.2-2: Temperature profile after 12 h of operation of the experiment depicted in Figure 4.2.2-1.

Figure 4.2.2-2 displays several abrupt changes in temperature near the bottom of the catalyst zone, but this effect is simply a result of round-off error. The temperatures are stored by the computer to the nearest degree, and the rounding-off process can create the illusion of large temperature changes.

After 12 h of operation, the composition of the liquid in the reboiler shown in Figure 4.2.2-1 is 43.8 wt% acetone, 40.44 wt% DAA, 11.52 wt% MO, 1.2 wt% IP, and 3 wt% water. This is much higher than the equilibrium limit of 4.3 wt% DAA. Ignoring the small amount of IP, and normalizing the results, the mole fractions are 0.544 acetone, 0.2511 DAA, 0.0846 MO, 0.1202 water. With this composition and UNIFAC activity coefficients, a good prediction of the boiling temperature in the reboiler can be obtained. The result of this calculation is a temperature of 69.3°C, which compares very well with the measured temperature of 69°C at the bottom of the column in Figure 4.2.2-2.

An experiment with only 2 bags (41.5 mL) of catalyst was run at the same acetone feed rate and reboiler duty as the experiment with 4 bags. A plot of the composition in the reboiler vs. time is quite different from Figure 4.2.2-1, and is provided in Figure 4.2.2-3.

The results in Figure 4.2.2-3 show a slow decline in MO and IP concentration over time, which is typical of other continuous CD experiments. Figure 4.2.2-3 also shows an unusual change in the reboiler DAA composition. Between 10 and 18 h, the composition reached steady state at 32.8 wt% DAA. This steady state is referred to as Experiment 1a. Between 28 and 44 h, however, the composition reached a new steady state at 27.8 wt% DAA. The second portion of this run is referred to as Experiment 1b. The change in the DAA composition between experiments 1a and 1b is very significant, representing a 15% decline in the production rate of DAA.

This experiment was conducted in the summer. In the late afternoon, the sun tends to shine directly into the lab and warm the insulation surrounding the column. Late afternoon arrived approximately 10 h into the experiment and the ensuing solar energy had a measurable impact on the condenser duty! The reflux flow rate of acetone returning from the condenser is plotted with the diamond shaped points in Figure 4.2.2-3.

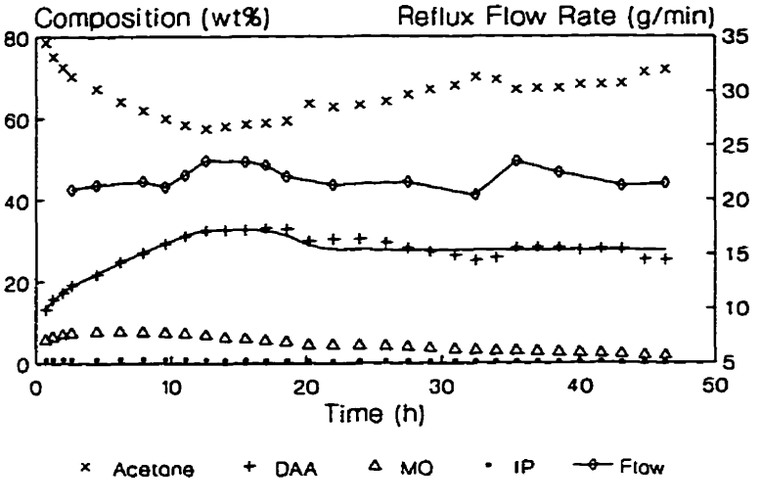

Figure 4.2.2-3: Liquid composition in the reboiler and the reflux flow rate during a continuous CD experiment with 41.5 mL of catalyst in 2 catalyst bags and an acetone feed rate of 152 mL/h (see Expt. #1a and 1b in Table 4.2.2-II).

After 18 h the sun set and the reflux flow rate declined to its previous level. It is interesting that the concentration of DAA declined at the same time as the sunset. The sun was back the next afternoon, of course, and another increase in the condenser duty was observed between 34 - 38 h. This increased the reflux flow rate and a simultaneous resurgence in the production rate of DAA is observed. Even though the condenser duty reached previous levels, the DAA concentration remained lower than the levels observed during the previous steady state. This suggests that the flow pattern during the latter portion of the experiment (expt. 1b, 35 - 43 h) was different from the flow pattern during the initial portion (expt. 1a, 12-19 h).

The similarity between the curves showing the reflux flow rate in the column and the reboiler DAA composition is undeniable. It seems that the sun is able to cause the reflux rate, the flow pattern, and thus, the DAA production rate to change. One important consequence of these findings was the eventual installation of air conditioning.

Another experiment at the same acetone feed rate and reboiler duty was conducted with 6 catalyst bags. After approximately 30 h of operation, however, the reboiler duty was purposely reduced to confirm that there would be changes in the observed catalyst activity. A plot of the composition in the reboiler, and the reflux flow rate, is shown in Figure 4.2.2-4.

In Figure 4.2.2-4, there is a small spike in the reflux flow rate around 7 h. This was caused by a brief appearance by the late afternoon sun. Fortunately, it was generally overcast and raining during this experiment and the sun was not a significant factor. The next afternoon, between 31 and 33 h, the weather was still cloudy. The sun shone intermittently, causing some fluctuations in the reflux flow rate, but the changes were not as severe as those observed in Figure 4.2.2-3.

Figure 4.2.2-4 clearly shows the dramatic change in DAA production that takes place when the reflux flow rate in the column is altered. The reflux flow rate drops very quickly at 29 h when the reboiler duty is reduced. The DAA composition in the reboiler then declines

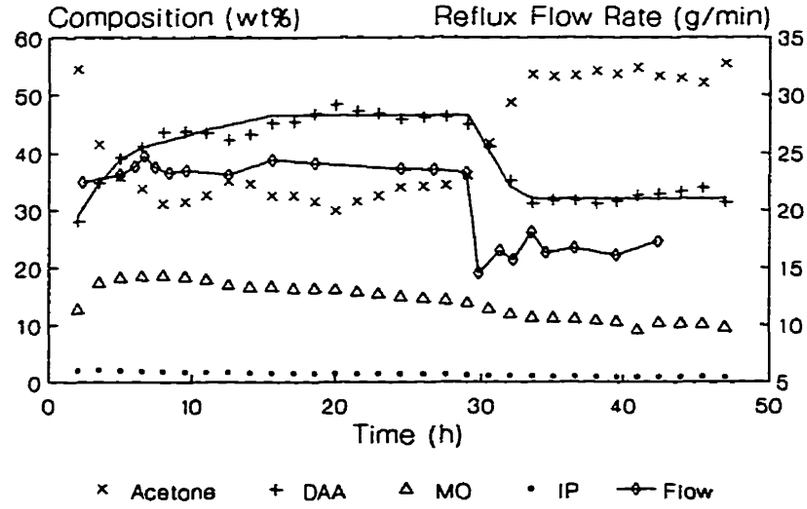

Figure 4.2.2-4: Liquid composition in the reboiler and reflux flow rate for the experiment with 131 mL of catalyst in 6 catalyst bags and an acetone feed rate of 152 mL/h (see Expt. #4a and 4b in Table 4.2.2-II).

from approximately 46 wt% to 32 wt%. The first portion of this experiment is referred to as experiment 4a and the portion following the drop in reboiler duty is experiment 4b. It is very interesting to note that the production of MO in Figure 4.2.2-4 was not seriously influenced by the large change in the flow rate. Only a small decline in the MO concentration is noticed following the change in the reboiler duty. This is a consequence of the pseudo-zero order nature of MO production. The maximum concentrations of MO and IP were 18.7 and 2.1 wt%, declining to 9.6 and .86 wt%, respectively, by the end of the run.

Table 4.2.2-II: Summary of the results from continuous CD experiments.

Expt. #	No. of Bags	Catalyst (mL in water)	Batch k_1 (M^{-1} min^{-1})	Batch k_2 (M min^{-1})	Reflux Flow (g/min)	Activity DAA (g/mL·h)	Activity MO[a] (g/mL·h)
1a	2	41.5	0.36×10^{-3}	0.0008	22.0	0.83	0.16
1b	2	41.5	0.36×10^{-3}	-	22.0	0.69	-
2a[c]	2	42.8	0.34×10^{-3}	0.00117[b]	25.4	0.78	0.21
2b[c]	2	42.8	0.34×10^{-3}	-	15.6	0.63	-
3	4	91.3	0.36×10^{-3}	0.0008	22.9	0.49	0.14
4a	6	131.1	0.36×10^{-3}	0.0008	23.6	0.41	0.15
4b	6	131.1	0.36×10^{-3}	-	16.3	0.29	-

[a]measured after 15 h of operation
[b]catalyst exchanged to 0.45 mmol OH^-/mL within 3 h (see Table 3.1.3-V)
[c]data for experiment #2 (a and b) is provided in Appendix G

Table 4.2.2-II provides a summary of the results from all of the continuous CD experiments. The most important sources of error in calculating the catalyst activities in this table are from minor fluctuations in the compostion of the liquid in the reboiler and from the error in the feed rate provided by the pump. The feed pump is very accurate, and a flow rate of 152 mL/h would be supplied within a fairly tight range of ±0.8 % of the calibrated flow rate. Because of the averaging that takes place, it is felt that the composition of the samples is

known within ±4%. Thus, the catalyst activity is known within approximately ±5%. As an example, the catalyst activity for DAA in experiment 4a would be 0.41 ● 0.02 g/mL·h.

A number of interesting observations can be made from the data in Table 4.2.2-II, and some of these are summarized below:

- A comparison of Expt. 1a, 3 and 4a shows that the rate of DAA production declines as more catalyst is placed into the column. The MO production rate decreases slightly, but this is not nearly as significant as the changes in DAA production.
- A comparison of Expt. 4a and 4b, and a comparison of Expt. 2a and 2b, show that the reflux flow rate of acetone (ie. the reboiler duty) has a very strong impact on the reaction rate in the CD column. Higher reflux flow rates increase the rate of external mass transfer, which increases the rate of DAA production and improves the product selectivity toward DAA.
- The product selectivity of these experiments is much lower than initially observed in batch reactions with loose catalyst. The molar DAA:MO ratio is 75:1 initially in batch reactions, and varies between 3.3:1 (Expt. 1a) and 2.2:1 (Expt. 4a) for the catalyst with $k_2 = 0.0008$ M min^{-1} in continuous CD reactions. The continuous CD results are very similar to the results obtained from a batch reaction with bagged catalyst in Section 3.1.5, where a ratio of DAA:MO of 2.4:1 was observed.

The results from Figure 4.2.2-3 (Expt. 1a and 1b in Table 4.2.2-II) also show that the random nature of flow through packed columns is a problem in these experiments. Flow patterns tend to remain constant with respect to time, but small disturbances may cause them to change. Changes in the flow pattern over the catalyst have a significant effect on the DAA activity and the product selectivity. The random nature of flow through packed columns was also observed in the results of Section 4.1.2, where attempts were made to measure the liquid flow rate that passes through the catalyst bag. Clearly, the product selectivity, the DAA activity, and the reproducibility of the results could be improved by controlling the liquid flow distribution in the column more precisely.

4.3 Controlling the Liquid Distribution

The use of random packing to distribute the refluxing liquid over the catalyst bag has a number of undesirable consequences. Perhaps the most significant problem is wall flow. When liquid flows along the wall of the column it bypasses the catalyst altogether, and results in lower mass transfer rates between the catalyst particles and the flowing liquid. This ultimately reduces the observed catalyst activity and the product selectivity. A logical step would be to design a liquid distributor that improves the contact between the liquid and the bag and reduces the variability of the system. A similar type of action was required in Section 3.3 to improve the reproducibility of the solid-liquid mass transfer experiments.

4.3.1 Experimental

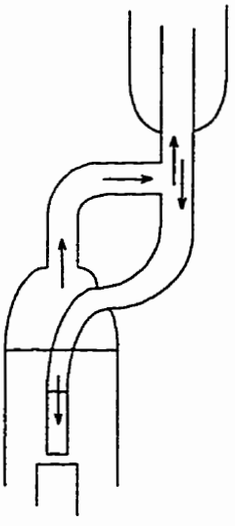

Figure 4.3.1-1: Schematic of the new liquid distributor.

Experiments were conducted in the bench-scale glass distillation column depicted in Figure 3.4.2-1. For these experiments, however, a new distributor was designed to direct the liquid onto the top of the catalyst bag. A schematic diagram of the top portion of the column is provided in Figure 4.3.1-1. This diagram indicates the vapour flow into the condenser, and the liquid flow down to the catalyst bag.

Three sample ports (not shown in Figure 4.3.1-1) were installed near the top of the distillation column to allow the removal of liquid samples from within the catalyst bag. This will provide the composition of each species inside the bag, and will be useful for confirming the results of the modelling work in Chapter 5.

The procedure for these experiments is identical to the procedure outlined in Section 4.1.1.

4.3.2 Results from Controlling the Liquid Distribution

Figure 4.3.2-1 summarizes an experiment with 22.32 mL of catalyst and the reboiler set to 75 V (the rate constants for this catalyst will be presented later in this section). This figure can be compared to Figure 4.1.3-3 to emphasize the changes that occur with the new liquid distributor. A visual inspection of the flow pattern also confirmed a dramatic reduction in the amount of wall flow. The activity of the catalyst for DAA production increased from 0.60 to 1.70 g DAA/mL_{cat}·h at a reboiler setting of 75 V. The product selectivity also improved tremendously. The molar ratio of DAA:MO increased from 2.85 to 10.12 through the use of the new liquid distributor. This improvement in performance is remarkable.

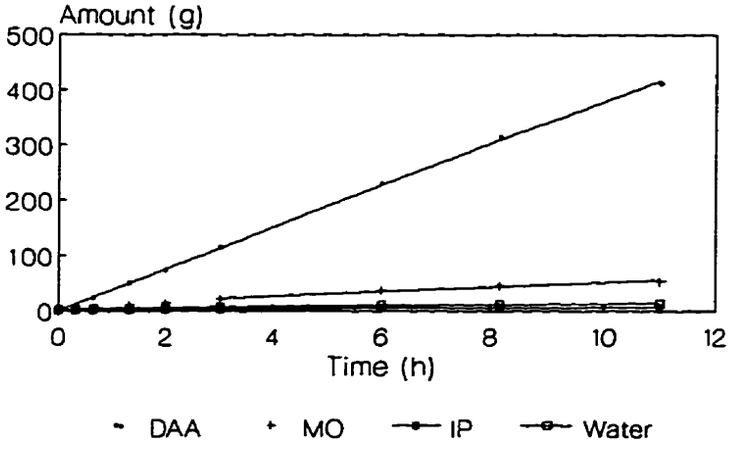

Figure 4.3.2-1: Results of the experiment with 22.32 mL of catalyst, the reboiler set at 75 V, and the new liquid distributor in place.

The rate of MO production is relatively insensitive to the flow rate and liquid distribution technique but the rate of DAA production changes dramatically when the new liquid distributor is used. The amounts of DAA and MO produced with the new liquid distributor are provided in Figures 4.3.2-2 and 4.3.2-3, respectively.

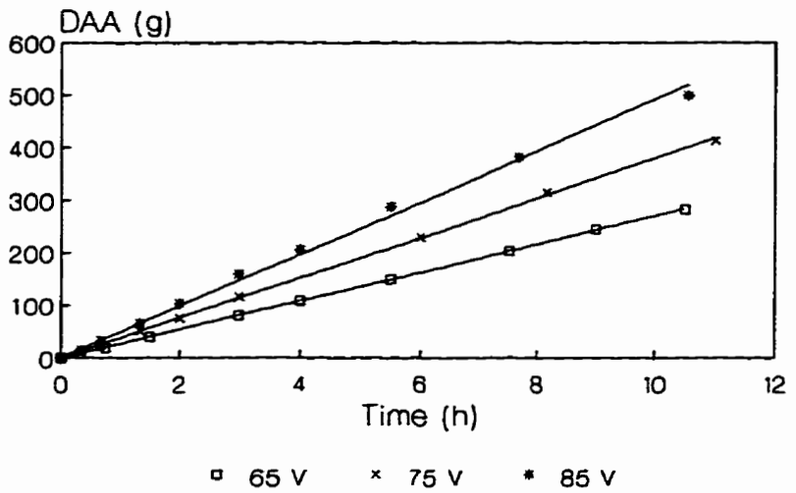

Figure 4.3.2-2: A comparison of DAA production from three different reboiler duties with the new liquid distributor.

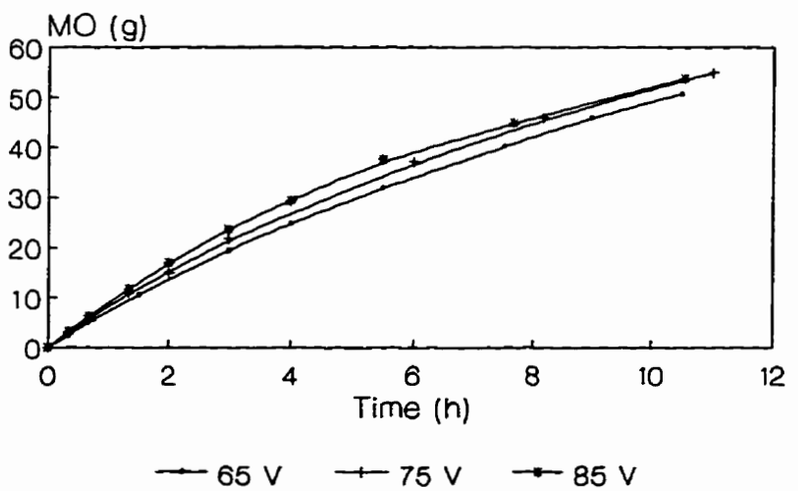

Figure 4.3.2-3: A comparison of MO production from three different reboiler duties with the new liquid distributor.

Table 4.3.2-I: Batch CD results with the new liquid distributor.

Reboiler Setting (V)	Flow Rate (g/min)	Amount of Catalyst (mL)	DAA Activity ($g/mL_{cat} \cdot h$)	MO Activity[a] ($g/mL_{cat} \cdot h$)	Selectivity (mol DAA/ mol MO)
65	8.76	22.45	1.20	.14	7.24
75	12.27	22.32	1.70	.14	10.26
85	16.36	22.70	2.17	.14	13.10

[a]measured after 10 h of operation

The results from three experiments are summarized in Table 4.3.2-I and composition data for the experiments at 65 and 85 V are available in Appendix G. A comparison of the results in Tables 4.1.3-I and 4.3.2-I clearly demonstrates that controlling the liquid distribution over the catalyst in the CD column is the key to obtaining good product selectivity and catalyst activity.

In these experiments, as in previous batch and batch CD experiments, the plots of the amount of MO vs. time are non-linear. This is likely caused by the catalyst deactivating toward a "steady state" activity. As was the procedure in Section 4.1, the MO production rate is determined by measuring the slope of the data near 10 h.

One possible explanation for the curvature observed in Figure 4.3.2-3, apart from catalyst deactivation, is an increase in the water concentration in the reaction zone of the column as a function of time. As the water concentration in the reaction zone of the column increases, the rate of MO production should decrease. In order to monitor the water concentration at the top of the column, three samples of the overhead condensate were taken during the batch CD experiment at 65 V. Samples were removed at 1, 4, and 8 h and the composition of these samples is shown in Table 4.3.2-II.

The results of Table 4.3.2-II show that the water content appears to change very little over time. While one would expect the amount of water in the overhead product to slowly increase over time, any increase which takes place is very small. Indeed, any increase in the

water concentration that did occur was too small to be discerned by the GC. This is due to the fact that a very small amount of water (on the order of 15 g after 10 h of operation) is produced by the reaction and distillation can easily separate mixtures of water and acetone because of the large difference in the volatility of the two components. Since the concentration of water is now known to remain fairly constant over time, this leaves catalyst deactivation as the most likely cause of the non-linear MO vs. time data in Figure 4.3.2-3.

Table 4.3.2-II: Overhead samples taken from the batch CD experiment at 65 V with the new liquid distributor.

Time (h)	Acetone (wt%)	DAA (wt%)	MO (wt%)	Water (wt%)
1	99.11	trace	trace	0.89
4	99.02	trace	trace	0.98
8	99.13	trace	trace	0.87

As mentioned in the Experimental description (Section 4.3.1), sample ports were installed to permit sampling within the catalyst bag. The liquid samples were approximately 0.55 mL in volume and were removed by a small syringe. Samples had to be taken quite slowly, as vapour could be easily drawn into the syringe rather than liquid. A summary of the samples taken is provided in Table 4.3.2-III. For some unknown reason, obtaining a reliable sample half way down the bag was difficult to do, with the only success occurring during the experiment at 75 V.

The data in Table 4.3.2-III show that the water concentration, in all cases, is higher than 0.4 wt% which is present as an impurity in the ACS Reagent grade acetone used for batch experiments. This is caused by an azeotrope in the acetone/water system which will be discussed in Section 5.1.6, and the fact that water is produced by the reaction. These data also confirm that the water concentration inside the bag becomes lower at higher flow rates

Table 4.3.2-III: Samples taken from within the catalyst bag.

Reboiler - 65 V time = 5.5 h	Taken .2-.7 cm from the top	Taken 1.5-2 cm from the bottom
DAA (wt%)	0.16	4.65
MO (wt%)	0.03	0.67
Water (wt%)	1.03	1.30

Reboiler - 75 V time = 4 h	Taken 1.5-2 cm from the top	Taken near the middle	Taken 1-1.5 cm from the bottom
DAA (wt%)	2.29	2.71	4.16
MO (wt%)	0.10	0.21	0.53
Water (wt%)	0.84	1.00	1.33

Reboiler - 85 V time = 4 h	Taken 1.5-2 cm from the top	Taken 1-1.5 cm from the bottom
DAA (wt%)	2.10	4.71
MO (wt%)	0.08	0.52
Water (wt%)	0.60	0.80

(ie. higher reboiler voltages). Since water concentrations inside the bag are lower at higher reflux flow rates, one would expect to find that MO production rates become higher at higher flow rates. Indeed, this trend has been reported in Sections 4.1 and 4.3.

Table 4.3.2-III also shows the concentration of DAA reaching levels of 4.7 wt% inside of the bag. This is somewhat surprising since the data in Table 2.2.4-I show that at 54°C, which is near the boiling point of acetone, the maximum DAA concentration is 4.3 wt%. In order to exceed this concentration of DAA, the temperature of the reaction zone must be lower than the boiling point of acetone. The temperature in the reaction zone of the column was not measured, but a good estimate can be obtained from the data in Table 4.3.2-I.

An average DAA concentration in the liquid descending from the reaction zone can be estimated from the total production rate of DAA and the total flow rate in the column. This leads to 5.14 wt% DAA at 65 V, 5.15 wt% DAA at 75 V, and 5.01 wt% at 85 V. These numbers are very consistent, and are likely close to the equilibrium concentration of DAA. While this may be close to the equilibrium value, the true equilibrium value must be slightly higher than this. A value of 5.5 wt% DAA was selected as a reasonable value for the equilibrium concentration of DAA. The data in Table 4.3.2-III also shows that there is approximately 1.3 wt% water and 0.7 wt% MO in the liquid phase, which leaves the remaining 92.5 wt% as acetone. Based on these composition data, the equilibrium constant was determined to be 2.43×10^{-3} M^{-1}. From the data in Table 2.2.4-I or Figure 2.2.4-1, the temperature of the reaction zone of the distillation column is estimated to be near 45°C.

Because of this significant change in the reaction temperature, a batch reaction had to be performed to obtain the rate constants for this catalyst. The batch reactor was operated at 45°C with 2 mL of catalyst and 100 mL of acetone. This experiment showed that $k_1 = 0.27 \times 10^{-3}$ M^{-1} min^{-1}, $k_2 = 0.00057$ M min^{-1}, $K_{EQ} = 2.56 \times 10^{-3}$ M^{-1}. The value of the equilibrium constant is quite close to the value estimated above. Therefore, it appears that 45°C is a reasonable estimate for the temperature in the reaction zone of the column, and these constants will be used when modelling these experiments in Chapter 5.

The estimated reaction temperature of 45°C is much lower than the 54°C measured in the pilot scale distillation column. Why should such a drop in temperature occur during these

experiments when none was reported for the results of Sections 4.1 and 4.2? The explanation rests with the use of the new liquid distributor. Any condenser at the top of a distillation column will usually subcool the liquid returning to the top of the column. In the columns used in Sections 4.1 and 4.2, a portion of the column above the catalyst bag was filled with distillation packing. This packing provides an area for heat transfer to take place, and raise the temperature of the refluxing liquid back up to the boiling point. With the new liquid distributor, however, the refluxing liquid is directly returned to the top of the catalyst bag and has almost no chance of being re-heated to its boiling temperature.

-5-

PHASE IV - CATALYTIC DISTILLATION SIMULATIONS

Models of catalytic distillation are an extension of conventional distillation models. In order to understand the current state of CD modelling, it is helpful to take a brief look at the history and evolution of distillation models.

Written references to distillation date back to at least 800 AD, but these early applications were batch operations. The first continuous multi-stage distillation process resembling modern units was designed by Cellier-Blumenthal and Coffey in 1813 to meet the increasing demand for brandy and whisky (Gentry, 1995).

While applications of distillation have a long history, the theory and equations which describe the distillation process lagged well behind. It was not until the 1890's that distillation models began to appear. In 1925, a landmark publication from McCabe and Thiele (1925) provided a simple and reasonably accurate way of solving distillation problems. Since then, distillation models have improved dramatically, but there is still a need for fundamental research (Porter, 1995).

Distillation models are usually based on the concept of the ideal equilibrium stage. The key assumption is that the vapour and liquid phases leaving an equilibrium stage are in physical and chemical equilibrium. The equations which are used to describe distillation can be categorized as follows:

- Material balances around each stage
- Vapour-Liquid Equilibrium (VLE) relationships
- Mole fraction Summations
- Energy (H) balance equations

Solving this set of equations provides the vapour and liquid compositions, the temperature, and the vapour and liquid flow rates at each stage. These equations are commonly referred to as the MESH equations, and have formed the basis of distillation models for 100 years.

Over time the MESH equations have remained essentially unchanged, but our ability to solve these equations has steadily improved. A wide variety of solution methods have been developed, with newer methods providing solutions in situations where previous methods have had difficulty. These methods are grouped into the categories of Tearing Methods, Newton's Methods, Homotopy-Continuation Methods, and Collocations Methods. An overview of the features of these methods is provided by Taylor and Lucia (1995) . For a more detailed discussion, however, a text specializing in this area should be consulted (Kister, 1992).

Reactive distillation models also lagged behind applications of the technology. Early patents for reactive distillation date back to 1920, yet one of the first models debuted in 1971 (Doherty and Buzad, 1992). Simulations of reactive distillation are treated as an extension of existing distillation models. The MESH equations are altered to include terms for the reaction kinetics, and are solved using existing methods. The main reason for the delay in solving reactive problems is the increased non-linearity introduced by the reaction terms. This necessitates the use of more complex and robust solution methods (such as Newton's method) which have only become practical because of the availability of powerful digital computers. Many examples of reactive distillation models and the various techniques used to solve them are available in the literature (Abufares and Douglas, 1995; Paludetto et. al., 1992; Simandl and Svrcek, 1991; Bogacki et. al., 1989; Grosser et. al. 1987; Izarraraz et. al. 1980; Mommessin et. al., 1980). Reactive distillation modelling techniques have been reviewed by Doherty and Buzad (1992) and Sundmacher et. al. (1994). These models are now quite mature, and are available in commercial packages (Venkataraman, 1990).

There is some debate about the definition of the ideal equilibrium-stage in a reactive distillation column. Some authors stipulate that an ideal reactive stage should include vapour-liquid equilibrium, thermal equilibrium, and reaction equilibrium. Barbosa and Doherty (1988) use this definition of an equilibrium stage and have studied the influence of the chemical

reaction in the liquid phase on VLE behaviour.

In non-reactive systems, azeotropes may exist. The condition for a non-reactive azeotrope is that the composition of the vapour and liquid phases are equal (ie. $y_i = x_i$). The addition of a liquid phase reaction can introduce 'reactive azeotropes' in VLE systems which are otherwise ideal. A reactive azeotrope occurs when distillation produces no further changes in composition. The compositions of the two phases, however, are not necessarily equal. Barbosa and Doherty (1987) have derived the mathematical condition describing a reactive azeotrope for a system with c components.

$$\frac{y_1 - x_1}{\nu_1 - \nu_T x_1} = \frac{y_i - x_i}{\nu_i - \nu_T x_i} \qquad i = 2, 3, \ldots . c$$

$$\textit{where:} \quad \nu_T = \sum_{i=1}^{c} \nu_i \tag{5.1}$$

In equation (5.1), ν_i represents the stoichiometric coefficient for component 'i'. The existence of reactive azeotropes depends on the VLE behaviour of the system and the value of the reaction equilibrium constant. Thus, by changing the operating temperature (or pressure), the azeotrope may be eliminated.

Barbosa and Doherty (1988) have also shown that the inclusion of an equilibrium chemical reaction can eliminate non-reactive azeotropes. Consideration was given to the production of MTBE as shown in Figure 1.2.1-1. In this system, isobutylene is more volatile than the reaction product (MTBE), and methanol is less volatile than the reaction product. The system is highly non-ideal, and binary azeotropes exist between methanol/MTBE and isobutylene/methanol. In a three-component, two-phase system with an equilibrium liquid phase reaction there are 2 degrees of freedom ($F = c+2-p-r$). Thus, by setting the total pressure and one mole fraction the entire system is specified. VLE calculations were made for this system at 101.3 kPa and all possible isobutylene compositions. The resulting T vs. x, y (mole fraction) diagram is displayed in Figure 5-1. Although the phase behaviour is rather strange, there is no azeotrope.

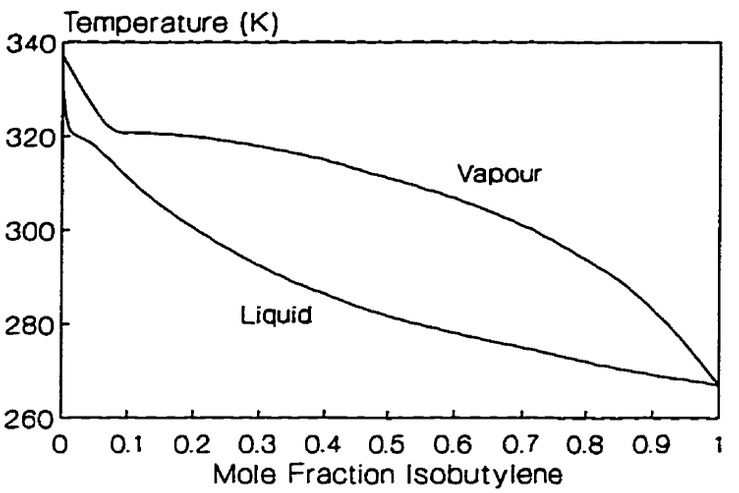

Figure 5-1: Temperature-composition diagram for the reactive isobutylene-methanol-MTBE system at 101.3 kPa.

Pekkanen (1995) does not endorse the use of the term "reactive azeotrope" to describe this phenomenon. In non-reactive systems, the existence of an azeotrope is determined only by thermodynamic properties. The existence of a "reactive azeotrope" in a *kinetically controlled* reactive distillation column, however, depends on the operating conditions of the column, such as liquid hold-up, flow rates, and reaction rates, as well as thermodynamic variables (Pekkanen, 1995). Therefore, the term "reactive pinch" has been suggested as a suitable alternative. Equations describing the conditions for a reactive pinch were developed.

The ubiquitous equilibrium stage distillation model is not without its detractors. Taylor and Lucia (1995) make the following statement:

> The (equilibrium stage) model is so simple in conception, so elegant from the mathematical viewpoint, has inspired so many algorithms, and has been used to simulate and design so many real columns that it seems almost heretical to mention that the model is fundamentally flawed!

It is a well known fact that the liquid and vapour phases leaving trays in an actual distillation column are not in equilibrium. The usual correction method is to introduce an efficiency

parameter. Despite a large body of efficiency data, however, this approach has many pitfalls (Taylor and Krishna, 1993).

Satisfying the reaction equilibrium condition on each ideal stage is just as questionable as the VLE assumption. It is not economical to operate reactive distillation columns close to reaction equilibrium conditions (Doherty and Buzad, 1992). Clearly, this assumption is reasonable only for fast reactions or for large residence times. As a result, most reactive distillation models do not adhere to this condition, and incorporate kinetic terms.

One method of completely avoiding the equilibrium stage concept is through the use of "Non-Equilibrium" or "Rate-Based" models. A good description of this type of distillation model is provided by Krishnamurthy and Taylor (1985). The rate-based model includes:

- Material balances for each phase
- Vapour-Liquid Equilibrium relationships
- Rates of mass and energy transfer between phases
- Energy (Q) balance equations

These are commonly called the MERQ equations. In the rate-based approach, the material balance and energy balance equations are written for each phase on each stage. Only at the vapour-liquid interface does equilibrium exist. Thus, equilibrium data must be calculated at the interfacial composition and temperature.

Mass and energy are transferred across the vapour-liquid interface at a rate which depends on the extent to which the phases are <u>not</u> in equilibrium. Of course, use of this model hinges on the availability of reliable mass transfer coefficients and interfacial areas. This is not a trivial task, and is the subject of a text by Taylor and Krishna (1993).

The use of rate based models requires the knowledge of reaction rates and reaction equilibrium data. Rate expressions are often quite simple for homogeneous catalysts, but can be considerably more complicated for heterogeneous catalysts. Mass transfer to the catalyst surface and pore diffusion within the catalyst particles seriously alter reaction rates, and add complexity to the rate expressions. This has discouraged their use in catalytic distillation

models. However, these mass transfer effects must be taken into account.

Toward this end, Berg and Harris (1993) have conducted an analysis of multi-component diffusion effects inside of the catalyst for the MTBE process. Zheng and Xu (1992b) have used a rate based model of catalytic distillation, but assumed that the conditions on the catalyst surface were identical to the conditions in the bulk liquid phase. Jianhua and Fu (1995) modelled the esterification of acetic acid and ethanol in a CD column, but also neglected mass transfer between the liquid and catalyst.

All of the discussions to this point have been directed toward tray-columns. The literature tends to focus on this area because of the historical importance of tray columns and the existing modelling infrastructure. The reality of the situation, however, is that the catalyst in a CD column behaves like a distillation packing. One of the most important characteristics of CD is that the catalyst acts as a catalyst for the reaction and a packing for distillation. The structures housing the catalyst inside of the column are designed with this task in mind. However, there are surprisingly few reactive or catalytic distillation models in the literature that describe the process in a packed column.

Distillation in a packed column is a "continuous contact" process, rather than a stagewise process. Packed distillation models, therefore, are capable of providing composition data as a function of height rather than only at specific stages. These types of models are much less popular than staged models. However, with recent improvements in liquid distributors, the industrial use of packed columns is increasing and there is strong interest in improving these models.

Rather than a series of algebraic equations, however, packed column models express the MERQ equations in a differential form. A discussion of these equations is provided in the text by Hines and Maddox (1985). The solution to a packed column distillation problem involves solving a series of differential equations. This is not a simple task, as the equations tend to be "stiff". As a result, very stable methods, such as orthogonal collocation, must be used (Wardle and Hapoglu, 1994).

There are surprisingly few studies in the literature that discuss reactive or catalytic distillation in a packed column. Sawistowski and Pilavakis (1988, 1979) develop equations

that describe the influence of the heat of reaction on the mass transfer fluxes. These flux equations are then used in a packed column model of reactive distillation for the esterification of methanol and acetic acid. Sawistowski (1983) also demonstrates that exothermic reactions improve distillation in packed columns.

Hen and Zhang (1989) also use a packed column model to describe the production of MTBE and propylene glycol (the hydration of propylene oxide) in a catalytic distillation column. Their experiments were run at total reflux, meaning that no overhead product was collected, and they took advantage of this fact to simplify their equations. As a result of these simplifications, solutions were obtained with standard numerical integration techniques and a fairly simple convergence algorithm. Unfortunately, they also ignored the mass transfer that takes place between the solid catalyst and the bulk liquid phase.

As the literature currently stands, there are no models of catalytic distillation that account for mass transfer between the liquid and catalyst. This is mainly because the problem has been treated as an extension of reactive distillation problems, and because mass transfer data in CD columns are generally unavailable. However, it is difficult to understand why Zheng and Xu (1992b) ignored mass transfer to the catalyst surface after determining the liquid-catalyst mass transfer coefficients in earlier experiments (Zheng and Xu, 1992).

The focus of the model developed in this thesis will be on the mass transfer that takes place between the catalyst and the liquid. This subject has not received any attention in the literature, and must be addressed in order to make accurate predictions of catalyst activity and reaction selectivity in catalytic distillation. Such a model would be extremely useful, as it would permit the use of kinetic data obtained in the absence of external mass transfer. This type of kinetic data is often the result of standard batch or CSTR laboratory experiments. The model should have the following characteristics:

- The model should be conceptually simple.
- The model should be as easy as possible to use.
- The model should focus on predicting catalyst activity and product selectivity.

Without exception, models in the literature describe compositions in the entire distillation column. However, modelling the distillation that occurs in the non-reactive sections of the column is not especially novel or important. One can quite easily adjust the product purity by simply changing the height of the column or altering the reflux ratio. However, if product selectivity or catalyst activity is unacceptable, no amount of distillation will correct the problem. Rather than attempting to describe the entire distillation column, the model in this thesis will concentrate on the reaction zone, and on predicting catalyst activity and product selectivity.

5.1 Model Overview and Equations

A schematic diagram depicting the concepts of the proposed CD model is shown in Figure 5.1-1. The liquid which flows down the column is shown to split into two portions. A fraction of the total liquid flow, $0 \le f \le 1$, passes through the bed of catalyst particles inside of the bag. The remainder of the liquid, 1-f, bypasses the catalyst bag. Housing the catalyst inside of a fibreglass bag creates a physical barrier between the liquid inside and outside of the catalyst bag. Because of this barrier, concentration differences exist between the liquid inside and outside of the bag, and mass transfer will take place with this concentration difference as the driving force. This exchange of material is represented by the bidirectional arrow between the bag and the liquid flowing outside of the bag.

Distillation also takes place in the reactive zone of the CD column. This is represented by a bidirectional arrow between the liquid flowing outside of the bag and the vapour phase. It is assumed that no mass transfer takes place between the vapour and the liquid inside of the bag. This assumption is reasonable at higher liquid flow rates, where the bag is completely wetted with liquid.

The catalyst particles are quite small ($d_p = 0.9$ mm). With such small particles, it is reasonable to assume that capillary action will keep the catalyst particles completely wetted, and keep the void spaces in the catalyst bag nearly full of liquid. For the purposes of modelling, it is assumed that the void space in the bag is completely full of liquid. Clearly, this assumption will be more reasonable at higher liquid flow rates.

Since mass transfer occurs through the wall of the catalyst bag, radial concentration gradients will exist inside of the catalyst bag. Thus, the local conditions inside of the catalyst bag, and local reaction rates, are a function of radial and axial position. The simplest method of mathematically describing this situation is to treat the catalyst bag as a plug flow reactor with radial dispersion.

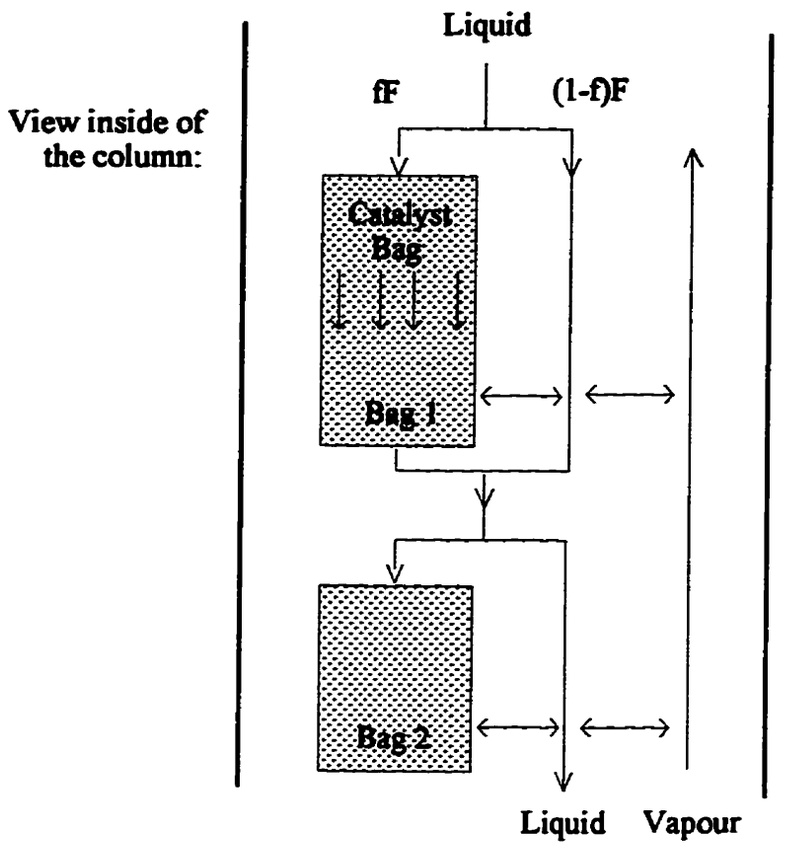

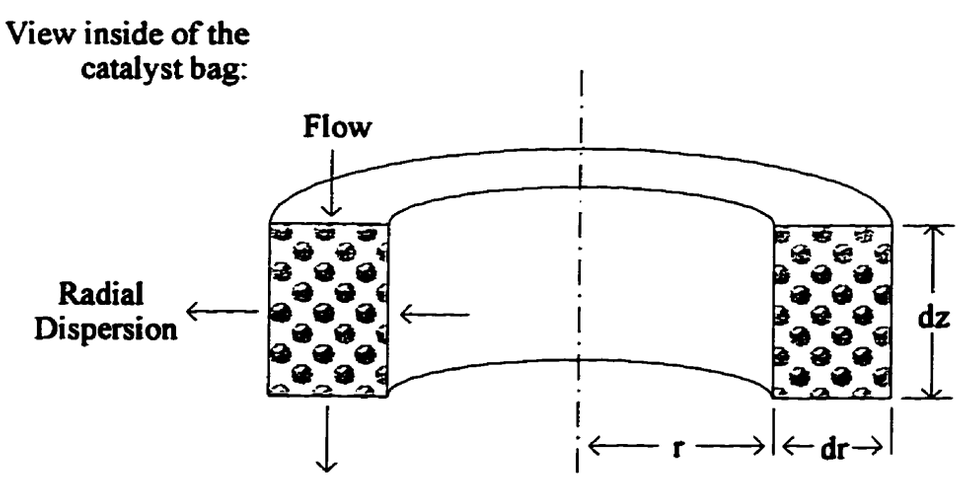

Figure 5.1-1: Diagram outlining the flows inside of the column and inside of the catalyst bag.

A differential slice within the catalyst bag is shown at the bottom of Figure 5.1-1. This diagram shows the downward flow of liquid through the reactor and the radial transfer of reaction products toward the wall of the bag. Constructing a mass balance around this differential element results in the following partial differential equation (PDE).

$$-f\left(\frac{F}{\pi R^2}\right)\frac{\partial C_{i,bag}(z,r)}{\partial z} + Đ\left(\frac{1}{r}\right)\frac{\partial\left(r\dfrac{\partial C_{i,bag}(z,r)}{\partial r}\right)}{\partial r} + R_i(z,r) = 0 \qquad (5.2)$$

Convection *Radial Disperson* *Generation*

where: F = volumetric liquid flow in the column (m^3/s)
f = fraction of liquid flowing through the bag
r = radial position from centre of bag (m)
R = radius of the bag (m)
z = axial position from top of bag (m)
$C_{i,bag}$ = concentration of component i in the catalyst bag (mol/m^3)
Đ = radial dispersion coefficient (m^2/s)
R_i = rate of generation of component i ($mol/m^3 \cdot s$)

Similar mass balances around a differential height element are used to derive the equations for the liquid phase (ie. the liquid outside of the bag) and the vapour phase. Since the liquid and vapour are assumed to be well mixed, no radial effects need to be considered, and ordinary differential equations (ODE) result. The ODEs for the liquid and vapour phases are shown in equation (5.3) and (5.4), respectively.

$$(1-f)F\frac{dC_i(z)}{dz} = k_{C,i}A\,(C_{i,bag}(z,R) - C_i(z)) - K_{OG,i}A\,(y_{i,EQ}(z) - y_i(z)) \qquad (5.3)$$

$$V\frac{dc_i(z)}{dz} = -K_{OG,i}A\,(y_{i,EQ}(z) - y_i(z)) \qquad (5.4)$$

where: V = vapour phase flow rate (m^3/s)
C_i = concentration of i in the liquid outside of the bag (mol/m^3)
c_i = vapour phase concentration of component i (mol/m^3)
$k_{C,i}A$ = liquid-solid mass transfer for component i (m^2/s)

$K_{OG,i}A$ = overall vapour-liquid mass transfer for component i (mol/m·s)
$y_{i,EQ}$ = vapour mole fraction in equilibrium with bulk liquid
y_i = vapour mole fraction

Heat of reaction effects are conspicuously absent from equations (5.2) - (5.4). Heat released by a reaction can influence mass transfer fluxes and phase flow rates. However, it was shown in Section 2.2.4 that the formation of DAA is only slightly exothermic (ΔH_R = -27 kJ/mol). The formation of MO is only slightly endothermic (ΔH_R = +25 kJ/mol), and will utilize some of the energy released by DAA formation. As a result of these considerations, the heat of reaction was assumed to be negligible.

The flow terms, F and V, are outside of the differential operators in equations (5.2) - (5.4), which implies that these terms are constant. This is a reasonable assumption since the heat effects are negligible, and the liquid and vapour in the reaction section of the column are dilute mixtures of water, MO, and DAA in acetone. The fact that the liquid in the reaction zone of the column is a dilute solution also permits the use of pseudo-binary mass transfer coefficients (Taylor and Krishna, 1993). In concentrated solutions, one should consider multicomponent mass transfer in a more rigorous way.

One final issue that needs to be discussed is the fate of the enthalpy balance equations. These equations are required in rigorous distillation models to accurately calculate phase flow rates and temperatures. However, the volumetric flow rates are assumed to be constant in this model. Preliminary experiments also reveal that the reaction section of the CD column is essentially isothermal, and that its temperature is near the boiling point of acetone (ie. the concentrations of DAA, MO, and water are not high enough to significantly raise the boiling point). Thus, there is little need for an enthalpy balance. This approach is similar to the method of McCabe and Thiele, where the need for an enthalpy balance is eliminated by assuming equimolar counter diffusion (EMCD), which gives constant molar flow rates on each stage (McCabe and Thiele, 1925).

We can write equations (5.2) - (5.4) for each of the four components present. With the assumption of constant volumetric flow rates, however, only three of the mass balances are independent. Thus, by solving three of the mass balance equations, the problem is

completely specified. It was decided to solve the equations for DAA, MO, and water, and determine the acetone concentration by difference as required.

Although this is not a rigorous approach, it is highly doubtful that the inclusion of an enthalpy balance would improve the accuracy of the model. It was clearly demonstrated in Section 2.2.4 that the thermodynamic data for this system are not accurate. The reader may recall that predictions of the heats of reaction were errant by roughly 200%! Water and MO also behave non-ideally, meaning that accurately predicting the enthalpy of liquid and vapour phases would be difficult. Thus, the inclusion of enthalpy balance equations would greatly complicate the model, yet do little to improve its accuracy.

It is important to calculate the total molar flow rate of each component emerging from the bottom of the catalyst bag. Since the concentration of each component is a function of radius, integration is required. The total molar flow rate of i can be obtained by multiplying the volumetric flow rate inside the catalyst bag (fF) by the average concentration of component i. The average concentration of component i is

$$\overline{C_i} = \int_{r=0}^{r=R} \frac{2rC_{i,bag}(Z,r)}{R^2}\, dr. \tag{5.5}$$

It may also be interesting to evaluate the total amount of product which is transported through the wall of the bag in the radial direction. This will permit a comparison of the relative importance of the radial mass transfer and plug flow mechanism of removing product from within the catalyst bag. The equation giving the total amount of production of component i obtained through radial mass transfer is given below.

$$\textit{Wall Production} = \int_{z=0}^{z=Z} k_{C,i}A\ [C_{i,bag}(z,R) - C_i(z)]\, dz \tag{5.6}$$

In equation (5.3) and (5.4), mole fractions are used in the vapour-liquid mass transfer expressions. However, concentrations (mol/m^3) are usually used to measure composition. It

is clear that a method of converting between these two measures of composition is required. In general, mole fractions can be determined by dividing the molar concentration of component i by the total molar concentration of the phase. The total molar concentration of the vapour phase can be calculated with the ideal gas law. The total molar concentration of the liquid phase will have to be estimated. The following approximation was used:

$$C_{L,tot} = C_{DAA}+C_{MO}+C_{Wat}+C^{o}_{Ac}\left[\,1 - \left(\frac{C_{DAA}}{C^{o}_{DAA}}+\frac{C_{MO}}{C^{o}_{MO}}+\frac{C_{Wat}}{C^{o}_{Wat}}\right)\right] \qquad (5.7)$$

where : $C_{L,tot}$ = total molar concentration of liquid phase (mol/m^3)
C°_i = molar concentration of pure component i (mol/m^3)
C_i = molar concentration of component i in the mixture (mol/m^3)

Equation (5.7) assumes that the volumes of liquids in a mixture are additive. Although this has been demonstrated for mixtures of DAA and acetone (Ray and Ghosh, 1974), it is likely not true for mixtures of acetone and water. However, the water concentration in the reactive zone of the column is quite low, and minimal errors will result from this assumption. The molar concentrations of the pure components can be obtained from the density data provided in Table 3.1.2-III.

Many parameters are required to use this proposed model, such as mass transfer coefficients, dispersion coefficients, VLE relations, kinetic data, and others. It is very important to understand how these values are obtained. The following sections of this chapter will briefly outline the sources of all of these parameters.

5.1.1 Radial Dispersion - Đ

The dispersion model is an acknowledgement that flow patterns in chemical reactors are seldom ideal. Bischoff (1966) and Wilhelm (1962) reviewed the progress made in reactor modelling, and revealed that the first reports of dispersion in chemical reactors date back to

the early 1900's. The theory and equations describing dispersion were presented by 1937, and many other valuable contributions followed. Most of the experimental work in this field was published in a flurry of activity between 1950 and 1960.

Chemicals will naturally mix in stagnant systems through the slow process of molecular diffusion. In flow systems, however, mixing occurs much more quickly because of the presence of small eddies. Despite the fact that the mixing takes place via a different mechanism, the dispersion process is analogously modelled with the equations that describe diffusion (Levenspiel, 1972). Rather than a diffusion coefficient, a *dispersion coefficient* (Đ) is used to characterize the mixing that takes place. The dispersion method of modelling a fixed bed reactor begins with the plug flow assumption. Dispersion is then superimposed on the ideal plug flow pattern to account for the non-ideal mixing.

In the proposed CD model, the catalyst bag is treated as a small fixed bed reactor with mass transfer taking place through the side wall of the bag. Since mass transfer occurs at the walls, the assumption of a uniform concentration in the radial direction is not acceptable. Thus, a radial dispersion term is included in equation (5.2). The model assumes plug flow in the axial direction.

Dispersion coefficients are often reported as part of a dimensionless group known as the Peclet number. The radial Peclet number is commonly displayed in a graphical format as a function of the particle Reynolds number, which characterizes the flow rate through the packed bed. The definitions of the Peclet and Reynolds numbers used in characterizing dispersion are shown in equation (5.8).

$$Pe_r = \frac{d_p v_0}{\varepsilon Đ} \qquad Re_p = \frac{d_p v_0 \rho}{\mu} \tag{5.8}$$

Where: d_p = catalyst particle diameter (m)
v_0 = superficial fluid velocity (m/s)
ε = void fraction of catalyst bed
Đ = radial dispersion coefficient (m^2/s)

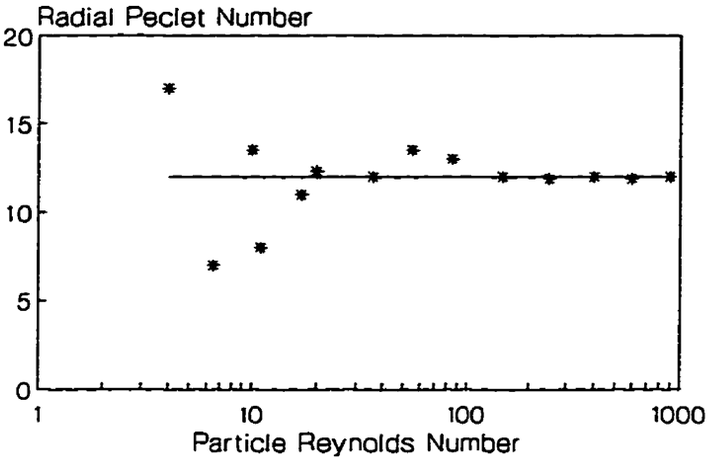

Figure 5.1.1-1: Radial dispersion in a bed of 1 mm and 3 mm spherical particles (Bernard and Wilhelm, 1950).

Radial dispersion data are available in the reviews by Wilhelm (1962) and Bischoff (1966), and in the text by Froment and Bischoff (1990). A graph of the Peclet number versus the Reynolds number from the often cited work of Bernard and Wilhelm (1950) is displayed in Figure 5.1.1-1.

These data show that Pe_r remains essentially constant over a wide range of flow conditions. However, at low values of Re_p, the data become rather unstable and a sharp rise in the value of the Peclet number is observed at very low Reynolds numbers. Froment and Bischoff (1990) compared 5 different sources of radial dispersion data, and found that some researchers did not report a sharp rise in the Peclet number at low flow rates. There is general agreement on the value of Pe_r at high flow rates, but various correlations diverge at low flow rates. Owing to the wide range of values in the literature, we will assume that Pe_r has a value near 12 for all flow conditions. This rule of thumb is endorsed by Froment and Bischoff (1990).

5.1.2 Mass Transfer between Catalyst Bag and Bulk Liquid - k_cA

An important aspect of this model is mass transfer between the liquid outside of the catalyst bag, and the outer edge of the catalyst bag. These mass transfer coefficients are involved in equations (5.3) and (5.6), and in a boundary condition in Section 5.2.

These mass transfer coefficients were experimentally determined as part of this thesis. A full discussion of the procedures and a j-factor correlation of the results is presented in Section 3.3.

5.1.3 Mass Transfer between Vapour and Liquid - $K_{OG}A$

The distillation which occurs in the reaction section of the CD column is described with a rate-based distillation model. The terms which describe the rate of mass transfer between the liquid and vapour phases appear in equations (5.3) and (5.4). It was decided to use overall gas phase mass transfer coefficients ($K_{OG}A$) in the model.

These mass transfer coefficients were also obtained experimentally. A discussion of the procedures and the j-factor correlations is provided in Section 3.4 of this thesis.

5.1.4 Film Mass Transfer - k_fA

Experimental data in Section 3.3 demonstrate that external mass transfer is not important in the well mixed batch reactor. This situation will almost certainly change when the catalyst is placed inside of fibreglass bags and subjected to low relative velocities of acetone. There will likely be a significant difference between concentrations inside of the catalyst bag, and concentrations at the outer surface of the catalyst pellets. A stagnant "film" will exist around the catalyst surface, through which the reagents and products must be transported. For the purposes of this model, we will superimpose the catalyst surface and the

bulk liquid phase on the same domain.

The presence of a "film" surrounding the catalyst particles has implications for reaction kinetics. The R_i term in equation (5.2) is a mass transfer term rather than a kinetic term. The rate of generation of component i depends on the rate at which it is transported through the film surrounding the catalyst surface. This is shown below:

$$R_i(z,r) = k_f A''(C_{i,film}(z,r) - C_i(z,r)) \tag{5.8}$$

where: $C_{i,film}$ = concentration of i at catalyst surface (mol/m^3)
A'' = interfacial area per unit bulk volume (m^2/m^3)
k_f = film mass transfer coefficient (m/s)

Correlations are available in the literature that relate values of k_f to the particle Reynolds number for the case of flooded liquid flow through packed beds of solids (Goto and Smith, 1975; Satterfield et. al., 1978; Satterfield, 1981). This subject has also been treated from a theoretical viewpoint by Carberry (1960), and his theoretical predictions are in good agreement with a wide range of experimental data. It was decided to use Carberry's equation to estimate the film mass transfer coefficient for this work, and this correlation is shown in equation (5.10).

$$k_f = 1.15 \frac{v_0}{\sqrt{\varepsilon}} Re_p^{-1/2} Sc^{-2/3} \tag{5.10}$$

The interfacial area for mass transfer per unit bulk volume (A") is required to accompany the values of the film mass transfer coefficient (k_f). This is typically estimated as the outer surface area of the spherical particles. This can be calculated as a function of the particle diameter and the void fraction of the bed as follows:

$$A'' = \frac{6(1-\varepsilon)}{d_p} \tag{5.11}$$

5.1.5 Reaction Kinetics

Although reaction kinetics are a very important aspect of the CD model, they do not assume the role that may have been initially envisaged. The reaction kinetic expressions are simply used to determine the composition of the stagnant film surrounding the catalyst, rather than directly calculating rates of generation. Since this is a steady state model, the rate of reaction generating component i in the film must equal the rate of mass transfer of component i out of the film. Since different components have different reaction rate equations, these expressions are different for each component.

For DAA:
$$k'_1 C^2_{Ac,film} - \frac{k'_1}{K_{EQ}} C_{DAA,film} = k_{f,DAA} A''(C_{DAA,film}(z,r) - C_{DAA}(z,r)) \quad (5.12)$$

For MO:
$$k'_2 = k_{f,MO} A''(C_{MO,film}(z,r) - C_{MO}(z,r)) \quad (5.13)$$

For Water:
$$k'_2 = k_{f,Water} A''(C_{Water,film}(z,r) - C_{Water}(z,r)) \quad (5.14)$$

Since water is produced in a 1:1 ratio with MO, the rate of water production equals the rate of MO production, and this is reflected in equation (5.14).

The k′ symbol indicates that the rate of generation of each component is expressed per unit bulk volume of catalyst. These constants can be calculated from the constants determined in batch experiments. A detailed batch study of reaction kinetics was presented in Section 3.1, and these data will be used in the CD model. Results from the batch experiments were typically obtained with 2 mL of catalyst (1.384 mL in acetone) in 100 mL (0.1 L) of acetone, and reaction rates were typically reported in units of M min^{-1}. The conversion of these units to mol/(m^3·s) is shown in equation (5.15).

$$\frac{M}{\min} \cdot 0.1L \cdot \frac{1}{1.384\ mL} \cdot \frac{1000000\ mL}{1\ m^3} \cdot \frac{1\ \min}{60\ s}\ [=]\ \frac{mol}{m^3 \cdot s} \qquad (5.15)$$

Thus, the reaction rates from the batch reactor must be multiplied by a factor of 1204 to convert to the appropriate units for the model. For the MO production rate, $k'_2 = 1204 \times k_2$. The procedure is similar for the rate constants for DAA production.

The data presented in Section 3.1.4 clearly show that the values of k_1 and k_2 depend on the concentration of water in the batch reactor. Thus, the rate constants in equations (5.12) - (5.14) are a function of the concentration of water in the film. For the model, it is convenient to mathematically describe the values of k_1 and k_2 as a function of water concentration. Using the data in Figures 3.1.4-1 and 3.1.4-2, some empirical correlations were developed.

It was rather difficult to find a function that would fit the kinetic data through the entire range of water concentrations. As a result, the data were divided into two regions. Equation (5.16) shows the correlations used to describe k_1 as a function of water concentration, and the range over which each correlation is valid. These correlations are also plotted in Figure 5.1.5-1.

$$\begin{aligned} 1000k_1 &= -0.6446\,[H_2O] + 0.4697 \qquad 0.17 \le [H_2O] \le 0.498\,M \\ 1000k_1 &= 0.0302 + \frac{0.0471}{[H_2O] + 0.13273} \qquad 0.498 \le [H_2O] \le 2.4\,M \end{aligned} \qquad (5.16)$$

Figure 5.1.5-1 shows that a linear model adequately describes the data at fairly low water concentrations. However, at water concentrations exceeding 0.498 M, a non-linear model is used. Neither correlation is valid below water concentrations of 0.17 M. This is not a concern, however, since it is not possible to realize such dry conditions in the reaction zone of the CD column.

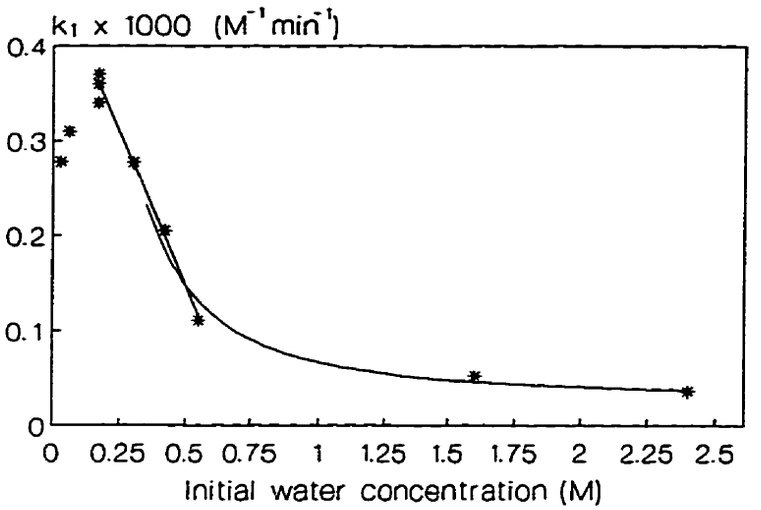

Figure 5.1.5-1: The correlations in equation (5.16) which describe k_1 as a function of water concentration.

A similar procedure was followed for the MO production rate data. The correlations describing the rate of MO production are provided in equation (5.17), and Figure 5.1.5-2 shows a plot of the correlations and the experimental data.

$$1000k_2 = -3.15([H_2O] - 0.17)^2 + 0.81 \qquad 0.06 \le [H_2O] \le 0.42M$$

$$1000k_2 = -0.07837 + \frac{0.19449}{[H_2O] - 0.13877} \qquad 0.42 \le [H_2O] \le 2.4M \qquad (5.17)$$

Figure 5.1.5-2 emphasizes the importance of using the correlations only within their defined range, as they deviate very rapidly from the experimental data.

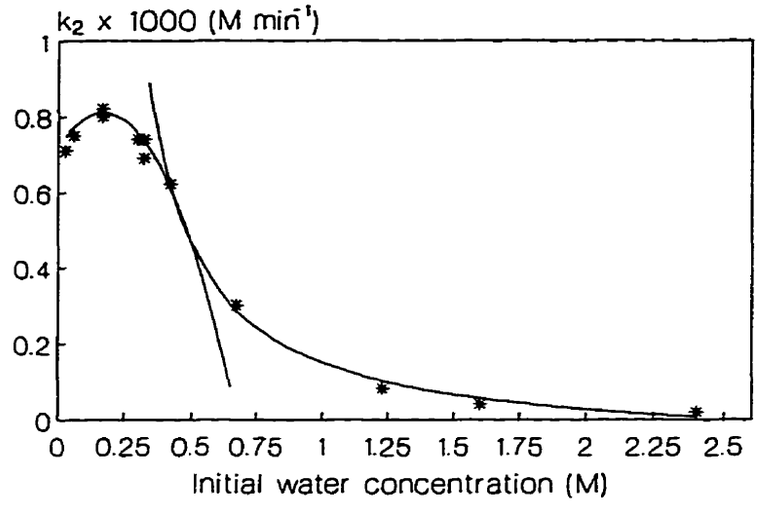

Figure 5.1.5-2: The correlations in equation (5.17) used to describe k_2 as a function of water concentration.

Equations (5.16) and (5.17) are incorporated into the CD model to account for the effects of water on the reaction kinetic expressions. These empirical expressions are preferred over the kinetic expressions developed in Chapter 3 because the kinetic expressions in Chapter 3 do not account for the non-ideality of water.

Equations (5.16) and (5.17) were developed for a catalyst exchanged to 0.49 mmol OH^-/mL for 24 h, however, and many catalysts do not exactly match these conditions. Therefore, it is assumed that the dependence of the reaction rate on water concentration is 'similar' for other catalysts. Thus, by incorporating a proportionality constant, equations (5.16) and (5.17) can be corrected and used to describe other catalysts. Once the appropriate rate constant is determined, the model then uses equation (5.15) to correct the units of the rate constant.

5.1.6 Vapour Liquid Equilibrium

Vapour-liquid equilibrium (VLE) data are necessary for distillation calculations. Vapour pressure data for each pure component, and a way of estimating liquid phase activity coefficients are required to obtain this VLE data. In our system, acetone, DAA, and MO are all fairly similar in structure, and no serious non-idealities are anticipated in mixtures of these compounds. Water has quite a different structure and polarity when compared to the ketones, and it is likely that water will behave non-ideally.

Using the UNIFAC group contribution method (Smith and Van Ness, 1987) good estimates of the liquid phase activity coefficients (γ_i) can be obtained. Component i behaves ideally if γ_i=1. Assuming that the vapour phase behaves ideally, the vapour composition can be calculated from the liquid composition, the liquid phase activity coefficient, and the vapour pressure of pure i. This relationship is

$$y_i P_T = \gamma_i x_i P_i^{vap}. \tag{5.18}$$

The vapour pressure of each pure component (P_i^{vap}) must be known. Vapour pressure is a function of temperature (T), and is often correlated by Antoine's equation (5.19).

$$\ln\left(P_i^{vap}\right) = A - \frac{B}{T + C} \tag{5.19}$$

In Antoine's equation, T is measured in K and the vapour pressure is reported in bar (1 bar = 100 kPa). Values of the constants A, B, and C were obtained from Daubert and Danner (1989) and Himmelblau (1982), and are shown in Table 5.1.6-I.

Activity coefficients for the binary systems acetone-DAA, acetone-MO, and acetone-water were calculated at 1.013 bar over the entire composition range to check for non-ideal behaviour. These results are shown in Table 5.1.6-II.

Table 5.1.6-I: Constants for Antoine's equation (5.19).

	Acetone	Water	DAA	MO
A	9.9734	11.6832	8.3601	9.0212
B	2879.49	3816.44	2900	2900
C	-38.411	-46.13	-100.013	-80.447

Table 5.1.6-II: Activity coefficients (γ_i) at 1.013 bar for the indicated binary systems.

Mole Frac. Acetone	Binary System: Acetone-DAA		Binary System: Acetone-MO		Binary System: Acetone-Water	
x_1	Acetone	DAA	Acetone	MO	Acetone	Water
.000001	.9060	1.0000	.9826	1.0000	11.0456	1.0000
.1	.9340	.9993	.9893	1.0000	5.0713	1.0397
.2	.9539	.9973	.9939	.9994	3.0783	1.1334
.3	.9691	.9941	.9971	.9989	2.2104	1.2641
.4	.9808	.9900	.9992	.9984	1.7544	1.4301
.5	.9896	.9853	1.0005	.9982	1.4819	1.6407
.6	.9958	.9806	1.0010	.9983	1.3032	1.9190
.7	.9995	.9769	1.0010	.9991	1.1779	2.3157
.8	1.0009	.9760	1.0007	1.0010	1.0875	2.9477
.9	1.0006	.9814	1.0002	1.0044	1.0258	4.1279
.999999	1.0000	.9996	1.0000	1.0102	1.0000	6.9371

The data in Table 5.1.6-II show that the acetone-DAA and acetone-MO systems are essentially ideal throughout the entire composition range. Since we will be dealing with dilute solutions of DAA and MO in acetone, it is reasonable to assume that these three compounds behave ideally. The value of γ_{water} for dilute mixtures of water in acetone is very much higher than 1, and indicates that water behaves non-ideally.

The VLE behaviour of the acetone-water system was studied by Brunjes and Bogart (1943), and their experimentally determined activity coefficients agree well with the data presented in Table 5.1.6-II. A plot of the activity coefficients for the acetone-water system is shown in Figure 5.1.6-1.

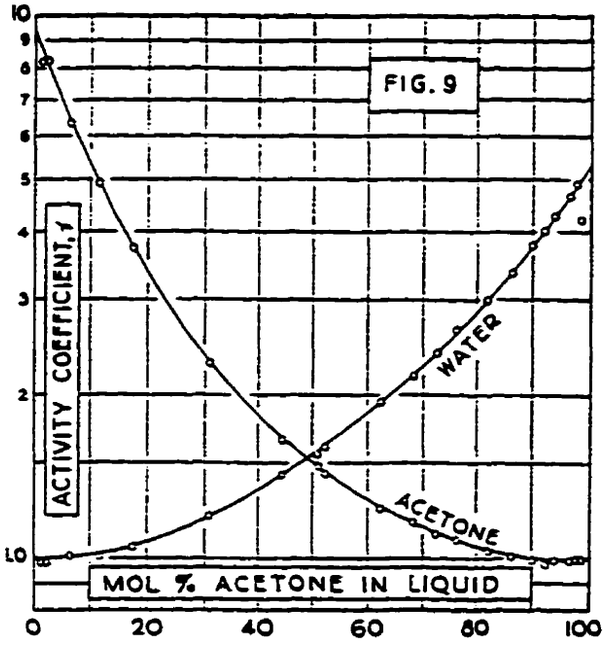

Figure 5.1.6-1: Activity coefficients for the binary system acetone-water at 101.3 kPa (Brunjes and Bogart, 1943). Reprinted, with permission, from *Industrial and Engineering Chemistry.* ©American Chemical Society, 1943.

Brunjes and Bogart (1943) constructed a VLE diagram for this system, and compared their work with data from two additional sources in Figure 5.1.6-2. As the mole fraction of acetone approaches 1, the equilibrium curve and the diagonal come in close proximity. Based on these experimental data, it does not appear that an azeotrope exists. However, Braithwaite (1995) states that there is an azeotrope at 98.7 wt% acetone (≈ 96 mol% acetone).

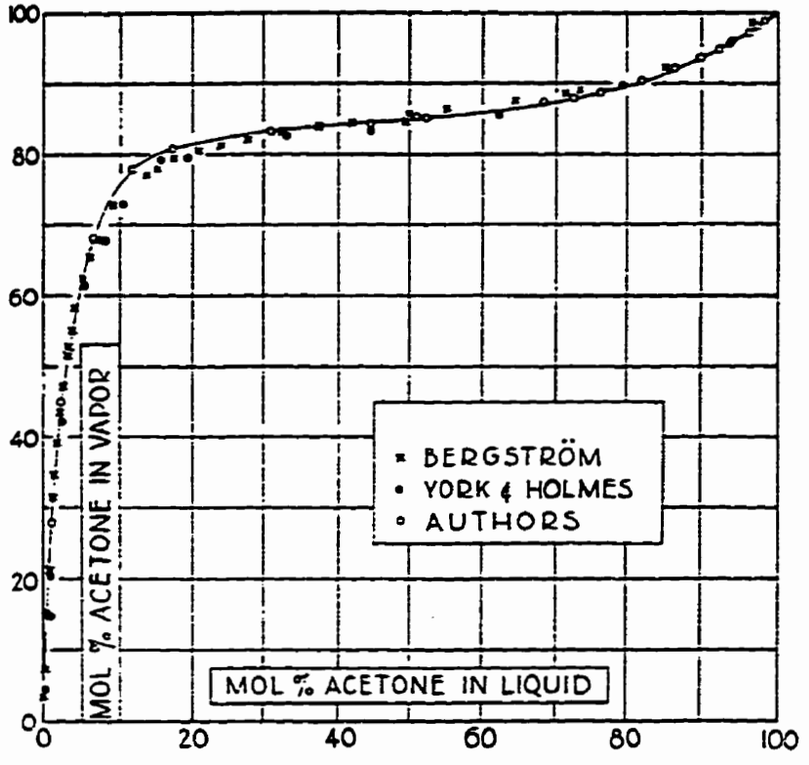

Figure 5.1.6-2: VLE diagram for acetone-water at 101.3 kPa (Brunjes and Bogart, 1943). Reprinted, with permission, from *Industrial and Engineering Chemistry*. ©American Chemical Society, 1943.

Since the reaction rate equations in Section 5.1.5 are sensitive to very low concentrations of water, a closer examination of the VLE behaviour of the acetone-water system is warranted. A VLE plot at high acetone concentrations was constructed from UNIFAC data to investigate the existence of an azeotrope. Figure 5.1.6-3 shows the results of the UNIFAC calculations, which predict an azeotrope for this system. There is a minimum boiling azeotrope at 97.9 mol% acetone. The close proximity of the equilibrium curve and the diagonal in the vicinity of the azeotrope is likely the reason that this azeotrope was undetected by Brunjes and Bogart (1943). Extremely accurate measurements would be required to verify the UNIFAC prediction.

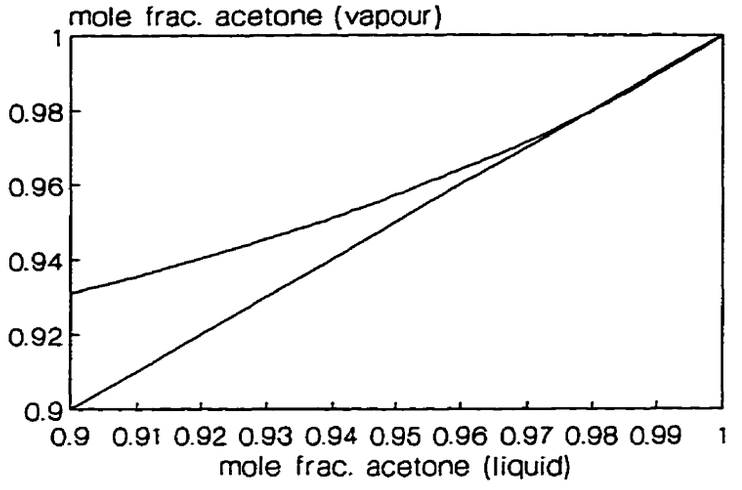

Figure 5.1.6-3: VLE diagram for acetone-water at 101.3 kPa based on UNIFAC activity predictions.

In Table 4.3.2-II, the composition of several overhead samples from a batch CD experiment was determined. An average of 99.08 wt% acetone and 0.92 wt% water was found in these samples. Braithwaite (1995) claims that an azeotrope exists at 98.7 wt% acetone. This seems unlikely, however, since the samples obtained from the batch CD experiment have a higher concentration of acetone than the Braithwaite's azeotrope would permit. When converted to a molar basis, the average composition of the samples in Table 4.3.2-II is 2.91 mol% water and 97.09 mol% acetone. This concentration of acetone does not exceed the azeotropic composition predicted by UNIFAC. Therefore, it was decided to use the UNIFAC prediction of the VLE behaviour in the model.

It is clear from Figure 5.1.6-3 that Raoult's law will not adequately describe the VLE behaviour of acetone/water. This non-ideality must somehow be incorporated into the CD model. However, it is not practical to include the UNIFAC equations in the model, since they are rather cumbersome. Thus, a simplified correlation must be developed.

To develop this correlation, activity data from the acetone-water system was regressed in the area of the azeotrope ($0.02 \leq x_{water} \leq 0.06$). The data is fairly linear over this narrow

region of interest, and is approximated very well by equation (5.20).

$$\gamma_{water} = -29.84x_{water} + 6.6798 \qquad (5.20)$$

Equation (5.20) is used by the model to take into account the non-ideality of water. The composition of MO and DAA in the vapour phase is simply calculated using Raoult's Law, which assumes that γ=1.

5.1.7 Fraction of Liquid Flowing Through the Bag - f

Only a fraction of the liquid refluxing inside of the column will actually flow through the catalyst bag. Because of problems with liquid distribution, a good portion of the liquid will bypass the bag. A discussion of liquid maldistribution and flow patterns in packed columns was presented in Section 4.1. The literature suggests that flow patterns in narrow packed columns are impossible to control, and are plagued by 'wall effects'. As a result, it was anticipated that determining the amount of liquid that passes through the catalyst bags would be difficult, and the results presented in Section 4.1.2 verify this expectation.

Attempts to measure the fraction of the total liquid flow passing through the catalyst bag were summarized in Table 4.1.2-I, and these data showed a tremendous amount of scatter. Consequently, f is the only parameter for which we cannot provide a reliable method of prediction. Thus, the value of f will be adjusted to fit the model to the experimental data. The value of the f will be varied until the simulated catalyst activity for DAA production matches the experimentally observed value. Based on the data of Porter and Templeman (1968), it is expected that the value of f will fall somewhere between 0.05 and 0.3.

Section 4.3 presents results from batch CD experiments where the liquid distribution was more carefully controlled. No random packings were used, and all of the liquid returning from the condenser directly contacted the catalyst bag. The simulation of these results will follow the same procedure of varying f until the simulated and measured DAA activities match. However, one would anticipate much higher values of f from these simulations.

5.2 Solving the PDEs and ODEs

Two issues involved in solving the differential equations of Section 5.1 are discussed in this section. Firstly, the boundary conditions are specified. Secondly, a basic method of actually obtaining a solution to the system of equations and boundary conditions will be presented.

5.2.1 The Boundary Conditions

In order to solve the PDEs and ODEs presented in equations (5.2) - (5.4), boundary conditions are required. One must not only determine the form of the boundary conditions, but the number of boundary conditions which are required. The ODEs in (5.3) and (5.4) contain derivatives which are first order with respect to the height variable, z. Thus, only one boundary condition is required for each ODE. Since equation (5.2) is second order with respect to radial position and first order with respect to height, it is necessary to specify two conditions for $C_{i,bag}$ at any r, and one condition for $C_{i,bag}$ at any z (Lapidus, 1962).

It should be stressed that equations (5.2) - (5.4) are written for each component, and our system involves three independent components (ie. DAA, MO, and water). For a problem involving one catalyst bag, there are 6 ODEs and 3 PDEs. For problems involving more than one catalyst bag, equations (5.2) - (5.4) are written for *each bag* placed in the CD column. The experiments presented in Section 4.2 were conducted with as many as 6 bags. This means solving a system with as many as 54 ODEs and PDEs.

In order to improve the flexibility of the model, the number of catalyst bags (N) is supplied by the user. Therefore, it is necessary to develop boundary conditions that are general enough to be applied to any number of bags. Since each catalyst bag requires 3 equations each from (5.2), (5.3), and (5.4), 15 boundary conditions (3x3 + 3x1 + 3x1) are required for each catalyst bag. The total number of boundary conditions is 15N. Each of the boundary conditions is now briefly explained in the following paragraphs, and the total

number of conditions will be tallied to ensure that the problem is not over or under-specified.

The boundary conditions for the PDEs (5.2) are as follows:

1) As a condition of symmetry, the derivative of $C_{i,bag}$ with respect to radius is zero at the center of the bag. This is written for each component in each bag (3N times).

$$\frac{\partial C_{i,bag}(z,r)}{\partial r} = 0, \quad \textit{for all } z,\ r=0 \tag{5.21}$$

2) At the wall of the bag, the rate of mass transfer to the liquid outside of the bag must equal the rate of radial dispersion inside of the bag. This is another condition on r, and may be written for each component in each bag (3N times). No further conditions on r are required.

$$2\pi R\mathcal{D} \frac{\partial C_{i,bag}(z,r)}{\partial r} = k_{C,i}A\ (C_{i,bag}(z,r) - C_i(z)), \quad \textit{for all } z,\ r=R \tag{5.22}$$

3) The composition of the liquid entering the top of a catalyst bag must be specified, and is assumed to be constant for all r. This is a condition on z, and may be written for each component. This condition, however, is written differently for the top bag than for the bags that are placed underneath. Since the column is at total reflux., the liquid composition at $z = 0$ equals the vapour composition at $z=0$.

$$C^{1}_{i,bag}(z,r) = \frac{V}{L} c_i^{1}(z)\ , \quad \textit{for all } r,\ z=0 \tag{5.23}$$

In equation (5.23), the superscript 1 signifies that this equation is only valid for the bag at the top of the column. For subsequent bags ($n = 2..N$), $C_{i,bag}(0,r)$ is determined by mixing the liquid exiting bag n-1 (at $z=Z$) and the liquid descending from outside of bag n-1. The bag numbering system, and the mixing of the two liquid streams is depicted in Figure 5.1-1. This boundary condition is expressed as:

$$C_{i,bag}^{n}(z=0,r) = f\overline{C_i^{n-1}} + (1-f)C_i^{n-1}(z=Z), \quad \textit{for all } r \tag{5.24}$$

In equation (5.24), $\bar{C}_i^{n-1}$ is the average concentration emerging from the bottom of bag n-1, and is determined by evaluating the integral in equation (5.5). Equation (5.23) is written 3 times, and equation (5.24) can be written 3(N-1) times, for a total of 3N boundary conditions.

The boundary conditions for the ODEs in equation (5.3) and (5.4) will now be presented.

4) The feed to the reactive section of the CD column is the vapour which enters from the bottom of the reaction zone. Therefore, the vapour composition at the bottom of the reaction zone must be specified as a boundary condition. A reasonable approximation of this composition is obtained if the vapour entering the reaction zone is assumed to be in equilibrium with the liquid leaving the reaction zone. This is expressed as

$$y_i^N(z) = \frac{\gamma_i x_{i,Avg.}^N P_i^o}{P_{tot}}, \; at \; z=Z. \tag{5.25}$$

It is important to realize that the mole fraction composition of the liquid leaving the reaction zone ($x^N_{i,Avg}$) must be determined by mixing the liquid that exits the lowest (N^{th}) bag with the liquid that bypasses the lowest bag. As in equation (5.24), this mixing is assumed to be complete, and instantaneous after each bag in the column. This equilibrium approximation is reasonable since most of the product separation takes place in the reboiler of the CD column. Therefore, as the vapour passes upward through the inert distillation packing, it is exposed to liquid of nearly constant composition, which allows time for equilibration.

Equation (5.25) is written at the bottom (z=Z) of the catalyst bag furthest down the column, which is indicated by the superscript N. This equation can be written 3 times.

The vapour composition must also be specified at the bottom (z=Z) of each of the

other catalyst bags (n = 1 .. N-1). The vapour composition at the bottom of bag n-1 equals the composition of the vapour leaving the top of bag n. This is shown in equation (5.26).

$$c_i^n(0) = c_i^{n-1}(Z) \qquad (5.26)$$

This boundary condition links together the vapour flows that pass each bag. Figure 5.1-1 helps visualize the physical situation. In the pilot scale distillation column, a few Intalox saddles were placed between the catalyst bags to improve liquid mixing. In this model, however, it is assumed that this small amount of packing does not change the vapour composition between the bags. Equation (5.26) can be written for n=2..N, or 3(N-1) times. Therefore, equations (5.25) and (5.26) comprise an additional 3N boundary conditions.

5) At the very top of the reactive zone, the composition of the liquid which does not pass through the catalyst bag equals the composition of the vapour at the top of the reaction zone. This is similar to boundary condition (5.23), which sets the composition of the liquid at the top of catalyst bag 1. In fact, for each bag in the reaction zone of the column, the composition of the liquid entering the top of the bag equals the composition of the liquid bypassing the top of the bag. This condition is written as

$$C_i^n(z) = C_{i,bag}^n(z,r) \ , \quad at\ z=0,\ r=0,\ for\ all\ n. \qquad (5.27)$$

This is a fairly simple boundary condition, and is possible since the liquid streams are assumed to mix completely and instantaneously at the bottom of each catalyst bag. Equation (5.27) contributes an additional 3N boundary conditions.

At this point, 15N boundary conditions have been specified. This matches the number of boundary conditions that are required, and the problem is completely specified.

5.2.2 The Method of Solution

The complexity of the system of equations and boundary conditions presented in Sections 5.1 and 5.2 suggests that obtaining an analytical solution is impractical. In order to solve these equations, therefore, numerical methods must be used. These methods are frequently based on the concept of finite differences.

Let f(x) be a single valued, finite, continuous function of x for the following discussion of finite difference methods. Using Taylor's expansion theorem, the following two relationships can be obtained (Finlayson, 1980; Smith et. al., 1970):

$$f(x+\Delta x) = f(x) + \Delta x \frac{df(x)}{dx} + \frac{\Delta x^2}{2}\frac{d^2f(x)}{dx^2} + \frac{\Delta x^3}{6}\frac{d^3f(x)}{dx^3} + \cdots \qquad (5.28)$$

$$f(x-\Delta x) = f(x) - \Delta x \frac{df(x)}{dx} + \frac{\Delta x^2}{2}\frac{d^2f(x)}{dx^2} - \frac{\Delta x^3}{6}\frac{d^3f(x)}{dx^3} + \cdots \qquad (5.29)$$

If these series are truncated after two terms, and rearranged, the following expressions are obtained for the derivatives of f(x):

$$\frac{df(x)}{dx} = \frac{f(x+\Delta x) - f(x)}{\Delta x} \qquad (5.30)$$

$$\frac{df(x)}{dx} = \frac{f(x) - f(x-\Delta x)}{\Delta x} \qquad (5.31)$$

Equation (5.30) is called a *forward difference* approximation of the first derivative, and (5.31) is a *backward difference* approximation of the first derivative. Ignoring the higher order terms in (5.28) and (5.29) introduces error, however, and these errors are said to be on the order of Δx.

A technique used to reduce the error of these approximations involves the subtraction of equation (5.29) from (5.28). If this is done, and all terms involving Δx^3 and higher are neglected, the following approximation of the first derivative is obtained:

$$\frac{df(x)}{dx} = \frac{f(x+\Delta x) - f(x-\Delta x)}{2\Delta x} \tag{5.32}$$

Equation (5.32) is called a *central difference* approximation of the first derivative, and has errors on the order of Δx^2. If equations (5.28) and (5.29) are added together, and all terms involving Δx^4 and higher are neglected, the following expression for the second derivative is obtained:

$$\frac{d^2f(x)}{dx^2} = \frac{f(x+\Delta x) - 2f(x) + f(x-\Delta x)}{\Delta x^2} \tag{5.33}$$

Equation (5.33) is also said to have errors on the order of Δx^2.

The significance of equations (5.30) - (5.33) is that values of the first and second derivatives of an unknown function can be expressed in terms of the values of the function at discrete points. These approximations can be substituted into the original differential equations and boundary conditions, transforming them into algebraic equations. For simplicity, this discussion dealt with a function of one variable. However, this technique may be readily extended to partial derivatives of a function of several variables.

To solve a practical problem, the region being considered is usually divided into an appropriate number of equally spaced finite differences. This produces a grid of points at which values of the function will be determined. The differential equations, or boundary conditions, are written at each grid point, which produces an equal number of equations and unknowns. Using various matrix methods, the unknowns in this system of equations are solved simultaneously. There are a wide variety of techniques used to solve these types of problems, and many of these methods are discussed in the texts by Lapidus (1962), Smith et. al. (1970), or Finlayson (1980). Dieterich et. al. (1994) provide a good review of numerical techniques used to solve systems of equations, and also provide some insight into the attitude of an engineer:

> In contrast to the computer scientist, or the (numerical) mathematician, the engineer usually considers numerical simulation as a tool with whose details he wants to become acquainted only up to a point which is necessary for its practical application.

Thus, a lengthy discussion of these mathematical techniques will not be presented.

A software package called *gPROMS* (version 1.3c) was ultimately used to solve the simulations for this thesis. *gPROMS* was developed at Imperial College, in London, England, and is available to the Chemical Engineering Department at the University of Waterloo on the CAPE computer system. Several different numerical techniques are included in the *gPROMS* package. Due to its improved accuracy over the forward and backward finite difference techniques, the *central difference* method was selected for this work.

Although *gPROMS* is a powerful package, there is no documentation describing the program in any detail. It is necessary to learn the program by studying the example problems which are provided, and by consulting with others who have already studied the example problems. Another consequence of having no manual is that the user is unclear of the exact techniques used to solve the equations.

In order for *gPROMS* to work properly, the problem must be translated into a language that *gPROMS* understands. This requires the creation of a text file in which the following sections are provided:

- definition of *variables*, *parameters*, and units (variables are unknowns which are solved for as part of the problem, while parameters are user supplied constants)
- definition of the *domain*, or the region over which the ODEs and PDEs will be solved
- statement of the *boundary* conditions
- statement of the differential *equations*
- *setting* of the parameters
- specification of the numerical method (*CFDM* = central finite difference method)
- statement that the simulation is at *steady state*.

A sample of the code is provided in Appendix H, and the reader will notice the italicized words (above) appear in various sections of this code.

The height of a catalyst bag, Z, was usually near 8 cm. This is referred to as the AXIAL domain, and is described by 11 grid points. The radius of a bag is roughly .75 cm. This is the RADIAL domain, and is described by 9 grid points. Typically, the accuracy of a solution improves when the number of grid points increases. Several tests, however, showed

that very small changes in the outcome of the simulation resulted when the number of points was increased beyond these values. Therefore, this grid spacing was deemed to be adequate.

The amount of time required to solve a simulation depends strongly on the number of bags specified. A problem with only one catalyst bag is usually solved within 1 minute, while a problem with 6 catalyst bags could take nearly 15 minutes.

The correlations used to obtain various mass transfer coefficients are not incorporated into the code. The user must supply these values as parameters. This was done since the inclusion of mass transfer correlations in the code increased the time required to reach a solution. A problem with one catalyst bag required nearly 20 minutes! This is due to the non-linear nature of the correlations, which makes converging to a solution much more difficult. Therefore, values of these parameters were determined on a separate spreadsheet. A sample of this spreadsheet is provided in Appendix I.

5.3 Simulation Results

Simulations were run for most of the experiments presented in Chapter 4. The results from the simulation of the batch CD experiments in Section 4.1 will be presented first, followed by the results from Sections 4.2 and 4.3.

5.3.1 Simulation of the Batch CD Experiments

Although batch distillation is a dynamic process, the reaction zone of the batch CD column can adequately be described with a steady state model since the conditions in the reaction zone remain essentially constant for a long period of time. The results of these simulations will be necessarily summarized in this section. The model produces far more information than is actually useful, and presenting the complete results of a simulation would be rather uninteresting. The simulation of the batch CD experiment at 75 V (see Figure 4.1.3-3 and Table 4.1.3-I) will be presented in more detail, however, to provide insight into the internal workings of the catalyst bag.

In order to obtain the required mass transfer coefficients, the following variables must be specified:

- the flow rate of acetone (the reflux flow rate)
- the fraction of liquid that flows through the bag (f)
- the radii of the bag and the column
- the temperature
- the total pressure
- the vapour and liquid phase diffusivity of each component in acetone
- the density of acetone
- the catalyst particle diameter
- the void fraction of the catalyst
- the vapour and liquid phase viscosity

These variables are input to a spreadsheet which calculates the values of the mass transfer coefficients. A sample spreadsheet for the experiment at 75 V is available in Appendix I. The mass transfer coefficients are then entered into the gPROMS code as parameters.

The catalyst used for the experiments in Section 4.1 had $k_1 = 0.36 \times 10^{-3}$ M^{-1} min^{-1} and $k_2 = 0.001$ M min^{-1} when tested in a batch reaction. This catalyst was slightly different from the batch used to determine the constants in Section 5.1.5. Because of differences exchange time during the catalyst preparation the value of k_2 in the program (0.0008 M min^{-1} at 0.17 M H_2O) must be multiplied by 1.25 to raise it to match the experimental value of 0.001 M min^{-1}. A remark in the program code in Appendix H highlights this constant.

As indicated in Section 5.1.7, predicting the fraction of the liquid flow which passes through the catalyst bag (f) would be a Sisyphean effort. A more appropriate approach is to use f as an adjustable parameter. With a trial-and-error approach, the value of f was changed until the DAA catalyst activity from the simulation matched the value obtained in the experiment. For the run at 75 V, the catalyst activity was 0.60 g DAA/mL_{cat}·h. Five or six simulations were typically run before a satisfactory value of f was discovered.

The results of most interest from these simulations are as follows:

- the catalyst activity for MO production
- the product selectivity (mol DAA:mol MO)
- the percentage of the total production radially transferred through the wall of the bag

For the batch CD experiment at 75 V, the simulated DAA activity equalled 0.60 g DAA/mL_{cat}·h when f = 0.1952. The simulated MO production rate is 0.181 g MO/mL_{cat}·h. Thus, the simulated product selectivity is 2.80 mol DAA/mol MO. This compares very well with the data presented in Table 4.1.3-I.

Three dimensional concentration profiles within the catalyst bag were constructed with the data from this simulation, and are shown in Figures 5.3.1-1 to 5.3.1-3. Figure 5.3.1-1 provides a picture of the DAA concentration profile, and shows clearly that reaction equilibrium is reached within the first few centimeters of the top of the bag (z=0). This plot also shows that the concentration of DAA inside the bag is a strong function of the radial position. There is a significant concentration gradient near the outer edge of the bag, and the simulation predicts that 53.7% of the DAA which is produced is radially transferred through the sides of the bag.

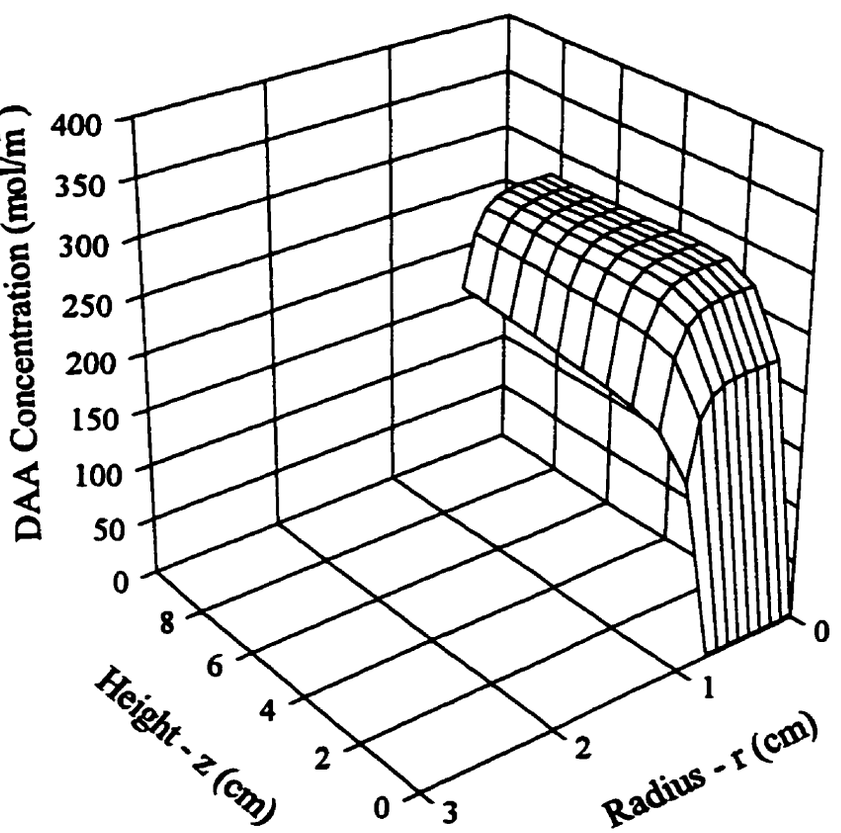

Figure 5.3.1-1: DAA concentration profile inside of the catalyst bag (from the simulation of the batch CD experiment at 75 V).

There are also radial concentration gradients for MO, as shown in Figure 5.3.1-2. Although MO production is not limited by equilibrium at these conditions, there is a significant radial concentration gradient. The simulation results suggest that 41.8% of the total amount of MO produced is radially transferred out of the catalyst bag, which is lower than the fraction of DAA which is radially transferred. A smaller fraction of the MO production is radially transferred because the driving force for radial mass transfer, the concentration difference between the outer edge of the bag and the liquid flowing outside of the bag, is lower for MO than for DAA. This can be visually confirmed by comparing Figures 5.3.1-4 and 5.3.1-5. These figures show the concentrations of DAA and MO inside and outside of the bag. The three sets of data represent the concentrations along the center of the bag (at r=0), at the outer edge of the bag (at r=R), and concentrations of the liquid flowing outside of the bag.

The concentration profile for water is shown in Figure 5.3.1-3, and is somewhat unique. The concentrations of MO and DAA at the top of the catalyst bag were both very close to zero. At z=0, the concentration of MO and DAA is 2.87 and 1.45 mol/m^3, respectively. The concentration of water, however, was 401 mol/m^3 at z=0. This elevated water concentration is a consequence of the azeotrope between water and acetone which was discussed in Section 5.1.6. A concentration of 401 mol/m^3 of water in acetone is equivalent to 0.96 wt% water. This mass fraction of water is very close to the amount determined in the overhead samples which were analysed in Table 4.3.2-II, and suggests that the VLE portion of the model is quite accurate.

Water is a byproduct of MO formation, and also exhibits radial concentration gradients inside of the catalyst bag. The simulation results indicate that 42.7% of the total amount of water produced is radially transferred out of the bag. As expected, this is very similar to the amount of MO radially transferred out of the bag, but is just slightly higher because of the higher mass transfer coefficients for water. The mass transfer coefficient for water is higher than for MO or DAA because the diffusivity of water in acetone is higher. This is shown in the spreadsheet in Appendix I.

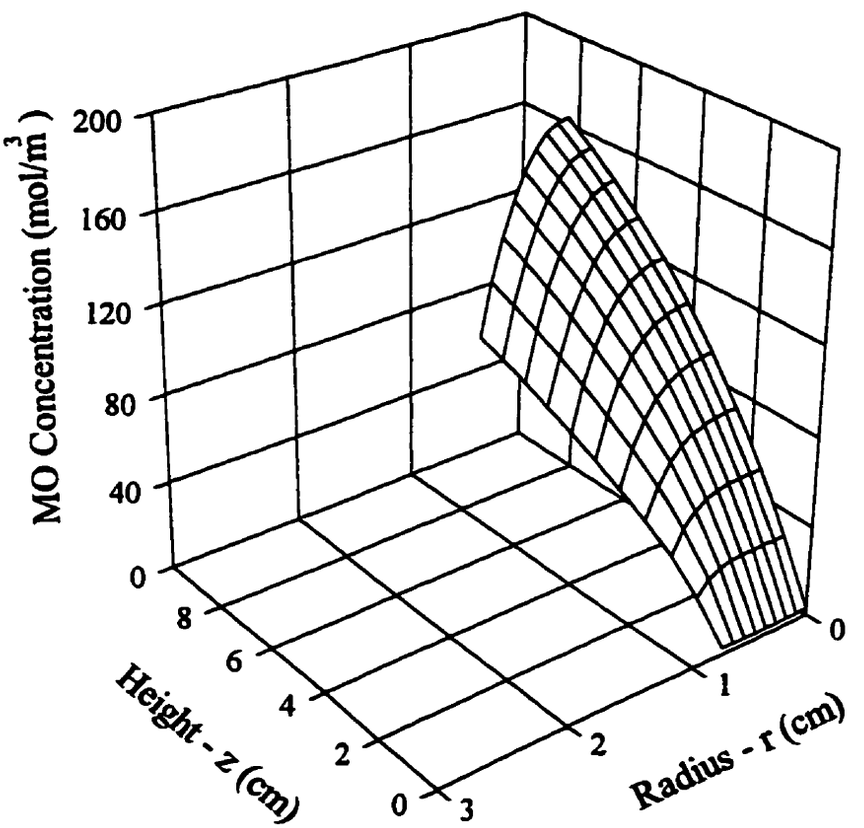

Figure 5.3.1-2: MO concentration profile inside of the catalyst bag (from the simulation of the batch CD experiment at 75 V).

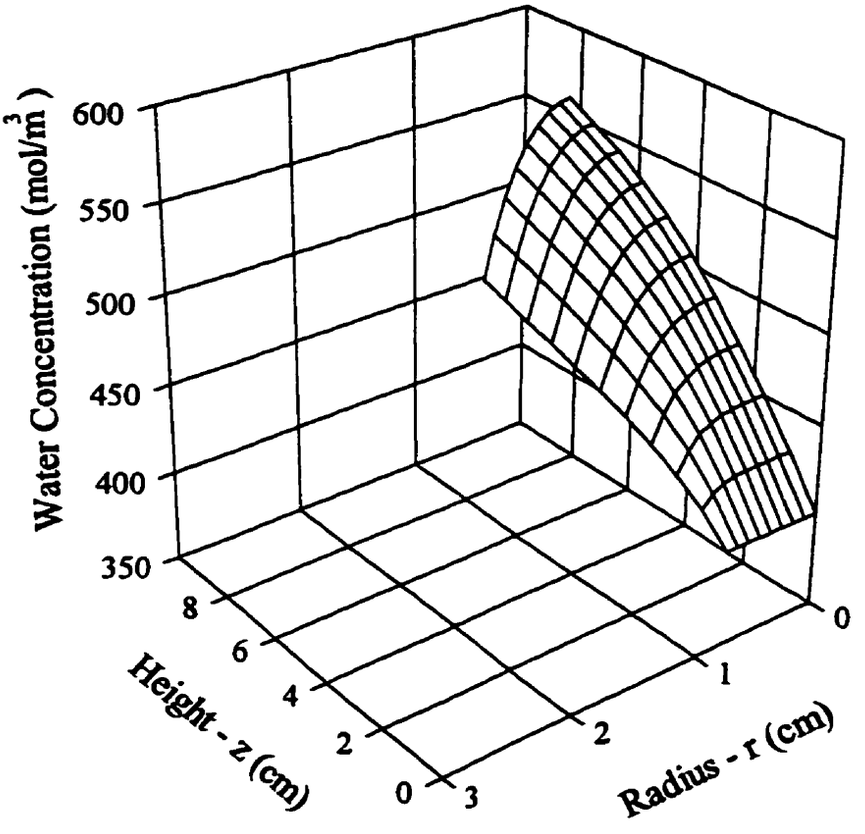

Figure 5.3.1-3: Water concentration profile inside of the catalyst bag (from the simulation of the batch CD experiment at 75 V).

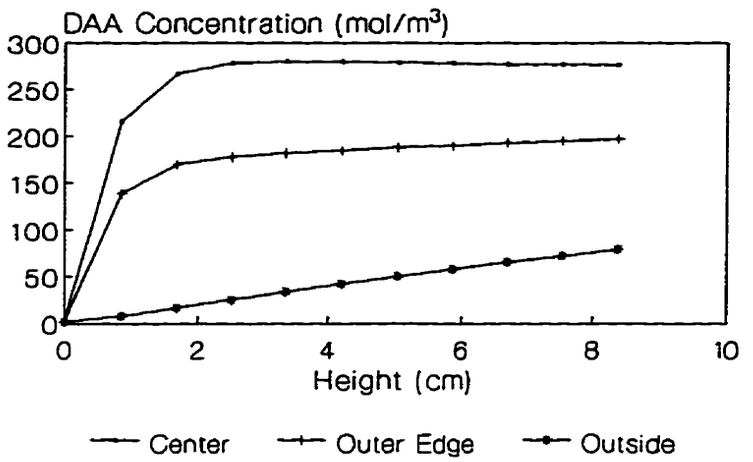

Figure 5.3.1-4: A comparison of DAA concentrations at the center of the catalyst bag (r=0), at the outer edge of the catalyst bag (r=R), and outside of the bag.

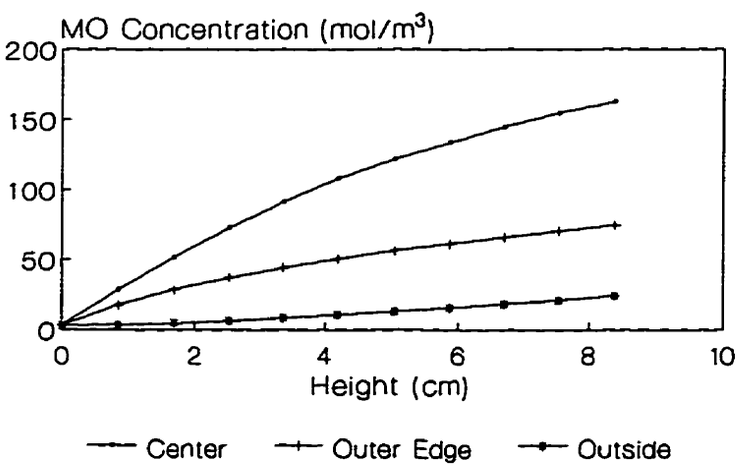

Figure 5.3.1-5: A comparison of MO concentrations at the center of the catalyst bag (r=0), at the outer edge of the catalyst bag (r=R), and outside of the bag.

A summary of the simulation results for the experiments of Section 4.1 is provided in Table 5.3.1-I. This table shows the values of f which balance the DAA production rates, the MO production rates, the product selectivities, and the percentages of the total production of each component which is credited by the simulation to radial mass transfer.

Table 5.3.1-I: Summary of the simulation results for the batch CD experiments of Section 4.1.

Reboiler (V)	Flow (g/min)	Z (cm)	f	DAA Activity ($g/mL_{cat} \cdot h$)	MO Activity[a] ($g/mL_{cat} \cdot h$)	Selectivity[a] (mol DAA /mol MO)	% Radial Production
65	8.76	8.54	.1045	0.33	0.145 (0.17)	1.928 (1.685)	67.8% DAA 54.9% MO 55.5% Wat.
75	12.27	8.38	.1952	0.60	0.181 (0.18)	2.801 (2.848)	53.7% DAA 41.8% MO 42.7% Wat.
85	16.36	6.66	.2837	1.07	0.222 (0.23)	4.053 (3.946)	36.9% DAA 26.9% MO 28.1% Wat.
85	16.36	9.15	.7316	1.54	0.214 (0.20)	6.077 (6.406)	15.7% DAA 11.5% MO 7.5% Wat.

[a]experimental data taken after 10 h of operation are shown in brackets

The results in Table 5.3.1-I show that there is good agreement between the model and the experimental data. The values of f in three of the four experiments fall between 0.05 and 0.3, as predicted from the work of Porter and Templeman (1968). The f-values also reveal that a higher fraction of the liquid tends to flow through the bag at higher flow rates. This trend was observed by Porter and Templeman (1968), but was not supported by attempts to measure the value of f in Section 4.1.2. However, the random nature of the distillation

packing is evident in the experiments at 85 V. These experiments, conducted at the same flow rate, resulted in different flow patterns and DAA activities.

The relative amount of product radially transferred out of the catalyst bag is quite high at lower flow rates, but decreases as the flow rate in the column is increased. Although the radial mass transfer rate tends to increase at higher flow rates, this is small when compared to the increase in the rate of product removal by convection through the bottom of the bag. For example, when the reboiler is increased from 65 V (f = 0.10) to 85 V (f = 0.28), the radial production rate of DAA increases by 37%, but the total production rate of DAA increases by 151%. Thus, the relative importance of radial mass transfer decreases at higher flow rates.

Although the simulation worked well for the experiments shown in Table 5.3.1-I, the simulation was not successful for the experiment conducted at 55 V. The results of this experiment were presented earlier in Table 4.1.3-I. The value of f required to have the model match the DAA activity was very low (ie. near 0.02), and the basic assumptions of the model likely broke down at such low flow rates.

A key assumption in the model is that the catalyst bag is completely filled with liquid. At the low liquid flow rates associated with a reboiler setting of 55 V and very low values of f, it is likely that the bag was not filled with liquid. A second assumption is that there is no contact between vapour and the liquid inside of the bag, which is reasonable only if the bag is filled with liquid. If the bag is not filled with liquid, acetone could enter the bag as a vapour and the reaction products could then trickle out of the bag in the liquid phase. Clearly, this mode of operation cannot be described by the current model.

It is of interest to change the values of the parameters in the model to determine the sensitivity of the final results to these changes. The simulation of the experiment at 85 V with f=0.28 was taken as the base-case, and was solved many times with different values of the parameters. Table 5.3.1-II shows a summary of the results of this 'Sensitivity Analysis'. The values of the parameters were varied by either ±10% or ±20% and the percentage of change in the observed DAA and MO production rates is reported.

Table 5.3.1-II: Sensitivity analysis for the CD model.

Variable(s)	Change	% change in DAA production		% change in MO production	
		- change	+ change	- change	+ change
Đ	±20%	-0.186	+0.215	-0.046	+0.057
k_fA''	±20%	-1.017	+0.301	-0.088	+0.077
$K_{OG}A$	±20%	-0.244	-0.186	-0.149	+0.160
k_CA	±20%	-2.313	+2.046	+0.036	-0.005
K_{EQ}	±20%	-18.245	+16.870	+0.015	-0.015
k_1 and k_2	±10%	-0.301	+0.272	-9.564	+9.492
f	±10%	-6.177	+6.034	-0.314	+0.263

The results in Table 5.3.1-II reveal the non-linear nature of this model. Note that the percentage increase in the DAA and MO production rates is seldom equal to the percentage decrease. It also appears that there are interactions between the various $K_{OG}A$ values, as increasing or decreasing the values of $K_{OG}A$ results in a slightly lower DAA production rate. Table 5.3.1-II also shows that the only variables which significantly change the MO production rate are $K_{OG}A$, f, and k_2. However, the MO production rate is most sensitive to the value of k_2. Several of the variables have a significant influence on the DAA production rate, and these variables include k_fA'', k_CA, K_{EQ}, and f. However, the rate of DAA production is most sensitive to the values of K_{EQ} and f.

These results are quite useful because they indicate the variables which must be known most accurately. For example, these results show that an error of ±20% in the value of Đ can easily be tolerated. However, the values of K_{EQ}, f, and k_2 must be known much more accurately in order to have the model function properly.

5.3.2 Simulation of the Continuous CD Experiments

The experiments conducted in the pilot scale distillation column were also simulated. These experiments are summarized in Table 4.2.2-II, and the results of the simulations are shown in Table 5.3.2-I. Again, the agreement between the actual and simulated MO production rates is quite good.

Table 5.3.2-I: Simulation of the continuous CD experiments of Section 4.2.

Expt. #	No. of Bags	Flow (g/min)	Z (cm)	f	DAA Activity ($g/mL_{cat}\cdot h$)	MO Activity[a] ($g/mL_{cat}\cdot h$)	Selectivity[a] (mol DAA /mol MO)	% Radial Production
1a	2	22.0	8.13	.2243	0.83	0.161 (0.16)	4.366 (4.449)	42.9% DAA 32.0% MO 41.2% Wat.
1b	2	22.0	8.13	.1478	0.69	0.157	-	52.3% DAA 39.9% MO 41.1% Wat.
2a	2	25.4	8.38	.1699	0.78	0.211 (0.21)	3.124 (3.109)	47.9% DAA 36.8% MO 38.1% Wat.
2b	2	15.6	8.38	.2559	0.63	0.183	-	44.3% DAA 33.7% MO 33.9% Wat.
3	4	22.9	8.94	.1581	0.49	0.124 (0.14)	3.312 (2.933)	52.9% DAA 41.0% MO 41.0% Wat.
4a	6	23.6	8.55	.1539	0.41	0.114 (0.15)	3.009 (2.270)	51.2% DAA 39.1% MO 38.8% Wat.
4b	6	16.3	8.55	.1586	0.29	0.100	-	54.9% DAA 42.1% MO 41.3% Wat.

[a]experimental data shown in brackets

The values of f reported in Table 5.3.2-I are fairly consistent. Although there are exceptions, between 14 - 17% of the total liquid flow usually passes through the catalyst bags. The flow pattern in these experiments was expected to be more reproducible since there was a much taller section of random packing above the reaction zone, which allows more time for the equilibrium flow pattern to become established in the column.

Only two experiments fell outside of this narrow range of f values. Experiment 2b had f = 0.2559, but this experiment was conducted at an unusually low flow rate. Experiment 1a had f = 0.2243, but this was shown not to be a stable situation. As depicted in Figure 4.2.2-3, the value of f declined to 0.1478 after the late-afternoon sun disturbed the normal operation of the column, influencing the liquid reflux flow rate and the flow pattern in the column.

It is possible to compare the predicted MO activity and product selectivity from the simulation with experimental data for experiments # 1a, 2a, 3, and 4a taken after 12-15 h of operation. It is not appropriate to make this comparison for all of the experiments because of excessive catalyst deactivation after this time. Agreement between the simulated data and the experimental data (shown in brackets) is quite good, but tends to worsen as the number of bags in the column increases. This could be caused by non-uniform flow patterns, which are more likely in taller reaction zones. The model assumes that the same fraction of liquid passes through each bag in the reaction zone. This is a major simplification of reality, and would likely become less valid as the height of the reaction zone increases.

The catalyst bundles are poor distillation packings (Cox, 1989). This is mainly due to their inability to distribute liquid evenly throughout the column. Thus, the task of ensuring that a reasonable portion of liquid contacts each catalyst bag rests with the short sections of Intalox saddles that are placed between the catalyst bags. A high fraction of liquid may contact the first catalyst bag, but one might reasonably expect the value of f to decline with each successive catalyst bag passed. It is not possible to investigate this idea, however, given the equipment as it currently exists. Modifying the column to include liquid redistributors between each catalyst bag would undoubtedly improve the performance and predictability of the column operation.

As was the case with the batch CD simulations in Section 5.3.1, a significant fraction

of the total production radially transfers through the sides of the bag. The results in Table 5.3.2-I show that the radial contribution becomes more significant at lower flow rates, and at lower values of f. Thus, if a high fraction of the liquid could be made to contact the catalyst bag, one would expect the relative importance of radial mass transfer to decline. In all cases, however, radial mass transfer is more significant for the production of DAA than for MO and water.

The activities listed in Table 5.3.2-I are determined by dividing the total production rate by the total amount of catalyst. A comparison of the results from experiments 1b, 3, and 4a (all with very similar values of f and the same batch of catalyst) reveals that the catalyst near the top of the reaction zone is more active than the catalyst near the bottom of the reaction zone. A steady decline in the catalyst activity for the production of DAA and MO is predicted as more bags are placed in the column. For the most part, this prediction is supported by the experimental data. The model, however, permits a closer examination of the production rates and the importance of radial mass transfer for each bag in the column. The data for experiments 1b, 3, and 4a is presented in Table 5.3.2-II.

The percentage of each reaction product which escapes each bag via radial mass transfer is surprisingly constant. Starting at the top of the reaction zone, the percentage of water that radially transfer out of the bag increases as the bottom of the reaction zone is approached. The percentage of MO which transfers radially, on the other hand, decreases as the bottom of the reaction zone is approached. These trends, however, are very subtle and their significance is questionable.

The data in Table 5.3.2-II clearly show that catalyst which is located further down the reaction zone is less active. Each catalyst bag's DAA activity is approximately 30% less than the activity of the bag above it. The decline for the MO (or water) productivity is much less, declining by 6%. Thus, the product selectivity depends strongly on the amount of catalyst loaded into the column. The decline in DAA productivity is due to reaction equilibrium restricting the concentration of DAA that is allowable. The decline in MO productivity is caused by the increasing concentration of water at lower points of the reaction zone.

Figure 5.3.2-1 shows the concentration profiles of DAA, MO, and water throughout

the entire catalyst zone from Experiment 4a. The instantaneous mixing of the liquid from inside and outside of the bag, which occurs at the bottom of each catalyst bag, is represented by the sharp vertical lines. This figure also shows that the concentration of DAA in each catalyst bag is restricted by equilibrium, and that the water concentration increases as the bottom of the reaction zone (z = 51.3 cm) is approached.

Table 5.3.2-II: Breakdown of the catalyst activity and the contribution of radial mass transfer by catalyst bag predicted by the simulations of experiments 1b, 3, and 4a.

		Expt. 1b		Expt. 3		Expt 4a	
		Activity ($g/mL_{cat}\cdot h$)	% Radial Prod'n	Activity ($g/mL_{cat}\cdot h$)	% Radial Prod'n	Activity ($g/mL_{cat}\cdot h$)	% Radial Prod'n
Bag 1	DAA	0.808	52.27	0.794	52.98	0.828	51.24
	MO	0.162	40.02	0.138	41.12	0.131	39.24
	Water	0.030	40.74	0.025	39.68	0.024	37.24
Bag 2	DAA	0.567	52.24	0.537	52.89	0.579	51.16
	MO	0.151	39.89	0.127	40.99	0.122	39.14
	Water	0.028	41.66	0.023	40.51	0.022	37.79
Bag 3	DAA			0.365	52.89	0.406	51.14
	MO			0.119	40.90	0.115	39.06
	Water			0.022	41.47	0.021	38.43
Bag 4	DAA			0.248	52.95	0.285	51.16
	MO			0.113	40.85	0.109	39.01
	Water			0.021	42.58	0.020	39.17
Bag 5	DAA					0.200	51.23
	MO					0.105	38.98
	Water					0.019	39.99
Bag 6	DAA					0.140	51.38
	MO					0.101	38.96
	Water					0.019	40.89

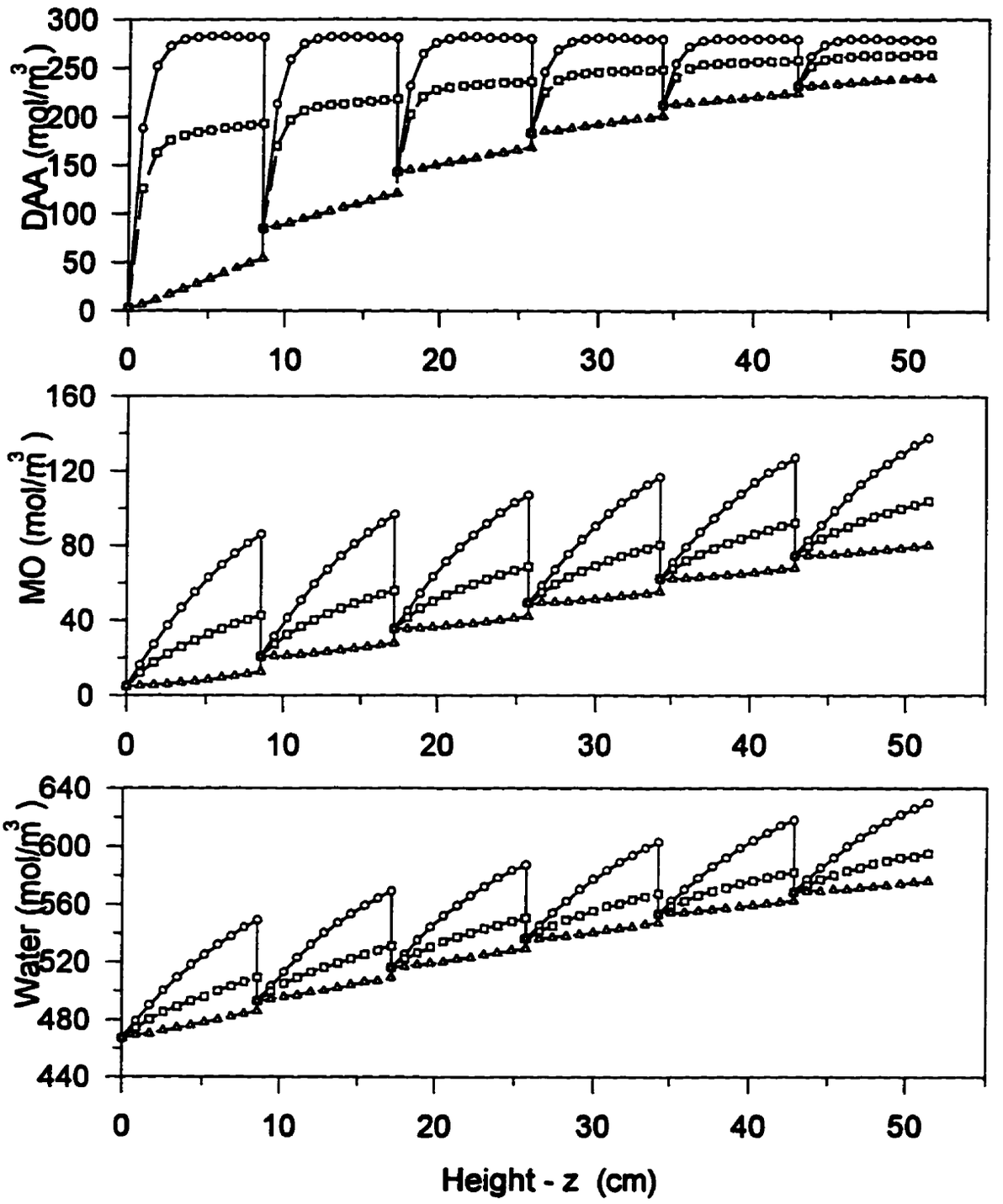

Figure 5.3.2-1: Liquid phase concentration profiles along the center of the catalyst bags, the wall of the catalyst bags, and outside of the catalyst bags.

5.3.3 Simulation of Batch CD Experiments with Controlled Liquid Distribution

Table 5.3.1-I provides a summary of the batch CD data with the liquid distributed by approximately 25 cm of ¼" Intalox saddles. The values of f reported in this table are often low, are sensitive to the flow rate, and vary over a wide range. The benefits of using a proper liquid distributor were experimentally demonstrated in Section 4.3. Other benefits of the new liquid distributor should also include much higher, and much more reproducible values of f. By fitting the model to the experimental data in Section 4.3, we can verify that these changes in the value of f do, in fact, take place. These experimental data will also provide an interesting test for the proposed model.

In Section 5.3.1, the predicted three-dimensional, liquid phase concentration profiles were plotted for the experiment at 75 V. These diagrams effectively show the concentration changes that take place as a function of height and radius in the catalyst bag. Three additional graphs were constructed which show the concentration profiles with the new liquid distributor at the same total liquid flow rate (reboiler setting of 75 V). The concentration profiles for DAA, MO, and water are shown in Figures 5.3.3-1, 5.3.3-2, and 5.3.3-3, respectively. These graphs were constructed on the same scale as the figures in Section 5.3.1 to facilitate a direct comparison.

A comparison of Figures 5.3.3-1 and 5.3.1-1 reveals the stark changes which are brought on by changing the value of f. The radial concentration gradients in Figure 5.3.3-1 are much less pronounced than in Figure 5.3.1-1. Also evident is the higher concentration of DAA at the bottom of the catalyst bag in Figure 5.3.3-1. This effect was fully discussed in Section 4.3, and is permitted by a lower reaction temperature in the catalyst bag, which increases the equilibrium concentration of DAA.

A comparison of Figure 5.3.3-2 with Figure 5.3.1-2 shows that the concentration of MO remains much lower with the new liquid distributor. The higher flow rates through the bag, combined with the lower MO production rate at a reaction temperature of 45°C, ensure that the MO concentration in the catalyst bag remains very low.

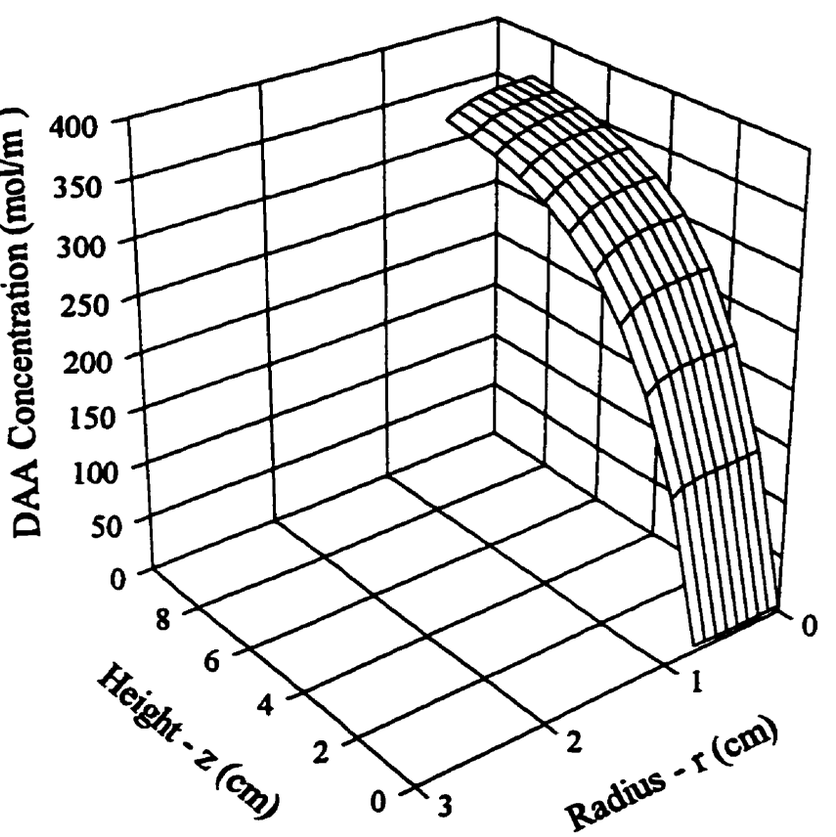

Figure 5.3.3-1: DAA concentration profile inside of the catalyst bag with the new liquid distributor (from the simulation of the batch CD experiment at 75 V).

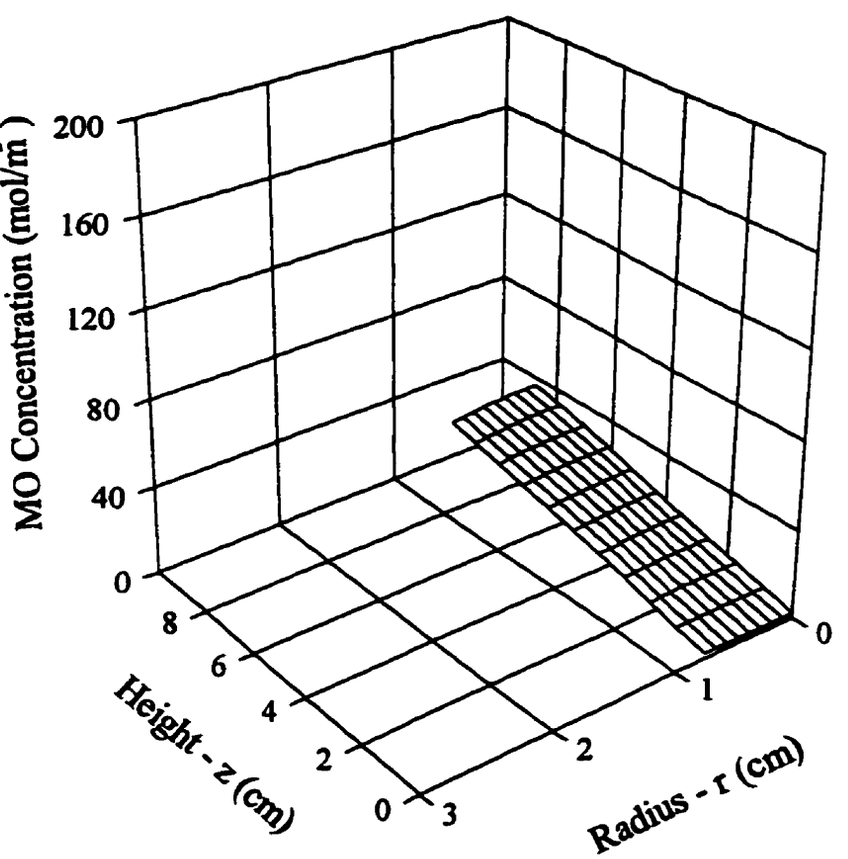

Figure 5.3.3-2: MO concentration profile inside of the catalyst bag with the new liquid distributor (from the simulation of the batch CD experiment at 75 V).

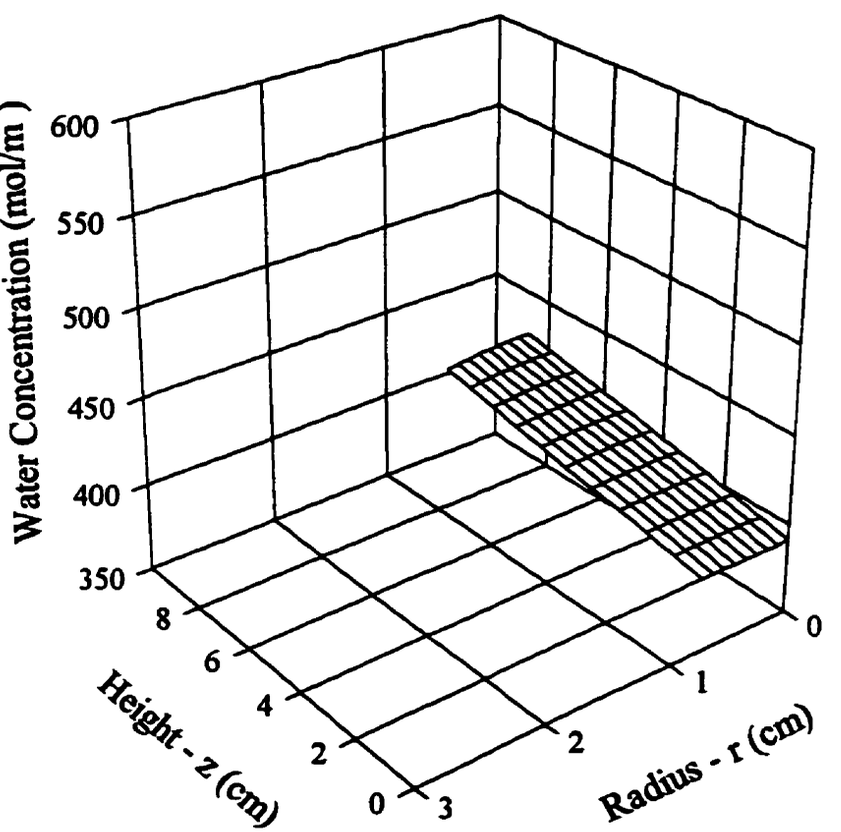

Figure 5.3.3-3: Water concentration profile inside of the catalyst bag with the new liquid distributor (from the simulation of the batch CD experiment at 75 V).

Not surprisingly, Figure 5.3.3-3 also shows that the concentration of water in the catalyst bag is much lower with the new liquid distributor in place. This is also a combined result of the higher liquid flow rate through the bag and the lower reaction temperature slowing down the rate of DAA dehydration. Another striking feature of Figures 5.3.3-2 and 5.3.3-3 is that the radial MO and water concentration gradients are small.

A comparison of Figures 5.3.3-1, 5.3.3-2, and 5.3.3-3 with their counterparts in Section 5.3.1 reinforces the literature reports that liquid distribution is an extremely important consideration in packed columns. Ensuring good liquid distribution may also eliminate the need for considering radial effects in the catalyst bags. The radial concentration gradients are very much smaller with the liquid distributor in place, which means that it may be possible to use 1-dimensional CD models without sacrificing accuracy.

A summary of the modelling results is presented in Table 5.3.3-I, and the values of f reported in this table are consistently high.

Table 5.3.3-I: Summary of the simulation results for the experiments of Section 4.3.

Reboiler (V)	Flow (g/min)	Z (cm)	f	DAA Activity ($g/mL_{cat} \cdot h$)	MO Activity[a] ($g/mL_{cat} \cdot h$)	Selectivity[a] (mol DAA /mol MO)	% Radial Production
65	8.76	8.79	.7965	1.204	0.119 (0.139)	8.549 (7.319)	14.9% DAA 11.3% MO 4.8% Wat.
75	12.27	8.74	.8479	1.701	0.129 (0.142)	11.142 (10.122)	10.5% DAA 7.9% MO 8.0% Wat.
85	16.36	8.89	.8489	2.167	0.137 (0.135)	13.365 (13.563)	9.4% DAA 7.1% MO 1.1% Wat.

[a]experimental data is shown in brackets

Table 5.3.3-I shows that the values of f are all very high, and within a fairly narrow range. While there are only three experiments shown in this table, this still represents an unprecedented level of reproducibility. At the lowest flow rate, the value of f drops slightly, but far exceeds the value of 0.1045 reported at the same flow rate in Section 5.3.1. There is also good agreement between the simulated and measured MO activity.

With such good contact between the liquid and the catalyst, the concentration of water inside the catalyst bag remains low at all of the flow rates investigated. Indeed, the average water concentrations at the bottom of the catalyst bag are 397, 423, and 457 mol/m^3 at reboiler settings of 85, 75, and 65 V, respectively. This is much more consistent than 446, 519, and 607 mol/m^3 of water predicted at the same total flow rates, but without the new liquid distributor. Since changes in the flow rate cause small changes in the water concentration with the liquid distributor, changes in the production rate of MO should also be small and rather difficult to detect experimentally. This is supported by the proximity of the MO production curves in Figure 4.3.2-3 and the MO production rates in Table 4.3.2-I.

The data in Table 5.3.3-I supports the fact that radial mass transfer inside of the bag is not as important when the flow rate through the bag is high. Radial mass transfer is credited with only 9.4 - 15% of the total DAA production. This is much lower than the 30 - 68% of total DAA production that was assigned to radial mass transfer in the batch CD experiments of Table 5.3.1-I. However, the batch CD experiment in Table 5.3.1-I with an unusually high f = 0.73 also shows that only 15.7% of the total DAA production rate is through radial mass transfer. This agrees well with the results in this section with the new liquid distributor.

During these experiments, several samples were taken with a syringe from inside the bottom of the catalyst bag. The composition of these samples was provided in Table 4.2.3-III. Some of these data are now compared to the model predictions in Table 5.3.3-II.

The agreement between the experimental data and the model predictions in Table 5.3.3-II is good. The simulated and measured DAA concentrations are fairly close, but the model seems to consistently over-predict the DAA composition of the actual samples. Not surprisingly, this may be caused by some error in the estimation of the reaction temperature.

Table 5.3.3-II: Comparison of predicted and measured compositions from inside the bottom of the catalyst bag.

Reboiler Setting (V)	Compound	Simulation Prediction (wt%)	Sample Composition (wt%)
65	DAA	5.37	4.65
	MO	0.58	0.67
	Water	1.06	1.30
75	DAA	5.34	4.16
	MO	0.44	0.53
	Water	0.99	1.33
85	DAA	5.25	4.71
	MO	0.36	0.52
	Water	0.93	0.80

However, there are many other possible sources of error which are related to the difficulty of collecting a representative sample. When sampling from within the catalyst bag, it is impossible to ensure that only liquid from the inside of the bag is obtained. Liquid travelling along the outside of the bag may have a tendency to be drawn in. As well, there may be flow channelling inside of the bag that is tapped into while sampling. Thus, one cannot be sure that the samples represent a true average composition in the bag. The bottom line is simply that this model is a simplified representation of the column, and it is unrealistic to expect perfect agreement.

Table 5.3.3-II does show that the compositions of DAA, MO, and water are of a similar order of magnitude. There appears to be some scatter in the amount of DAA in the samples, but the water and MO compositions closely follow the trends predicted by the model. Indeed, these compositions verify that the model is a reasonable representation of the conditions inside of the catalyst bag.

-6-

CONCLUSIONS AND RECOMMENDATIONS

In order to model Catalytic Distillation, many different types of data are required. Consequently, this thesis has dealt with a broad spectrum of topics in the field of Chemical Engineering. In the end, however, these varied topics are all incorporated into a unique model for Catalytic Distillation.

In Phase I of this work, the aldol condensation of acetone was selected as the reaction to be studied. This reaction initially produces diacetone alcohol (DAA), but also has a consecutive reaction whereby DAA is converted to mesityl oxide (MO). This reaction provides an excellent opportunity to test the ability of CD to improve the conversion of this reaction beyond its thermodynamic limit, and also permits an examination of the effect of CD on catalyst activity and product selectivity.

Batch reactions were conducted in Phase II of this thesis to study reaction kinetics. These experiments revealed that the aldol condensation of acetone can be treated as second order with respect to acetone in the forward direction, and first order with respect to DAA in the reverse direction. It was also confirmed that this reaction is strongly limited by equilibrium, with only 4.3 wt% acetone conversion at 54°C. MO formation was also observed during these experiments, and can be treated as a pseudo-zero order reaction.

The activation energy for the formation of DAA from acetone was experimentally determined to be 18.8 kJ/mol when whole catalyst beads were used. Such a low value of the activation energy, and the fact that the IRA-900 macroreticular ion exchange resin has an average pore radius of 178 Å, suggests that the reaction rate is controlled by pore diffusion. Through fitting a kinetic model (Gottifredi et. al., 1994) to our experimental data, it is estimated that the Thiele modulus for this catalyst is 11. Such a high value of the Thiele modulus is consistent with the suggestion that pore diffusion controls the reaction rate.

The activation energy of MO formation was found to be near 75 kJ/mol with the whole catalyst beads. This value is quite high, and is reasonable for kinetically controlled reactions. Unlike DAA formation, the rate of MO production is not severely controlled by pore diffusion.

Batch experiments also confirmed that water plays an important role in determining the reaction rate. This phenomenon has been commented on very little in the open literature. Generally, higher concentrations of water led to lower MO and DAA production rates, and also changed the product selectivity to favour DAA formation. Very low concentrations of water, however, also caused the rate of DAA and MO formation to decline. This was attributed to a shift in the rate controlling step of the reaction at very low water concentrations, and to catalyst deactivation. The maximum reaction rate was observed near a water concentration of 0.17 M.

Catalyst deactivation was observed in some of the batch experiments, and was studied in detail with CSTR experiments. The two main sources of catalyst deactivation were the formation of heavy byproducts which block the catalytic sites, and the neutralization of catalytic sites by trace acid impurities in the acetone feed. It was experimentally demonstrated that adding water to the acetone feed is an effective way of improving the catalyst lifetime. The addition of water inhibits the formation of the heavy byproducts.

Two batch reactions were conducted with the catalyst placed inside of a fibreglass catalyst bag, and the results were quite revealing. The bag creates an environment where mass transfer to the catalyst surface becomes important in determining the reaction rate. The activity of the catalyst, especially for DAA, was much lower with the catalyst bag in place. The product selectivity declined from 75 mol DAA/mol MO without the bag, to 2.4 mol DAA/mol MO with the bag. This test shows quite clearly that mass transfer to the catalyst surface is important, and must be considered in the CD model.

Given the importance of mass transfer, a correlation was developed describing mass transfer between the catalyst bag and the liquid flowing inside of the CD column. The results of these experiments were compared to the published work of Zheng and Xu (1992), and were found to agree within an order of magnitude. Differences in the geometries of this work and the literature study were likely responsible for the different mass transfer coefficients. A second correlation was also developed to describe vapour-liquid mass transfer in the reaction zone of the

CD column. A meaningful comparison could not be made with Zheng and Xu's (1992) findings due to insufficient data presented in their paper.

Phase III of this thesis involved the completion of CD experiments in a bench scale and a pilot scale column. The non-reactive sections of these columns were filled with ¼" Intalox saddles. The rate of DAA production in the CD column was only 0.5 - 7.5 % of the rate initially observed in batch reactions. There was a strong relationship between the liquid flow rate in the column and the DAA production rate, which confirms that mass transfer is extremely important in the CD column. The rate of MO production was between 40.1 - 79.0 % of the rate observed in batch reactions. The lower rate of MO production was attributed to higher concentrations of water in the reaction zone of the CD column than in the batch reactor. Higher water concentrations exist in the catalyst bag because of slow mass transfer, and an azeotrope that exists between acetone and water.

Although the rate of DAA production in the CD column is much lower than in the batch reactor, the column easily overcame the equilibrium limit of DAA composition. The bench scale column was able to reach a maximum of 55 wt% DAA. This is 12.3 times higher than the 4.3 wt% limit. The concentration of DAA which is possible in the CD product is only limited by the ability of distillation to separate acetone from DAA. This is a strong incentive for the use of CD with this reaction system, as it has the potential to dramatically reduce acetone recycling.

These experimental results showed that the operating conditions which favour the production of DAA are:

1) high reboiler duties (high liquid flow rates in the column)
2) short catalyst sections
3) high concentrations of water

The catalyst had a much longer lifetime in the CD column than in the CSTR. This was aided by the acetone/water azeotrope elevating the water concentrations in the reaction zone of the column, the constant removal of reaction products from the reaction zone of the column, and the fact that all acetone which came in contact with the catalyst was distilled. While these measures did not completely prevent deactivation, they did provide a vastly improved catalyst lifetime.

Initially, the deactivation of the IRA-900 catalyst was fairly rapid. However, as the

deactivation proceeded, the rate of deactivation declined until a period of nearly constant activity was reached. Nearly constant activity was observed after 20-30 minutes in the batch reactor, but it took approximately 10 h to become established in the CD column. As a result, the catalyst was able to provide "steady state" data over a reasonable period of time.

Attempts were made to measure the fraction of the total liquid flow which passed through the catalyst bag, and the results ranged widely from 12 to 80%. Unfortunately, this random behaviour is normal for dumped distillation packing. Porter and Templeman (1968) published valuable information about wall effects in packed columns. With a ratio of the column diameter to packing size of 4:1, anywhere between 70 - 95% of the total flow rate in a packed column may travel down the wall of the column. Based on these findings, it is expected that only 5 - 30% of the liquid flowing in the CD column would pass through the catalyst bag. While this provides a reasonable range for the percentage of the liquid which passes through the catalyst bag, there is no way to accurately predict the flow pattern in the column.

It is best to try to maximize contact between the liquid and the catalyst bag in the CD column. This maximizes the production rate of DAA and changes the product selectivity in favour of DAA. With this goal in mind, a new liquid distributor was designed and tested in the bench scale CD column. The DAA production rates were increased by 45 - 240%, and molar ratios of DAA:MO were increased by 112 - 343%. These incredible improvements in performance were achieved by doing nothing more than controlling the liquid flow pattern in the column.

Phase IV of this thesis involved modelling the reaction zone of the CD column. The original goal of this work was to bring together all of the data from Phases I and II, and build a model that could predict the performance of the column. The model predictions would then be compared to the data generated in Phase III. Unfortunately, it was not feasible to build a predictive model due to the impossibility of reproducing the liquid distribution in the column.

A two-dimensional rate-based model of catalytic distillation was created, however, and the fundamental kinetic and mass transfer data obtained in Phase II of this thesis was incorporated into the model. This is the first model of catalytic distillation that accounts for mass transfer between the catalyst and the liquid phase, and considers local concentrations that immediately

surround the catalyst. The model was fitted to the experimental CD data from Phase III. The fitting procedure involved changing the fraction of the total liquid flow that passes through the catalyst bag (f) until the DAA activity measured during the experiment matched the DAA activity calculated by the model. The model prediction of the MO activity was then compared with the experimental data, and the value of f was compared with the data published by Porter and Templeman (1968).

For the experiments involving the ¼" Intalox saddles, the values of f were usually between 0.1 and 0.28. There was one exception, however, when f was determined to be 0.73. In the pilot scale CD column, the values of f usually fell between the narrower range of 0.14 - 0.26. These values are well within the range of 0.05 to 0.3 anticipated from Porter and Templeman's (1968) data. The agreement between the predicted and the observed MO production rate was also quite good, but tended to worsen as a larger number of catalyst bags was placed into the column.

The main purpose of this model was to elucidate the effects of mass transfer on the reaction rate and product selectivity in the CD column. Although the DAA production rate was used to fit the model to the data, the experimental product selectivity data can be independently compared to the results of the simulations. It was found that the model worked very well for a wide range of catalyst zone heights, flow patterns, and flow rates. Thus, the model has achieved its intended purpose.

In addition to the model's ability to predict product selectivity data, there was also good agreement between the predicted and measured composition of DAA, MO, and water inside of the catalyst bag. This is strong evidence of the validity of this model.

The results of the model suggest that radial effects in the catalyst bag are very important. Between 36 and 70 % of the production of DAA was credited to the radial mass transfer mechanism. Three dimensional plots of the concentration profiles of DAA, MO, and water inside of the catalyst bag clearly show the magnitude of the radial concentration gradients.

The CD model was also fitted to the experiments conducted with the proper liquid distributor. The values of f seemed much more reproducible, and much higher than the previous experiments. Typically, $0.79 < f < 0.85$. The new liquid distributor also diminished the importance of radial mass transfer. Only 9 - 15% of the total amount of DAA produced was

removed from the catalyst bag in the radial direction. Thus, when contact between the liquid and the catalyst bag is good, a simplified one-dimensional CD model can likely be used.

Although the CD model developed in this thesis could be applied to other chemical systems, the simplified treatment of vapour-liquid mass transfer could pose problems for systems involving a gaseous reagent. For this reason, a more detailed treatment of vapour-liquid mass transfer is recommended. Knowledge of gas-side and liquid-side mass transfer coefficients in the catalyst zone of the CD column would be helpful, as these mass transfer coefficients can be used to calculate more accurate values for $K_{OG}A$.

One must never underestimate the importance of liquid distribution in packed columns. Wall effects and other flow maldistributions can seriously effect the performance of any packed column. However, these effects can be reduced by using a larger ratio of column diameter to packing diameter. A logical recommendation, therefore, is to test this reaction in a larger column. Perhaps some day, if the budget permits, a larger unit will be built at the University.

The catalyst bags are clearly a nuisance. They do not encourage contact between the liquid flow and the catalyst, and significant radial concentration gradients develop inside of them. Another logical recommendation is to move away from this type of catalyst structure. Work has already been initiated in this laboratory toward developing catalysts that are shaped like random distillation packings. This would greatly improve the contact between the liquid and the catalyst surface, and would also permit the use of much simpler 1-dimensional CD models. Other researchers have also begun to investigate this possibility (Flato and Hoffmann, 1992), but at this time there are no commercial applications of these specially shaped catalytic packings. It is also likely that some catalyst systems will never be amenable to shaping. For this reason, the standard fibreglass bag will likely be in service for many years to come.

Catalyst deactivation is the only major barrier to the commercialization of the work presented here. Clearly, a more detailed understanding of catalyst deactivation would be a useful for developing methods to prevent deactivation. Although several different catalysts were initially screened, there was not enough time to study the lifetime characteristics of each of them. It is very likely that catalysts with much better lifetime characteristics than IRA-900 resin already exist.

Therefore, it is recommended that future efforts be focused on catalyst selection and catalyst lifetime. The production of DAA via Catalytic Distillation could very easily be commercialized if a suitable catalyst is identified.

REFERENCES

Abufares, A.A. and Douglas, P.L., 1995, Mathematical Modelling and Simulation of an MTBE Catalytic Distillation Process using Speedup and Aspenplus. *Trans. Instn. Chem. Eng. Part A*, 73, pp. 3-12.

Agreda, H.V., Partin, L.R., and Heise, W.H., 1990, High-Purity Methyl Acetate via Reactive Distillation. *Chem. Eng. Prog.*, February, pp. 40-46.

Anderson, E.V., 1993, Health Studies Indicate MTBE Is Safe Gasoline Additive. *C&EN*, September, pp. 9-18.

Åkerlöf, G., 1926, Decomposition of Diacetone Alcohol in Alkali Hydroxide-Alkali Salt Solutions. *J. Am. Chem. Soc.*, 48, pp. 3046-3063.

Åkerlöf, G., 1928, Decomposition of Diacetone Alcohol by Sodium Hydroxide in Water Mixtures of Organic Solvents. *J. Am. Chem. Soc.*, 50, pp. 1272-1275.

Barbosa, D. and Doherty, M.F., 1987, Theory of phase diagrams and azeotropic conditions for two-phase reactive systems. *Proc. R. Soc. London A*, 413, pp. 443-458.

Barbosa, D. and Doherty, M.F., 1988, The Influence of Equilibrium Chemical Reactions on Vapour-Liquid Phase Diagrams. *Chem. Eng. Sci.*, 43, pp. 529-540.

Belck, L.H., 1955, Continuous Reactions in Distillation Equipment. *A.I.Ch.E. J.*, 1, pp. 467-470.

Bell, A., 1995, Methanex profit soars. *Globe & Mail*, Toronto, January 31, p. B13.

Bell, V.A. and Gold, H.S., 1983, Carbon-13 Nuclear Magnetic Resonance Studies of the Aldol Condensation Products of Acetone on an Activated Alumina Catalyst. *J. Catalysis*, 79, pp. 286-290.

Berg, D.A. and Harris, T.J., 1993, Characterization of Multicomponent Diffusion Effects in MTBE Synthesis. *Ind. Eng. Chem. Res.*, 32, pp. 2147-2158.

Bernard, R.A. and Wilhelm, R.H., 1950, Turbulent Diffusion in Fixed Beds of Packed Solids. *Chem. Eng. Prog.*, 46, pp. 233-244.

Billet, R. and Schultes, M., 1993, Predicting Mass Transfer in Packed Columns. *Chem. Eng. Technol.*, 16, pp. 1-9.

Bischoff, K.B., 1966, Mixing and Contacting in Chemical Reactors. *Ind. Eng. Chem.*, 58, 11, pp. 18-32.

Bogacki, M.B., Alejski, K. and Szymanowski, J., 1989, The Fast Method of the Solution of a Reacting Distillation Problem. *Computers Chem. Engng.*, 13, pp. 1081-1085.

Box, G.E.P., Hunter, W.G. and Hunter, J.S., 1978, *Statistics for Experimenters*. John Wiley & Sons, New York.

Braithwaite, J., 1995, Ketones. In Howe-Grant, M., ed., *Kirk-Othmer Encyclopedia of Chemical Technology*, 4th Ed. John Wiley & Sons, New York, 14, pp. 978-1021.

Bravo, J.L., Pyhalahti, A. and Järvelin, H., 1993, Investigations in a Catalytic Distillation Pilot Plant: Vapour/Liquid Equilibrium, Kinetics, and Mass-Transfer Issues. *Ind. Eng. Chem. Res.*, 32, pp. 2220-2225.

Brunjes, A.S. and Bogart, M.J.P., 1943, Vapour-Liquid Equilibria for Commercially Important Systems of Organic Solvents. *Ind. Eng. Chem.*, 35, pp. 255-260.

Carberry, J.J., 1960, A Boudary-Layer Model of Fluid-Particle Mass Transfer in Fixed Beds. *A. I. Ch. E. J.*, 6, pp. 460-463.

Chase, J.D. and Galvez, B.B., 1981, Maximize Blend Ethers with MTBE and TAME. *Hydrocarbon Proc.*, 60, March, pp. 89-94.

Ciric, A.R. and Miao, P., 1994, Steady State Multiplicities in an Ethylene Glycol Reactive Distillation Column. *Ind. Eng. Chem. Res.*, 33, pp. 2738-2748.

Convers, A., Juguin, B. and Torck, B., 1981, Make pure butenes via MTBE. *Hydrocarbon Proc.*, 60, March, pp. 95-98.

Cox, M.C., 1989, *Catalytic Distillation*. Research proposal presented to the University of Waterloo, Department of Chemical Engineering.

Craven, E.C., 1963, The Alkaline Condensation of Acetone. *J. Appl. Chem.*, 13, pp. 71-76.

Daubert, T.E. and Danner, R.P. eds., 1989, Physical and Thermodynamic Properties of Pure Chemicals: Data Compilation. Design Institute for Physical Property Data, A. I. Ch. E., Hemisphere Publishing Corp., New York.

Davis, G.L. and Burrows, G.H., 1936, Equilibrium and Free Energy Relationships in the System Acetone-Diacetone Alcohol. *J. Am. Chem. Soc.*, 58, pp. 311-312.

Delion, A., Torck, B. and Hellin, M., 1986, Equilibrium Constant for the Liquid-Phase Hydration of Isobutylene over Ion-Exchange Resin. *Ind. Eng. Chem. Process Des. Dev.*, 25, pp. 889-893.

Dieterich, E., Sorescu, G. and Eigenberger, G., 1994, Numerical methods for the simulation of chemical engineering processes. *Intl. Chem. Eng.*, 34, pp. 455-468.

Doherty, M.F. and Buzad, G., 1992, Reactive Distillation By Design. *Trans. Instn. Chem. Eng. Part A*, 70, pp. 448-458.

Ecklund, E.E. and Mills, G.A., 1989, Alternative fuels: Progress and prospects. Part 1. *Chemtech*, September, pp. 549-556.

Fessenden, R.J. and Fessenden, J.S., 1986, *Organic Chemistry*, 3rd ed. Brooks/Cole, Monterey, California.

Finlayson, B.A., 1980, *Nonlinear Analysis in Chemical Engineering*. McGraw Hill, New York.

Flato, J. and Hoffmann, U., 1992, Development and Startup of a Fixed Bed Reaction Column for Manufacturing Antiknock Enhancer MTBE. *Chem. Eng. Technol.*, 15, pp. 193-201.

Freifelder, M., 1971, *Practical Catalytic Hydrogenation*. John Wiley & Sons, New York.

French, C.C., 1929, Basic Catalysis in the Decomposition of Diacetone Alcohol. *J. Am. Chem Soc.*, 51, pp. 3215-3225.

Froment, G.F. and Bischoff, K.B., 1990, *Chemical Reactor Analysis and Design*, 2nd ed. John Wiley & Sons, New York.

Fuchigami, Y., 1990, Hydrolysis of Methyl Acetate in Distillation Column Packed with Reactive Packing of Ion Exchange Resin. *J. Chem. Eng. Japan*, 23, pp. 354-358.

Gentry, J.W., 1995, The 19TH Century Legacy to Distillation from Kidd to Young. *Chem. Eng. Education*, 29, pp. 250-255.

Gianetto, A. and Silveston, P.L., 1986, *Multiphase Chemical Reactors - Theory, Design, Scale-up*. Hemisphere Publishing Corp., Washington.

Gmehling, J. and Onken, U., 1977, *Vapour-Liquid Equilibrium Data Collection, Chemistry Data Series VI*, part 2a. Dechma, Frankfurt.

Godet, P., 1957, Process for Producing Diacetone Alcohol. US. Patent #2 889 369, July 19.

Goto, S. and Smith, J.M., 1975, Trickle-Bed Reactor Performance Part 1. Holdup and Mass Transfer Effects. *A. I. Ch. E. J.*, 21, pp. 706-713.

Gottifredi, J.C., Gonzo, E.E. and Froment, G.F., 1994, Diffusion and Reaction Inside a Catalyst Pellet for a Parallel-Consecutive Reaction Scheme. *Chem. Eng. Sci.*, 49, pp. 2399-2403.

Griffiths, D.M. and Rochester, C.H., 1978, Infrared Study of the Adsorption of Acetone on Rutile. *J. C. S. Faraday I*, 74, pp. 403-417.

Grosser, J.H., Doherty, M.F. and Malone, M.F., 1987, Modeling of Reactive Distillation Systems. *Ind. Eng. Chem. Res.*, 26, pp. 983-989.

Guang-run, W. and Nai-ju, Y., 1991, The Application of Catalytic Distillation in Petrochemicals Production and its Technical Aspects. In Hou, X. ed., *Proc. Int. Conf. Pet. Refin. Petrochem. Proc.*, pp. 350-354.

Harriott, P., 1989, Effects of Liquid Maldistribution on the Performance of Packed Stripping Columns. *Environ. Sci. Technol.*, 23, pp. 309-314.

Hen, Y. and Zhang, R., 1989, Simulation of Catalytic Distillation Columns with Total Reflux. *J. of East China Institute of Chemical Technology* (in Chinese), 15, pp. 331-338.

Himmelblau, D.M., 1982, Basic Principles and Calculations in Chemical Engineering, 4th ed. Prentice Hall, Englewood Cliffs, NJ.

Hines, A.L. and Maddox, R.N., 1985, Mass Transfer in Continuous Differential Contactors. In *Mass Transfer Fundamentals and Applications*. Prentice Hall, Englewood Cliffs, NJ., pp. 410-441.

Hoek, P.J., Wesselingh, J.A. and Zuiderweg, F.J., 1986, Small Scale and Large Scale Liquid Maldistribution in Packed Columns. *Chem. Eng. Res. Des.*, 64, pp. 431-449.

Hung, J. and Taylor, R., 1990, A Second Generation Nonequilibrium Model for Computer Simulation of Multicomponent Separation Processes. In Bussemaker, H.T.; Ledema, P.D. eds., *Computer Applications in Chemical Engineering*. Elsevier Science Publishers, Amsterdam, p. 19.

Huss, A. Jr. and Kennedy, C.R., 1990, Hydrocarbon Processes Comprised of Catalytic Distillation using Lewis Acid Promoted Inorganic Oxide Catalyst Systems. US. Patent #4 935 577, June 19.

Hutchings, G.J., Nicolaides, C.P. and Scurrell, M.S., 1992, Developments in the production of methyl *tert*-butyl ether. *Catalysis Today*, 15, pp. 23-49.

Hydrocarbon Processing, 1994, Hydrocarbon Processing's refining processes '94. *Hydrocarbon Proc.*, November, pp. 85-148.

Izarraraz, A., Bentzen, G.W., Anthony, R.G. and Holland, C.D., 1980, Solve more distillation problems Part 9 - When chemical reactions occur. *Hydrocarbon Proc.*, April, pp. 195-203.

Jianhua, Z. and Fu, S., 1995, The Modelling and Simulation of Reactive Distillation Processes. In Biegler, L.T. and Doherty, M.F., eds., *Foundations of Computer Aided Process Design*, A.I.Ch.E. Symposium Series No. 304, 91, pp. 297-300.

Jones, E.M. Jr., 1984, Contact Structure for use in Catalytic Distillation. US. Pat. #4 439 350, March 27.

Jones, E.M. Jr., 1985, Contact Structure for use in Catalytic Distillation. US. Pat. #4 536 373, August 20.

Kim, Y.K. and Hatfield, J.D., 1985, Kinetics and Equilibrium Data of the Dehydration-Hydration Reaction between Diacetone Alcohol and Mesityl Oxide in Phosphoric Acid. *J. Chem. Eng. Data*, 30, pp. 149-153.

Kirschner, E.M., 1994, Environment, Health Concerns Force Shift in Use of Organic Solvents. *C&EN*, June 20, pp. 13-20.

Kirschner, E.M., 1995, Production of Top 50 Chemicals Increased Substantially in 1994. *C&EN*, April 10, pp. 16-19.

Kister, H.Z., 1992, *Distillation Design*. McGraw Hill, New York.

Krishnamurthy, R. and Taylor, R., 1985, A Nonequilibrium Stage Model of Multicomponent Separation Processes Part I: Model Description and Method of Solution. *A. I. Ch. E. J.*, 31, pp. 449-456.

Kunin, R., 1972, Catalysis with Ion Exchange Resins. *amber-hi-lites*, Rohm and Haas Company, May.

Kunin, R., 1972b, *Ion Exchange Resins*. Robert E. Krieger Publishing Co., Malabar, Florida.

Kunin, R., 1973, Catalysis with Ion Exchange Resins. *amber-hi-lites*, Rohm and Haas Company, July.

Kyowa Yuka Co., Ltd., 1983, Jpn. Patent #58-59935 (in Japanese), April 9.

Kyowa Yuka Co., Ltd., 1983b, Jpn. Patent #58-59936 (in Japanese), April 9.

La Mer, V.K. and Miller, M.L., 1935, Temperature Dependence of the Engergy of Activation in the Dealdolization of Diacetone Alcohol. *J. Am. Chem. Soc.*, 57, pp. 2674-2680.

Lander, E.P., Hubbard, J.N. and Smith, L.A. Jr., 1983, Revving-up refining profits with catalytic distillation. *Chemical Engineering*, April, pp. 36-39.

Lapidus, L., 1962, *Digital Computation for Chemical Engineers*. McGraw Hill, New York.

Levenspiel, O., 1972, *Chemical Reaction Engineering*, 2nd ed. John Wiley, New York.

Lippert, S., Baumann, W. and Thomke, K., 1991, Secondary reactions of the base-catalyzed aldol condensation of acetone. *J. Mol. Catal.*, 69, pp. 199-214.

Lorette, N.B., 1958, Addition of Alcohols to Mesityl Oxide Using an Acid Ion Exchange Resin Catalyst. *J. Org. Chem.*, 23, p. 937.

Maple, S.R. and Allerhand, A., 1987, Analysis of Minor Components by Untrahigh Resolution NMR. 2. Detection of 0.01% Diacetone Alcohol in "Pure" Acetone and Direct Measurement of the Rate of the Aldol Condensation of Acetone. *J. Am. Chem. Soc.*, 109, pp. 6609-6614.

March, J., 1985, *Advanced Organic Chemistry*, 3rd ed. John Wiley, New York.

McCabe, W.L., Smith, J.C. and Harriott, P., 1985, *Unit Operations of Chemical Engineering*, 4th ed. McGraw Hill, New York.

McCabe, W.L. and Thiele, E.W., 1925, Graphical Design of Fractionating Columns. *Ind. Eng. Chem.*, 17, pp. 605-611.

Mills, G.A. and Ecklund, E.E., 1989, Alternative fuels: Progress and prospects. Part 2. *Chemtech*, October, pp. 626-631.

Mills, P.L., Beaudry, E.G. and Duduković, M.P., 1984, Comparison and Prediction of Reactor Performance for Packed Beds with Two-Phase Flow: Downflow, Upflow, and Countercurrent Flow. *I. Chem. E. Symposium Series*, 87, pp. 527-534.

Momessin, P.E., Bentzen, G.W. and Holland, C.D., 1980, Solve more distillation problems Part 10 - Another way to handle reactions. *Hydrocarbon Proc.*, July, pp. 144-148.

Morsi, B.I., 1989, Mass Transfer Coefficients in a Trickle-Bed Reactor with High and Low Viscosity Organic Solutions. *Chem. Eng. J.*, 41, pp. 41-48.

Murphy, G.M., 1931, Salt and Medium Effects on the Temperature Coefficient of Velocity of Decomposition of Diacetone Alcohol. *J. Am. Chem. Soc.*, 53, pp. 977-981.

Østergaard, K., 1961, An Example of the Influence of Intraparticle Diffusion on the Kinetics of Consecutive Heterogeneous Catalytic Reactions. *Acta Chem. Scand.*, 15, pp. 2037-2042.

Paludetto, R., Paret, G. and Donati, G., 1992, Multicomponent Distillation with Chemical Reaction Mathematical Model Analysis. *Chem. Eng. Sci.*, 47, pp. 2891-2896.

Papa, A.J. and Sherman, P.D. Jr., 1978, Ketones. In Grayson, M., ed. *Kirk-Othmer Encyclopedia of Chemical Technology*. John Wiley, New York, 13, pp. 894-941.

Papageorgiou, J.N. and Froment, G.F., 1995, Simulation Models Accounting for Radial Voidage Profiles in Fixed-Bed Reactors. *Chem. Eng. Sci.*, 50, pp. 3043-3056.

Paushkin, Ya.M., Panidi, I.S., Ryabtseva, N.V., Kazanskaya, A.S., Sladkov, A.M. Meshcheryakov, S.V., Yatsko, O.I. and Lunin, A.F., 1970, Catalytic Activity of Polymers with a system of Conjugated Bonds in the Dehydration of Diacetone Alchohol. *Kinet. Catal.*, 11, pp. 1131-1133.

Pekkanen, M., 1995, Pinches in Reactive Distillation: Conditions of Existence. In Biegler, L.T. and Doherty, M.F., eds. *Foundations of Computer Aided Process Design*, A.I.Ch.E. Symposium Series No. 304, 91, pp. 301-304.

Perry, D., Nutter, D.E. and Hale, A., 1990, Liquid Distribution for Optimum Packing Performance. *Chem. Eng. Prog.*, January, pp. 30-35.

Perry, R.H. and Green, D.W. eds., 1984, *Perry's Chemical Engineers' Handbook*, Sixth Edition, McGraw Hill, New York.

Podrebarac, G.G., 1992, *The Dimerization of 1-Butene using Catalytic Distillation*. MASc. Thesis, University of Waterloo.

Podrebarac, G.G., 1994, *Development and Modelling of a New Catalytic Distillation Process*. Research proposal presented to the University of Waterloo, Department of Chemical Engineering.

Podrebarac, G.G., Ng, F.T.T. and Rempel, G.L., 1996, The Effect of Butadiene and Reaction Conditions on the Dimerization of 1-Butene over NiY Zeolite. *Appl. Catal.*, in press.

Porter, K.E., 1968, Liquid Flow in Packed Columns Part I: The rivulet model. *Trans. Instn. Chem. Engrs.*, 46, pp. T69-T73.

Porter, K.E., 1995, Why Research is Needed in Distillation. *Trans. Instn. Chem. Eng. Part A*, 73, pp. 357-362.

Porter, K.E. and Templeman, J.J., 1968, Liquid Flow in Packed Columns Part III: Wall Flow. *Trans. Instn. Chem. Engrs.*, 46, pp. T86-T94.

Rao, G.B., Ibrahim, S.H. and Kuloor, N.R., 1966, Ketolization of Acetone to Diacetone Alcohol in a Batch Reactor. *Indian J. Technol.*, 4, pp. 364-367.

Rao, G.B., Ibrahim, S.H. and Kuloor, N.R., 1967, Kinetics of Ketolization of Acetone to Diacetone Alcohol in a Trickle Bed Reactor. *Indian J. Technol.*, 5, pp. 119-124.

Ray, D. and Ghosh, D.N., 1974, Catalytic Conversion of Acetone to Diacetone Alcohol. *Indian J. Technol.*, 12, pp. 57-60.

Rehfinger, A. and Hoffmann, U., 1990, Kinetics of Methyl Tertiary Butyl Ether Liquid Phase Synthesis Catalyzed by Ion Exchange Resin - I. Intrinsic Rate Expression in Liquid Phase Activities. *Chem. Eng. Sci.*, 45, pp. 1605-1617.

Reichle, W.T., 1980, Pulse Microreactor Examination of the Vapour-Phase Aldol Condensation of Acetone. *J. Catalysis*, 63, pp. 295-306.

Reichle, W.T., 1984, Catalysts for Aldol Condensations. US. Patent #4 458 026, July 3.

Reichle, W.T., 1985, Catalytic Reactions by Thermally Activated, Synthetic, Anionic Clay Minerals. *J. Catalysis*, 94, pp. 547-557.

Reid, R.C., Prausnitz, J.M. and Poling, B.E., 1987, *The Properties of Gases & Liquids*, 4th ed. McGraw Hill, New York.

Rohm and Haas Company, 1991, *Amberlite IRA-900 Anion Exchange Resin*. Rohm and Haas, Philedelphia, Pennsylvania.

Satterfield, C.N., 1975, Trickle-Bed Reactors. *A. I. Ch. E. J.*, 21, pp. 209-227.

Satterfield, C.N., Van Eek, M.W. and Bliss, G.S., 1978, Liquid-Solid Mass Transfer in Packed Beds with Downward Concurrent Gas-Liquid Flow. *A. I. Ch. E. J.*, 24, pp. 709-717.

Satterfield, C.N., 1981, *Mass Transfer in Heterogeneous Catalysis*. Robert E. Krieger Publishing, Malabar, Florida.

Savković-Stevanović, J., Mišić-Vuković, M., Bončić-Caričic, G.,Trišović B. and Jezdić S., 1992, Reaction Distillation with Ion Exchangers. *Sep. Sci. Tech.*, 27, pp. 613-630.

Sawistowski, H., 1983, Distillation with Chemical Reaction. In Alper, E. ed. *NATO ASI Series E: Applied Sciences - No. 72*. Martinus Nijhoff, The Hague, pp. 391-414.

Sawistowski, H. and Pilavakis, P.A., 1979, Distillation with Chemical Reaction in a Packed Column. *Int. Symp. Distillation, London, I. Chem. Eng. Symp. Ser. 56*, pp. 4.2/49-4.2/63.

Sawistowski, H. and Pilavakis, P.A., 1988, Performance of Esterification in a Reaction-Distillation Column. *Chem. Eng. Sci.*, 43, pp. 355-360.

Scheidt, F.M., 1964, Vapour-Phase Aldol Condensations over Heterogeneous Catalysts. *J. Catal.*, 3, pp. 372-378.

Schmidle, C.J. and Mansfield, R.C., 1952, Catalysis by Anion Exchange Resins. *Ind. Eng. Chem.*, 44, pp. 1388-1390.

Sharma, M.M. and Danckwerts, P.V., 1970, Chemical methods of measuring interfacial area and mass transfer coefficients in two-fluid systems. *Brit. Chem. Eng.*, 4, pp. 522-528.

Shoemaker, J.D. and Jones, E.M. Jr., 1987, Cumene by Catalytic Distillation. *Hydrocarbon Proc.*, 66, June, pp. 57-58.

Simandl, J. and Svrcek, W.Y., 1991, Extension of the Simultaneous-Solution and Inside-Outside Algorithms to Distillation with Chemical Reactions. *Computers Chem. Engng.*, 15, pp. 337-348.

Sišul, N., Ciković, N., Jelenčić, J. and Wolf, N., 1989, Contribution to the Study of the Aldol Condensation Process. *React. Kinet. Catal. Lett.*, 40, pp. 227-233.

Sišul, N., Ciković, N. and Jelenčić, J., 1991, Catalytic Preparation of Diacetone Alcohol in Controlled Flow Conditions. *React. Kinet. Catal. Lett.*, 45, pp. 111-117.

Sišul, N., Cikovič, N., Wolf, N. and Jelenčič, J., 1992, Catalytic Preparation of Mesityl Oxide from Acetone. *React. Kinet. Catal. Lett.*, 47, pp. 65-71.

Smith, C.L., Pike, R.W. and Murrill, P.W., 1970, *Formulation and Optimization of Mathematical Models*. International Textbook, Scranton, Pennsylvania.

Smith, J.M. and Van Ness, H.C., 1987, *Introduction to Chemical Engineering Thermodynamics*, 4th ed. McGraw Hill, New York.

Smith, L.A. Jr., 1980, Catalytic Distillation Process. US. Patent #4 232 177, Nov. 4.

Smith, L.A. Jr., 1982, Catalytic Distillation Process and Catalyst. Can. Patent #1 125 728, June 15.

Smith, L.A. Jr., 1984, Catalytic Distillation Structure. US. Patent #4 443 559, April 17.

Smith, L.A. Jr., 1985, Deetherification Process. US. Patent #4 551 567, November 5.

Smith, L.A. Jr., Hearn, D. and Jones, E.M. Jr., 1991, Oligomerization Process. US. Pat. #5 003 124, March 26.

Smith, N.L. and Amundson, N.R., 1951, Intraparticle Diffusion in Catalytic Heterogeneous Systems. *Ind. Eng. Chem.*, 43, pp. 2156-2167.

Spiegel, M.R., 1968, *Mathematical Handbook of Formulas and Tables, Schaum's Outline Series*. McGraw Hill, New York.

Stadig, W.P., 1987, Catalytic Distillation - Combining chemical reaction with product separation. *Chemical Processing*.

Steinberger, R.L. and Treybal, R.E., 1960, Mass Transfer from a Solid Soluble Sphere to a Flowing Liquid Stream. *A. I. Ch. E. J.*, 6, pp. 227-232.

Sumitomo Chemical Co., 1986, Jpn. Patent #61-5040 (in Japanese), January 10.

Sundmacher, K., Rihko, L.K. and Hoffmann, U., 1994, Classification of Reactive Distillation Processes by Dimensionless Numbers. *Chem. Eng. Comm.*, 127, pp. 151-167.

Tada, A., 1975, Basic Properties of Metal Phosphates and Their Catalytic Activity in the Decomposition of Diacetone Alcohol. *Bull. Chem. Soc. Jpn.*, 48, pp. 1391-1393.

Tanabe, K., Misono, M., Ono, Y. and Hattori, H., 1989, Ion Exchange Resins. In Delmon, B. and Yates, J.T., eds. *Stud. Surf. Sci. Catal., New Solid Acids and Bases: Their Catalytic Properties*. Elsevier Science Publishers, Amsterdam, 51, pp. 173-183.

Tanabe, K., Zhang, G. and Hattori, H., 1989, Addition of Metal Cations to Magnesium Oxide Catalyst for the Aldol Condensation of Acetone. *Appl. Catal.*, 48, pp. 63-70.

Taylor, R. and Lucia, A., 1995, Modeling and Analysis of Multi-Component Separation Processes. In Biegler, L.T.; Doherty, M.F., eds.; *Foundations of Computer Aided Process Design*, A.I.Ch.E. Symposium Series No. 304, 91, pp. 19-28.

Taylor, R. and Krishna, R., 1993, *Multicomponent Mass Transfer*. John Wiley, New York.

Tencer, Y., Michman, M. and Goldenfeld, I., 1991, Catalysis by cobalt compounds of aldol and retroaldol reactions. *J. Organomet. Chem.*, 412, pp. 203-214.

Thomas, J.H., 1994, MTBE: Its Impact and Promise. *Hydrocarbon Proc.*, 73, May, pp. 66-G - 66-P.

Trambouze, P., 1990, Countercurrent Two-Phase Flow Fixed Bed Catalytic Reactors. *Chem. Eng. Sci.*, 45, pp. 2269-2275.

Treybal, R.E., 1980, *Mass-Transfer Operations*, 3rd ed. McGraw-Hill, New York.

Umland, J.B., 1993, *General Chemistry*. West Publishing Co., New York.

Venkataraman, S., Chan, W.K. and Boston, J.F., 1990, Reactive Distillation Using Aspen Plus. *Chem. Eng. Prog.*, August, pp. 45-54.

Wardle, A.P. and Hapoglu, H., 1994, On the Solution of Models of Binary and Multicomponent Packed Distillation Columns using Orthogonal Collocation on Finite Elements. *Trans. Instn. Chem. Eng. Part A*, 72, pp. 551-564.

Watanabe, H. and Seto, J., 1991, The Catalysis of Maghemite and Hematite on the Aldol and Retro-Aldol Condensation of Acetone. *Bull. Chem. Soc. Jpn.*, 64, pp. 2411-2415.

Weirauch, W., 1995, MTBE future looks 'bright', according to EFOA analysis. *Hydrocarbon Proc.*, August, pp. 23-24.

Weisz, P.B. and Hicks, J.S., 1962, The behaviour of porous catalyst particles in view of internal mass and heat diffusion effects. *Chem. Eng. Sci.*, 17, pp. 265-275.

Weiszmann, J.A., D'Auria, J.H., McWilliams, F.G. and Hibbs, F.M., 1992, Octane Options. In McKetta, J.J. ed. *Petroleum Processing Handbook*. Marcel Dekker, New York, pp. 50-64.

Westheimer, F.H. and Cohen, H., 1938, The Amine Catalysis of the Dealdolization of Diacetone Alcohol. *J. Am. Chem. Soc.*, 60, pp. 90-95.

Wheeler, A., 1951, Reaction Rates and Selectivity in Catalyst Pores. In Frankenberg, W.G., Rideal, E.K. and Komarewsky, V.I. eds. *Advances in Catalysis and Related Subjects*. Academic Press, New York, 3, pp. 249-327.

Wilhelm, R.H., 1962, Progress Towards the A Priori Design of Chemical Reactors. *Pure Appl. Chem.*, 5, pp. 403-421.

Zhang, G., Hattori, H. and Tanabe, K., 1988, Aldol Addition of Acetone Catalyzed by Solid Base Catalysts: Magnesium Oxide, Calcium Oxide, Strontium Oxide, Barium Oxide, Lanthanum (III) Oxide and Zirconium Oxide. *Appl. Catal.*, 36, pp. 189-197.

Zhang, G., Hattori, H. and Tanabe, K., 1988b, Aldol Condensation of Acetone/Acetone d_6 over Magnesium Oxide and Lanthanum Oxide. *Appl. Catal.*, 40, pp. 183-190.

Zheng, Y. and Xu, X., 1992, Study on Catalytic Distillation Processes Part I. Mass Transfer Characteristics in Catalyst Bed within the Column. *Trans. I. Chem. E. Part A*, 70, pp. 459-464.

Zheng, Y. and Xu, X., 1992b, Study on Catalytic Distillation Processes Part II. Simulation of Catalytic Distillation Processes - Quasi-Homogeneous and Rate-Based Model. *Trans. Instn. Chem. Eng. Part A*, 70, pp. 465-470.

Zhukova, T.B., Pisarenko, V.N. and Kafarov, V.V., 1990, Modeling and design of industrial reactors with a stationary bed of catalyst and two-phase gas-liquid flow - a review. *Intern. Chem. Eng.*, 30, pp. 57-102.

Appendix A

Heat of Reaction

The properties required for the heat of reaction calculations are shown in the following table: (taken from Daubert and Danner, 1989)

Property	Acetone	DAA	MO	Water
Heat of formation (kJ/mol)[a]	-217.2	-545.8	-195.6	-241.8
Heat of vaporization (kJ/mol)[a]	31.39	47.45	42.91	44.58
Liquid Heat Capacity (J/mol·K)[b]	129.2	229.43	216.24	72.44

[a] at 25°C [b] at 40°C

For the conversion of acetone (gas) to DAA (gas):

$\Delta H^\circ_{IG,298} = -2(-217.2) + (-545.8) = -111.4$ J/mol

Heats of formation are given for the formation of the compounds in the gas phase. This must be corrected to the liquid phase using the enthalpy of vaporization. Consider that 2 mol of acetone is vaporized, reacted to 1 mol of DAA, then condensed to the liquid phase.

$\Delta H^\circ_{298} = 2(31.38) + (-111.4) - 47.45 = -96.1$ kJ/mol

This value can then be corrected to 56°C. In the complete cycle, 2 mol of acetone is cooled to 25°C, vaporized, reacted to 1 mol of DAA which is then condensed, and reheated to 56°C. The correction to 56°C is shown below using heat capacities evaluated at the average temperature of 40°C.

$\Delta H^\circ_{329} = -96.1 + (2(129.2)(25-56) + 1(229.43)(56-25))/1000 = -97$ kJ/mol

Thus, for every mole of DAA produced, 97 kJ of energy is released.

Following a similar procedure, we can estimate the enthalpy of reaction for the dehydration of DAA to MO to be $\Delta H^\circ_{329} = 70.2$ kJ/mol. The dehydration is endothermic to the extent that 70.2 kJ of energy are required for each mole of MO produced.

Appendix B

Representative Data from Batch Reactions

Sample of the Spreadsheet used to convert mass fraction data to Molar concentration data

Experiment 75 New batch of catalyst at .45 mmol/mL Sept 8,1995

Catalyst used in Big CD #4 (2 bags)

2 mL of IRA-900 catalyst, 100 mL acetone, no added water.

Samp. #	Time	Weight % Acetone	DAA	MO	Water	Density of mixture	[Ac]	[DAA]	[MO]	[H20]
1	2	98.09402	1.427841	0.038496	0.439643	0.754625	12.74526	0.092759	0.00296	0.184159
2	4	97.1426	2.315488	0.094357	0.447555	0.755841	12.64197	0.150667	0.007267	0.187775
3	8	96.01018	3.292436	0.21085	0.486539	0.757275	12.51832	0.214643	0.016269	0.204519
4	14	95.27447	3.854416	0.358103	0.513012	0.758166	12.43699	0.251575	0.027663	0.2159
5	25	94.77336	4.071902	0.602985	0.551748	0.758691	12.38015	0.265954	0.046613	0.232363
6	35	94.48141	4.120935	0.800632	0.597022	0.758974	12.34661	0.269257	0.061915	0.251523
8	45	94.30366	4.09146	0.973001	0.631878	0.759116	12.3257	0.267381	0.075259	0.266258
9	65	93.96705	4.072352	1.273979	0.686614	0.759397	12.28625	0.266231	0.098575	0.289429
10	85	93.62535	4.090696	1.556823	0.727134	0.759689	12.24628	0.267533	0.120506	0.306828

REQUIRED DATA

density of	acetone	0.791 at room temperature	Mol. Wt.	Acetone	58.0798
		0.75195 at 54 C		DAA	116.1596
	DAA	0.938 at room temperature		MO	98.1444
		0.90903 at 54 C		Water	18.0152
	water	0.998 at room temperature			
		0.98587 at 54 C			
	MO	0.856 at room temperature			
		0.82585 at 54 C			

Calculations in the Spreadsheet on p. 219:

1) To calculate the density of the liquid mixture (in g/mL):

$$\rho_{mix} = \frac{100\ g}{\left(\frac{wt\%\ Ac}{\rho^0_{Ac}} + \frac{wt\%\ DAA}{\rho^0_{Ac}} + \frac{wt\%\ MO}{\rho^0_{MO}} + \frac{wt\%\ Wat}{\rho^0_{Wat}} \right)}$$

2) To calculate the molar concentration in mol/L of a component, i:

$$[i] = \frac{(wt\%_i\ /\ MW_i)}{(100\ g\ /\ \rho_{mix})}\ x\ 1000\ mL/L = \left(\frac{wt\%_i}{MW_i} \right) \rho_{mix}\ x\ 10$$

In order to use these equations, the molecular weights of each component (MW) and the density of each pure component (ρ^0) are required. These values are all available in the spreadsheet on p. 206.

In this way, data from the GC in wt% are converted to concentrations in mol/L.

Raw Data for Some Representative Batch Reactions

Experiment #4 - Compositions in wt%, MO data not integrated

· 100 mL of acetone, temperature = 54°C
· 2 mL of catalyst exchanged for 3 h to 0.49 mmol OH^-/mL
· stir speed set to 1
· water content assumed to be constant

Time	Ac	DAA	Water
2	97.713	1.887	0.4
4	96.991	2.609	0.4
7	96.297	3.303	0.4
11	95.742	3.858	0.4
17	95.505	4.095	0.4
25	95.344	4.256	0.4
40	95.336	4.264	0.4

from regression: $k_1 = 0.377 \times 10^{-3}\ M^{-1}\ min^{-1}$

Experiment #5 - Compositions in wt%

· 100 mL of acetone, temperature = 54°C
· 2 mL of catalyst exchanged for 3 h to 0.49 mmol OH^-/mL
· stir speed set to 1
· water content assumed to be constant

Time	Ac	DAA	MO	Water
2	98.03883	1.536207	0.024968	0.4
4	97.10243	2.424439	0.073127	0.4
8	96.04457	3.422243	0.133183	0.4
12	95.42621	3.975888	0.197904	0.4
17	95.29142	4.026641	0.281941	0.4
25	94.91166	4.251474	0.436864	0.4
30	94.78401	4.300879	0.515115	0.4
39	94.64391	4.289391	0.666698	0.4

from regression: $k_1 = 0.370 \times 10^{-3}\ M^{-1}\ min^{-1}$, $k_2 = 0.00135\ M\ min^{-1}$

Experiment #6 - Compositions in wt%

- 100 mL of acetone, temperature = 54°C
- 2 mL of catalyst exchanged for 3 h to 0.49 mmol OH^-/mL
- stir speed set to 1
- water content assumed to be constant

Time	Ac	DAA	MO	Water
2	97.60231	1.997687	0	0.4
4	96.83166	2.768335	0	0.4
7	95.96627	3.560102	0.073626	0.4
11	95.59231	3.792284	0.215402	0.4
16.5	95.12534	4.163602	0.311053	0.4
22	94.90588	4.224371	0.46975	0.4
30	94.64572	4.260644	0.693633	0.4
40	94.55263	4.203692	0.843681	0.4
77	93.89649	4.263348	1.440159	0.4

from regression: $k_1 = 0.365 \times 10^{-3}\ M^{-1}\ min^{-1}$, $k_2 = 0.00131\ M\ min^{-1}$

Experiment #7 - Compositions in wt%

- 100 mL of acetone, temperature = 54°C
- 2 mL of catalyst exchanged for 24 h to 0.49 mmol OH^-/mL
- stir speed set to 1
- water content assumed to be constant

Time	Ac	DAA	MO	Water
2	97.9153	1.656112	0.028589	0.4
4	97.0623	2.473192	0.064508	0.4
7	96.38802	3.102163	0.109812	0.4
12	95.8474	3.576395	0.176208	0.4
17	95.70603	3.611791	0.282179	0.4
23	95.06901	4.156294	0.374699	0.4
29	94.8762	4.255789	0.468016	0.4
38	94.81163	4.219155	0.569217	0.4
50	94.71098	4.214676	0.674348	0.4
150	93.73085	4.19669	1.672464	0.4

from regression: $k_1 = 0.36 \times 10^{-3}\ M^{-1}\ min^{-1}$, $k_2 = 0.00079\ M\ min^{-1}$

Experiment #8 - Compositions in wt%

· 100 mL of acetone, temperature = 54°C
· 2 mL of catalyst exchanged for 3 h to 0.49 mmol OH^-/mL
· stir speed set to 2
· water content assumed to be constant

Time	Ac	DAA	MO	Water
2	97.73462	1.814397	0.050978	0.4
4	96.8359	2.683168	0.080933	0.4
7	96.14257	3.325983	0.131443	0.4
12	95.49597	3.875787	0.228247	0.4
17	95.18435	4.103366	0.312284	0.4
23	94.9925	4.192443	0.415058	0.4
29	94.91275	4.197222	0.490025	0.4
35	94.6923	4.225	0.6827	0.4
42	94.59089	4.277924	0.731186	0.4

from regression: $k_1 = 0.365 \times 10^{-3}\ M^{-1}\ min^{-1}$, $k_2 = 0.00136\ M\ min^{-1}$

Experiment #10 - Compositions in wt%

· 100 mL of acetone, temperature = 54°C
· 2 mL of catalyst exchanged for 3 h to 0.49 mmol OH^-/mL
· stir speed set to 2
· water content assumed to be constant

Time	Ac	DAA	MO	Water
2	97.62722	1.934279	0.038502	0.4
4	96.91774	2.603671	0.078587	0.4
7	96.20529	3.290314	0.1044	0.4
12	95.58519	3.823938	0.190873	0.4
17	95.27432	4.049433	0.276246	0.4
25	94.92057	4.229876	0.449552	0.4
32	94.84055	4.222007	0.537446	0.4
41	94.72555	4.178968	0.695482	0.4
62	94.41578	4.223055	0.96117	0.4

from regression: $k_1 = 0.375 \times 10^{-3}\ M^{-1}\ min^{-1}$, $k_2 = 0.00116\ M\ min^{-1}$

Experiment #11 - Compositions in wt%

- 100 mL of acetone, temperature = 54°C
- 2 mL of catalyst exchanged for 3 h to 0.49 mmol OH^-/mL
- stir speed set to 2
- water content assumed to be constant

Time	Ac	DAA	MO	Water
2	97.71252	1.887483	0	0.4
4	97.0319	2.568098	0	0.4
7	96.33696	3.263039	0	0.4
12	95.49188	3.836853	0.271265	0.4
17	95.14186	4.008399	0.449742	0.4
24	94.96766	4.090445	0.541892	0.4
31	94.79756	4.138605	0.663832	0.4
40	94.48177	4.175082	0.943151	0.4
60	94.29189	4.16322	1.144886	0.4

from regression: $k_1 = 0.365 \times 10^{-3}$ M^{-1} min^{-1}, $k_2 = 0.00132$ M min^{-1}

Experiment #13 - Compositions in wt%

- 100 mL of acetone, temperature = 54°C
- 1 mL of catalyst exchanged for 24 h to 0.49 mmol OH^-/mL
- stir speed set to 1
- water content assumed to be constant, only two good MO analyses obtained

Time	Ac	DAA	MO	Water
3	98.28457	1.315429	0	0.4
10	96.97057	2.629428	0	0.4
17	96.35572	3.244279	0	0.4
24	96.01551	3.584489	0	0.4
31	95.55347	3.748561	0.297973	0.4
38	95.10731	3.921349	0	0.4
45	95.57852	4.021483	0	0.4
58	94.80269	4.107283	0	0.4
75	94.68961	4.14729	0	0.4
150	94.41831	4.240338	0.941355	0.4

from regression: $k_1 = 0.175 \times 10^{-3}$ M^{-1} min^{-1}, $k_2 = 0.00042$ M min^{-1}

Experiment #14 - Compositions in wt%

· 100 mL of acetone, temperature = 54°C
· 1 mL of catalyst exchanged for 24 h to 0.49 mmol OH^-/mL
· stir speed set to 1
· water content assumed to be constant

Time	Ac	DAA	MO	Water
3	98.2596	1.312792	0.027605	0.4
10	96.82759	2.679512	0.092894	0.4
17	96.15997	3.297969	0.142057	0.4
24	95.79492	3.626057	0.179021	0.4
31	95.50733	3.851243	0.241425	0.4
38	95.44078	3.896222	0.263003	0.4
48	95.24135	4.046247	0.312404	0.4
58	95.07871	4.146021	0.375271	0.4
68	95.03704	4.124054	0.438911	0.4
85	94.87307	4.216135	0.510792	0.4

from regression: $k_1 = 0.175 \times 10^{-3}$ M^{-1} min^{-1}, $k_2 = 0.00044$ M min^{-1}

Experiment #16 - Compositions in wt%

· 100 mL of acetone, temperature = 54°C
· 1 mL of catalyst exchanged for 24 h to 0.49 mmol OH^-/mL
· stir speed set to 2
· water content assumed to be constant

Time	Ac	DAA	MO	Water
3	98.3287	1.271299	0	0.4
10	96.85412	2.646548	0.099333	0.4
18	96.10027	3.33535	0.16438	0.4
24	95.83815	3.568882	0.192966	0.4
31	95.5176	3.838805	0.243594	0.4
38	95.34185	3.974281	0.283864	0.4
48	95.16485	4.090914	0.34424	0.4
59	95.0114	4.174133	0.414466	0.4
70	94.89962	4.206645	0.493734	0.4
85	94.79627	4.245669	0.558056	0.4

from regression: $k_1 = 0.17 \times 10^{-3}$ M^{-1} min^{-1}, $k_2 = 0.00047$ M min^{-1}

Experiment #33 - Compositions in wt%

- 100 mL of acetone, temperature = 54°C
- 2 mL of catalyst exchanged for 24 h to 0.49 mmol OH^-/mL
- stir speed set to 2
- water content measured but assumed to be constant

Time	Ac	DAA	MO	Water
2	97.57187	2.038129	0	0.39
4	97.02897	2.535575	0.045451	0.39
7	96.28734	3.230906	0.091756	0.39
12	95.61965	3.841788	0.148563	0.39
17	95.31349	4.101839	0.194668	0.39
23	95.07931	4.254649	0.27604	0.39
32.5	95.06632	4.198342	0.34534	0.39
40	94.83583	4.360464	0.41371	0.39
51	94.74727	4.37111	0.491616	0.39

from regression: $k_1 = 0.35 \times 10^{-3}\ M^{-1}\ min^{-1}$, $k_2 = 0.0008\ M\ min^{-1}$

Experiment #62 - Compositions in wt%

- 100 mL of acetone, temperature = 54°C
- 2 mL of catalyst exchanged for 3 h to 0.61 mmol OH^-/mL
- stir speed set to 2
- water content measured but assumed to be constant

Time	Ac	DAA	MO	Water
3	97.16927	2.378092	0.072635	0.38
6	96.10933	3.340581	0.170579	0.379509
10	95.46407	3.868871	0.28706	0.38
16	94.84439	4.312016	0.463592	0.38
25	94.61811	4.3211	0.68079	0.38
40	94.1152	4.443537	1.061268	0.38
60	93.71654	4.462683	1.440775	0.38

from regression: $k_1 = 0.44 \times 10^{-3}\ M^{-1}\ min^{-1}$, $k_2 = 0.00173\ M\ min^{-1}$

Experiment #74 - Compositions in wt%

- 100 mL of solution, temperature = 54°C
- 2 mL of catalyst exchanged for 3 h to 0.35 mmol OH^-/mL
- stir speed set to 2
- water content measured but assumed to be constant

Time	Ac	DAA	MO	Water
2.1833	97.94867	1.620263	0.031067	0.4
4.766667	96.91621	2.600073	0.083715	0.4
8	96.18144	3.271312	0.147251	0.4
15.33333	95.38393	3.942043	0.274029	0.4
26	94.93852	4.222498	0.438983	0.4
45	94.60078	4.313739	0.685481	0.4
62.41667	94.43041	4.302288	0.867304	0.4
86	94.24677	4.292212	1.061017	0.4

from regression: $k_1 = 0.30 \times 10^{-3}$ M^{-1} min^{-1}, $k_2 = 0.00086$ M min^{-1}

Experiment #76 - Compositions in wt%

- 100 mL of solution, temperature = 54°C
- 2 mL of catalyst exchanged for 3 h to 0.45 mmol OH^-/mL
- stir speed set to 2
- several samples analyzed for water, and water composition interpolated
- experiment started with $[DAA]_0 = 0.32$ M

Time	Ac	DAA	MO	Water
1	94.57501	4.910754	0.037905	0.476333
5	95.00552	4.358719	0.149211	0.486553
13	94.86061	4.274644	0.350169	0.514581
20	94.75157	4.181491	0.512532	0.554404
30	94.54614	4.142242	0.721173	0.590447
40	94.33078	4.14011	0.908185	0.620923
60	94.06652	4.047845	1.215547	0.670088
80	93.65673	4.100712	1.512335	0.730223

from regression: k_1 cannot be determined, $k_2 = 0.00121$ M min^{-1}

Experiment #77 - Compositions in wt%

- 100 mL of solution, temperature = 54°C
- 2 mL of catalyst exchanged for 3 h to 0.45 mmol OH^-/mL
- stir speed set to 2
- several samples analyzed for water, and water composition interpolated
- experiment started with $[DAA]_0 = 0.58$ M

Time	Ac	DAA	MO	Water
1	90.59358	8.879182	0.057236	0.470004
5	92.5565	6.786036	0.169088	0.488377
12	94.06884	5.049311	0.349939	0.531911
20	94.45922	4.44241	0.539886	0.55848
30	94.44124	4.204594	0.751611	0.602557
40	94.27037	4.144646	0.93772	0.64726
60	93.96449	4.085899	1.259024	0.690588
80	93.64982	4.036325	1.558002	0.755853

from regression: $k_1 = 0.270 \times 10^{-3}$ M^{-1} min^{-1}, $k_2 = 0.00124$ M min^{-1}

Experiment #78 - Compositions in wt%

- 100 mL of solution, temperature = 54°C
- 2 mL of catalyst exchanged for 3 h to 0.45 mmol OH^-/mL
- stir speed set to 2
- several samples analyzed for water, and water composition interpolated
- experiment started with $[DAA]_0 = 1.08$ M

Time	Ac	DAA	MO	Water
1	83.11799	16.2634	0.096797	0.521812
5	87.9608	11.31201	0.198937	0.52825
12	91.91921	7.140007	0.364671	0.576115
20	93.59152	5.250807	0.542535	0.615138
30	94.16158	4.460999	0.737716	0.639703
40	94.20693	4.194683	0.909756	0.688635
60	93.97384	4.076815	1.208064	0.74128
80	93.70688	4.042367	1.451926	0.798831

from regression: $k_1 = 0.20 \times 10^{-3}$ M^{-1} min^{-1}, $k_2 = 0.0011$ M min^{-1}

Experiment #79 - Compositions in wt%

- 100 mL of solution, temperature = 54°C
- 2 mL of catalyst exchanged for 3 h to 0.45 mmol OH^-/mL
- stir speed set to 2
- several samples analyzed for water, and water composition interpolated
- experiment started with $[DAA]_0 = 2.77$ M

Time	Ac	DAA	MO	Water
1	59.33158	39.87639	0.197066	0.594966
5	68.58979	30.53033	0.277447	0.60243
12	78.70282	20.23051	0.415532	0.651142
20	85.71512	13.04322	0.559329	0.68233
30	90.32214	8.250781	0.721686	0.705395
40	92.36285	5.973768	0.871288	0.792096
60	93.55526	4.503511	1.128197	0.81303
80	93.6655	4.150297	1.336856	0.847342

from regression: $k_1 = 0.11 \times 10^{-3}$ M^{-1} min^{-1}, $k_2 = 0.00094$ M min^{-1}

Experiment #80 - Compositions in wt%

- 100 mL of solution, temperature = 54°C
- 2 mL of catalyst exchanged for 3 h to 0.45 mmol OH^-/mL
- stir speed set to 2
- several samples analyzed for water, and water composition interpolated
- experiment started with $[DAA]_0 = 6.75$ M

Time	Ac	DAA	MO	Water
0	10.50212	88.63181	0.375258	0.490812
1	15.05665	84.02335	0.385742	0.534255
5	24.09822	74.95579	0.436274	0.509719
12	33.90979	65.01334	0.529584	0.547308
20	41.82737	56.95066	0.620417	0.601554
30	49.43832	49.24257	0.725381	0.593729
40	55.41777	43.13808	0.816765	0.627388
60	64.37078	33.97742	0.979478	0.672332
80	72.52157	25.63218	1.146288	0.699953

from regression: $k_1 = 0.03 \times 10^{-3}$ M^{-1} min^{-1}, $k_2 = 0.00062$ M min^{-1}

Experiment #81 - Compositions in wt%

· 100 mL of solution, temperature = 54°C
· 2 mL of catalyst exchanged for 3 h to 0.29 mmol OH^-/mL
· stir speed set to 2
· several samples analyzed for water, and water composition interpolated

Time	Ac	DAA	MO	Water
2	98.25992	1.266717	0.02461	0.448754
4	97.44717	2.034138	0.063368	0.455325
8	96.41892	2.980367	0.138568	0.462143
15	95.71441	3.568168	0.240138	0.477288
23	95.28585	3.874059	0.345235	0.494861
30	94.98613	4.034997	0.448101	0.530768
40	94.81187	4.07677	0.565543	0.545817
60	94.55983	4.094726	0.764809	0.580631
80	94.34301	4.099163	0.931967	0.625864

from regression: $k_1 = 0.24 \times 10^{-3}$ M^{-1} min^{-1}, $k_2 = 0.00075$ M min^{-1}

Experiment: MO Hydration - Compositions in wt%

· 100 mL of solution (20 mL water/20 mL MO in isopropanol), temperature = 54°C
· 5 mL of catalyst exchanged for 3 h to 0.45 mmol OH^-/mL
· stir speed set to 2
· added water measured, water content then interpolated

Time	Ac	DAA	MO	Water
2	2.827954	0.012499	17.45651	23.63852
60	2.726789	0.013808	17.54087	23.65402
150	2.907024	0.021394	17.38219	23.62487
240	3.02179	0.025635	17.28165	23.60641

Very slight rate of MO hydration: 0.00012 M min^{-1}

Appendix C

Estimation of the DAA concentration profile inside of the catalyst bead

To determine $k^*_{V,B}$:

from expt #6:

MO prod'n (mol/s) = (volume of liquid in batch reactor) x (production rate)
= 0.1 L x 0.0012 M/min x 1 min/60 s = 2×10^{-6} mol/s

2 mL (total volume) of catalyst was used in the reaction. This is equivalent to 1.38 mL of catalyst in acetone solvent. The void fraction of the catalyst is taken as 0.386. Therefore, there are 0.85 mL of catalyst beads in the reactor.

Rate constant comes from the equation --> MO prod'n = catalyst vol. x $k^*_{V,B}$ x [DAA]

$$k^*_{V,B} = 2 \times 10^{-6} \text{ mol/s} / (8.5 \times 10^{-7} \text{ m}^3 \times 280 \text{ mol/m}^3) = 8.4 \times 10^{-3} \text{ 1/s}$$

To estimate the effective diffusivity of acetone and DAA in the catalyst:

Satterfield (1981) states: $D_{12,eff} = D_{12} \times \theta / \tau$, where θ = void fraction of the pores or the porosity of the catalyst, and τ = tortuosity or labyrinth factor. Tortuosity is a correction factor applied since the pores are not straight. Therefore, the length of the diffusion path is often longer than the length used to characterize the catalyst particle. The porosity of the resin is estimated to be 27% (Tanabe, 1989), while typical tortuosities for catalysts vary widely between 0.5 and 10 (Satterfield, 1981). Most catalysts and theoretical predictions, however, give a value of τ near 2. We will assume that D_{eff} = 15% of D_{AB}.

The same value of the diffusion coefficient will be used for Acetone and DAA since the Fick diffusion coefficients for components in a binary mixture are equal (ie. $D_{12}=D_{21}$). Since this work is concerning dilute solutions of different components in acetone, pseudo-binary mass transfer can be assumed. The following expression shows the estimate of the effective diffusivity:

$$D_{A,eff} = D_{B,eff} = 4.6 \times 10^{-9} \text{ m}^2/\text{s} \times 0.15 = 6.9 \times 10^{-10} \text{ m}^2/\text{s}.$$

Production Rates of DAA:

From experiment:

DAA = 0.1 L x 0.36×10^{-3} M^{-1} min^{-1} x $(12.95 \text{ M})^2$ x 1 min/60 s = 1×10^{-4} mol/s

For the Concentration profile:

Surface Area of 1 particle = $4\pi(0.00045)^2 = 2.54 \times 10^{-6}$ m^2
Volume of 1 particle = $4\pi(0.00045\text{m})^3/3 = 3.82 \times 10^{-10}$ m^3

Total volume of particles in the reactor = 8.5×10^{-7} m^3
Thus, # of particles = 2226
Total surface area of particles = $2226 \times 2.54 \times 10^{-6} = 5.67 \times 10^{-3}$ m^2

Therefore, the DAA production rate is:

$$1 \times 10^{-4} \text{ mol/s} = (d[DAA]/dx) \times (1/0.00045m) \times 6.9 \times 10^{-9} \text{ m}^2/\text{s} \times 5.67 \times 10^{-3} \text{ m}^2$$

The value of the Thiele modulus should be varied in equation (3.16) so that the dimensionless concentration gradient (d[DAA]/dx in mol/m^3) satisfies the above equation. The value of (d[DAA]/dx) will be determined numerically, rather than trying to differentiate (3.16) at the outer edge of the catalyst where x=1. The slope will be evaluated between the dimensionless positions x = 1 and x = 0.99.

Through iteration using a spreadsheet, a Thiele modulus of 11 satisfies the above relation for the DAA production rate.

$$h_L^2 = (0.00045m/3)^2 \times (k^*_{V,A} / 6.9 \times 10^{-10} \text{ m}^2/\text{s}) = 11^2$$

From this expression, the intrinsic rate constant $k^*_{V,A} = 3.71$ 1/s.
This is very much higher than the observed $k^*_{V,A}$ estimated from experiment to be 0.01 1/s.

With a final value of $k^*_{V,A}$, we can specify a final value of the parameter w, which is

$$w = k^*_{V,B} / k^*_{V,A} = 0.00226.$$

Appendix D

Comparison of Kinetic Models

Due to the influence of pore diffusion, reactions may exhibit a reaction order which is different from intrinsic kinetics. The formation of DAA is strongly influenced by pore diffusion, so different rate models were tested to determine whether or not they would provide a better fit for the experimental data. First order, 1.5 order, and second order models were tested. All models were tested with $[Ac]_0$=12.95 M, and the models used are outlined below:

First order model:
k_1=0.0047, K_{EQ}=0.0227

$$\frac{d[DAA]}{dt} = k_1([Ac]_0 - 2[DAA]) - \frac{k_1}{K_{EQ}}[DAA]$$

1.5 order model:
k_1=0.00128, K_{EQ}=0.00645

$$\frac{d[DAA]}{dt} = k_1([Ac]_0 - 2[DAA])^{1.5} - \frac{k_1}{K_{EQ}}[DAA]$$

Second order model:
k_1=0.00036, K_{EQ}=0.00185

$$\frac{d[DAA]}{dt} = k_1([Ac]_0 - 2[DAA])^2 - \frac{k_1}{K_{EQ}}[DAA]$$

As shown in the Figure below, all three models can be made to appear virtually identical by using the above constants!

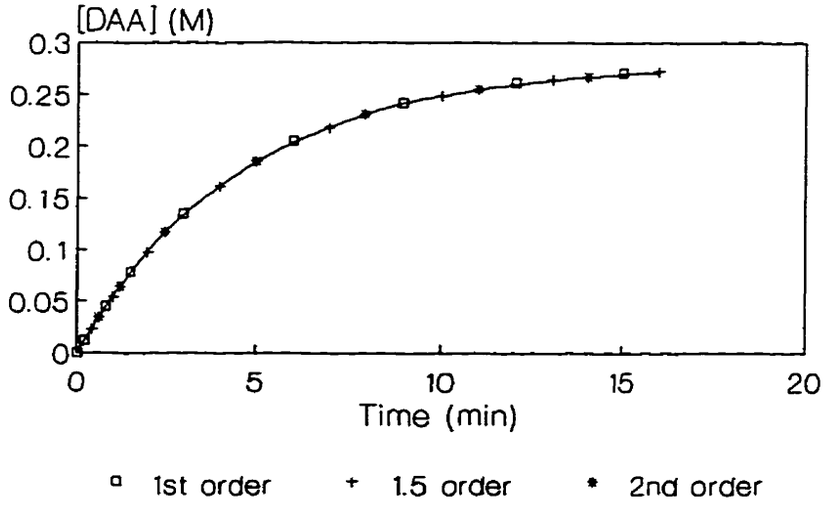

First order, 1.5 order, and second order models can be made to appear virtually identical.

Appendix E

Solid-Liquid Mass Transfer Data

To calculate Reynolds numbers, the following constants are required:

$\mu_L = 0.982 \times 10^{-3}$ Pa·s
$\rho_L = 997$ kg/m^3
$\mu_G = 0.0175 \times 10^{-3}$ Pa·s
$\rho_G = 1.218$ kg/m^3
d = column diameter = 2.54 cm
$D = 1.21 \times 10^{-9}$ m^2/s (diffusion coefficient of benzoic acid in water)

The following table shows the observed and predicted (Section 3.3, equation (3.23)) solid-liquid mass transfer coefficients and j-factors.

Liquid (mL/min)	Gas (L/min)	[B. Acid] (mol/L)	Height (m)	kCa (m2/s)	jD	N-Re Liquid	N-Re Gas	Predict jD	Predict kCa
11	15	8.41E-03	0.125	5.24E-07	4.690	10.181	872.219	4.925	5.09E-07
11	30	8.32E-03	0.125	5.17E-07	4.628	10.181	1744.438	4.586	4.74E-07
11	45	8.09E-03	0.125	5.00E-07	4.475	10.181	2616.658	4.398	4.55E-07
32.5	15	5.25E-03	0.125	9.00E-07	2.727	30.079	872.219	2.549	7.79E-07
32.5	30	4.85E-03	0.125	8.25E-07	2.499	30.079	1744.438	2.373	7.25E-07
32.5	45	4.42E-03	0.125	7.45E-07	2.257	30.079	2616.658	2.276	6.95E-07
70	15	3.59E-03	0.125	1.28E-06	1.800	64.785	872.219	1.599	1.05E-06
70	30	3.15E-03	0.125	1.11E-06	1.561	64.785	1744.438	1.489	9.79E-07
70	45	3.08E-03	0.125	1.09E-06	1.533	64.785	2616.658	1.428	9.39E-07
70	62.68	2.47E-03	0.125	8.62E-07	1.212	64.785	3644.713	1.380	9.08E-07
90	15	2.80E-03	0.125	1.27E-06	1.389	83.295	872.219	1.372	1.16E-06
90	30	see Table	3.3.2-II	1.38E-06	1.510	83.295	1744.438	1.278	1.08E-06
90	45	2.75E-03	0.125	1.24E-06	1.357	83.295	2616.658	1.225	1.04E-06
90	62.68	2.24E-03	0.125	1.00E-06	1.094	83.295	3644.713	1.184	1E-06
117	15	2.53E-03	0.125	1.48E-06	1.245	108.284	872.219	1.170	1.29E-06
117	30	2.51E-03	0.125	1.47E-06	1.237	108.284	1744.438	1.089	1.2E-06
117	45	1.86E-03	0.125	1.07E-06	0.900	108.284	2616.658	1.045	1.15E-06
117	62.68	1.74E-03	0.125	1.00E-06	0.842	108.284	3644.713	1.010	1.11E-06
144	15	2.23E-03	0.125	1.59E-06	1.087	133.272	872.219	1.031	1.4E-06
144	30	1.82E-03	0.125	1.29E-06	0.882	133.272	1744.438	0.960	1.3E-06
144	45	1.70E-03	0.125	1.21E-06	0.827	133.272	2616.658	0.921	1.25E-06
144	62.68	1.52E-03	0.125	1.08E-06	0.738	133.272	3644.713	0.890	1.2E-06
170	15	1.68E-03	0.125	1.40E-06	0.811	157.335	872.219	0.932	1.49E-06
170	30	1.46E-03	0.125	1.21E-06	0.701	157.335	1744.438	0.868	1.39E-06
170	45	1.17E-03	0.125	1.09E-06	0.631	157.335	2616.658	0.832	1.33E-06
170	62.68	1.35E-03	0.125	1.12E-06	0.649	157.335	3644.713	0.804	1.29E-06

Appendix F

The use of overall mass transfer coefficients and a derivation of Equation 3.27

The meaning of an 'overall mass transfer coefficient' - K_{OG}

When mass transfer occurs from vapour to liquid phase, component 'A' transfers from the bulk vapour to the vapour-liquid interface, then proceeds from the interface to the bulk liquid. In the figure below, y_A represents the mole fraction of A in the vapour phase, and x_A represents the composition of the liquid phase. Note that VLE exists at the interface.

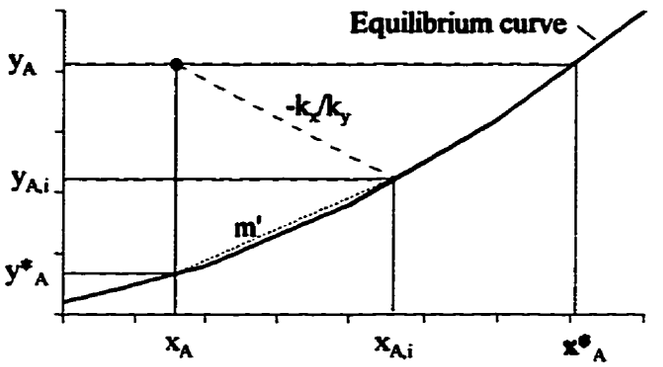

The flux of component A is given by the following expression:

$$N_A = k_y(y_A - y_{A,i}) = k_x(x_{A,i} - y_A)$$

It is convenient if the interfacial concentrations can be eliminated by using overall mass transfer coefficients. The overall gas phase mass transfer coefficient is shown below:

$$N_A = K_{OG}(y_A - y_A^*)$$

From the geometry in the above figure, it can be seen that:

$$y_A - y_A^* = (y_A - y_{A,i}) + (y_{A,i} - y_A^*) = (y_A - y_{A,i}) + m'(x_{A,i} - x_A)$$

In the above expression, the concentration differences can be replaced by the appropriate expression for (flux/coefficient), which then leads to the following relationship:

$$\frac{1}{K_{OG}} = \frac{1}{k_y} + \frac{m'}{k_x}$$

This equation provides the relationship between the overall gas phase mass transfer coefficient and the liquid side and gas side mass transfer coefficients.

The definition of the number of transfer units is: $$NTU_{OG} = \int_{y_b}^{y_t} \frac{dy}{y_{EQ} - y}$$

From the VLE relationship, $y_{EQ} = m\,x + b$: $$NTU_{OG} = \int_{y_b}^{y_t} \frac{dy}{(mx + b) - y}$$

Since the column is at total reflux (no overhead product is removed), the vapour and liquid molar flow rates are equal, and the operating line is simply y=x. Thus, in the expression used to evaluate y_{EQ}, one can substitute y in place of x.

This changes the expression as follows: $$NTU_{OG} = \int_{y_b}^{y_t} \frac{dy}{(my + b) - y}$$

Integration of this expression leads to :

$$NTU_{OG} = \frac{1}{m-1} \ln \left[\frac{(m-1)y_t + b}{(m-1)y_b + b} \right]$$

$$= \frac{1}{1-m} \ln \left[\frac{(1-m)y_b - b}{(1-m)y_t - b} \right]$$

Since samples are removed from the reboiler, y_b is unknown. The composition in the reboiler (x_r) is known, however. If we assume that the reboiler comprises 1 theoretical stage, then $y_b = mx_r + b$. This can be substituted into the equation to give the final form of (3.27).

$$NTU_{OG} = \frac{1}{1-m} \ln \left[\frac{(1-m)(mx_r + b) - b}{(1-m)y_t - b} \right]$$

An analogous procedure leads to the equation for NTU_{OL}.

Appendix G

Data from representative CD Experiments

Batch CD Experiment with reboiler at 55V:

- reflux rate = 5.49 g/min as acetone
- 20.5 mL of catalyts in 1 catalyst bag, catalyst's rate constants shown in Table 4.1.3-I
- 750 mL (592.5 g) of acetone initially charged into reboiler
- initial composition - 99.6 wt% acetone/0.4 wt% water

Time (h)	Ac (g)	DAA (g)	MO (g)	IP (g)	Wat (g)
0	590.7225	0	0	0	1.7775
1.5	578.5671	3.862073	5.386447	1.521328	3.163062
2.7	570.5104	6.340281	8.976008	2.300586	4.079164
4.116667	560.9779	9.588317	13.19375	3.205274	5.112935
6.05	548.3971	14.06357	18.80989	4.225394	6.436711
7.683333	538.6907	17.17667	23.15045	5.237239	7.525377
9.4	529.0607	20.70064	27.31742	6.041975	8.524965
11.66667	514.8039	25.43155	32.8128	8.298363	10.14961
23.21667	436.6551	62.64892	60.23277	14.23352	16.8855
25.88333	429.1773	64.09402	67.08471	12.38519	17.7009

Batch CD Experiment with reboiler at 65V:

- reflux rate = 8.76 g/min as acetone
- 21.8 mL of catalyts in 1 catalyst bag, catalyst's rate constants shown in Table 4.1.3-I
- 750 mL (592.5 g) of acetone initially charged into reboiler
- initial composition - 99.6 wt% acetone/0.4 wt% water

Time (h)	Ac (g)	DAA (g)	MO1 (g)	IP (g)	Wat (g)
0	590.7225	0	0	0	1.7775
1	581.8429	2.959069	3.495498	1.414463	2.788024
3	563.238	10.38104	11.48603	2.783032	4.611871
4.666667	545.1753	18.77034	18.27005	4.086937	6.197345
6.016667	529.6743	26.57309	23.96866	4.843203	7.44077
7.666667	507.3009	39.08902	30.99934	6.06155	9.049226
9.2	489.7423	48.02699	37.35384	6.933589	10.44325
11.13333	467.8879	60.15428	44.56081	7.883032	12.01397
14.25	428.0617	83.66043	56.49122	9.62748	14.65917
25.61667	292.7762	168.9716	91.36157	16.52984	22.86081
30.43333	245.9611	202.8174	101.8648	16.95624	24.90038

Batch CD Experiment with reboiler at 75V:

· reflux rate = 12.27 g/min as acetone
· 21.4 mL of catalyts in 1 catalyst bag, catalyst's rate constants shown in Table 4.1.3-I
· 750 mL (592.5 g) of acetone initially charged into reboiler
· initial composition - 99.6 wt% acetone/0.4 wt% water

Time (h)	Ac (g)	DAA (g)	MO (g)	IP (g)	Wat (g)
0	590.7225	0	0	0	1.7775
1.016667	567.0946	12.66823	7.782817	1.386432	3.567868
2	543.1796	27.55255	14.49241	2.250438	5.024996
3.083333	522.0729	39.93363	20.94335	3.115293	6.434855
4.016667	501.5996	52.50278	26.91206	3.781266	7.70433
5.5	469.4414	73.73536	34.7533	5.085863	9.48409
7.5	427.3695	103.669	43.88933	6.13674	11.43543
10.73333	373.35	138.557	57.78697	8.264308	14.54169
14.13333	321.2043	175.2565	69.48574	9.533116	17.02037
23.6	189.1867	276.6563	94.38465	10.44329	21.82909
26.41667	161.5583	295.2617	101.799	10.6395	23.24151

Batch CD Experiment with reboiler at 85V:

· reflux rate = 16.36 g/min as acetone
· 23.3 mL of catalyts in 1 catalyst bag, catalyst's rate constants shown in Table 4.1.3-I
· 750 mL (592.5 g) of acetone initially charged into reboiler
· initial composition - 99.6 wt% acetone/0.4 wt% water

Time (h)	Ac (g)	DAA (g)	MO (g)	IP (g)	Wat (g)
0	590.7225	0	0	0	1.7775
1	539.8167	35.28038	11.14973	1.926352	4.32679
2	487.9123	74.53124	20.87988	2.828208	6.34836
3.033333	438.1533	112.8147	29.55524	3.785973	8.190845
4.033333	394.3363	146.8318	37.27064	4.315689	9.74549
5	346.1155	185.8861	44.02204	5.248136	11.22814
7	261.1323	255.7135	55.68573	6.319549	13.64891
11.76667	71.98419	415.404	78.99407	7.80279	18.315

Batch CD Experiment with reboiler at 85V: see Figure 4.1.3-1

- reflux rate = 16.36 g/min as acetone
- 17.0 mL of catalyts in 1 catalyst bag, catalyst's rate constants shown in Table 4.1.3-I
- 750 mL (592.5 g) of acetone initially charged into reboiler
- initial composition - 99.6 wt% acetone/0.4 wt% water
- IP analysis was not done during this experiment

Time (h)	DAA (g)	MO (g)	Water (g)	Acetone (g)
0	0	0	2.37	590.13
2.35	44.028	19.8178	6.00747	520.2767
4.07	76.3351	32.2	8.280168	473.3147
6.13	141.987	44.4358	10.526	393.1812
16.05	298.169	111.869	22.90306	157.1889
18.72	321.535	115.591	23.58622	129.4178
22.85	324.9	135.057	27.15912	103.0139
29.65	314.234	164.593	32.58032	78.72268
41.57	274.048	214.024	41.65316	60.40484
49.3	255.666	241.414	46.68048	46.36952
53.88	234.878	258.338	49.7868	47.1272
65.8	196.756	298.848	57.22223	37.30377

Continuous CD data from experiment 2a and 2b: see Table 4.2.2-II

This was the only continuous experiment for which composition vs. time data were not shown in a figure in Section 4.2.2. These data are provided here.

- 42.8 mL of catalyst loaded into 2 catalyst bags
- reboiler duty dropped from 28% to 19% of maximum output after 10.5 h of operation
- reflux flow at 25.4 g/min during 2a, then dropped to 15.6 g/min during 2b
- catalyst properties and results for this experiment are shown in Table 4.2.2-II
- acetone flow rate held constant at 152 mL/h (120 g/h)

					Compositions given in wt%				
time (h)	Reboiler Output (%)	Reboiler T. (°C)	Catalyst Zone T (°C)	Diff. P.[a] (psi)	Ac	DAA	MO	IP	Water
1.50	28.00	57.60	54.90	0.80	59.30	25.43	10.82	1.59	2.86
3.00	28.00	65.50	54.80	0.80	57.08	27.47	11.04	1.49	2.92
4.50	28.00	65.00	54.70	0.90	60.18	25.23	10.08	1.37	3.14
6.00	28.00	64.30	55.00	0.90	60.81	25.25	9.73	1.31	2.90
7.50	28.00	64.60	55.00	0.90	60.26	25.84	9.74	1.28	2.90
9.00	28.00	64.80	54.60	0.80	58.91	27.77	8.76	1.31	3.26
10.50	28.00	64.30	54.60	0.80	59.30	26.92	9.08	1.17	3.54
12.00	19.00	64.00	54.20	0.80	63.88	24.48	8.13	1.02	2.49
13.50	19.00	62.40	54.50	0.70	66.59	22.54	7.61	0.93	2.34
15.00	19.00	61.60	54.00	0.70	67.83	22.02	7.14	0.89	2.12
16.50	19.00	61.70	54.00	0.70	67.86	21.99	7.01	0.85	2.29
18.00	19.00	61.90	54.00	0.70	67.92	22.05	6.85	0.81	2.36
19.50	19.00	61.40	54.00	0.60	67.42	22.77	6.85	0.81	2.15
21.00	19.00	61.40	54.00	0.70	67.90	22.37	6.62	0.76	2.36
22.50	19.00	61.00	54.00	0.60	70.26	20.57	6.15	0.72	2.30
24.00	19.00	61.00	54.00	0.70	72.03	19.15	6.01	0.66	2.15
26.00	19.00	61.00	54.20	0.70	70.56	20.24	6.24	0.73	2.24

[a]differential pressure measured across the entire height of the CD column

Batch CD Experiment with reboiler at 65V and New Liquid Distributor:

Data for the experiments with the new liquid distributor is shown graphically in Figures 4.3.2-2 and 4.3.2-3. A complete plot of the data obtained with the reboiler at 75 V is shown in Figure 4.3.2-1. In addition to this, it was decided to include from the experiments at 65 and 85 V.

- reflux rate = 8.76 g/min as acetone
- 22.45 mL of catalyts in 1 catalyst bag, catalyst's rate constants discussed in Section 4.3
- 750 mL (592.5 g) of acetone initially charged into reboiler
- initial composition - 99.6 wt% acetone/0.4 wt% water

Time (h)	Ac (g)	DAA (g)	MO1 (g)	IP (g)	Wat (g)
0	590.5448	0	0	0	1.95525
0.333	579.0528	7.798482	2.542547	0.54263	2.563525
0.75	562.948	19.41359	5.758564	1.084558	3.295266
1.5	535.4868	40.17736	10.6899	1.767318	4.378655
3	482.5859	81.15844	19.47874	2.970893	6.306058
4	448.0256	108.7198	24.82653	3.50174	7.426304
5.5	398.1011	149.2094	31.93619	4.310737	8.942544
7.5	331.3204	202.6233	40.21053	7.145146	11.20064
9	283.2615	245.2442	46.11288	5.917279	11.96421
10.5	240.4178	281.8099	50.76063	6.533496	12.97818

Batch CD Experiment with reboiler at 85V and New Liquid Distributor:

- reflux rate = 16.36 g/min as acetone
- 22.7 mL of catalyts in 1 catalyst bag, catalyst's rate constants discussed in Section 4.3
- 750 mL (592.5 g) of acetone initially charged into reboiler
- initial composition - 99.6 wt% acetone/0.4 wt% water

Time (h)	Ac (g)	DAA (g)	MO1 (g)	IP (g)	Wat (g)
0	590.5448	0	0	0	1.95525
0.333	570.2834	15.6249	3.204888	0.668791	2.718021
0.667	548.3174	33.0092	6.274452	1.421183	3.477742
1.333	508.0511	65.99598	11.72846	2.07491	4.649524
2	463.2729	103.454	16.94079	2.987845	5.84451
3	398.0162	159.3057	23.6392	4.159166	7.379702
4	344.2684	205.7806	29.36385	4.553573	8.53357
5.5	250.9345	287.8177	37.67609	5.710398	10.36128
7.667	147.063	382.2683	44.9231	6.379384	11.86624
10.55	19.32271	498.8614	53.75369	6.930892	13.63131

Appendix H

gPROMS Program Code

```
# Model of a Catalytic Distillation Reactor with Plug Flow,
#      Radial Dispersion, Film mass transfer inside the bag,
#      and counter-current liquid and vapour flow outside the bag.
#      Also featuring the Water/Acetone azeotrope...
#
#                              Gary Podrebarac, April 19, 1996
#

DECLARE
      TYPE

      CONC        = 100    :   0.0 : 1000       UNIT = "mol/m3"
      REACRATE    =  30.0  : -10.0 :  120       UNIT = "mol/m3.s"
      PRODRATE    =   1E-4 :  -0.1 :    0.1     UNIT = "mol/s"
      FLOWRATE    =   5E-6 :   0.0 :    0.1     UNIT = "m3/s"
      MOLFRAC     =   0.01 :   0.0 :    1       UNIT = "mol/mol"

END

MODEL TUBULAR_REACTOR

      PARAMETER

      NOBAG              AS INTEGER  # No. OF CATALYST BAGS
      FLOW               AS REAL     # FLOW FROM CONDENSER (g/min)
      SPLIT              AS REAL     # FRACTION OF FLOW THRU BAG
      RB,ZB              AS REAL     # REACTOR RADIUS & LENGTH (m)
      Dr                 AS REAL     # RADIAL DISPERSION (m2/s)
      KsaD,KsaM,KsaW     AS REAL     # WALL MASS TRANS. (m2/s)
      KGaD,KGaM,KGaW     AS REAL     # GAS/LIQUID MASS TRANS. (mol/m.s)
      KfaD,KfaM,KfaW     AS REAL     # FILM MASS TRANS. (1/s)
      ADAA,BDAA          AS REAL     # KINETIC PARAMETERS
      DDAA,EDAA,FDAA     AS REAL     # KINETIC PARAMETERS
      AMO,BMO,CMO        AS REAL     # KINETIC PARAMETERS
      DMO,EMO,FMO        AS REAL     # KINETIC PARAMETERS
      Keq                AS REAL     # REACTION EQ. CONST. (m3/mol)
      M,B                AS REAL     # WATER/ACETONE VLE CORRELATION
      VPD,VPM,VPW        AS REAL     # VAPOUR PRESS AT 56C (kPa)
      AcCON,DAACON       AS REAL     # LIQUID CONC. AT 56C (mol/m3)
      MOCON,WATCON       AS REAL     # LIQUID CONC. AT 56C (mol/m3)
      PT                 AS REAL     # TOTAL PRESSURE (kPa)
      PI                 AS REAL     # 3.14159...


      DISTRIBUTION_DOMAIN

            AXIAL   AS (0:ZB)
            RADIAL  AS (0:RB)


      VARIABLE

      F,FOUT,V           AS                                          FLOWRATE
      CVAP               AS                                          CONC
      OD,OM,OW           AS                                          CONC
      OXD,OXM,OXW        AS                                          MOLFRAC
      BD,BM,BW           AS DISTRIBUTION (NOBAG,AXIAL,RADIAL) OF     CONC
      FD,FM,FW           AS DISTRIBUTION (NOBAG,AXIAL,RADIAL) OF     CONC
      RDAA,RMO           AS DISTRIBUTION (NOBAG,AXIAL,RADIAL) OF     REACRATE
      LD,LM,LW           AS DISTRIBUTION (NOBAG,AXIAL)        OF     CONC
```

```
VD,VM,VW          AS DISTRIBUTION (NOBAG,AXIAL)        OF   CONC
XDL,XML,XWL       AS DISTRIBUTION (NOBAG,AXIAL)        OF   MOLFRAC
YDEQ,YMEQ,YWEQ    AS DISTRIBUTION (NOBAG,AXIAL)        OF   MOLFRAC
BAGD,BAGM,BAGW    AS        ARRAY (NOBAG)              OF   CONC
WALD,WALM,WALW    AS        ARRAY (NOBAG)              OF   PRODRATE

BOUNDARY  #-------------------------------------------  THE BC'S

#1) FOR ALL BAGS-> dC/dr=0 AT r=0 FOR ALL z

FOR x := 1 TO NOBAG DO
  FOR z := 0|+ TO ZB| DO

     PARTIAL(BD(x,z,0|),RADIAL) = 0;
     PARTIAL(BM(x,z,0|),RADIAL) = 0;
     PARTIAL(BW(x,z,0|),RADIAL) = 0;

  END
END

#2) FOR ALL BAGS-> DISPERSION = FLUX AT r=RB

FOR x := 1 TO NOBAG DO

   FOR z := 0|+ TO ZB| DO

      2*PI*RB*Dr*PARTIAL(BD(x,z,RB|),RADIAL) =
      KsaD*(LD(x,z)-BD(x,z,RB|));

      2*PI*RB*Dr*PARTIAL(BM(x,z,RB|),RADIAL) =
      KsaM*(LM(x,z)-BM(x,z,RB|));

      2*PI*RB*Dr*PARTIAL(BW(x,z,RB|),RADIAL) =
      KsaW*(LW(x,z)-BW(x,z,RB|));

   END
END

#3) AT INLET OF BAG 1 --> LIQUID CON. = VAPOUR CON. AT z=0

FOR r := 0| TO RB| DO
      BD(1,0|,r) = VD(1,0|)*V/(FOUT+F);
      BM(1,0|,r) = VM(1,0|)*V/(FOUT+F);
      BW(1,0|,r) = VW(1,0|)*V/(FOUT+F);
END


#4) FOR THE LAST BAG (NOBAG)-> SET VAPOUR CONC. AT z=ZB

      VD(NOBAG,ZB|) = CVAP*OXD*VPD/PT;
      VM(NOBAG,ZB|) = CVAP*OXM*VPM/PT;
      VW(NOBAG,ZB|) = CVAP*OXW*(M*OXW+B)*VPW/PT;

#5) AT TOP OF BAG --> LIQUID COMPN. IN BAG = COMPN. OUTSIDE BAG

      LD(1,0|) = BD(1,0|,0|);
      LM(1,0|) = BM(1,0|,0|);
      LW(1,0|) = BW(1,0|,0|);
```

```
EQUATION

#-------------------------  CALCULATE FLOW RATES

F = SPLIT*FLOW/(60*1000*749);              # FLOW IN BAG (m3/s)
FOUT = (1-SPLIT)*FLOW/(60*749*1000);       # FLOW BY BAG (m3/s)
V = FLOW*0.008314*329/(PT*60*58.08);       # VAPOUR FLOW (m3/s)
CVAP = PT/(0.008314*329);                  # VAPOUR CONC.(mol/m3)


#-------------------------  Mass Balance and Reaction Equations

FOR x := 1 TO NOBAG DO

   FOR z := 0|+ TO ZB| DO  #------------ LIQUID PHASE BALANCES

     FOUT*PARTIAL(LD(x,z),AXIAL) = KsaD*(BD(x,z,RB|)-LD(x,z))
      -KGaD*(YDEQ(x,z)-VD(x,z)/CVAP);

     FOUT*PARTIAL(LM(x,z),AXIAL) = KsaM*(BM(x,z,RB|)-LM(x,z))
      -KGaM*(YMEQ(x,z)-VM(x,z)/CVAP);

     FOUT*PARTIAL(LW(x,z),AXIAL) = KsaW*(BW(x,z,RB|)-LW(x,z))
      -KGaW*(YWEQ(x,z)-VW(x,z)/CVAP);


      FOR r := 0|+ TO RB|- DO   #------------ INSIDE THE BAG

      -(F*r/(PI*RB*RB))*PARTIAL(BD(x,z,r),AXIAL) +
      Dr * ( PARTIAL(BD(x,z,r),RADIAL) +
      r * PARTIAL(BD(x,z,r),RADIAL,RADIAL) ) +
      r * RDAA(x,z,r) = 0;

      -(F*r/(PI*RB*RB))*PARTIAL(BM(x,z,r),AXIAL) +
      Dr * (PARTIAL(BM(x,z,r),RADIAL) +
      r * PARTIAL(BM(x,z,r),RADIAL,RADIAL)) +
      r * RMO(x,z,r) = 0;

      -(F*r/(PI*RB*RB))*PARTIAL(BW(x,z,r),AXIAL) +
      Dr * (PARTIAL(BW(x,z,r),RADIAL) +
      r * PARTIAL(BW(x,z,r),RADIAL,RADIAL)) +
      r * RMO(x,z,r) = 0;

      END
   END
END

#-------------- FILM MASS TRANSFER

FOR x:= 1 TO NOBAG DO
   FOR z := 0| TO ZB| DO
      FOR r := 0| TO RB| DO

      KfaD*(FD(x,z,r)-BD(x,z,r)) = RDAA(x,z,r);
      KfaM*(FM(x,z,r)-BM(x,z,r)) = RMO(x,z,r);
      KfaW*(FW(x,z,r)-BW(x,z,r)) = RMO(x,z,r);

      END
   END
END
```

```
#--------------GAS PHASE BALANCES

FOR x := 1 TO NOBAG DO
   FOR z := 0| TO ZB|- DO

     V*PARTIAL(VD(x,z),AXIAL) = -KGaD*(YDEQ(x,z)-VD(x,z)/CVAP);
     V*PARTIAL(VM(x,z),AXIAL) = -KGaM*(YMEQ(x,z)-VM(x,z)/CVAP);
     V*PARTIAL(VW(x,z),AXIAL) = -KGaW*(YWEQ(x,z)-VW(x,z)/CVAP);

   END
END

# ----------KINETIC EXPRESSIONS = MASS TRANSFER RATE

FOR x := 1 TO NOBAG DO

   FOR z := 0| TO ZB| DO

      FOR r := 0| TO RB| DO    #Kinetics are based on film conc.

      IF (FW(x,z,r)/1000) < 0.42 THEN
        RMO(x,z,r) = 1.204*1.25*(AMO*((FW(x,z,r)/1000)-BMO)^2 + CMO);
      ELSE
        RMO(x,z,r) = 1.204*1.25*(DMO+EMO/((FW(x,z,r)/1000)+FMO));
      END

# A NOTE ABOUT THE CONSTANTS IN THESE KINETIC EQUATIONS...
# we assume 'simular' profiles for all catalysts...
# 1.25 = is a proportionality constant
# 1.204 converts from (1000*mol/mL.min) to (mol/m3.s)

      IF (FW(x,z,r)/1000) < 0.498 THEN
        RDAA(x,z,r) = 1.204*(ADAA+BDAA*FW(x,z,r)/1000)*
        ((AcCON*(1-(FD(x,z,r)/DAACON+FM(x,z,r)/MOCON+FW(x,z,r)/WATCON))
        /1000)^2-FD(x,z,r)/(1000*Keq)) - RMO(x,z,r);
      ELSE
        RDAA(x,z,r) = 1.204*(DDAA+EDAA/(FDAA+FW(x,z,r)/1000)^2)*
        ((AcCON*(1-(FD(x,z,r)/DAACON+FM(x,z,r)/MOCON+FW(x,z,r)/WATCON))
        /1000)^2-FD(x,z,r)/(1000*Keq)) - RMO(x,z,r);
      END

      END

#---------- MOL FR. AND VLE CALCULATIONS

      XDL(x,z) = LD(x,z)/
            (LD(x,z)+LM(x,z)+LW(x,z)+AcCON*(1-(LD(x,z)/DAACON
            +LM(x,z)/MOCON+LW(x,z)/WATCON)));
      XML(x,z) = LM(x,z)/
            (LD(x,z)+LM(x,z)+LW(x,z)+AcCON*(1-(LD(x,z)/DAACON
            +LM(x,z)/MOCON+LW(x,z)/WATCON)));
      XWL(x,z) = LW(x,z)/
            (LD(x,z)+LM(x,z)+LW(x,z)+AcCON*(1-(LD(x,z)/DAACON
            +LM(x,z)/MOCON+LW(x,z)/WATCON)));

      YDEQ(x,z) = XDL(x,z)*VPD/PT;
      YMEQ(x,z) = XML(x,z)*VPM/PT;
      YWEQ(x,z) = XWL(x,z)*(M*XWL(x,z)+B)*VPW/PT;
   END
END
```

```
FOR x := 1 TO NOBAG DO  #---- AVG. CONC AT ZB & PRODN RATE AT WALL

   BAGD(x) = INTEGRAL (r := 0| : RB| ; 2*r*BD(x,ZB|,r)/(RB*RB) );
   BAGM(x) = INTEGRAL (r := 0| : RB| ; 2*r*BM(x,ZB|,r)/(RB*RB) );
   BAGW(x) = INTEGRAL (r := 0| : RB| ; 2*r*BW(x,ZB|,r)/(RB*RB) );

   WALD(x) = INTEGRAL (z := 0| : ZB| ; KsaD*(BD(x,z,RB|)-LD(x,z)));
   WALM(x) = INTEGRAL (z := 0| : ZB| ; KsaM*(BM(x,z,RB|)-LM(x,z)));
   WALW(x) = INTEGRAL (z := 0| : ZB| ; KsaW*(BW(x,z,RB|)-LW(x,z)));

END

# These equations could also be listed as boundary conditions....

FOR x := 1 TO (NOBAG-1) DO


#-------LINK LIQUID OUTSIDE OF BAG (EQN 5.23)

   LD(x+1,0|) = SPLIT*BAGD(x) + (1-SPLIT)*LD(x,ZB|);
   LM(x+1,0|) = SPLIT*BAGM(x) + (1-SPLIT)*LM(x,ZB|);
   LW(x+1,0|) = SPLIT*BAGW(x) + (1-SPLIT)*LW(x,ZB|);


#-------LINK TOP OF EACH BAG (EQN 5.22)

   FOR r := 0| TO RB| DO

      BD(x+1,0|,r) = LD(x+1,0|);
      BM(x+1,0|,r) = LM(x+1,0|);
      BW(x+1,0|,r) = LW(x+1,0|);
   END


#-----------VAPOUR CONNECTIONS (EQN 5.26)

   VD(x,ZB|) = VD(x+1,0|);
   VM(x,ZB|) = VM(x+1,0|);
   VW(x,ZB|) = VW(x+1,0|);

END


#---------------------------- EXIT LIQUID COMPOSITION

OD = (F*BAGD(NOBAG)+FOUT*LD(NOBAG,ZB|))/(F+FOUT);
OM = (F*BAGM(NOBAG)+FOUT*LM(NOBAG,ZB|))/(F+FOUT);
OW = (F*BAGW(NOBAG)+FOUT*LW(NOBAG,ZB|))/(F+FOUT);

OXD = OD/(OD+OM+OW+AcCON*(1-(OD/DAACON+OM/MOCON+OW/WATCON)));
OXM = OM/(OD+OM+OW+AcCON*(1-(OD/DAACON+OM/MOCON+OW/WATCON)));
OXW = OW/(OD+OM+OW+AcCON*(1-(OD/DAACON+OM/MOCON+OW/WATCON)));

END
```

```
PROCESS SIMULATION

      UNIT
       REACTOR AS TUBULAR_REACTOR

      MONITOR

       REACTOR.BAG*(*) ; REACTOR.WAL*(*) ;
       REACTOR.L*(*,11) ; REACTOR.V*(*,11);
       REACTOR.BD(*,*,1) ; REACTOR.BM(*,1,1) ; REACTOR.BW(*,1,1) ;
       REACTOR.FD(*,*,1) ; REACTOR.FM(*,1,1) ; REACTOR.FW(*,1,1) ;
       REACTOR.F ; REACTOR.V ; REACTOR.FOUT ;
       #REACTOR.BD(*,*,*) ; REACTOR.BM(*,*,*) ; REACTOR.BW(*,*,*) ;
       #REACTOR.L*(*,*) ;

     SET     # Values for BATCH CD 75 (glass column)

      WITHIN REACTOR DO

      FLOW    := 12.27          ; # g/min
      SPLIT   := 0.1952         ; # fraction of liquid 'in' bag
      RB      := 0.0075         ; # Radius of catalyst bag (m)
      ZB      := 0.0838         ; # Hieght of catalyst bag (m)
      PT      := 101.3          ; # Reaction Pressure (kPa)
      NOBAG   := 1              ; # Number of catalyst bags
      Dr      := 5.837e-8       ; # Radial Dispersion (m2/s)
      KsaD    := 1.488e-6       ; # Wall Mass Trans. (m2/s)
      KsaM    := 1.527e-6       ; # Wall Mass Trans. (m2/s)
      KsaW    := 1.888e-6       ; # Wall Mass Trans. (m2/s)
      KGaD    := 3.097e-3       ; # Gas/Liquid Mass Trans. (mol/m.s)
      KGaM    := 3.288e-3       ; # Gas/Liquid Mass Trans. (mol/m.s)
      KGaW    := 1.029e-2       ; # Gas/Liquid Mass Trans. (mol/m.s)
      KfaD    := 1.472e-1       ; # Film Mass Trans. (1/s)
      KfaM    := 1.511e-1       ; # Film Mass Trans. (1/s)
      KfaW    := 1.869e-1       ; # Film Mass Trans. (1/s)
      Keq     := 1.95E-3        ; # Reaction Eq. (m3/mol)
      ADAA    := 0.4697         ; # Slope for DAA      \
      BDAA    := -0.6446        ; # Intercept for DAA  /
      DDAA    := 0.0302         ; # For DAA when       \
      EDAA    := 0.0471         ; # [water] > 0.49 M   -
      FDAA    := 0.13273        ; # (wet conditions)   /
      AMO     := -3.15          ; # Kinetic constants for MO  \
      BMO     := 0.17           ; # for cat exch. 0.49 mmol/mL-
      CMO     := 0.81           ; # Dry cond.                 /
      DMO     := -0.07837       ; # MO constants when    \
      EMO     := 0.19449        ; # [water] > 0.675 M    -
      FMO     := -0.13877       ; # Wet cond.            /
      M       := -29.84         ; # Acetone/water VLE
      B       := 6.6798         ; # Actone/water VLE
      VPD     := 1.38           ; # Vap Press. DAA (kPa)
      VPM     := 7.26           ; # Vap Press. MO (kPa)
      VPW     := 16.58          ; # Vap Press. Water (kPa)
      AcCON   := 12888          ; # Conc. of pure acetone (mol/m3)
      DAACON  := 7825.7         ; # Conc. of pure DAA (mol/m3)
      MOCON   := 8414.16        ; # Conc. of pure MO (mol/m3)
      WATCON  := 54724.9        ; # Conc. of pure Water (mol/m3)
      PI      := 3.14159265     ; #
      PT      := 101.3          ; # Total Pressure (kPa)
```

```
        #-------------- Specify centered finite difference method

        AXIAL  := [CFDM,2,10];
        RADIAL := [CFDM,2,8];

        END


        INITIAL

         STEADY_STATE

END
```

Appendix I

Sample Spreadsheet for Calculation of

Mass Transfer Coefficients

Spreadsheet for calculating Mass Transfer Coefficients

Constants for Batch CD at 75 V

Condensate Rate	12.27 g/min
f	0.1952 -
Radius of Bag	0.0075 m
Radius of Column	0.0127 m
Temperature	329 K
Pressure	101.3 kPa
DI of DAA in Ac	4.60E-09 m2/s
DI of MO in Ac	4.78E-09 m2/s
DI of Wat in Ac	6.57E-09 m2/s
Dv of DAA in Ac	5.47E-07 m2/s
Dv of MO in Ac	5.98E-07 m2/s
Dv of Wat in Ac	3.31E-06 m2/s
Gas Constant	0.008314 kPa.m3/mol.K
Liquid Density (Ac)	751.95 kg/m3
Cat. Particle dia.	9.00E-04 m
Void Fraction	0.386
Liquid Visc. (Ac)	2.32E-04 Pa.s
Vapour Visc. (Ac)	9.00E-06 Pa.s

Wall Mass Transfer (KcA)

Sup. Vel. of liquid outside of bag =	0.000432	m/s
Re Liquid =	35.62207	
Vapour Flow =	9.51E-05	m3/s
Vapour Density =	2.150949	kg/m3
Re Vapour =	1139.009	
jD =	2.2375161	
Sc DAA	67.020455	
Sc MO	64.445765	
Sc Water	46.879635	
KCAD =	1.488E-06	m2/s
KCAM =	1.527E-06	m2/s
KCAW =	1.888E-06	m2/s <----

Gas/Liquid Mass Transfer (KogA)

Total Flow in col	0.000537	m/s
Re Liquid	44.26201	
Sc DAA (vapour)	7.653557	
Sc MO (vapour)	6.996989	
Sc Wat (vapour)	1.264109	
ShG DAA	152.97032	
ShG MO	148.46467	
ShG Wat	83.929414	
KGaD =	0.0030971	mol/m.s
KGaM =	0.003288	mol/m.s
KGaW =	0.0102883	mol/m.s <----

Radial Dispersion

(1-f)F -flow in bag	5.309E-08	m3/s
Superf. velocity =	0.0003004	m/s
Particle Re =	0.8778184	
Pe Number =	12	
Dispersion (D) =	5.837E-08	m2/s <----

Film Mass Transfer (KfA)

Area/Volume =	4093.333	m2/m3
KfaD =	0.1472377	1/s
KfaM =	0.1511336	1/s
KfaW =	0.1868535	1/s <----